University of Reading

Investigation of the functional effects of auto-immune ionotropic glutamate receptor antibodies in representative in vitro CNS preparations

PhD Thesis

School of Pharmacy

Charlotte Day

December 2021

Supervisors:

Angela Bithell

Gary Stephens

Abstract

The NR1 subunit of N-methyl-D-aspartate receptors (NMDARs) and the GluR3 subunit of α-amino-3-hydroxy-5-methyl-4-isoxazolepropionic acid receptors (AMPARs) have been identified as targets of autoantibodies (Aabs) in autoimmune encephalopathy, whereby seizures, cognitive impairment and memory loss are key symptoms. Recent studies have proposed mechanisms by which these Aabs act on their respective receptors, but their role in neuronal excitability, seizures and autoimmune epilepsy is yet to be established. Patient Aabs have been shown to bind to specific regions within the NR1 and GluR3 subunits. Therefore, peptide immunisation was used to generate Aabs in rabbits against these specific sequences, and 'protein A' purification to obtain total IgG, or peptide purification to obtain target specific Aabs. Binding and specificity of these Aabs were determined using a range of methodologies including enzyme-linked immunosorbent assay (ELISA), immunocytochemistry (ICC) and immunohistochemistry (IHC). Functional effects were determined using a range of *in vitro* electrophysiology techniques, including two-electrode voltage-clamp on *Xenopus* oocytes, long-term potentiation (LTP) in hippocampal brain slices using multi-electrode arrays, and excitatory postsynaptic currents (EPSCs) from primary hippocampal neurons using whole-cell patch-clamp. This study has shown NMDAR and AMPAR Aabs generated from peptide immunisation demonstrated specificity for NR1 and GluR3 immunisation peptides as well as target-specific binding to their native proteins in ELISA, IHC and ICC. Upon further purification, NMDAR Aabs were shown to prevent the induction of LTP at Schaffer collateral-CA1 synapses, supporting the proposed Aab-induced internalisation of NMDARs mechanism of action. Acute and chronic application of AMPAR Aabs elicited a reduction in spontaneous and miniature EPSC frequency in hippocampal neurons. Our data is consistent with NMDAR Aabs decreasing the number of synaptic NMDARs via internalisation, and AMPAR Aabs acting via an inhibitory mechanism at the synaptic level, in both cases an effect consistent with a disruption to the excitatory/inhibitory network. This work provides a solid basis to address outstanding questions regarding the mechanism of both these Aabs; for example, future work using internalisation assays or applying Aabs to *in vitro* models of epileptiform activity to determine their roles on network activity. The basic science presented here can contribute to the development of novel AEDs with respect autoimmune epilepsy.

Declaration

I confirm that this is my own work and the use of all material from other sources has been properly and fully acknowledged.

Charlotte Day

Acknowledgements

I would like to start by thanking the University of Reading and UCB for both funding this project and giving me the opportunity to undertake this PhD. I would like to specifically thank the team at UCB; Christian, John, Brice and Becci. The wisdom and support that you have contributed throughout these last four years have been invaluable. In addition, the time and resources you have dedicated to helping me perform experiments, allowing me to visit both Braine l'Alleud and Slough on multiple occasions has been most beneficial. I simply could not have completed this research without you all!

I would also like to thank my supervisors, Dr Angela Bithell and Prof Gary Stephens for their unwavering support and guidance throughout. I have been incredibly lucky to have supervisors who always found time to listen to any problems I encountered throughout this PhD, and supported me both personally and with the research. Thank you for always being calm and collected in response to my many stressed emails, I would not have succeeded without your wisdom, dedication, knowledge and endless dog anecdotes, for this I am forever grateful!

My family who have endured this PhD with me; words can't fully encompass what it's meant to have your support, guidance and love over the years. I know my endless breakdowns and tears have driven you insane, so thank you for believing in me and picking me up when I was down. The motivational talks, the jokes and hugs were priceless and has helped me become the person I am today.

To Nathan, you are my rock. Thank you for putting up with me, bringing me endless coffees, cooking for me and dealing with the endless madness that has been this PhD. You have been my constant voice of reason throughout, and your unwavering support and love has made completing this PhD so much easier. You have made these last four years possible, and I wouldn't trade any of it!

Conferences/Publications

Conferences:

2020: Federation of European Neuroscience Societies (FENS) (Virtual conference; Poster)

2021: British Neuroscience Association (BNA) (Virtual conference; 10 min presentation)

Publications:

Ion channels as Targets in Drug Discovery – Chapter on 'autoantibodies against ionotropic glutamate receptors' (**In progress**)

Functional effects of AMPAR Aabs **(In progress)**

Table of Contents

Abstract ..... *ii*

Declaration ..... *iii*

Acknowledgements ..... *iv*

Conferences/Publications ..... *v*

List of Figures ..... *xiv*

List of Tables ..... *xix*

List of Abbreviations ..... *xx*

1. Introduction *1*

1.1 Autoimmune encephalitis *1*

1.2 Epilepsy *2*

1.2.1 Classification of epilepsy *3*

1.2.1.1 Seizure classification *3*

1.2.1.2 Classification by aetiology *6*

1.2.2 Current management of epilepsy *7*

1.3 Autoimmune Epilepsy *10*

1.4 The immune system *11*

1.4.1 Adaptive immune system *11*

1.4.2 Antibody structure *12*

1.4.2.1 Autoantibodies *14*

1.4.3 Autoimmune diseases *15*

1.4.3.1 Anti-NMDAR Encephalitis *15*

1.4.3.2 Rasmussen's encephalitis 17

1.5 Glutamate receptors 18

1.5.1 NMDA Receptors 19

1.5.1.1 NMDAR Structure 20

1.5.1.2 NMDAR CNS distribution 22

1.5.1.3 Physiological function of NMDARs 22

1.5.1.4 Autoantibodies against NMDARs 23

1.5.1.4.1 Binding of Aabs to NMDARs 23

1.5.1.4.2 In vitro effects of NMDAR Aabs 25

1.5.1.4.3 In vivo effects of NMDAR Aabs 26

1.5.2 AMPA Receptors 29

1.5.2.1 AMPAR structure 29

1.5.2.2 AMPAR CNS distribution 31

1.5.2.3 Physiological function of AMPARs 31

1.5.2.4 Autoantibodies to AMPARs 34

1.5.2.4.1 Binding of Aabs to AMPARs 34

1.5.2.4.2 In vitro effects of AMPAR Aabs 35

1.5.2.4.3 In vivo effects of AMPAR Aabs 36

1.6 Aims 37

2 Materials and Methods 39

2.1 NR1 and GluR3 autoantibody production and purification 39

2.1.1 Rabbit immunisation and antibody production 41

2.1.2 Serum screening and antibody titre 42

2.1.3 Protein A purification of polyclonal IgG antibody from rabbit serum 43

2.1.4 Peptide purification of polyclonal IgG from protein A purified Aabs 43

2.1.5 SDS-PAGE analysis of anti-NMDAR/anti-AMPAR antibody purity..... 44

2.2 Binding specificity of generated autoantibodies 45

2.2.1 NMDAR transfection in HEK cells 46

2.2.1.1 Immunocytochemistry on NR1-transfected HEK cells 47

2.2.2 Immunocytochemistry on primary neurons..... 48

2.2.3 Immunohistochemistry 48

2.2.4 SDS PAGE and Western blotting 49

2.2.4.1 Cell lysate preparation..... 49

2.2.4.2 Whole brain homogenisation and protein lysate preparation 50

2.2.4.3 Quantification of protein concentration..... 51

2.2.4.4 SDS-PAGE Gel preparation 51

2.2.4.4.1 Preparation of protein lysate samples 53

2.2.4.4.2 SDS-PAGE Gel electrophoresis 53

2.2.4.4.3 Wet transfer of gel to membrane 54

2.2.4.4.4 ECL Western Blot Imaging 55

2.3 Tissue preparation for functional studies 55

2.3.1 Animals 55

2.3.1.1 Generation of acute hippocampal slices 55

2.3.1.2 Primary hippocampal neuronal cultures 57

2.3.1.2.1 Preparation of laminin coated coverslips 57

2.3.1.2.2 Removal and dissociation of E18 primary neuronal cells 58

2.3.1.2.3 Primary hippocampal neuronal cell culture 59

2.3.2 Xenopus oocyte expression system 60

2.3.2.1 mRNA preparation and GluN1/GluN2A receptor expression 60

2.4 Electrophysiology 60

2.4.1 Multi-electrode array (MEA) electrophysiology 61

2.4.1.1 MEA recordings and long-term potentiation 61

2.4.2 Patch clamp electrophysiology 63

2.4.3 TEVC in Xenopus oocytes 64

2.4.4 Whole cell patch clamp and primary hippocampal cultures 66

2.4.4.1 Patch pipettes 67

2.4.4.2 Whole-cell patch-clamp 67

2.4.4.3 Spontaneous excitatory postsynaptic currents (sEPSCs) 68

2.4.4.4 Miniature excitatory postsynaptic currents (mEPSCs) 68

2.5 Statistical Analysis 69

3. Generation and characterisation of NMDAR Aabs 71

3.1. Introduction 71

3.2 Production of rabbit polyclonal NMDAR 1 Aabs (rabbit #1) 71

3.2.1 Titres and ELISA of antibody sera 74

3.2.2 Purification and analysis of NMDAR1 Aabs 76

3.3 Characterisation of NMDAR1 Aabs using in vitro models. 79

3.3.1 NMDAR1 Aab detection of NMDARs in NR1-transfected HEK cells 79

3.3.2 NMDAR1 Aab detection of NMDARs to native NMDARs 82

3.4 Production of rabbit polyclonal anti-NMDAR2 Aabs (rabbit #2) 94

3.4.1 Titres and ELISA of sera of NMDAR2 Aabs 96

3.4.2 Purification and analysis of NMDAR2 Aabs 98

3.5 Characterisation of NMDAR2 Aabs on in vitro systems 102

3.5.1 NMDAR2 Aab detection of NMDAR in NR1-transfected HEK cells 102

3.5.2 NMDAR2 Aab detection of NMDAR to native NMDARs 105

3.6 Peptide purification of NMDAR1 Aabs 111

3.7 Characterisation of NMDAR1pp Aabs on in vitro systems 114

3.7.1 NMDAR1pp Aab detection of NMDAR in NR1-transfected HEK cells 114

3.7.1.1 NMDAR Aab detection of NMDAR to native NMDARs 117

3.8 Discussion 124

3.8.1 Peptide immunisation generates NMDAR Aabs 125

3.8.2 Anti-NMDAR Aabs bind to native NMDARs 127

3.8.3 Conclusions 130

4. Assessing the functionality of NMDAR Aabs 132

4.1 Introduction 132

4.2 Xenopus oocytes experimental setup 133

4.2.1 Known NMDAR antagonists reduce NMDAR current 135

4.2.2 NMDAR1 Aabs have no functional effects on NMDAR expressing oocytes following acute incubation 137

4.2.3 NMDAR1 Aabs have no functional effects on NMDAR expressing oocytes following chronic incubation 140

4.2.4 NMDAR1 Aabs do not alter NMDAR current via allosteric modulation 143

4.3 Effects of Aabs on NMDAR-dependent LTP 148

4.3.1 Schaffer collateral long-term potentiation (LTP) 148

4.3.2 Commercial anti-NMDAR antibodies and class specific negative controls have no significant effect on NMDAR-dependent LTP 148

4.3.3 NMDAR1 protein A purified Aabs do not inhibit NMDAR-dependent LTP 151

4.3.4 NMDAR2 Aabs do no alter NMDAR-dependent LTP 155

4.3.5 NMDAR1pp reduces NMDAR-dependent LTP 157

4.4 Effects of NMDAR1pp Aabs on hippocampal neurons 160

4.4.1 Spontaneous excitatory postsynaptic currents 160

4.4.2 NMDAR1pp Aabs do not affect sEPSC frequency or amplitude 161

4.5 Discussion 166

4.5.1 NMDAR1 Aabs do not display any functional effects in NR1/NR2A expressing Xenopus oocytes 167

4.5.2 Schaffer collaterals-CA1 LTP is NMDAR dependent, but NMDAR1 & 2 Aabs have no significant effect 169

4.5.3 Peptide purification of NMDAR Aabs elicited a significant reduction in LTP 170

4.5.4 NMDAR1pp Aabs have no significant effect on sEPSC frequency following acute exposure 172

4.5.5 Limitations of techniques used in this chapter 173

4.5.6 Conclusions 174

5 Generation and characterisation of AMPAR Aabs 176

5.1 Introduction 176

5.2 Production of rabbit polyclonal antibodies 176

5.2.1 Titres and ELISA of antibody sera 179

5.2.2 Purification and analysis of AMPAR Aabs 181

5.3 Characterisation of AMPAR Aabs on in vitro systems 184

5.3.1 AMPAR Aab detection of native AMPAR 184

5.4 Discussion 191

5.4.1 Peptide immunisation generates a strong immune response 191

5.4.2 Anti-AMPAR Aabs bind to native AMPARs 193

5.4.3 Conclusions 194

6. Assessing the functionality of AMPAR Aabs 196

6.1 Introduction 196

6.2 Aab effects on spontaneous excitatory postsynaptic currents 197

6.2.1 Acute 10min AMPAR Aab incubation 197

6.2.2 Acute 30 min AMPAR Aab incubation 200

6.2.3 Effects of chronic (24 h) AMPAR Aab incubation 205

6.3 Miniature excitatory postsynaptic currents (mEPSCs) 207

6.3.1 Effect of AMPAR Aabs application on mEPSCs 208

6.4 Discussion 213

6.4.1 AMPAR Aabs exhibit an inhibitory functional effect 213

6.4.2 Conclusions 216

7. General discussion and final conclusions 218

7.1. Can inhibitory functional effects of Aabs lead to seizures? 218

7.2 NMDAR and AMPAR Aabs: causative or compensatory? 227

7.3 Conclusions and future work 227

8. References 230

9. Appendices 250

9.1. Vector maps of recombinant plasmid pcDNA3.1(-) NR1-4a Hs and pcDNA3.1(+) NR2B Hs 250

9.2 Optimisation of organotypic hippocampal brain slice cultures 252

9.2.1 Organotypic hippocampal brain slice cultures (OHSCs) 252

9.2.2 Spontaneous epileptic bursting in OHSCs 253

9.3 Additional AMPAR Aabs Western blots 255

9.3.1 AMPAR Aabs detect GluR3, but also other non-specific bands 255

9.4 Acute and chronic incubation of primary neurons with AMPAR Aabs resulted in significant differences in cumulative inter-event intervals 257

9.5 Preliminary cell death experiments following AMPAR Aab incubation 259

9.5.1 No obvious changes in neuronal cell death were observed following acute or chronic AMPAR Aab incubation 259

List of Figures

Figure 1.1: Classification of different seizure types. 5

Figure 1.2: Mechanism of action of anti-epileptic drugs 9

Figure 1.3: Structure of a typical antibody 13

Figure 1.4: Structure of NMDAR, including the amino terminal domain (ATD), ligand binding domains (LBD) and transmembrane domains (TMD) 20

Figure 1.5: Schematic identifying location of the immunogenic amino acids within the NR1 subunit 24

Figure 1.6: Structure of a hetero-tetrameric GluR2/GluR3 AMPAR highlighting the amino-terminal domain (ATD), ligand binding domain (LBD) and trans-membrane domains (TMD) 30

Figure 1.7: Schematic identifying the location of the immunogenic GluR3B peptide within the ATD 33

Figure 2.1: Dissection and slicing of mouse brain 57

Figure 2.2: Schaffer collaterals within hippocampal slice 62

Figure 2.3: A schematic of two-electrode voltage clamp on Xenopus oocytes 65

Figure 2.4: Schematic of all experiments performed throughout this thesis with each generated Aab 70

Figure 3.1: NMDAR peptide sequences used for the immunisation of rabbit #1 73

Figure 3.2: Rabbit anti-NMDAR1 immunogenicity response 75

Figure 3.3: Protein A purification of NMDAR1 Aabs 77

Figure 3.4: Protein A purified NMDAR1 Aabs are comparable to control rabbit IgG 78

Figure 3.5: ICC staining of NR1 and empty vector transfected HEK cells 80

Figure 3.6: Immunocytochemical staining of fixed primary cortical neurons 83

Figure 3.7: Immunocytochemical staining of fixed primary cortical neurons.....85
Figure 3.8: Immunohistochemical staining of fixed mouse brain sections 87
Figure 3.9: Immunohistochemical staining of fixed mouse brain 88
Figure 3.10: Human ATD of NR1 subunit probed with NMDAR1 Aabs.....90
Figure 3.11: Western blot of primary cortical cells, whole brain and NR1- and empty vector-transfected HEK cells 93
Figure 3.12: NMDAR peptide sequences used for the immunisation of rabbit #2.....95
Figure 3.13: Rabbit anti-NMDAR2 Aab immunogenicity response 97
Figure 3.14: Protein A purification of NMDAR2 Aabs 100
Figure 3.15: Protein A purified NMDAR Aabs are comparable to control rabbit IgG. 101
Figure 3.16: ICC staining of NR1 and empty vector transfected HEK cells.....103
Figure 3.17: Immunocytochemical staining of fixed primary cortical neurons.....106
Figure 3.18: Representative image of immunohistochemical staining of dentate gyrus of fixed hippocampal brain slice 108
Figure 3.19: Human ATD of NR1 subunit probed with NMDAR2 Aabs.....109
Figure 3.20: Representative western blot assessing binding specificity of protein A purified NMDAR2 Aabs to NR1 transfected HEK cells, whole brain and NR1- and empty vector-transfected HEK cells. 111
Figure 3.21: Peptide purification of NMDAR1 Aabs. 113
Figure 3.22: ICC staining of NR1 and empty vector transfected HEK cells.....115
Figure 3.23: ICC staining of primary cortical neuronal cells 118
Figure 3.24: Representative image of immunohistochemical staining of dentate gyrus of fixed hippocampal brain slice 120
Figure 3.25: Human ATD of NR1 subunit probed with NMDAR1pp Aabs.....122

Figure 3.26: Binding specificity of NMDAR1pp Aabs in western blot 123
Figure 4.1: Schematic of oocyte experimental setup. 134
Figure 4.2: Known NMDAR antagonists significantly reduce NMDAR current 136
Figure 4.3: No significant change in NMDAR current is seen following acute NMDAR1 Aabs incubation. 139
Figure 4.4: No significant change in NMDAR current is seen following chronic Aabs incubation 142
Figure 4.5: No significant effect of NMDAR1 Aab incubation was observed when co-incubated with increasing concentrations of the NR1 allosteric modulator TCN-201... 144
Figure 4.6: No significant changes in NMDAR current was seen following acute NMDAR1pp Aab incubation. 147
Figure 4.7: Normalised traces of HFS induced LTP for vehicle, as well as both positive (mNMDAR and rNMDAR) and negative controls (mIgG2b and rIgG). 150
Figure 4.8: Normalised traces of HFS induced LTP for vehicle, NMDAR1 Aabs incubated and APV treated..... 153
Figure 4.9: Normalised traces of HFS induced LTP for vehicle, NMDAR2 Aabs incubated and APV treated..... 156
Figure 4.10: Normalised traces of HFS induced long term potentiation (LTP) for vehicle, NMDAR1pp Aabs incubated and APV treated. 159
Figure 4.11: Effects of acute (30 min) NMDAR1pp Aabs and rIgG application on sEPSC frequency 162
Figure 4.12: Effects of acute (30 min) NMDAR1pp Aabs and rIgG application on sEPSC amplitude 163

Figure 4.13: Effects of chronic (overnight) NMDAR1pp Aabs and rIgG application on sEPSC frequency and amplitude. 165
Figure 5.1: AMPAR peptide sequence used for the immunisation of rabbit #3 178
Figure 5.2: Rabbit anti-AMPAR immunogenicity response 180
Figure 5.3: Protein A purification of AMPAR Aabs 182
Figure 5.4: Protein A purification of AMPAR Aabs 183
Figure 5.5: Immunocytochemical staining of fixed primary cortical neurons 185
Figure 5.6: Immunocytochemical staining of fixed primary cortical neurons 186
Figure 5.7: Immunohistochemical staining of fixed hippocampal brain slice 188
Figure 5.8: Western blot assessing binding specificity of protein A purified AMPAR Aabs to mouse whole brain lysate 190
Figure 6.1 Effects of acute (10 min) AMPAR Aabs (1:1000 dilution) and rIgG application (1:1000 dilution) on sEPSC frequency 198
Figure 6.2: Effects of acute (10 min) AMPAR Aabs and rIgG application on sEPSC amplitude 199
Figure 6.3: Effects of acute (30 min) AMPAR Aabs and rIgG application on sEPSC frequency 201
Figure 6.4: Effects of acute (30 min) AMPAR Aabs and rIgG application on sEPSC amplitude 202
Figure 6.5: sEPSC frequency of AMPAR Aabs and rIgG incubated cells compared to their respective baselines 204
Figure 6.6: Effects of chronic (24 h) AMPAR Aabs and rIgG (1:1000 dilution) application on sEPSC frequency and amplitude 206

Figure 6.7: mEPSC frequency following 30 min AMPAR Aabs and rIgG incubation (1:1000 dilution) compared to their respective baselines 209
Figure 6.8: Effects of acute (30 min) and chronic (24 h) AMPAR Aabs and rIgG application on mEPSC frequency.....211
Figure 6.9: Effects of acute (30 min) and chronic (24 h) AMPAR Aabs and rIgG application on mEPSC amplitude 212
Figure 7.1: Schematic of how NMDAR Aabs may cause seizures 222
Figure 7.2 Schematic of potential mechanisms of AMPAR Aabs.....226
Figure 9.1: Vector map for pcDNA3.1(-)-NR1-4a Hs, used for HEK cell transfections described in section 2.2.1. 250
Figure 9.2: Vector map for pcDNA3.1(-)-NR1-4a Hs, used for HEK cell transfections described in section 2.2.1. 251
Figure 9.3: Western blot assessing binding specificity of protein A purified AMPAR Aabs to mouse whole brain lysate and cortical cell lysate.....256
Figure 9.4: Effects of acute (30 min) AMPAR Aabs and rIgG application on sEPSC cumulative inter-event interval.....257
Figure 9.5: Effects of acute (30 min) AMPAR Aabs and rIgG application on mEPSC cumulative inter-event interval.....258
Figure 9.6: Immunocytochemical staining of fixed primary hippocampal neurons.....260
Figure 9.7: Immunocytochemical staining of fixed primary hippocampal neurons.....261

List of Tables

Table 1: NMDAR peptide sequences used for the immunisation of rabbit #1 40

Table 2: NMDAR peptide sequences used for the immunisation of rabbit #2 40

Table 3: AMPAR peptide sequence used for the immunisation of rabbit #3 40

Table 4: Details of primary antibodies used. 45

Table 5: Details of secondary antibodies used. 46

Table 6: Composition of lysis buffer for HEK cell lysates 50

Table 7: Composition of lysis buffer for mouse brain lysates. 50

Table 8: Composition of 10% separating gel 52

Table 9: Composition of 3% stacking gel 52

Table 10: Composition of 3x sample loading buffer. 53

Table 11: Composition of 1X running buffer 53

Table 12: Composition of 1X transfer buffer. 54

Table 13: Culture medium used for growth of primary hippocampal neuronal cells. 59

Table 14: Composition of intracellular and extracellular patch clamp solution 66

Table 15: Summary of reagents used in organotypic culture medium 253

List of Abbreviations

aa	-	amino acids
Aabs:	-	autoantibodies
(a)CSF	-	(artificial) cerebrospinal fluid
AEDs	-	anti-epileptic drugs
AMPA(R)	-	α-amino-3-hydroxy-5-methyl-4-isoxazoleproprionic acid (receptor)
ANOVA	-	analysis of variance
ANRE	-	anti-NMDAR encephalitis
AP	-	action potential
APS	-	ammonium persulfate
ATD	-	amino terminal domain
ATP	-	adenosine triphosphate
AUC	-	area under the curve
BCA	-	bicinchonic Acid
BL	-	bleed
BSA	-	bovine serum albumin
CA1	-	cornu ammonis area 1
CA3	-	cornu ammonis area 3
CAMKII	-	calcium/calmodulin-dependent kinase II
CFA	-	complete freunds adjuvant

CNS	-	central nervous system
CNQX	-	6-cyano-7-nitroquinoxaline-2,3-dione
CTD	-	C-terminal domain
DAPI	-	4′,6-diamidino-2-phenylindole
DIV	-	days *in vitro*
DG	-	dentate gyrus
DL-APV	-	DL -2-Amino-5-phosphonopentanoic acid
DNA	-	deoxyribonucleic acid
DMEM	-	dulbeccos modified Eagles medium
E18	-	embryonic day 18
EAATs	-	excitatory amino acid transporters
ECL	-	enhanced chemiluminescence
EEG	-	electroencephalogram
ELISA	-	enzyme linked immunosorbent assay
eNT1	-	equilibrative Nucleoside Transporter 1
(m/s)EPSC	-	(miniature/spontaneous) excitatory post-synaptic current
Fab	-	antigen binding fragment
FBS	-	fetal bovine serum
Fc	-	fragment crystallizable region
FDG-PET	-	fluorodeoxyglucose-positron emission tomography

fEPSP	-	field excitatory postsynaptic potential
FTD	-	fronto-temporal dementia
GΩ	-	giga ohm
GABA(R)	-	gamma-aminobutyric acid (receptor)
GFAP	-	glial fibrillary acidic protein
GluR	-	glutamate receptors
HBSS	-	hanks balanced salt solution
HEK	-	human embryonic kidney
HFS	-	high frequency stimulation
HRP	-	horseradish peroxidase
ICC	-	immunocytochemistry
icv	-	intracerebroventricular
IFA	-	incomplete freunds adjuvant
Ig	-	immunoglobulin
IHC	-	immunohistochemistry
IL	-	interleukin
ILAE	-	international league against epilepsy
IVIg	-	Intravenous immunoglobulin
KLH	-	keyhole limpet hemocyanin
LBD	-	ligand binding domain

LT (D, P)	-	long-term (depression, potentiation)
MEA	-	multi-electrode array
mGluRs	-	metabotropic glutamate receptors
MRI	-	magnetic resonance imaging
MWCO	-	molecular weight cut off
nAChRs	-	nicotinic acetylcholine receptors
NMDA(R)	-	N-methyl-D-aspartate (receptor)
NeuN	-	neuronal nuclei
OVA	-	ovalbumin
PBMCs	-	peripheral blood mononuclear cells
PBS	-	phosphate buffered saline
PDL	-	poly-D-lysine
PEI	-	polyethylenimine
PFA	-	paraformaldehyde
PI	-	propidium iodide
PTZ	-	pentylenetetrazole
PVDF	-	polyvinylidene fluoride
RE	-	Rasmussen's encephalitis
R_S	-	series resistance
SD	-	standard deviation

SDS-(PAGE)	-	sodium dodecyl sulphate – (poly acrylamide gel electrophoresis)
TEMED	-	tetramethylethylenediamine
TEVC	-	two electrode voltage clamp
TMB	-	3,3′,5,5′-tetramethylbenzidine
TMD	-	transmembrane domain
TTX	-	tetrodotoxin
VGKC	-	voltage gated potassium channel

1. Introduction

1.1 Autoimmune encephalitis

Autoimmune encephalitis encompasses a range of disorders where the body's immune system mistakenly targets self-proteins within the central nervous system (CNS), leading to inflammation of the brain (Uy *et al.*, 2021). The underlying causes of autoimmune encephalitis and autoantibody generation are not well understood, in some cases occurring due to neuronal receptor presence in peripheral tumours (Dalmau *et al.*, 2007), following an infection such as herpes simplex virus (Alexopoulos *et al.*, 2018) or in some cases sporadically. Patients with autoimmune encephalitis often present with neurologic symptoms such as impaired memory and cognition, psychiatric symptoms and seizures, with current treatments focussing on the removal of any autoantibodies and suppressing the immune system (Uy *et al.*, 2021). However, due to the lack of understanding of the underlying cause of these conditions, and the lack of specific treatments, conditions can worsen and result in progressive neurologic deterioration and status epilepticus (SE).

In addition, and increasing number of patients with epilepsy have been shown to have an autoimmune component to their disorder, whereby patients harbour autoantibodies (Aabs) (Bien and Holtkamp, 2017), similar to autoimmune encephalitis but without the accompanying neurological symptoms. Aabs are antibodies produced by the body to self-proteins, in this case, self-neurotransmitter receptors such as N-methyl-D-aspartate receptors (NMDARs), α-amino-3-hydroxy-5-methyl-4-isoxazoleproprionic acid receptors (AMPARs), and gamma-aminobutyric acid receptors (GABARs) (Dalmau *et al.*, 2017). This increasing prevalence of autoimmune encephalitis, autoimmune epilepsy and Aabs has sparked interest into

investigating the functionality of Aabs (Dalmau *et al.*, 2007; Bauer *et al.*, 2017). Here, the current evidence behind autoimmune epilepsy will be discussed, with a focus on two of the most common Aab targets: NMDARs and AMPARs.

1.2 Epilepsy

Epilepsy, a disease encompassing many neurological syndromes, is one of the most common neurological disorders, affecting approximately 50 million people worldwide (WHO, 2019). Epilepsy has been defined by the International League against Epilepsy (ILAE) as "*a disorder of the brain characterised by an enduring predisposition to generate epileptic seizures, and by the neurobiological, cognitive, psychological, and social consequences of this condition"* (Fisher et al., 2005; Fisher et al., 2014). Approximately 10% of the population will have at least one seizure in their lifetime, many of which do not result in an epilepsy diagnosis. A seizure alone can be defined as the abnormal synchronous neuronal activity within the brain resulting in transient symptoms such as jerking and loss of consciousness (Fisher *et al.*, 2014). In these cases, seizures may be caused by other physical conditions such as diabetes, or may have an underlying psychological cause (Mellers, 2005). Broadly speaking, epilepsy is characterised by recurrent seizures, resulting from a hyper-excitable neuronal network, which occurs due to an imbalance of excitatory and inhibitory neurotransmission. This can arise from an alteration in brain function at several different levels (Engelborghs *et al.*, 2000): (1) a dysfunction at the genetic level (for example, a mutation in the *SCN1A* gene encoding the neuronal voltage-gated sodium channel (Nav1.1) most commonly results in non-functional sodium channels on inhibitory neurons and therefore causes seizures in 70-90% of patients with Dravet Syndrome (Dravet and Oguni, 2013)), (2) a modification in protein expression may lead to changes in signalling cascades, resulting in a hyper excitable network (one example has been shown

following the reduced intensity status epilepticus (RISE) model, whereby an increase in hippocampal PSD95 was observed (Needs *et al.*, 2019)). This hyper-excitable state, regardless of underlying cause, can occur in different regions of the brain and with different patterns of propagation, thus presenting different seizure types and clinical symptoms (Stafstrom and Carmant, 2015).

1.2.1 Classification of epilepsy

Due to a better understanding of epilepsy and ongoing research into the area, a revision of the definitions, terminology and classification of both epilepsy and seizures was undertaken in 2017 by the ILAE (Fisher *et al.*, 2017). Epilepsy can be classified by seizure type or by underlying aetiology, both of which are investigated on diagnosis as this impacts the choice of treatment.

1.2.1.1 Seizure classification

Seizures can be classified into three main categories: focal, indicating seizures that originate in one hemisphere or region within the brain (and in some cases can evolve to bilateral); generalised, seizures that occur suddenly and affect both hemispheres at once; and unknown onset (Scheffer *et al.*, 2017) (Figure 1.1). This can be further characterised by awareness level (awareness of self and environment during a seizure) as well as by motor or non-motor presentation (Stafstrom and Carmant, 2015). Motor seizures involve muscle movement and may be due to either an increase or decrease in muscle contraction. Briefly, myoclonic seizures involve sudden involuntary movements that are not associated with a loss of consciousness. Tonic-clonic seizures are the most well-known type of generalised seizure, involving bilateral convulsive movements accompanied by a loss of consciousness, where tonic is defined by a stiffening in muscle tone, and clonic is regular, repetitive myoclonus (Blume *et al.*, 2001). Non-

motor seizures can be generalised, including absence seizures, identified by an abrupt onset and offset of altered awareness without any changes in muscular tone, or focal, non-motor seizures, including emotional seizures. Emotional seizures are characterised by alterations in mood or emotion without the subjective emotion at seizure onset, e.g., focal emotional seizure with laughing without the appropriate related emotion of happiness (Fisher *et al.*, 2017).

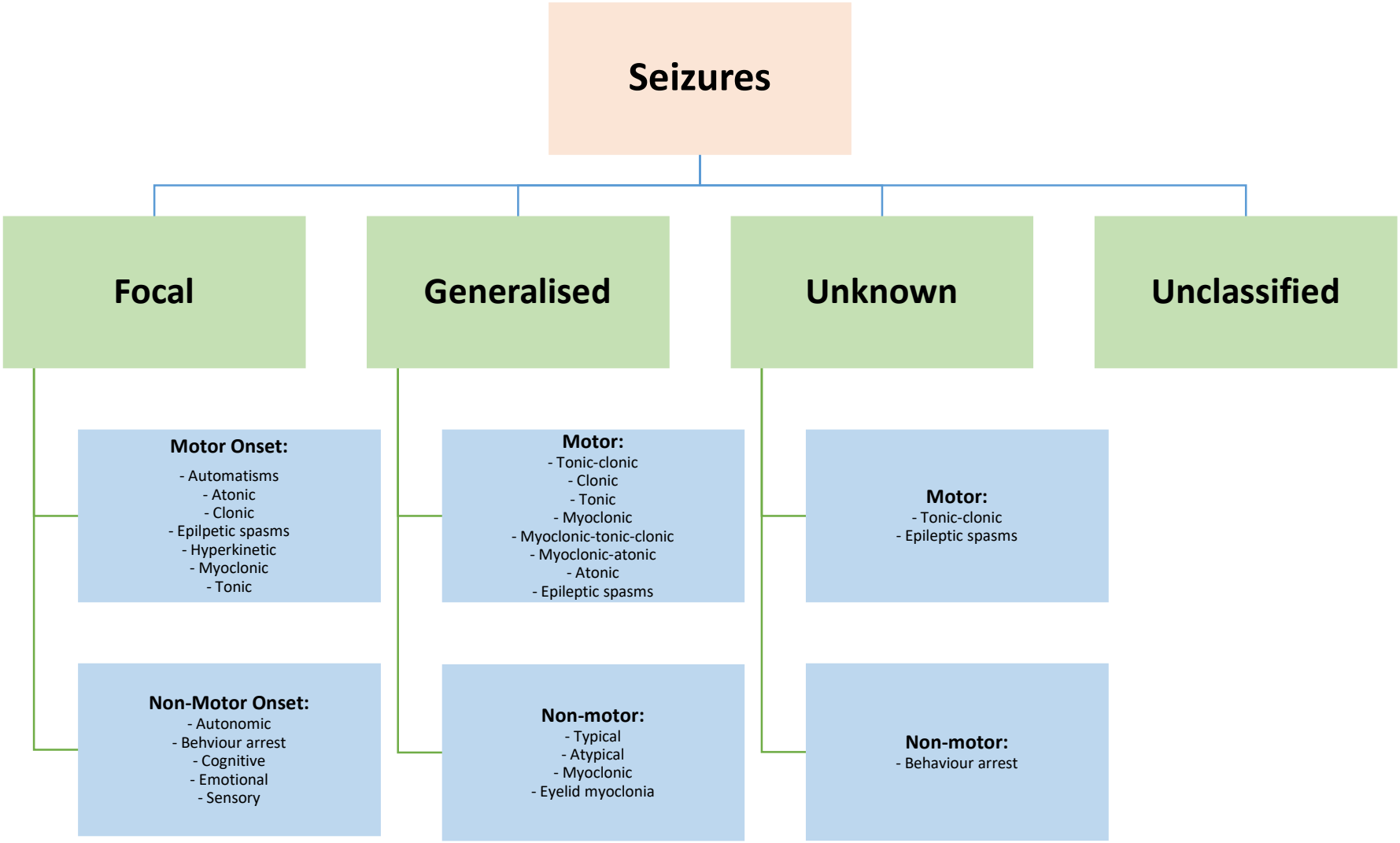

Figure 1.1: Classification of different seizure types. Adapted from the ILAE Revised Terminology for Organisation of Seizures and Epilepsies 2011 – 2013 (Scheffer et al., 2017).

Seizures can vary in length, depending upon the type (Jenssen *et al.*, 2006). Generally, the seizure will self-terminate via several mechanisms, returning the neuronal network to a non-seizing state. These mechanisms can be at the neuronal level, such as activation of potassium channels and/or a diminishment of adenosine triphosphate (ATP) to limit further excitability, or the self-termination can occur at a network level, including glutamate depletion, glial buffering and GABAergic inhibition (Lado and Moshé, 2008).

1.2.1.2 Classification by aetiology

In recent years, epilepsy has been classified as idiopathic, cryptogenic or symptomatic (Fisher *et al.*, 2014). However, with increasing understanding of the aetiologies underpinning epilepsy, these terms have been replaced with more suitable categories based on the underlying cause, importantly including immune (and autoimmune) as well as genetic, metabolic, structural, infectious or unknown (Scheffer *et al.*, 2017). The 'genetic' category replaces idiopathic, where a known gene is the primary cause of the syndrome, such as in Dravet syndrome, where a mutation in the *SCN1A* gene causes seizures (Dravet and Oguni, 2013). 'Unknown' replaces the classification of cryptogenic and is only used when there is no evidence for any cause of seizures. The categories 'metabolic', 'structural', 'infectious' and 'immune' replace the previous classification of 'symptomatic' when there is a suspected cause of the syndrome, of which infectious is the most common etiology of epilepsy worldwide. In the case of immune (or autoimmune) causes of epilepsy, antibodies targeting brain proteins are the cause of the observed seizures (Scheffer *et al.*, 2017; Husari and Dubey, 2019).

1.2.2 Current management of epilepsy

At present, there are more than 20 AEDs that can be used for the treatment and management of epileptic disorders (Löscher *et al.*, 2013; Ghosh *et al.*, 2021). Current AEDs work generally to reduce seizure frequency by decreasing the electrical activity of the brain, although due to the multi-causal aspect of epilepsy and inter-individual variability, these do not treat the underlying pathological cause. The decision of which drug to use is dependent on the seizure type, patient age and whether the disorder has been identified as having a genetic/symptomatic cause, or whether its cause is unknown (Stafstrom and Carmant, 2015; (NICE), 2021).

AEDs work to decrease the activity of the neuronal networks within the brain via an array of mechanisms, via inhibition of glutamate-mediated excitatory pathways through blockade of NMDARs or AMPARs (using antagonists such as felbamate or perampanel, respectively (Figure 1.2) (Rho *et al.*, 1994; Greenwood and Valdes, 2016)). Voltage-gated Na^+ channels are also common targets, with different drugs such as phenytoin and carbamazepine acting to prolong the duration for which sodium channels are inactivated (Macdonald and Kelly, 1995). Alternatively, hyper-excitability can be treated by augmenting GABA-mediated inhibitory neuronal pathways, for example by enhancing the inhibitory effect of GABA (e.g., benzodiazepines in status epilepticus)or by enhancing potassium channel function (Stafstrom and Carmant, 2015), as also shown in Figure 1.2. Currently, AEDs prescribed as first-line therapy are dependent upon the type of seizures/epilepsy, as well as the demography of the patient. For example, for focal seizures first line treatment involved carbamazepine, lamotrigine, levetiracetam or oxcarbazepine, whereas for generalised seizures the current first line treatment is sodium valproate, for boys, men and women not of childbearing potential, with lamotrigine being the next choice when valproate is not applicable. NICE guidelines in

the UK advise prescribing a single drug to control newly developed seizures, and progressing to combination treatment where necessary ((NICE), 2021).

Despite the range of available AEDs, approximately 30% of epilepsy patients are resistant to the current therapies, with the mechanisms underlying this resistance still unknown. This has led to the development of many new AEDs over recent decades that aim to target the pathological cause rather than the symptoms, but these have shown no greater efficacy than previous AEDs due to a lack of understanding of the underlying pathophysiology of a lot of epilepsy conditions (Perucca *et al.*, 2007; Schmidt and Schachter, 2014). In addition, it has been shown that seizures themselves can increase disease progression, due to seizure-induced excitotoxicity; therefore, if AEDs fail to control seizure occurrence and frequency, breakthrough seizures may occur, which can exacerbate the disease and develop into refractory seizures (Kwan and Brodie, 2000; Lee, 2014; Zeiler *et al.*, 2014).

AEDs are also associated with a variety of adverse effects, some of which can be severe enough to cause the patient to discontinue the drug treatment completely. These effects can include sedation, cognitive dysfunction, psychiatric effects, appetite and weight variability and cardiovascular risks (Perucca *et al.*, 2009; Perucca and Gilliam, 2012; Lee, 2014).

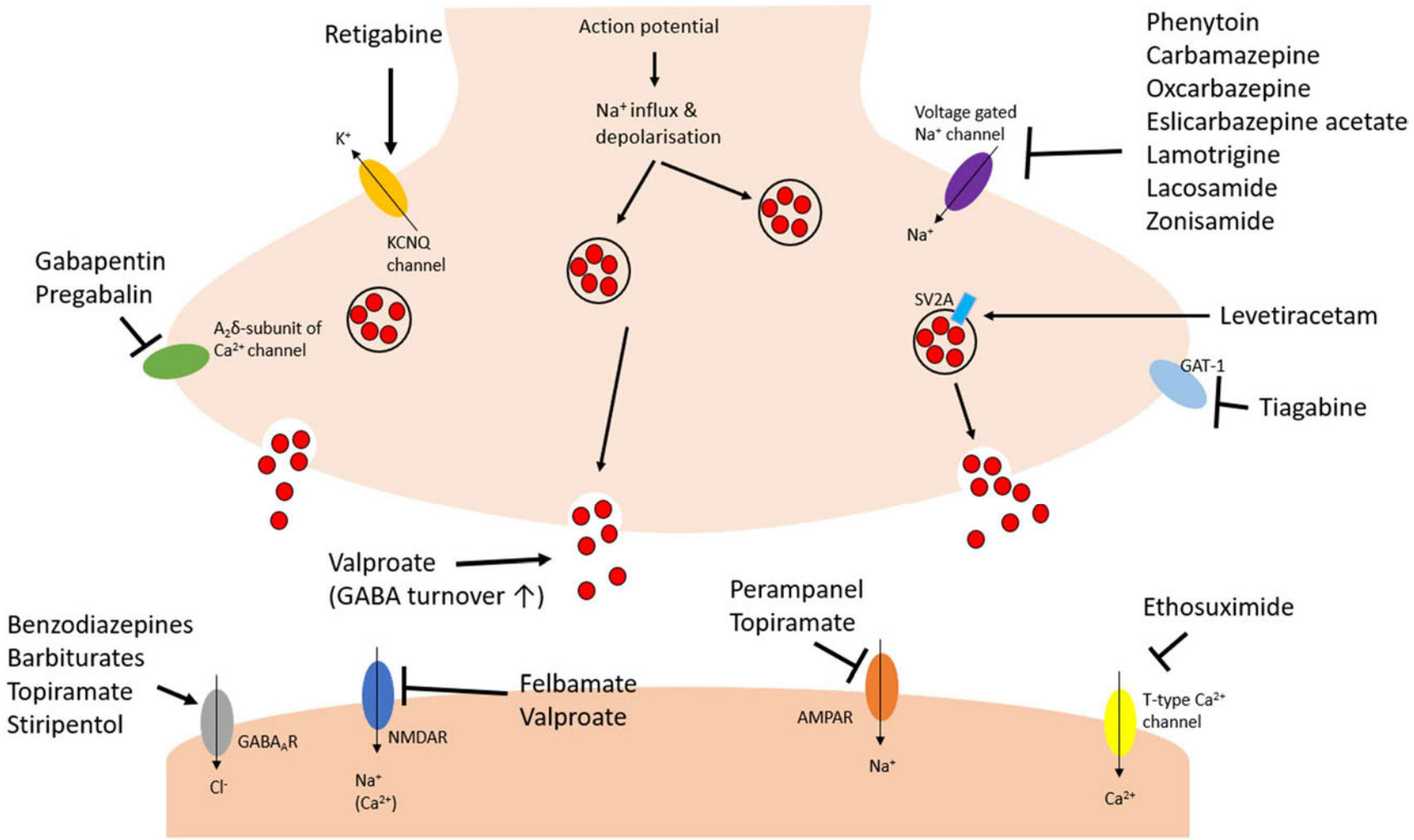

Figure 1.2: Mechanism of action of anti-epileptic drugs. AEDs target and inhibit voltage gated Na^+ channels and Ca^{2+} channels to reduce excitability, as well as activating K^+ channels and $GABA_A$Rs to augment inhibition. Glutamate receptors AMPAR and NMDAR are also targeted with less success. GABA-T: GABA aminotransferase, GAT: GABA transporter, Adapted from (Loscher et al., 2016).

1.3 Autoimmune Epilepsy

At present, there is a large and complex body of literature describing the presence of inflammation and immune activation in many disorders of the central nervous system (CNS) (Billiau *et al.*, 2005; Hammer *et al.*, 2014). In recent years, it has been recognised that immune dysfunction and autoimmunity can be a cause of epilepsy, especially drug-resistant epilepsy (Ong *et al.*, 2014; Ramanathan *et al.*, 2014; Fang *et al.*, 2017). Despite this, the mechanisms and causes of this immune dysfunction are not well understood, and thus the prevalence of epilepsies with an associated immune component remains poorly defined and is likely to be underestimated (Greco *et al.*, 2016).

The recognition and diagnosis of autoimmune epilepsy has improved substantially over recent years owing to the landmark discovery of potentially pathogenic Aabs, which have the ability to be discriminating biomarkers of disease (Chefdeville *et al.*, 2016). Patients with autoimmune epilepsy often do not respond well to conventional AEDs, but may respond to immunotherapy, thus it is necessary to identify those patients with suspected autoimmune epilepsy for rapid, optimum treatment (Bien, 2013; Ekizoglu *et al.*, 2014; Iorio *et al.*, 2015a). Importantly, an ever-growing number of Aabs have been observed in patients with epilepsy. Much of what is known thus far about autoimmune epilepsies originated from studies of paraneoplastic syndromes affecting the CNS. These diseases are caused by peripheral tumours, which express CNS proteins. The immune system identifies these CNS proteins as foreign, and generates Aabs which target these proteins, and hence an autoimmune response against the brain follows. Classic examples of these syndromes are teratomas that cause paraneoplastic anti-NMDAR encephalitis (ANRE) and small-cell lung carcinoma that causes limbic encephalitis (Dalmau *et al.*, 2007; Dalmau *et al.*, 2017).

1.4 The immune system

Physiologically, the immune system is a complex network that aims to protect the body against foreign pathogens via the production of antibodies. However, the immune system occasionally produces an abnormal response to self-proteins in the body, resulting in the production of Aabs, which can then bind to these self-proteins and alter their function (Elkon and Casali, 2008).

Under normal circumstances, the mechanisms by which the body's immune system fights pathogens can be broadly divided into two systems: innate and adaptive. Innate immunity is a cell-mediated, non-specific response to foreign cells and includes internal systems such as phagocytosis and cell lysis. The body has also developed external barriers such as skin and mucous membranes that prove effective against environmental agents. The adaptive immune system can be further divided into humoral, and cell mediated systems, and in contrast to the innate system, the effectiveness of the adaptive immune system improves with re-exposure to foreign molecules (Alberts *et al.*, 2014).

1.4.1 Adaptive immune system

The adaptive immune response is the body's second line of defence, which is often activated by specific cells of the innate immune system. The main cells involved in adaptive immunity are the T and B lymphocytes. B lymphocytes originate from hematopoietic stem cells in the bone marrow, which give rise to immature B cells (Bonilla and Oettgen, 2010). These B cells migrate to the spleen, where further differentiation occurs into mature naïve B cells, which circulate peripherally through the lymphatic system where they interact with foreign antigens, which once encountered gives rise to a plasma B cell or a memory B cell. Memory B cells have surface bound antibodies, whereas plasma B-cells secrete antibodies that are specific for the activating antigen (Janeway *et al.*, 2001).

1.4.2 Antibody structure

Antibodies are Y-shaped glycoproteins of the immunoglobulin family, with three functional domains, two fragment antigen binding domains (Fabs) and the fragment crystallisable (Fc) region. All immunoglobulins (Igs) are formed from four polypeptide chains comprising of two identical light chains (~25 kDa each) and two identical heavy chains (~50 kDa each) as shown in Figure 1.3. There are two types of light chain; kappa and lambda, and five main heavy chains: μ, δ, ϒ, α and ε, where the heavy chain determines the overall class and function of antibody (IgM, IgD, IgG, IgA and IgE respectively) (Schroeder and Cavacini, 2010). All Igs have two domains termed the variable and constant domains. The variable domain is located at the N-terminus and is designated as VL in the light chain, and VH in the heavy chain. Similarly, constant domains are designated CL in the light chain, and CH for those in the heavy chain. The hinge region is a short amino acid sequence that permits flexibility of between 60-180 degrees of the two Fab arms and is located between the CH regions of the Ig heavy chains and is composed primarily of proline and cysteine residues (Janeway *et al.*, 2001).

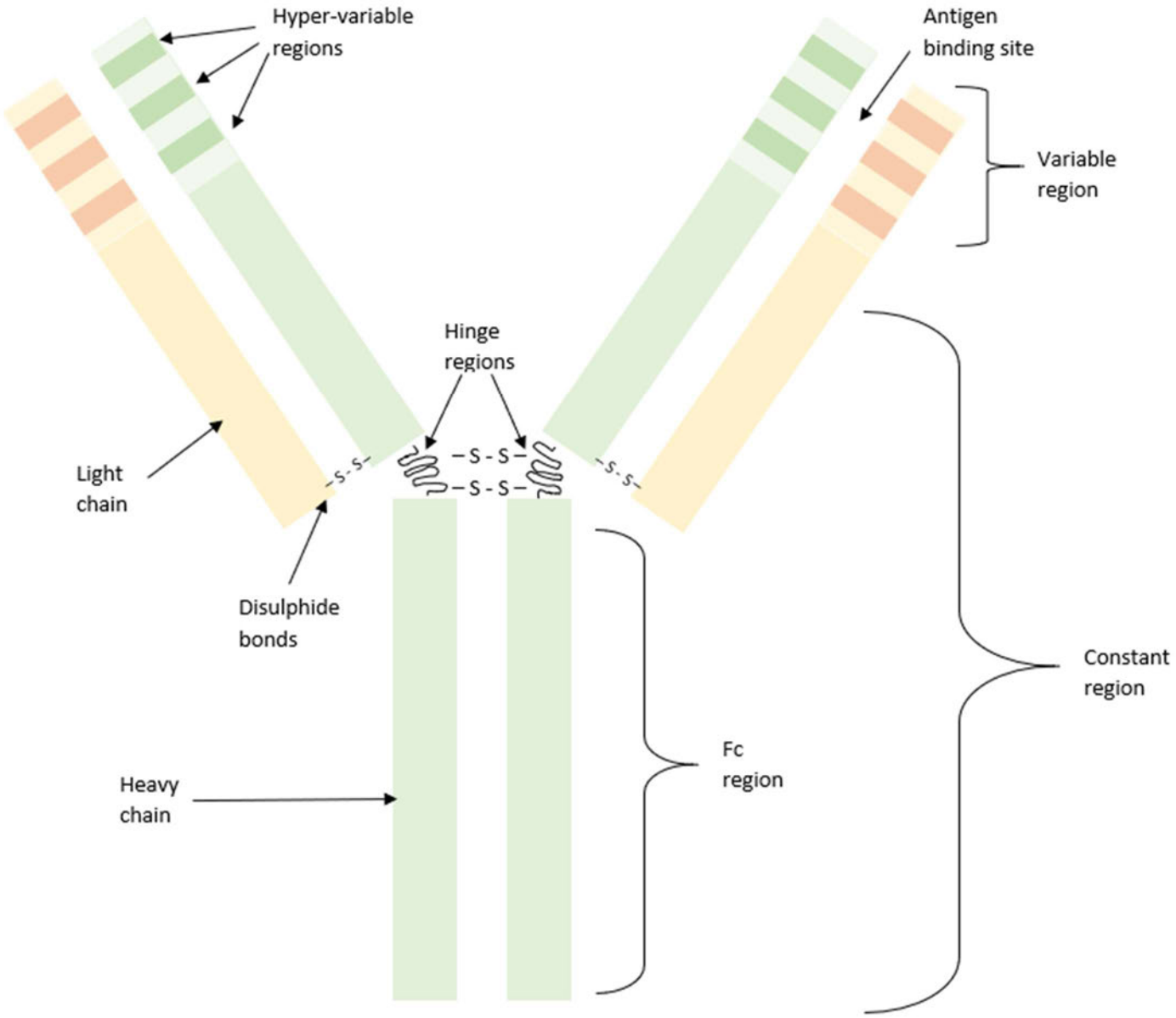

Figure 1.3: Structure of a typical antibody. Antibodies are Y-shaped, flexible molecules consisting of two heavy and two light chains linked together by disulphide bonds. Hypervariable regions make up the antigen binding sites.

1.4.2.1 Autoantibodies

Currently, more than 2.5% of the population is estimated to be affected by an Aab-driven autoimmune disease, although with increasing knowledge, this percentage is rapidly rising (Ludwig *et al.*, 2017). Aabs to neural antigens have been found to arise idiopathically (as a result of breaches in central or peripheral tolerance), paraneoplastically (immune responses to neural proteins expressed on peripheral tumours, such as ANRE), or as a result of bacterial or viral infections (Iorio *et al.*, 2015b; Alexopoulos *et al.*, 2018). There are multiple mechanisms in place to limit B-cell self-reactivity: receptor editing, clonal deletion and anergy. However, in autoimmune conditions, a breakdown in self-tolerance and a persistent immune response against self-proteins is observed, resulting in the production of Aabs (Parkin and Cohen, 2001; Medina, 2016; Siloşi *et al.*, 2016).

Aabs have been identified against many neuronal proteins, including extracellular epitopes of membrane proteins such as NMDARs, voltage gated potassium channels (VGKCs), AMPARs and GABARs, as well as intracellular proteins such as Hu (RNA-binding proteins involved in post-transcriptional regulation) (Gold *et al.*, 2012). The most common neuronal Aabs target NMDARs and VGKCs (Suleiman *et al.*, 2013; Pollak *et al.*, 2016). Aabs against neuronal proteins such as NMDARs and AMPARs have been identified in epileptic patients, where seizures are a symptom of other neurological disorders as well as healthy volunteers (Ludwig *et al.*, 2017). These Aabs can cause pathogenic effects via several pathways, dependent on their target protein (Bien, 2013; Toledano and Pittock, 2015; Bauer *et al.*, 2017). Generally, pathogenic effects of all Aabs can be classified into seven main groups: 1) mimicking of receptor stimulation, 2) blockade/alteration of neural transmission (e.g., anti-nicotinic acetylcholine receptor (nAChR) Aabs bind to and cause internalisation of nAChRs in myasthenia gravis), 3) induction of altered signalling, 4) causing micro-thrombosis, 5) causing cell lysis, 6) neutrophil recruitment and activation, and 7) induction of inflammation (e.g., anti-

rheumatoid factor Aabs in rheumatoid arthritis, triggering complement prolonging B-cell survival, maintaining their own production) (Ludwig *et al.*, 2017).

At present, the majority of evidence for all Aab types suggests a pathogenic, causal role in *in vivo* mouse models, whereby removal of Aabs via plasmapheresis results in a temporary alleviation of symptoms, such as that observed in myasthenia gravis (Vincent, 2005). However, not all Aabs are pathogenic, with Aabs being detected in healthy people without any associated symptoms; whether these Aabs target different epitopes or are present in lower levels is unclear (Ludwig *et al.*, 2017). In addition, it has been shown that natural, autoreactive IgM antibodies can protect from autoimmune diseases (Mannoor *et al.*, 2013). Therefore, it is necessary to establish whether Aabs associated with epilepsy are pathogenic or are produced as a compensatory mechanism in an attempt to reduce hyper-excitability.

1.4.3 Autoimmune diseases

1.4.3.1 Anti-NMDAR Encephalitis

ANRE, officially described as a singular disease in 2008, has been increasingly recognised as a neurological disorder in both adults and children, and as one of the most common causes of encephalitis (Gable *et al.*, 2012). In 2007, Dalmau *et al,* described a paraneoplastic syndrome, based on 12 women with an ovarian teratoma, with high levels of IgG Aabs against the NR1 subunit of NMDARs in serum and cerebrospinal fluid (CSF) (Dalmau *et al.*, 2007). Clinically, ANRE occurs in two main stages: the initial stage is characterised by flu-like symptoms, while the subsequent phase is characterised by neuropsychiatric symptoms (Dalmau *et al.*, 2008). These symptoms can include confusion, hallucinations and personality changes as well as memory loss and seizures (Dalmau *et al.*, 2008; Dalmau *et al.*, 2011; Bapka *et al.*, 2016). In addition, distinct patterns in electroencephalogram (EEG) and in glucose metabolism have

been identified in patients. A distinguishing EEG pattern has been detected in the most severe cases, known as 'extreme delta brush', consisting of rhythmic delta activity with superimposed beta frequency (Dionisio *et al.*, 2013; Wright and Vincent, 2016). Changes in glucose metabolism have been identified by fluorodeoxyglucose positron emission tomography (FDG-PET), showing an increased fronto-temporal to occipital gradient that correlates with disease severity (Leypoldt *et al.*, 2012). As not all patients display teratomas and/or Aabs, knowledge of these characteristics may be helpful in both the diagnosis and treatment of ANRE and may be translated to those cases where patients display only seizures without other symptoms of encephalitis.

It is known that the Aabs target the NR1 subunit of NMDAR. Whether the origin of the antibody is solely intrathecal (in CSF), peripheral or both, is still not fully understood (Gleichman *et al.*, 2012). *In vitro* studies have demonstrated that patient NMDAR Aabs bind to NMDARs and cause internalisation of the receptor, and thus a reduction in NMDAR currents (Hughes *et al.*, 2010). Additionally, it has also been shown that Aabs have the ability to activate membrane attack complex on NMDAR-expressing cells, which may be responsible for a subset of symptoms observed in patients (Irani *et al.*, 2010). Patients often seek treatment prior to the onset of seizures but are misdiagnosed as having schizophrenia or bipolar disorder and placed on anti-psychotic medications, which have little or no effect (Dalmau *et al.*, 2011). As the Aabs target the extracellular domain of surface-expressed receptors, immunotherapy is the first line treatment, with steroids, intravenous immunoglobulin (IVIg) and plasmapheresis working to suppress the immune system and physically remove the pathogenic Aabs (Vincent *et al.*, 2006). If first line therapy is ineffective, second line therapies may be employed; these includes rituximab and cyclophosphamide. Rituximab is a monoclonal antibody therapy that targets CD20-expressing B-cells, thus destroying the 'self-reactive' B-cells (Yeshokumar and Pardo, 2017), and cyclophosphamide targets several immunomodulatory mechanisms such as

suppression of lymphocyte proliferation to decrease the immune system response (Shin *et al.*, 2018). These treatment protocols have been demonstrated to be effective in several case studies where the patient seizures were uncontrolled with any currently available AEDs but were effectively controlled using either first or second-line immunotherapy (Toledano *et al.*, 2014; Lee and Lu, 2016).

1.4.3.2 Rasmussen's encephalitis

Rasmussen's encephalitis (RE) is an extremely rare neurological disease affecting approximately 2 per 10 million people aged 18 years or under (Varadkar *et al.*, 2014). RE has been linked with Aabs against glutamate receptors. This neurological disease usually presents in children around 6 years of age. There are two main stages, which in some cases is preceded by a prodromal phase. The first stage, typically lasting 4-8 months, can be characterised by inflammation, weakening of one side of the body (hemiparesis), loss of vision of one side of the visual field (hemoanopia), cognitive difficulties and focal seizures (Bien *et al.*, 2002). In the second (residual) stage, the peak inflammatory response is reached, and progression of the diseases slows, but the patient is left with some or all of the symptoms because of the damage caused by inflammation. In the long-term, most patients are left with epilepsy, paralysis, and cognitive problems, but the severity among patients varies (Granata *et al.*, 2003). Magnetic resonance imaging (MRI) and EEG are the two main ways in which RE is diagnosed. Within months of onset of the acute stage, most patients show unilateral enlargement of the ventricular system and mild focal cortical atrophy (Granata and Andermann, 2013). These changes occur alongside changes in EEG, whereby a slowing of background activity and epileptic abnormalities are observed, which progressively worsen over time (Longaretti *et al.*, 2012; Granata and Andermann, 2013).

The exact mechanism underlying RE is not fully understood. Over the years, there have been many hypotheses regarding the primary cause of RE, including T-cell and microglial activation (Bauer *et al.*, 2002; Wirenfeldt *et al.*, 2009) as well as GluR3 (a subunit of AMPARs)-targeted Aabs (Rogers *et al.*, 1994; Levite and Hermelin, 1999). However more recent studies have shown GluR3 Aabs to be present in patients with other types of epilepsy, as well as Aabs targeting other neurotransmitter receptors in RE patients, hence these are not specific to RE (Wiendl *et al.*, 2001; Mantegazza *et al.*, 2002; Watson *et al.*, 2004). As the mechanism underlying RE is not fully understood, no specific treatment targeting the primary cause is currently available, with all available therapeutics focusing on alleviating the inflammation and subsequent symptoms (Varadkar *et al.*, 2014). Similar to ANRE, corticosteroids, IVIgs and plasmapheresis are all used throughout the acute stage of RE. All have shown some efficacy, but none are able to permanently alleviate the patient's symptoms (Varadkar *et al.*, 2014). Once the patient enters the residual stage, these therapeutics have minimal effect due to the lack of inflammation. If seizure occurrence remains severe, a hemispherectomy is one of the remaining effective treatments whereby the affected hemisphere is surgically removed (Bien and Schramm, 2009) (Varadkar *et al.*, 2014).

1.5 Glutamate receptors

Glutamate is the major excitatory neurotransmitter in the mammalian central nervous system (Zhou and Danbolt, 2014) The glutamatergic system is important for synaptic plasticity, which underlies many advanced brain functions such as learning and memory. To use glutamate as a neurotransmitter, it must first be synthesised from local precursors, such as glutamine, which is released by glial cells, and subsequently taken up by neurons via excitatory amino acid transporters (EAATs). Once in the presynaptic terminal, glutamine is metabolised into glutamate (Anderson and Swanson, 2000), packaged into synaptic vesicles and awaits release (Purves *et al.*, 2004). Once released, glutamate binds to its receptors on the postsynaptic

membrane. These receptors can be classed into ionotropic and metabotropic glutamate receptors. NMDARs, AMPARs and kainate receptors make up the ionotropic receptors, and are named after the agonists that activate them. All three are non-selective cation channels, allowing the passage of both sodium and potassium ions (Na^+ and K^+ respectively), and in some cases (for NMDARs and GluR2-lacking AMPARs), calcium ions (Ca^{2+}) (Dingledine *et al.*, 1999). The metabotropic receptors are G protein-coupled receptors (mGluRs), of which there are 8 types, named mGluR1-8. These are divided into three major groups, based on their structure, location and function (Niswender and Conn, 2010). Group 1 mGluRs include mGluR1 and mGluR5, Group 2 mGluRs include mGluR2 and mGluR3 and Group 3 mGluRs include mGluR4, 6, 7 and 8 (Niswender and Conn, 2010).

1.5.1 NMDA Receptors

NMDARs belong to the class of ionotropic glutamate receptors (Traynelis *et al.*, 2010), which are physiologically activated by glutamate, with glycine acting as a co-agonist, resulting in an opening of the channel and increased permeability to Ca^{2+}, Na^+, and K^+ (Vyklicky *et al.*, 2014). NMDARs are widely distributed throughout the CNS and play important roles in neuronal excitability, synaptic plasticity and learning and memory (Hedegaard *et al.*, 2012; Hansen *et al.*, 2017).

1.5.1.1 NMDAR Structure

NMDARs are hetero-tetrameric receptors that consist of NR1, NR2 or NR3 subunits (Karakas and Furukawa, 2014). All NMDAR subunits share a common topology, with a large extracellular amino-terminal domain (ATD), transmembrane domains (M1, M3 & M4), a re-entrant loop M2, and an intracellular C-terminal domain (CTD), that can vary in size depending upon the subunit (Figure 1.4). The ion channel is formed when the transmembrane domain (TMD) of the four subunits come together, with the M3 segment and the M2 re-entrant loop being the major pore lining structures. All these domains are critical to the normal physiology of NMDARs (Paoletti and Neyton, 2007; Paoletti, 2011; Paoletti *et al.*, 2013; Hansen *et al.*, 2018).

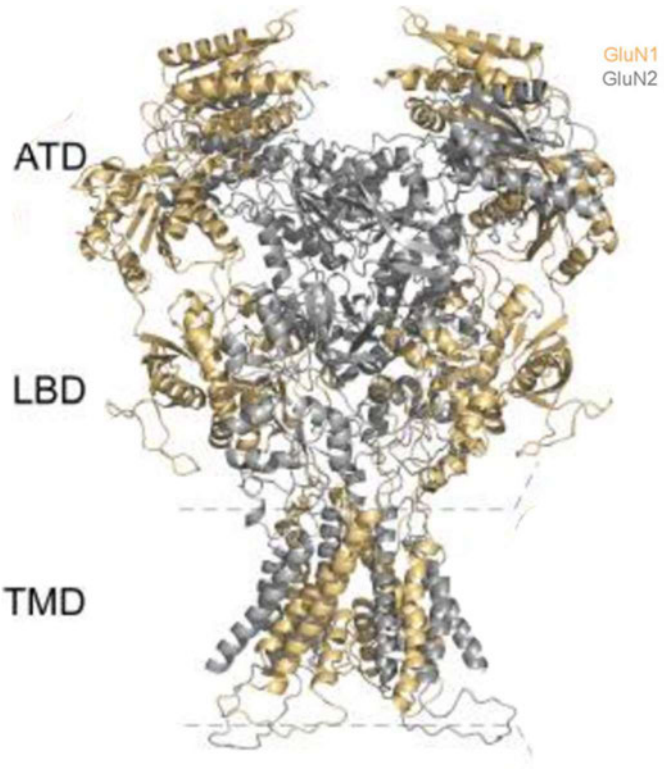

Figure 1.4: Structure of NMDAR, including the amino terminal domain (ATD), ligand binding domains (LBD) and transmembrane domains (TMD). Adapted from (Amin et al., 2017).

The ATD and CTD modulate the core gating function, as well as roles in receptor assembly (Hansen *et al.*, 2010), trafficking to the membrane and downstream signalling (Gladding and Raymond, 2011). The ligand binding domain (LBD) and the short polypeptide chains connecting these domains (LBD-TMD linkers) are directly involved in converting agonist binding into ion channel opening, as well as participating in receptor assembly and trafficking. In the absence of agonist, the ligand binding domains are in the open configuration, and the M3 gate is closed. Agonist binding induces LBD closure which translates into movement away from the membrane via LBD-TMD linkers, opening the M3 gate, thus opening the ion channel pore (Kazi *et al.*, 2014; Twomey and Sobolevsky, 2018).

NMDAR composition can vary by brain localisation and by different variants of each subunit. Post-translational RNA splicing results in eight splice variants of NR1, whereas subunits NR2 and NR3 are encoded for by six separate genes (4 genes for NR2 and 2 genes for NR3). Different combinations of these subunits result in specificity among different brain regions, with the NR1 subunit being obligatory for a fully functioning receptor (Paoletti and Neyton, 2007). The NMDAR tetramer most often consists of two NR1 subunits and two NR2 subunits, both of which are needed for agonist binding (glycine to NR1 and glutamate to NR2). The presence of a NR3 subunit in place of an NR2 subunit decreases the functional channel activity and creates a functional glycine receptor that cannot be activated by glutamate due to the lack of an NR2 subunit (Levite, 2014).

1.5.1.2 NMDAR CNS distribution

As the NR1 subunit is obligatory for fully functional NMDARs, it is ubiquitously expressed throughout the CNS, both in the embryonic and adult brain, although the NR1 splice variant expressed can vary. For example, the NR1a isoform is expressed abundantly in principal layers throughout the hippocampus, while NR1b isoforms are restricted to principal cells of *Cornu Ammonis* (CA3) (Paoletti, 2011). NR2 subunit expression changes with developmental stage. In the embryo, only NR2B and NR2D are expressed while NR2A and NR2C expression increases rapidly with development (Dalmau *et al.*, 2007; Paoletti, 2011), where NR2A is abundantly expressed, NR2B is restricted to the forebrain, with NR2C and NR2D localised prominently in the cerebellum and select populations of interneurons (Szczurowska and Mares, 2013). NR3A expression is low embryonically, peaks in the first few postnatal weeks, and then gradually decreases to low levels in adulthood (with widespread expression). Whereas NR3B is expressed in low levels in early life, increasing throughout adulthood, where it is expressed ubiquitously in the CNS (Paoletti, 2011; Szczurowska and Mares, 2013).

1.5.1.3 Physiological function of NMDARs

In the brain, NMDARs (generally consisting of NR1 and NR2 subunits) are activated by the binding of glutamate to the ligand binding site on the NR2 subunit and glycine to the binding site located on the NR1 subunit. However, unlike AMPARs, low levels of glutamate cannot elicit a response due to the presence of a magnesium ion (Mg^{2+}) block within the channel pore. The presence of the magnesium block ensures only a full depolarisation and sufficient glutamate binding allows the entry of permeable cations (Vyklicky *et al.*, 2014).

NMDARs are necessary for excitability and synaptic plasticity, as well as being involved in processes such as learning and memory. Once a full depolarisation occurs, there is an influx in

cations; Ca^{2+} and Na^{+} where this increase in intracellular Ca^{2+} triggers multiple downstream signalling events in the post-synaptic neuron, leading to both short-term and long-term effects. The strength and duration of NMDAR activation can result in potentiation or depression of synaptic events (Hansen *et al.*, 2017); such plasticity can be measured as long term potentation (LTP) and/or long term depression (LTD) (Bliss and Collingridge, 1993). Evidence has shown that hyper-activation of NMDARs mediates acute neuronal death and chronic neurodegeneration, whereas hypo-activation of NMDARs can lead to the development of psychiatric states, the mechanisms of which are not yet fully understood (Miya *et al.*, 2014). This evidence has strengthened the hypothesis that NMDAR Aabs represent a pathogenic cause of seizures and epilepsy, with the mechanisms of how these Aabs implicate network activity being increasingly studied (Fang *et al.*, 2017).

1.5.1.4 Autoantibodies against NMDARs

Aabs of the IgG class directed against the NR1 subunit of NMDARs were originally linked with ANRE, a condition characterised by seizures, psychosis, and cognitive deficits, often with the presence of Aabs in both serum and CSF (Dalmau *et al.*, 2007). Increasing numbers of patients have been identified with anti-NMDAR Aabs who present with seizures without the array of other symptoms that are usually associated with ANRE. However, the prevalence of autoimmune epilepsy (seizures without other encephalitis symptoms) and the presence of NMDAR Aabs is likely to be highly underestimated due to the lack of testing and diagnosis.

1.5.1.4.1 Binding of Aabs to NMDARs

Human Aabs targeting NMDARs from patients with ANRE have been shown to recognise the amino acids N368/G369 of the amino-terminal domain of NR1 subunit of the NMDAR (Figure 1.5) (Gleichman *et al.*, 2012). Experiments including site-directed mutagenesis detected two amino acids near the hinge region within the ATD as being crucial for antibody recognition

and binding, confirmed by functional studies, whereby when one of the amino acids was altered (G369I), patients Aabs no longer bound to the receptor (Gleichman *et al.*, 2012).

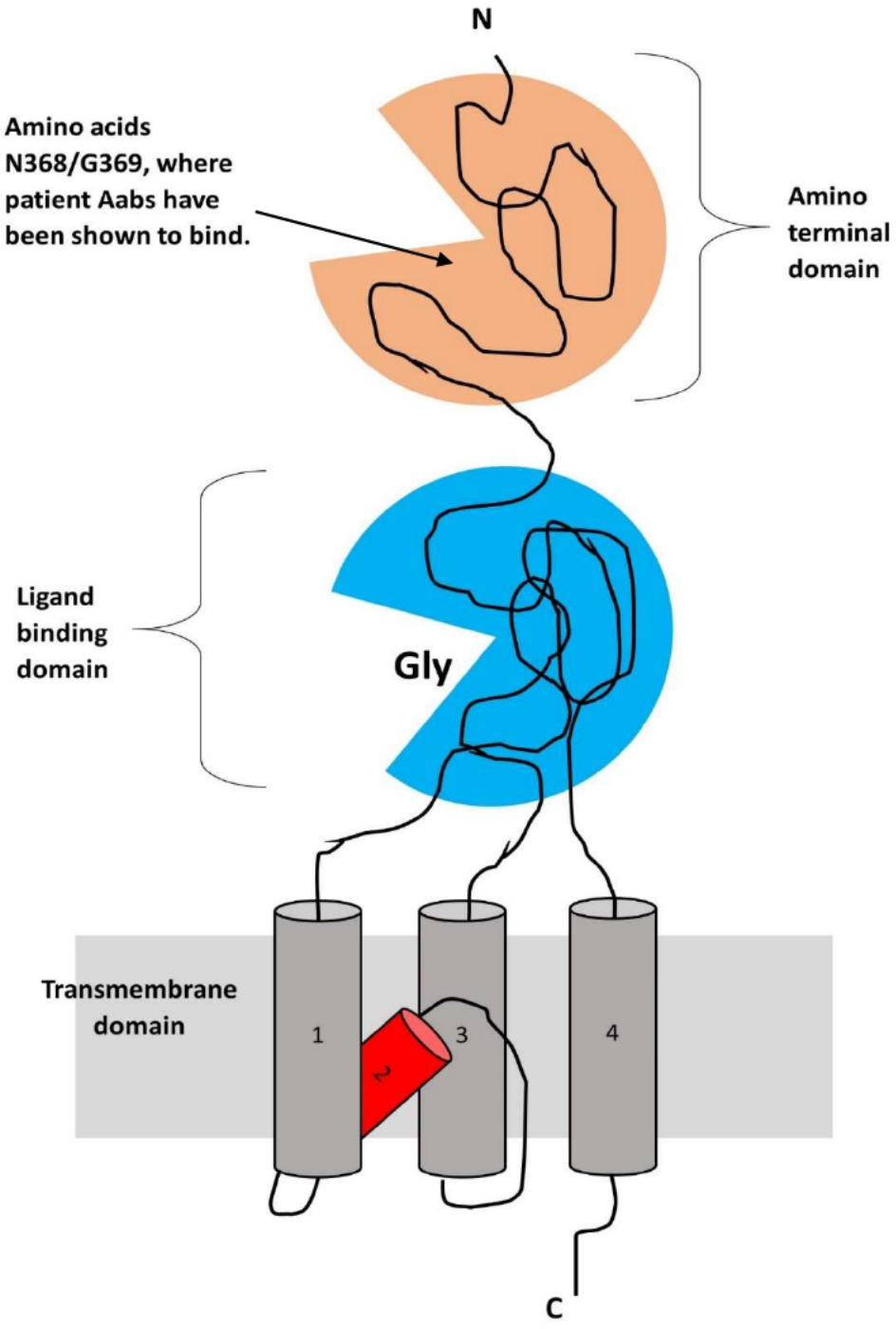

Figure 1.5: Schematic identifying location of the immunogenic amino acids within the NR1 subunit, in relation to the transmembrane domain and ligand binding domain, where glycine (Gly) binds.

1.5.1.4.2 In vitro effects of NMDAR Aabs

Since the identification of NMDAR Aabs, several studies have been performed to identify potential pathological mechanisms by which they may cause the clinical phenotypes seen in patients. Early *in vitro* studies showed that incubation of primary hippocampal neurons with patient anti-NMDAR Aabs resulted in a significant reduction in the synaptic density of NMDARs on both excitatory and inhibitory neurons in a titre-dependent manner (Hughes *et al.*, 2010). This resulted in a subsequent reduction in NMDAR synaptic current when isolated using pharmacological agents and measured via whole-cell patch-clamp (Hughes *et al.*, 2010; Kreye *et al.*, 2016). Following these findings, NMDAR Aabs were found to bind to NMDARs, crosslink and cause receptor internalisation and consequently degradation (Moscato *et al.*, 2014), therefore, reducing total number of synaptic NMDARs on both excitatory and inhibitory neurons. This is hypothesised to subsequently reduce feedback inhibition, which may contribute to a hyper-excitable network (Wright *et al.*, 2015). There has been some evidence to support this hypothesis, via *in vivo* micro-dialysis studies where patient NMDAR Aabs were infused into the CA1 region of the hippocampus and premotor cortex of rats (Manto *et al.*, 2010). Analysis identified that patient Aabs, but not control IgG, caused high concentrations of glutamate to accumulate in the extracellular space following an infusion of NMDA.

These alterations in synaptic expression of NMDARs were also shown via a reduction in synaptic plasticity following NMDAR Aab application (Zhang *et al.*, 2012; Würdemann *et al.*, 2016; Blome *et al.*, 2018; Kersten *et al.*, 2019). Treatment with patients Aabs specifically decreased synaptic NMDAR-specific currents, without affecting AMPAR specific currents, consistent with a reduction in surface NMDARs, however no change in miniature excitatory postsynaptic current frequency of hippocampal neurons was observed, indicating a lack of presynaptic effect (Hughes *et al.*, 2010). Some of these findings have been confirmed in a study

using post-mortem hippocampus from human patients with ANRE, who had significantly less NMDARs than age-matched controls (Hughes *et al.*, 2010). However, these effects have not been investigated with respect to epilepsy or seizures, so the pathway that occurs between the reduction of NMDARs and the development of seizures remains unknown (Hughes *et al.*, 2010; Dalmau, 2017).

Whether these Aabs mediate their effects primarily via synaptic NMDARs or extra-synaptic NMDARs, or whether this binding is preferentially to NMDARs on excitatory or inhibitory neurons is not yet fully understood and needs further investigation. Both circumstances would ultimately result in reduced NMDAR synaptic density, but their downstream effects and hence therapeutics would be opposing in mechanism (Hunter *et al.*, 2021).

1.5.1.4.3 In vivo effects of NMDAR Aabs

In vivo experiments in mice and rats have been performed with results that recapitulate some of the specific features of ANRE. The experiments performed used either a passive transfer model, whereby CSF from patients was infused into the animals, which were subsequently monitored for any functional effects (Planagumà *et al.*, 2015), or an active immunisation model, where peptides or full receptors were used to immunise the animals, generating their own immune response and Aabs (Jones *et al.*, 2019). Continuous intracerebroventricular (icv) infusions in mice of CSF pooled from individuals with ANRE reproduced some of the neuropsychiatric features observed in patients such as memory deficits and depressive-like behaviours (Planagumà *et al.*, 2015), however, no seizures were observed. NMDAR Aab binding and a subsequent decrease in NMDAR clusters on hippocampal neurons were detected in NMDAR Aab-injected mice, which was reversed following the termination of infusion (Planagumà *et al.*, 2015). This binding of Aabs to NMDAR clusters was shown to disrupt the

normal interaction of NMDARs with other synaptic proteins, in particular the Ephrin B2 receptor (EPHB2R) (Planaguma *et al.*, 2016); an interaction, which normally stabilises NMDARs at the membrane surface, hence promoting internalisation of NMDARs. When the Ephrin B2 ligand was co-administered with CSF infusion, the pathogenic behavioural effects seen previously (memory deficits and depressive like behaviours) were prevented and cell-surface levels of NMDARs were maintained (Planaguma *et al.*, 2016). Electrophysiological analysis further supports the internalisation findings described previously, where a reduction in the amplitude of NMDAR-mediated excitatory post-synaptic potentials (EPSPs) was seen following bilateral stereotactic injection into rat dentate gyrus (DG) with patient NMDAR Aabs (Würdemann *et al.*, 2016), an effect that has also been seen in other groups (Hughes *et al.*, 2010).

In another mouse model, icv injection of NMDAR Aabs from individuals with ANRE was co-administered with a subthreshold dose of pentylenetetrazol (PTZ), a $GABA_AR$ antagonist, which is regularly used as a drug to induce seizures/epilepsy. This resulted in increased frequency and severity of seizures when compared to those injected with control IgG (Wright *et al.*, 2015). In addition, human NMDAR Aabs were bound to CA1, CA3 and DG regions within the hippocampus at 48 h post-icv infusion, where NMDAR expression is high, with minimal binding in areas where NMDAR expression is lower (e.g., cortex) compared to control IgG, which showed little binding within the hippocampus. In addition, binding intensity of NMDAR Aabs from ANRE patients correlated to the number and severity of seizures seen. Despite this, no internalisation of NMDARs was observed following NMDAR Aab infusion (Wright *et al.*, 2015), which is in contrast with previous studies *in vitro* and *in vivo* (Hughes *et al.*, 2010; Planagumà *et al.*, 2015). In a more recent study, EEG recordings of mice infused intraventricularly for 14 days with ANRE patient CSF showed a higher frequency of seizures compared with control mice, associated with variable behavioural effects (Taraschenko *et al.*,

2019). Subsequent studies infused C57BL6 mice with purified serum IgG from patients with ANRE, which exhibited increased seizure frequency and a subsequent increased mRNA expression of hippocampal CCL2, a pro-inflammatory cytokine (Taraschenko *et al.*, 2021a). In addition, NMDAR Aab-infused mice were subsequently treated with anakinra (a selective interleukin-1 (IL-1) receptor antagonist) to assess the role of IL-1 in antibody-induced seizures. It was shown that anakinra significantly decreased the frequency and duration of seizures induced by NMDAR Aabs as well as improving memory behaviour, suggesting that IL-1 may be implicated in Aab-induced seizures (Taraschenko *et al.*, 2021b).

Using active immunisation of four peptides against epitopes within the NR1 ATD, Pan *et al* (2018) showed that mice immunised against NMDAR did not show behavioural changes. Only when these mice were treated concomitantly with MK-801 (an NMDAR antagonist) was a psychosis-like phenotype observed in NMDAR-immunised mice, an effect not observed in control mice. In addition, no T-cell or microglial activation was detected on immunopathology (Pan *et al.*, 2018). In contrast, immunisation with purified NR1/NR2B fully assembled NMDARs embedded in liposomes induced a phenotype similar to that in patients (Jones *et al.*, 2019); this phenotype was characterised by hyperactivity and seizures in association with neuroinflammation and immune cell infiltrates. Distinct from the passive transfer models, these immunised mice produced NR1 and NR2 antibodies that reacted with the linear epitopes of the NMDAR protein, and not the amino terminal domain of NR1 seen with the human-derived antibodies (Gleichman *et al.*, 2012). Nevertheless, this model may prove useful for testing novel treatments acting on the cellular inflammatory component of the disease. In line with Jones *et al* (2019), a subsequent study using active immunisation of NR1 amino acids 359-378, resulted in mice developing cognitive, emotional, and behavioural impairments, including anxiety- and depressive-like behaviours, as well as increased seizure activity two weeks after immunisation (Wagnon *et al.*, 2020). Interestingly, this immunisation also induced a B-cell

mediated autoimmune response, where infiltrates into the meninges, periventricular spaces and ventricles was observed, followed by a differentiation into plasmacytes. When the B-cell response was blocked using a depleting cocktail of antibodies, a reduction in the severity of symptoms was observed, confirming the role of B-cells in the development of symptoms, and that intervening in this B-cell response is a suitable therapeutic option.

1.5.2 AMPA Receptors

AMPARs are also ionotropic glutamate receptors that are physiologically activated by glutamate and responsible for the primary depolarisation in glutamate-mediated neurotransmission (Traynelis *et al.*, 2010). Similar to NMDARs, AMPARs are widely distributed throughout the CNS and play pivotal roles in basal synaptic transmission and synaptic plasticity, with their dysfunction being implicated in many disease states, such as epilepsy (Gouaux, 2004).

1.5.2.1 AMPAR structure

All AMPARs share a common topology, similar to NMDARs, consisting of an extracellular ATD, a LBD, three TMDs (M1, M3 and M4), a cytoplasmic facing re-entrant loop (M2) and an intracellular CTD (Figure 1.6) (Amin *et al.*, 2017; Greger *et al.*, 2017). AMPARs can be made up of GluR1-4 subunits (which are encoded for by four separate genes), which assemble as tetramers, with a pore diameter of approximately 0.8mm permitting the movement of Na^+ and K^+, AMPARs lacking the GluR2-subunit are also permeable to Ca^{2+} (Dravid, 2009).

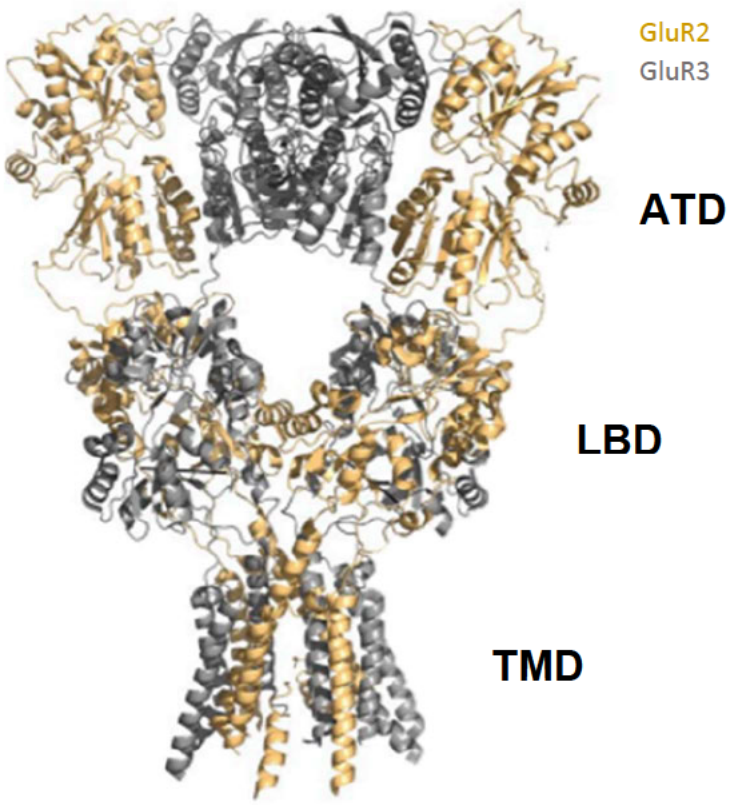

Figure 1.6: Structure of a hetero-tetrameric GluR2/GluR3 AMPAR highlighting the amino-terminal domain (ATD), ligand binding domain (LBD) and trans-membrane domains (TMD). Taken from (Amin et al., 2017).

All domains within the receptor have different functions. The ATD makes up approximately 45% of the mature polypeptide and is involved in receptor assembly and trafficking (Dravid, 2009), the LBD is required for agonist (and antagonist) binding, TMDs are vital to the central pore-forming channel, and the CTD is implicated in receptor localisation (Sukumaran *et al.*, 2012).

Typically, AMPARs are hetero-tetrameric, consisting of a dimer of dimers, however homo-tetrameric complexes can occur. Different combinations of these subunits result in variations in their properties and in specificity within different brain regions (Cantanelli *et al.*, 2014). In addition, alternative splicing produces two variants for each GluR gene, known as 'flip' or

'flop' forms, resulting in 8 possible subunits for receptor assembly. This splicing involves a 38-amino acid sequence found prior to M4 in all four subunits that determines the speed of desensitisation and re-sensitisation of the receptor, whereby 'flop' isoforms exhibit faster desensitisation (Sommer *et al.*, 1990). In embryonic and early postnatal development, the 'flip' isoforms predominate, whereas the 'flop' isoform begins to be expressed during the early stages of postnatal development, meaning a difference in receptor kinetics is observed at different ages (Miller, 2017). A clear understanding of the different isoforms at different ages is vital to understanding any electrophysiological experiments performed involving AMPARs.

1.5.2.2 AMPAR CNS distribution

AMPARs are abundant and widely distributed throughout the CNS. GluR1, 2 and 3 subunits are enriched in the hippocampus, outer layers of the cortex, basal ganglia, olfactory regions, lateral septum and amygdala, whereas the GluR4 subunit is expressed at lower levels in most regions except in the cerebellum, thalamus and brain stem where expression is high (Dravid, 2009). Studies have shown that the hippocampus predominantly expresses AMPARs composed of GluR1/2 with a smaller proportion composed of GluR2/3 subunits (Lu *et al.*, 2009; Schwenk *et al.*, 2014; Renner *et al.*, 2017).

1.5.2.3 Physiological function of AMPARs

Each AMPAR subunit has an agonist binding site for glutamate which, when bound, promotes a movement in the LBD, which is stabilised by the formation of several hydrogen bonds between glutamate and the LBD (Dravid, 2009). Briefly, the LBD is formed by two extracellular stretches of amino acids, named S1 and S2. LBDs form a clamshell-like conformation, where the polypeptide segment S1 forms one half of the clamshell (Domain 1; D1), and segment S2 forms the opposite half of the clamshell (Domain 2; D2), with these domains linked to the TMDs via short linker segments (Figure 1.7). The agonist binding pocket

is located within the cleft between D1 and D2, whereby a conformational change occurs upon agonist binding, closing the clamshell structure. This triggers re-arrangement of the linker segments and subsequently TMDs, resulting in channel opening (Traynelis *et al.*, 2010; Twomey and Sobolevsky, 2018). AMPARs open and close quickly (~1 ms) and are responsible for most of the fast excitatory synaptic transmission in the CNS (Platt, 2007), although once open, the channel may undergo rapid desensitisation, closing the pore (Armstrong *et al.*, 2006).

AMPAR permeability to Ca^{2+} and other cations, such as Na^{+} and K^{+}, is governed by the GluR2 subunit. If an AMPAR lacks GluR2, it will be permeable to Na^{+}, K^{+} and Ca^{2+}, whereas those containing GluR2 will only be permeable to Na^{+} and K^{+}. This characteristic of GluR2 is determined by post-transcriptional modification of Q/R (Q607), promoting a glutamate to arginine substitution in the channel forming section of TM2, the presence of which inhibits permeability to divalent cations (Dravid, 2009).

AMPARs are vital for physiological functions within the CNS, such as neurotransmission and synaptic plasticity (Gouaux, 2004). The most heavily studied form of plasticity is LTP, which is an increase in EPSP size due to postsynaptic upregulation of AMPARs (Bliss and Collingridge, 1993). Glutamate binding to postsynaptic AMPARs causes the opening of AMPARs, and hence an influx of Na^{+} and subsequent depolarisation. Binding of glutamate to NMDARs and postsynaptic depolarisation caused by AMPAR opening then relieves the Mg^{2+} block on NMDARs, allowing the influx of both Na^{+} and Ca^{2+}. Influx of Ca^{2+} triggers the activation of calmodulin-dependent kinase II (CaMKII), thus phosphorylating AMPARs and increasing their conductance as well as the number of AMPARs inserted into the postsynaptic membrane (Malenka, 2003; Malinow, 2003). As well as being vital for basal neurotransmission

and physiological functions, AMPARs are also heavily implicated in disease states such as epilepsy due to their key role in the generation of seizures (Chater and Goda, 2014).

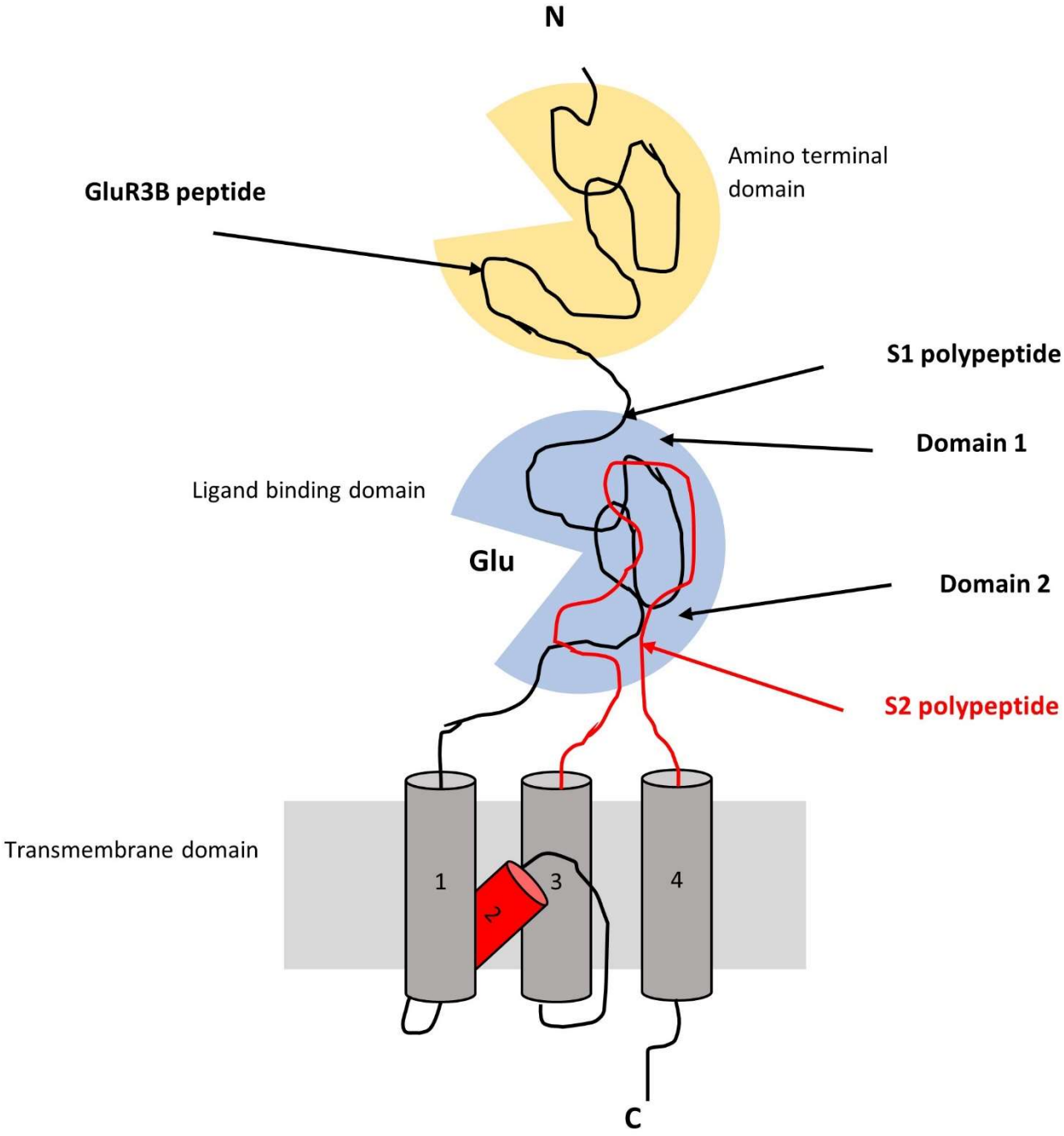

Figure 1.7: Schematic identifying the location of the immunogenic GluR3B peptide within the ATD. The GluR3 subunit is composed of an ATD where the GluR3B peptide is located, a ligand binding domain (which is composed of two domains: domain 1 and 2), four transmembrane domains and an intracellular C terminal.

1.5.2.4 Autoantibodies to AMPARs

Anti-GluR3 Aabs were originally discovered in patients with RE (Rogers *et al.*, 1994). Further studies showed that these were not exclusive to RE patients but were also present in patients with other types of epilepsy (Wiendl *et al.*, 2001; Mantegazza *et al.*, 2002; Watson *et al.*, 2004). It has been estimated that GluR3 Aabs are present in up to 20-30% of epilepsy patients (Levite, 2014), as well as in 20-25% of patients with frontotemporal dementia (FTD) (Borroni *et al.*, 2017).

1.5.2.4.1 Binding of Aabs to AMPARs

The key antigenic epitope recognised by human GluR3 Aabs is a 24 amino acid sequence within the GluR3 ATD (372-395; NEYERFVPFSDQQISNDSSSSENR), termed the GluR3B peptide (Figure 1.7) (Stern-Bach *et al.*, 1994; Levite *et al.*, 1999). A number of studies have assessed binding, including generation of recombinant Aabs, site-directed mutagenesis and immunostaining to determine the functional effects of GluR3 Aabs (Rogers *et al.*, 1994; Twyman *et al.*, 1995; Levite *et al.*, 1999). One particular study identified key residues within the GluR3B sequence necessary for Aab binding using deletion mapping and site-directed mutagenesis, whereby amino acids 375 and 378-380 were preferred for binding (Carlson *et al.*, 1997). These GluR3B Aabs have been shown to have an agonistic-like effect on GluR3B-containing AMPARs; co-application of Aabs with the GluR3B peptide blocked any Aab agonist-like activity (Twyman *et al.*, 1995). Taken together, these data indicate the GluR3B sequence as being the active epitope for patient anti-GluR3 Aabs, being important for both binding and functionality on native AMPARs.

1.5.2.4.2 In vitro effects of AMPAR Aabs

In recent years, it has been shown that several neurotransmitters, such as dopamine, can interact with their respective receptors on T-cells, and subsequently trigger T-cell functions (Levite *et al.*, 2001). Therefore, human peripheral T-cells were used to assess whether this was also the case of GluR3B Aabs, and if so, could this be one mechanism for how these Aabs originate. A high expression of GluR3 was identified on human peripheral T-cells, which could be directly activated by the addition of glutamate, resulting in T-cell adhesion to extracellular matrix proteins (Ganor *et al.*, 2003). It was also identified that the GluR3 Aab antigenic epitope, i.e., the GluR3B peptide, can be generated by specific cleavage of GluR3 via granzyme B (a serine protease released by activated immune cells) (Gahring *et al.*, 2001; Ganor *et al.*, 2003). Therefore, it has been hypothesised that Aabs may be generated against a peripheral GluR3 and subsequently enter the CNS and, from there, disrupt neuronal signalling via binding, activation and killing AMPAR-expressing neurons. This hypothesis involves peripheral T-cells being exposed to foreign antigen, thus activating, and releasing granzyme B. This cleaves any GluR3 from the surface of neighbouring T-cells, solubilising GluR3 protein containing the GluR3B peptide. This soluble peptide is detected by immune cells as a foreign antigen, where Aabs are then generated (Ganor *et al.*, 2007).

Several studies have investigated the binding specificity and functionality of both patient and recombinant GluR3B Aabs in *in vitro* experimental setups. Immunohistochemistry and electrophysiology studies have demonstrated the ability of these Aabs to not only bind to both GluR3-transfected cells (Rogers *et al.*, 1994) and cultured neurons (Twyman *et al.*, 1995), but also to activate and evoke GluR3-specific currents in GluR3-expressing oocytes (Malina *et al.*, 2006), primary neurons and rat neocortical slices (Levite *et al.*, 1999). In addition, it was shown that incubation of primary neurons with GluR3 Aabs resulted in increased cell death, which

was apoptotic in nature, as identified by the positive labelling with Annexin V, and a lack of binding with propidium iodide (PI) (Levite *et al.*, 1999). More recent studies have revealed the presence of GluR3 Aabs (selective for both GluR3 peptide A and B) in 20-25% of FTD patients, providing further mechanistic insight into the pathogenic role of Aabs (Borroni *et al.*, 2017). *In vitro* studies have shown that acute treatment with GluR3 Aabs results in a reduction in GluR3-containing AMPARs and a reduction in dendritic spine density in rat hippocampal neuronal primary cultures and human iPSC-derived neurons (Borroni *et al.*, 2017).

Whether these Aabs mediate their effects primarily via an agonistic-like effect and subsequent neuronal death (Levite *et al.*, 1999), via a presynaptic mechanism of action (Palese *et al.*, 2020) or via an internalisation of GluR3-containing AMPARs, as detailed more recently in FTD patients (Borroni *et al.*, 2017) is yet to be fully determined and needs further investigation.

1.5.2.4.3 In vivo effects of AMPAR Aabs

The pathogenic features associated with GluR3B Aabs such as cognitive deficits and seizures are in line with behaviours seen in previous mouse models of GluR3 deficiency. These GluR3-deficient mice showed reduced exploratory behaviour (Sanchis-Segura *et al* 2006), hypo-activity in open field (Steenland, 2008) and minor deficits in motor and balance (Adamczyk *et al.*, 2012).

GluR3B Aabs have been studied in several animal models using Aabs generated by immunisation with GluR3-specific peptides (Rogers *et al.*, 1994; Ganor *et al.*, 2014; Goldberg-Stern *et al.*, 2014). Rogers *et al* immunised rabbits with a portion of the GluR3 subunit (aa245-457); rabbits subsequently developed seizures and behavioural abnormalities, accompanied by inflammatory pathology in the brain (Rogers *et al.*, 1994), similar to that of RE. However, this has not been fully reproducible in subsequent studies, and has generated conflicting results

(Levite and Hermelin, 1999; Levite *et al.*, 1999). Immunisation with GluR3B peptide in rats led to the generation of highly specific GluR3 Aabs, which were present in both the serum and CSF (Ganor *et al.*, 2005). In line with *in vitro* studies (He *et al.*, 1998; Levite *et al.*, 1999), histopathology showed an increase in neuronal death and associated reactive gliosis. As the rats did not spontaneously generate seizures as previously observed in rabbits by Rogers *et al* (1994), multiple doses of PTZ were administered to lower the seizure threshold. Unexpectedly, GluR3B Aabs were shown to confer partial protection from seizures when compared to control rats (Ganor *et al.*, 2005). In a subsequent study in mice, animals immunised with a GluR3B peptide to generate Aabs also did not exhibit seizures spontaneously, thus several doses of PTZ were administered to see if the seizure threshold was altered. In this case, mice with GluR3B Aabs developed more seizures compared to control mice and the severity of seizures correlated to the titre of Aabs in the serum (Ganor *et al.*, 2014). Taking these studies together, the precise effects of GluR3B Aabs remain unclear with regard to seizure generation across different species. Several hypotheses have been made that might explain the conflicting results. Firstly, GluR3B Aabs confer partial protection from PTZ-induced seizures via a chronic depolarisation of GABAergic inhibitory neurons or via excitatory neuronal death, leading to an over-inhibition of neuronal networks (Ganor *et al.*, 2005). However, it has also been postulated that GluR3B Aabs lower seizure threshold via over-activating and subsequently killing GluR3-expressing neurons (Ganor *et al.*, 2014). It is clear that future *in vivo* studies are required to fully understand the impact of GluR3B Aabs on network activity.

1.6 Aims

Much of the information in the current literature is conflicting with regards to the mechanism of action of patient Aabs associated with seizure and epilepsy. We hypothesise that Aabs directed against NMDARs and AMPARs are largely pathogenic in nature and contribute to

seizures identified in patients with autoimmune epilepsy and autoimmune encephalitis. Therefore, taking all the above into consideration, this PhD project aimed to:

1) Design and generate Aabs targeting the GluR3 subunit of AMPARs, and NR1 subunit of NMDARs.
2) Purify and characterise Aabs using techniques such as enzyme linked immunosorbent assay (ELISA), immunofluorescence, and western blot to ensure specificity for the target receptor.
3) Test functional effects of Aabs on synaptic and network activity using a range of *in vitro* electrophysiological techniques, including two-electrode voltage clamp (TEVC), multi-electrode arrays (MEAs) and whole-cell patch-clamp.

Together, this will aim to provide information regarding the functional effects of anti-glutamate receptor Aabs on neuronal excitability and determine any putative link with seizure activity observed in patients, thus supporting or disproving the hypothesis outlined above.

2 Materials and Methods

2.1 NR1 and GluR3 autoantibody production and purification

Human Aabs against the NR1 subunit of NMDARs are known to bind to two amino acids within the NR1 ATD (Gleichman *et al.*, 2012). These data, combined with the known structure of NMDARs, enabled the design of peptides to be used for immunisation. Extracellular protruding loops within the NR1 subunit are expected to be of high immunogenicity and were used as targets for the design of 9 peptides (Table and Table for NMDAR1 and 2 respectively; design and generation of peptides performed by UCB and Peptide Synthetics, UK). In an effort to increase the immune response, peptides 2, 4, 5 and 8 were cyclised via a thioester, improving the metabolic stability of the peptides as well as mimicking the natural 3D structure (Skwarczynski and Toth, 2016), therefore increasing the chances of generating Aabs that bind to the NR1 subunit in its natural conformation. In addition, all peptides were modified with N-terminal acetylation and C-terminal amidation to help prevent degradation (Purcell *et al.*, 2007). A mixture of peptides 1-5 and peptides 6-8 were injected into two separate rabbits to generate anti-NMDAR Aabs (NMDAR1 and 2 Aabs respectively).

Table 1: NMDAR peptide sequences used for the immunisation of rabbit #1. All peptides were generated and modified with N-terminal acetylation and C-terminal amidation. Peptides 2, 4 and 5 were cyclised via a thioester to aid in mimicking the natural 3D structure of their respective epitopes.

Peptide number	Sequence
1 (aa125-135)	MSIYSDKSIHL
2 (aa249-266)	Cyclo-VGEREISGNALRYAPDGI
3 (aa272-281)	INGKNESAHI
4 (aa353-363)	Cyclo-IMNLQNRKLVQ
5 (aa365-375)	Cyclo-GIYNGTHVIPN

Table 2: NMDAR peptide sequences used for the immunisation of rabbit #2. All peptides were generated and modified with N-terminal acetylation and C-terminal amidation. Peptide 8 was cyclised via a thioester to aid in mimicking the natural 3D structure of the epitope.

Peptide number	Sequence
6 (aa34-53)	STRKHEQMFREAVNQANKRH
7 (aa386-399)	TEKPRGYQMSTRLK
8 (aa488-497)	Cyclo-ERVNNSNKKE
9 (aa685-710)	KQSSVDIYFRRQVELSTMYRHMEKHN

Table 3: AMPAR peptide sequence used for the immunisation of rabbit #3. The peptide was generated and modified with N-terminal acetylation and C-terminal amidation.

Peptide number	Sequence
10 (aa372-395)	NEYERFVPFSDQQISNDSSSSENR

The exact amino acids to which patient anti-GluR3 Aabs bind is less well-known than for NMDAR Aabs, therefore a longer sequence was used for peptide immunisation (Table). This sequence also corresponds to an extracellular hinge region within the GluR3 ATD considered to be an immunogenic region capable of stimulating an immune response (Levite and Hermelin, 1999). This sequence has been used in previous studies (Ganor *et al.*, 2005), whereby anti-GluR3 Aabs were successfully generated following peptide immunisation; therefore, no cyclisation of the immunising peptide was carried out. As for NR1 peptides, the GluR3 peptide was modified with N-terminal acetylation and C-terminal amidation to help prevent degradation by exopeptidases. Despite these Aabs being generated this way by previous studies, no conclusive mechanism has been determined.

2.1.1 Rabbit immunisation and antibody production

To elicit an immune response, an antigen must possess three characteristics: a high molecular weight, a degree of 'foreignness' to the host and chemical complexity. Adjuvants (e.g. Complete Freund's Adjuvant (CFA) or Incomplete Freund's Adjuvant (IFA)) and carrier proteins (e.g. keyhole limpet hemocyanin, KLH) were both used in this protocol in order to increase the immunogenicity of the NMDAR and AMPAR peptides (Janeway *et al.*, 2001). Peptides were designed and subsequently conjugated to three different carrier proteins: KLH, bovine serum albumin (BSA) and ovalbumin (OVA) (Peptide Synthetics, UK). These carrier proteins were chosen due to their large and complex structures, conferring immunogenicity to the conjugated peptide.

Three female New Zealand rabbits (>2kg) were immunised subcutaneously with 3-4 immunisations of either NMDAR or AMPAR peptides (Tables 1-3) at UCB Slough, in accordance with the UK Animals (Scientific Procedures) Act 1986. For each immunisation,

peptides were mixed in a 1:1 ratio with either CFA or IFA. In addition, for each immunisation dose, the peptides were conjugated to a different carrier protein, ensuring a minimal immune response to the carrier protein. Dosing was carried out every 21 days and blood samples were taken before initial immunisation and 14 days post immunisation. Rabbits were sacrificed 14 days after the final immunisation by Schedule 1 methods in accordance with the UK Animals (Scientific Procedures) Act 1986, at which time the spleen, bone marrow, peripheral blood mononuclear cells (PBMCs) and lymph nodes were taken, along with the terminal serum.

2.1.2 Serum screening and antibody titre

To determine the immune response and analyse the specificity of antibodies produced, ELISAs were carried out after each immunisation boost. 96-well microtiter plates were coated with streptavidin (2µg/mL; Jackson ImmunoResearch, Cambridge, UK) and incubated overnight at 4°C. The contents of the plates were emptied and washed (3x) with 1% PBS-Tween20 (PBS-T) using an automatic plate washer (BioStack 3 Microplate Stacker: BioTek). To block any uncoated sites, plates were incubated with 1% casein (VWR, UK) for 1 h at room temperature. Following three washes, biotin-tagged peptides (1µM) were added to the wells and incubated at room temperature for a further hour. Bleed 0, 1, 2, 3 (pre-immunisation, post 1st 2nd and 3rd boost) and terminal serum were added to the wells as a half-log dilution series, incubated for 1 h and subsequently washed (3x) with 1% PBS-T. Any peptide-sera complexes were detected using an HRP-conjugated secondary antibody (1:4000; Jackson ImmunoResearch, Cambridge, UK). Following a final three washes, the peptide-sera complexes were detected using 3,3',5,5' tetramethylbenzidine (TMB; Sigma Aldrich, UK) substrate, incubated at room temperature until the blue colour developed. The reaction was stopped by the addition of 2.5% NaF, and the level of absorbance was measured at 630nm using a microplate reader (Synergy 5; BioTek). The ELISA results following each immunisation identified any increases in binding to the

immunisation peptides, and thus any changes in EC_{50} values. These factors helped determine how many immunisation boosts were given to each rabbit.

2.1.3 Protein A purification of polyclonal IgG antibody from rabbit serum

Immunised rabbit terminal serum was purified using protein A resin (GE Healthcare, UK) in order to obtain total IgG. Protein A-Sepharose beads were added to a 20mL column, and subsequently washed five times with 10mL PBS, where on the final wash a cap was placed on the base of the column to prevent the column from drying out. Debris in the terminal serum was removed by filtration prior to addition to the column. The resin was re-suspended and mixed with the serum and left to mix gently on a roller overnight at 4°C. The serum and resin were re-added to the column and the flow-through collected. The column was washed (2x) with 50mL PBS and any antibody captured by the resin was eluted with 0.1M sodium citrate (pH 3.5). 12 x 8mL fractions were collected in tubes containing 1.2mL 2M Tris-HCl (pH8.4) for pH neutralisation. The column was washed again with 50mL PBS and stored at 4°C. The fractions were subsequently combined, washed, and concentrated through buffer exchange with PBS using 10kDa molecular weight cut off (MWCO) filters (Amicon; Sigma Aldrich, UK). Total IgG concentration was determined using absorbance at 280nm, and sodium dodecyl sulphate–polyacrylamide gel electrophoresis (SDS-PAGE) and ELISAs were performed and compared to an IgG control to check accuracy and specificity of chromatography.

2.1.4 Peptide purification of polyclonal IgG from protein A purified Aabs

Protein A purified Aabs (NMDAR 1; generated via immunisation of peptides 1-5 into rabbit #1) were purified further using high-capacity streptavidin agarose resin (Pierce; ThermoFisher Scientific, UK). Biotin-bound peptides used for immunisation (133µM each, peptides 1-5; Table 1) were mixed with 5mL streptavidin agarose resin to create a mixed peptide specific column. Once thoroughly mixed, the resin/peptide mix was combined with the protein A

purified Aab material and left to incubate overnight on a roller at 4°C. This material was then split over 4 separate columns and allowed to flow-through, collecting all material. The columns were then washed with PBS and any peptide specific antibody captured by the resin was eluted with 0.1M sodium citrate (pH 3.2). One pooled fraction was collected in a tube containing 1.2mL 2M Tris-HCl (pH 8.5) for pH neutralisation. The columns were washed once again with PBS and stored at 4°C. The fractions were concentrated through buffer exchange with PBS using 10kDa MWCO columns. Total peptide specific IgG concentration was determined using absorbance at 280nm, SDS-PAGE and ELISAs were performed and compared to an IgG control.

2.1.5 SDS-PAGE analysis of anti-NMDAR/anti-AMPAR antibody purity

To assess the quality of the chromatography, an aliquot from all stages of purification was kept and analysed via SDS-PAGE to ensure all IgG had been removed from the starting material. Samples from the starting material, flow-through, washes and eluates were all combined with loading buffer (2x sample buffer; ThermoFisher Scientific, UK) and added to each well of a 4-20% Novex Tris-Glycine gel (ThermoFisher Scientific, UK), along with a pre-stained marker to determine band sizes (ThermoFisher Scientific, UK). The gel was resolved at 220V until the blue tracker dye reached the bottom of the gel (approximately 40 min). The gel was removed and stained with Coomassie Blue (Generon, UK) for 1 h. Subsequently, the gels were de-stained overnight using ddH_20 and visualised using an ImageQuant LAS 4000 mini (GE Healthcare, UK).

2.2 Binding specificity of generated autoantibodies

Both NMDAR and AMPAR Aabs were tested in multiple systems to determine binding specificity. Aabs were tested via immunocytochemistry and -histochemistry (ICC/IHC) and co-stained with a range of other neuronal/glial antibodies to determine specific localisation. In addition, positive and negative control antibodies were also tested to compare specificity of binding. Primary and secondary antibodies used are detailed in Tables 4 and 5 respectively.

Table 4: Details of primary antibodies used.

Primary antibody	Supplier	Catalogue no.	Host	Type	ICC/IHC Conc.
NMDAR1 Aabs	UCB	n/a	Rabbit	IgG	1:100-1:1000
NMDAR2 Aabs	UCB	n/a	Rabbit	IgG	1:100-1:1000
AMPAR	UCB	n/a	Rabbit	IgG	1:100-1:1000
NMDAR	Synaptic Systems	114 103	Rabbit	IgG	1:100
NMDAR	Synaptic Systems	114011	Mouse	IgG2b	1:100
AMPAR	Alomone	AGC-010	Rabbit	IgG	1:100
IgG	Jackson ImmunoResearch	011-000-003	Rabbit	IgG	1:100
IgG2b	BioLegend	70-4732	Mouse	IgG2b	1:100
βIII-tubulin	BioLegend	801201	Mouse	IgG2a	1:500
GFAP	Millipore	MAB3402	Mouse	IgG1	1:400
NeuN	Chemicon (Merck)	MAB377	Mouse	IgG1	1:400

Table 5: Details of secondary antibodies used.

Secondary antibody	Supplier	Catalogue no.	Host	Type	Conc.
Anti-rabbit Alexa Fluor 488	Life Tech	A11008	Goat	IgG	1:1000
Anti-rabbit Alexa Fluor 594	Life Tech	A11012	Goat	IgG	1:1000
Anti-rabbit Alexa Fluor 647	Life Tech	A21244	Goat	IgG	1:1000
Anti-mouse Alexa Fluor 488	Life Tech	A21141	Goat	IgG2b	1:1000
Anti-mouse Alexa Fluor 594	Life Tech	A21145	Goat	IgG2b	1:1000
Anti-mouse Alexa Fluor 647	Life Tech	A21242	Goat	IgG2b	1:1000
Anti-mouse Alexa Fluor 488	Life Tech	A21121	Goat	IgG1	1:1000
Anti-mouse Alexa Fluor 594	Life Tech	A21125	Goat	IgG1	1:1000
Anti-mouse Alexa Fluor 647	Life Tech	A21240	Goat	IgG1	1:1000
Anti-mouse Alexa Fluor 488	Life Tech	A21131	Goat	IgG2a	1:1000
Anti-mouse HRP-conjugated	SeraCare	5450-0011	Goat	IgG	1:10,000
Anti-rabbit HRP-conjugated	SeraCare	5450-0010	Goat	IgG	1:10,000

2.2.1 NMDAR transfection in HEK cells

Human embryonic kidney 293 (HEK) cells were transiently transfected with plasmids expressing the NR1 or NR2 subunit using polyethylenimine (PEI). PEI is a cationic polymer that assembles positively charged complexes with DNA, which binds to the anionic surface of the cell, resulting in DNA: PEI complex endocytosis (Boussif *et al.*, 1995).

Cells were initially plated in 24 well plates at approximately $1.5x10^6$ cells per 35mm well in antibiotic-free DMEM (Gibco; ThermoFisher Scientific, UK) with 10% FBS (Sigma Aldrich, UK), typically resulting in ~90% confluency the following day. Cells were divided into three groups: (i) control group (transfected with an empty plasmid vector; pcDNA3.1(+)) and those transfected with plasmids encoding either (ii) NR1 or (iii) NR2 subunit of NMDARs

(pcDNA3.1(+) NR1-4a_HS and pcDNA3.1(-) NR2B_HS respectively; vector maps shown in Appendix 9.1). When the cells were ~90% confluent, medium was replaced with 1.5 ml fresh antibiotic free medium (DMEM + 10% FBS) 2 h prior to transfection. The transfection mix was prepared at a 2:1 ratio PEI:DNA (12 µg/well: 6 µg/well) in a total volume of 500µl OptiMem (Gibco; ThermoFisher Scientific, UK) and incubated at room temperature for 20 min to allow complex formation prior to being added to the cells. This mix was slowly added dropwise into each well and cells were subsequently incubated for 6 h before sub-culturing on coverslips for immunocytochemistry. Glass coverslips (13 mm; VWR, UK) were coated with poly-D-lysine (PDL; 20 µg/ml; Sigma Aldrich, UK) for 20 min to facilitate the attachment of cells. The coverslips were washed with PBS (3x) and cells were plated at $2.5x10^5$ cells/well and incubated for 24 h before fixing for immunocytochemistry experiments.

2.2.1.1 Immunocytochemistry on NR1-transfected HEK cells

The day after transfection, cells were washed (3x) with PBS, care was taken not to directly pipette onto the cells to prevent cell detachment. Cells were then fixed with 4% paraformaldehyde for 10 min (PFA; Sigma Aldrich, UK) and washed 3 x 5 min each with blocking buffer (1x PBS, 0.1% Triton X-100, 1% normal goat serum) on a shaker and subsequently transferred to a humid chamber. Primary antibodies (NMDAR Aabs, mNMDAR, rIgG and mIgG2b; Table 4) were added (in blocking buffer) and incubated overnight at 4°C. Coverslips were washed with blocking buffer and specific Alexa Fluor-coupled secondary antibodies were added (in blocking buffer) and incubated for 2 h at room temperature (Table 5). Following incubation, cells were washed 3x with blocking buffer and subsequently 3x PBS (all 5 min each). Nuclei were counterstained using 4',6-diamidino-2-phenylindole (DAPI; 1:10,000, Thermo Fisher Scientific, UK) and coverslips were mounted in ProLong Gold anti-fade mounting medium (Thermo Fisher Scientific, UK). Cells were visualised with an

AxioImager A1 microscope (Zeiss) and images acquired using Axiovision 4.6.3 imaging software with a 20x or 40x objective lens.

2.2.2 Immunocytochemistry on primary neurons

Primary neurons obtained from embryonic mice (E18), detailed later in section 2.3.1.2 were used for immunocytochemistry at DIV7-14. Cells were washed (3x) with PBS and fixed with PFA for 10 min and washed a further 3x with PBS. Primary antibodies (NMDAR Aabs, mNMDAR, rIgG and mIgG2b; Table 4) were added (in blocking buffer; PBS; 10% normal goat serum) and incubated for 2 h at room temperature. Coverslips were washed and permeabilised using 0.1% Triton X-100 and subsequently washed again. Additional primary antibodies were added (βIII tubulin, Glial fibrillary acidic protein (GFAP) or neuronal nuclei (NeuN); Table 4) for 2 h at room temperature. The cells were subjected to three further washes and subsequently specific Alexa Fluor-coupled secondary antibodies were added (in blocking buffer) and incubated for 30 min at room temperature (Table 5). Following incubation, cells were washed 3x with PBS. Nuclei were counterstained using DAPI and coverslips were mounted in ProLong anti-fade mounting medium. Cells were visualised with AxioImager A1 microscope (Zeiss) and images acquired using Axiovision 4.6.3 imaging software with a 20x or 40x objective lens.

2.2.3 Immunohistochemistry

Brains from male adult C57BL6/J mice (6-8 weeks) were removed (detailed further in section 2.3.1.1) and fixed/sectioned in two separate conditions. Brains were perfusion-fixed in 4% PFA and cryopreserved in 30% sucrose/PBS and subsequently cryosectioned sagitally at 12µm, collected and stored at -20°C until use (QPS Neuropharmacology Histology Services, Austria). Alternatively, brains were immersion fixed in 4% PFA overnight at 4°C and cryopreserved in 30% sucrose/PBS for 2-3 days at 4°C; cryosectioning was performed, obtaining transverse

sections at 12µm, collected, and stored at -20°C. Sections were permeabilised and blocked (0.3% Triton X-100, 10% normal goat serum in PBS: blocking buffer) for 1 h at room temperature. Incubation with primary antibodies was carried out at 4°C overnight in blocking buffer (Table 4); however, to test NMDAR staining, primary antibodies were added prior to permeabilization with Triton X-100 and incubated overnight, followed by permeabilization and subsequent co-labelling with neuronal and glial primary antibodies. Sections were then incubated with appropriate Alexa Fluor conjugated secondary antibodies (Table 5), all counterstained with DAPI (1:10,000; ThermoFisher Scientific, UK). Sections were mounted with ProLong Gold anti-fade and visualised using a Zeiss AxioImager A1 microscope.

IHC was also performed at UCB, where mouse brains were fixed and sectioned externally (QPS Neuropharmacology Histology Services, Austria), and subsequently permeabilised and blocked (0.3% Triton X-100, 5% BSA in PBS: blocking buffer) for 30 min at room temperature. Incubation with primary antibodies was carried out at 4°C overnight in blocking buffer (Table 4), followed by incubation with appropriate AlexaFluor conjugated secondary antibodies (Table 5), all counterstained with DAPI (1:10,000; ThermoFisher Scientific, UK). Sections were mounted with ProLong Gold anti-fade and visualised using a Zeiss AxioScan.

2.2.4 SDS PAGE and Western blotting

2.2.4.1 Cell lysate preparation

Western blotting was used to assess the specificity of NMDAR Aabs against protein lysate, whereby all steps were conducted at 4°C to prevent protein degradation. HEK cells were placed on ice and washed 3x with PBS (5 min each). Lysis buffer (Table 6) was added to each well in a 6 well plate and rocked at 4°C for 20 min. Lysed cells were scraped from the wells and

centrifuged for 10 min at 12,000rpm at 4°C. The supernatant was then removed and kept on ice or kept at -20°C if not used immediately.

Table 6: Composition of lysis buffer for HEK cell lysates. pH was adjusted to 7.4 using HCl

Component	Final concentration
Tris base	50mM
Sodium Fluoride	10mM
Sodium pyrophosphate	10mM
Sodium orthovanadate	0.1mM
Triton X-100	0.1%

2.2.4.2 Whole brain homogenisation and protein lysate preparation

Frozen hemispheres from adult male C57BL6/J mice were defrosted in 2mL ice-cold lysis buffer (Table 7) and homogenised using an upright homogeniser. This was repeated several times with samples being maintained at ice-cold temperature. Lysates were centrifuged at 14,000rpm at 4°C for 10 min, with the supernatant being removed, aliquoted and stored at -20°C if not being used immediately.

Table 7: Composition of lysis buffer for mouse brain lysates.

Component	Final concentration
NaCl	150mM
Triton-X-100	1% (v/v)
Glycerol	10% (v/v)
HEPES	30mM
SigmaFAST protease inhibitors	1 tablet/50mL

2.2.4.3 *Quantification of protein concentration*

A bicinchoninic acid (BCA) protein assay kit (ThermoFisher Scientific, UK) was used to determine the concentration of protein lysates. This method utilises the Biuret reaction; a reduction of copper ions (Cu^{2+} to Cu^{+}) mediated by the peptide bonds present in protein molecules. BCA chelates Cu^{+} ions resulting in the formation of a purple-coloured complex that absorbs light at 540nm (Smith *et al.*, 1985). BSA (2mg/ml; ThermoFisher Scientific, UK) was used as a protein standard and diluted to concentrations ranging from 0-2mg/ml; each of these standards were pipetted in triplicate on a 96-well plate. Protein lysates were diluted 1 in 4 with lysis buffer and pipetted in triplicate. BCA (Reagent A) and $CuSO_4$ (Reagent B) were mixed in a 50:1 ratio before subsequently adding to each well, incubating at 37°C for 30 min. The absorbance for each well was then measured using Emax Precision Microplate Reader (Molecular Devices, UK) at 540nm. Absorbance values were averaged and subtracted with the value obtained from the blank standard. A standard curve was plotted and the protein concentration for the lysate samples was determined via interpolation of the standard curve. Lysate concentrations were multiplied by 4 to account for initial dilution. The samples were stored at -20°C until needed.

2.2.4.4 *SDS-PAGE Gel preparation*

Polyacrylamide gels are extensively used for the separation and analysis of protein samples. Polymerisation of these gels is initiated by the addition of ammonium persulfate (APS; Sigma Aldrich, UK) and tetramethylenediamine (TEMED; Fisher Scientific, UK) via free radical formation (Shi and Jackowski, 1998). The separating gel solution (Table 8) was gently pipetted into the glass plates and left to polymerise for approximately 1 h. The formation of bubbles was prevented by the addition of water-saturated butanol on top of the separating gel solution.

Table 8: Composition of 10% separating gel. TEMED (2.5µl) was the last component to be added and was carried out in a fume cupboard.

Component	Volume per 10ml
ddH_20	4.8ml
1.5M Tris/HCl	2.5ml
40% Acrylamide	2.5ml
10% APS (w/v)	100ul
10% SDS (w/v)	100ul
TEMED	2.5ul

Table 9: Composition of 3% stacking gel. TEMED (2.5µl) was the last component to be added and was carried out in a fume cupboard.

Component	Volume per 5ml
ddH_20	3.275ml
0.5M Tris/HCl pH	1.25ml
40% Acrylamide	0.375ml
10% APS (w/v)	50ul
10% SDS (w/v)	50ul
TEMED	2.5ul

The stacking gel was prepared whilst waiting for the separating gel to set (Table 9). Upon polymerisation of the separating gel, water-saturated butanol was removed, the top of the gel was rinsed with ddH_2O, and dried using strips of filter paper. The stacking gel was added and the comb (1.5mm, 10 wells) was gently inserted into the plate ensuring that no air bubbles were present. The gel was left to polymerise.

2.2.4.4.1 *Preparation of protein lysate samples*

Table 10: Composition of 3x sample loading buffer.

Component	Final concentration
0.5M Tris/HCl pH 6.8	150mM
DTT	300mM
Glycerol	30% (v/v)
SDS	6% (w/v)
Bromophenol blue	0.3% (w/v)

2-mercaptoethanol, a reducing agent was added to the 3x loading buffer (Table 10) in a fume hood to a final concentration of 4% (v/v). Samples were made up to the appropriate concentration using the loading buffer/2-mercaptoethanol mix and denatured at 90°C for 5 min.

2.2.4.4.2 *SDS-PAGE Gel electrophoresis*

Gels were inserted into a Mini-Protean Tetra cell electrophoresis tank (Bio-Rad) with the combs removed and immersed in running buffer (Table 11), initially flushing the wells to remove any unpolymerized acrylamide, and subsequently fill the tank. Lysate samples and molecular weight markers (Precision Plus pre-stained marker; Bio-Rad, UK) were loaded into appropriate wells and the gel was run at a constant current of 0.02A per gel for approximately 2-3 h until the dye front reached the bottom of the gel using a Bio-Rad power pack.

Table 11: Composition of 1X running buffer. ddH2O was added to make up to 1L.

Component	Final concentration
Tris base	25mM
Glycine	190mM
SDS	0.10% (w/v)

2.2.4.4.3 *Wet transfer of gel to membrane*

Prior to completion of gel electrophoresis, a 9 x 7.5cm piece of polyvinylidene fluoride (PVDF; BioRad, UK) membrane was immersed in 100% methanol for approximately 15 s in order to activate the membrane. This was transferred to ddH_2O for 2 min and subsequently equilibrated by soaking in transfer buffer (Table 12), along with two filter papers and two sponges for 10 min on a rocker.

Table 12: Composition of 1X transfer buffer. ddH2O was added to make up to 1L.

Component	Final concentration
Tris base	25mM
Glycine	190mM
Methanol	20% (v/v)

Following electrophoresis, the gel was removed and equilibrated in transfer buffer on a rocker for 10 min. The transfer cassette was assembled, sandwiching the gel and PVDF membrane between two pieces of filter paper and two sponges (BioRad, UK), ensuring the cassette remained wet at all times. The cassette was secured and placed into the transfer tank (Bio-Rad) along with a magnetic stirrer and filled with transfer buffer. Wet ice was added to the tank for the entirety of the transfer and replaced every ~30 min to prevent overheating. Transfer was carried out at a constant current of 0.2A for 2 h. Following completion, the membrane was fixed in methanol for ~15 s, followed by 5 min in 1x PBS on a rocker. PBS was replaced with blocking buffer (PBS; 5% non-fat milk powder, 1% Tween 20) and the membrane was further incubated for 1 h at room temperature on a rocker. This was to prevent/minimise any non-specific binding.

Appropriate concentrations of primary antibody diluted in blocking buffer were added to the membrane and incubated overnight on a rocker at 4°C. The following day, the membrane was washed with 1x PBS-T for 5 min (6x) on a rocker and incubated with an appropriate concentration of HRP-conjugated secondary antibody for 1 h at room temperature (Table). Finally, the membrane was subjected to 6 more washes with PBS-T for 5 min each.

2.2.4.4.4 ECL Western Blot Imaging

A mix containing equal parts of each of the enhanced chemiluminescence detection buffers (Pierce; ThermoFisher Scientific, UK) was prepared. The PBS-T was drained from the membrane and the detection buffer mix was added for at least 5 min whilst being covered to prevent exposure to light. Membranes were then imaged using ImageQuant. An image of the protein ladder was initially taken followed by the membrane which was exposed at automatic detection.

2.3 Tissue preparation for functional studies

2.3.1 Animals

The housing and use of animals in all experiments were carried out in accordance with UK Home Office regulations under the Animals (Scientific Procedures) Act, 1986. C57BL6/J mice (Charles River Ltd, UK) were used throughout all experiments at embryonic day 18, postnatal day 7 or 4-6 weeks old depending on the specific method. Mice were housed at 21°C in a 12-hour light/dark cycle with food and water available *ad libitum.*

2.3.1.1 Generation of acute hippocampal slices

Transverse brain slices (400µm) were prepared from male wild type C57BL6/J mice, aged 4-6 weeks. Mice were terminally anaesthetised with 4% isoflurane and immediately underwent

cervical dislocation and decapitation. The brain was gently removed and immediately placed in ice-cold 'slushy' high sucrose cutting solution (pH 7.4, comprising: 75mM sucrose, 87mM NaCl, 25mM $NaHCO_3$, 2.5mM KCl, 1.25mM NaH_2PO_4, 0.5mM $CaCl_2$, 7mM $MgCl_2$, 25mM glucose), which was continually carboxygenated (95% oxygen, 5% carbon dioxide, BOC Gas, Reading). Remaining immersed in solution, the whole brain was placed on filter paper, and using a razor blade (Campden Instruments Ltd., Loughborough, UK) the cerebellum, olfactory bulbs and anterior part of the forebrain was removed, and the brain was cut down the midline. Each hemisphere was placed midline facing down and the extreme dorsal and ventral ends were removed, providing a flat base by which to attach the brain to the slicing block (Figure 2.1A-B).

The brain was fixed to the slicing block using a small amount of cyanoacrylate glue (Loctite Super Glue, Hatfield, UK) and transferred to the slicing chamber of a Leica VT1200S containing ice-cold 'slushy' high sucrose cutting solution (see Figure 2.1C). Transverse hippocampal brain slices (400μm) were cut and carefully transferred to a beaker using a glass pipette containing carboxygenated artificial cerebrospinal fluid (aCSF, pH 7.4; comprising; 126mM NaCl, 10mM Glucose, 2mM $MgCl_2$, 2.49mM KCl, 1.25mM NaH_2PO_4, 26mM $NaHCO_3$, 2mM $CaCl_2$), heated to 37°C for 30 min to overcome the cellular 'shock' of slicing and continually carboxygenated. Following this, slices were left to equilibrate at room temperature for at least 1 h prior to experimental use to encourage longer-term viability (Bazelot *et al.*, 2015). All chemicals for cutting solution and aCSF were purchased from Fisher Scientific (Loughborough, UK), where both solutions were made a maximum of 24 h before use in each experiment, and stored at 4°C, if not used immediately.

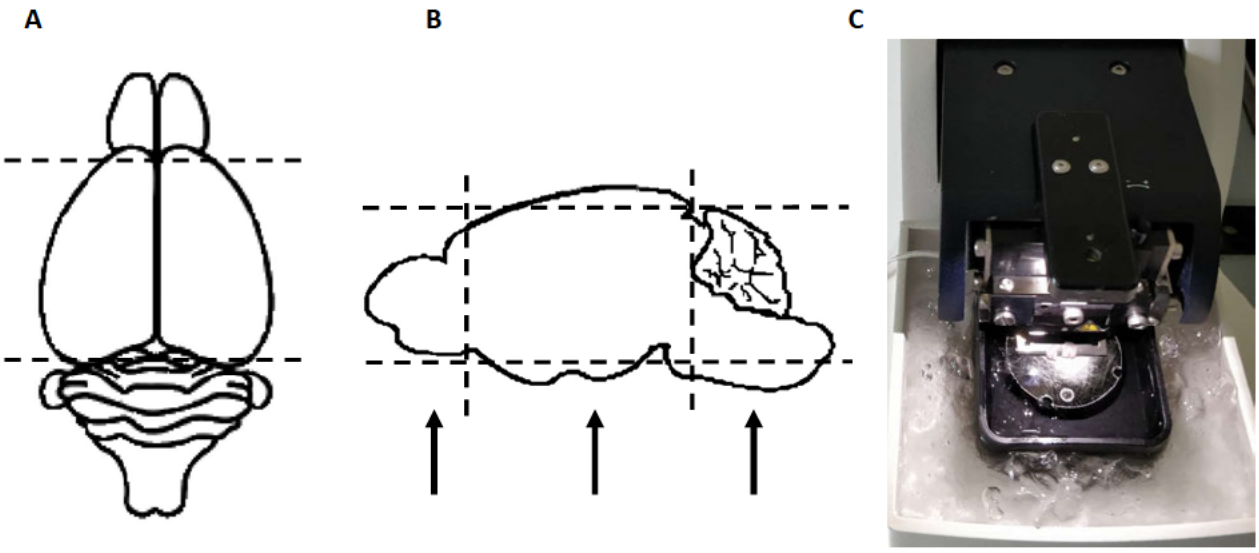

Figure 2.1: Dissection and slicing of mouse brain. A&B: Schematic showing top view **(A)** and side view **(B)** of mouse brain indicating cuts performed using a razor blade prior to slicing. Arrows indicate surface which was fixed to slicing block. **(C)** Representative image of trimmed mouse hemispheres mounted onto the vibratome slicing block within the ice-cold high sucrose cutting solution, surrounded by an ice-filled chamber.

2.3.1.2 Primary hippocampal neuronal cultures

2.3.1.2.1 Preparation of laminin coated coverslips

Coverslips (13mm; VWR, UK) were used as seeding surfaces inside 24-well plates. Coverslips were baked prior to use at 180° for 2-3 h to ensure sterility. To enhance cell adhesion to surfaces, coverslips were coated with PDL (20µg/mL) or 1-3 h followed by incubation with laminin (1µm/cm^2 in sterile ddH_20) overnight. Coverslips were washed thoroughly with PBS 3x prior to the addition of cells.

2.3.1.2.2 Removal and dissociation of E18 primary neuronal cells

Embryonic day 18 (E18) C57BL6/J mice were used for primary hippocampal neuronal cultures. Embryos were removed from the abdominal cavity of the adult female mouse following cervical dislocation. Heads were removed and placed in dissection media (DMEM-F12; Sigma Aldrich, UK). Once all brains had been isolated, the meninges were removed, and hippocampi and cortices dissected. Hippocampi were chemically dissociated using papain (20 min incubation at 37°C). DNase **(**deoxyribonuclease I from bovine pancreas**;** Sigma Aldrich, UK) was added (2mg/ml in PBS) for 30 s, to reduce any cell clumping caused by released DNA during dissociation. The papain and DNase solution were removed, and tissue washed 3x in dissection medium, and finally transferred to warm culture medium (Table 13). The cell suspension was then triturated using a P1000 pipette 30x. Cortical cell survival was low when dissociated with papain and triturated using P1000 pipette, therefore trypsin was used hereafter for dissociation of cortical cells (10 min incubation at 37°C), this reaction was inhibited by the addition of 10% FBS. The cells were transferred to warm culture medium and triturated using needles (3x21G followed by 3x23G). Both cell suspensions were topped up to 5ml and allowed to sit enabling any large clumps of debris to settle. Supernatant was transferred to new tubes and brief centrifugation (250rcf, 5 min) was performed to pellet the cells. The supernatant was removed and discarded, and pellet resuspended before topping up to 5ml with fresh culture medium. The number of healthy cells were determined via manual counting using a haemocytometer within a 10µl sample (using a Nikon TMS microscope) or using an automated cell counter (Countess II FL Automated Cell Counter; Invitrogen). The estimated number of cells was multiplied to calculate the number of cells in 5ml of culture medium. From this, cell suspensions were diluted in appropriate volumes of culture medium (as detailed in Table 13) to achieve a seeding density of $1.5x10^5$ hippocampal cells/well and $2x10^5$ cortical cells/well.

2.3.1.2.3 *Primary hippocampal neuronal cell culture*

Cells were subjected to a 50% medium change after 2-3 days in culture.

Table 13: Culture medium used for growth of primary hippocampal neuronal cells.

Reagent	Final Concentratio	Active Ingredients	Function	Supplier
Neurobasal medium	N/A	Vitamins, amino acids, inorganic salts	Basic stable medium for cell culturing	Gibco/Life Technologies
B27	1%	Serum free supplement	Promote stem cell differentiation towards neurons	Gibco/Life Technologies
GlutaMax	2mM	L-alanyl-L-glutamine dipeptide	Essential amino acids (stabilised form of L-Glutamine)	Gibco/Life Technologies
FBS	2.5%	N/A	Growth factors promote cell proliferation	Gibco/Life Technologies
Penicillin/Streptomycin	100U/ml/100µg/ml	Antibiotic	Prevents growth of bacteria, gram positive	Gibco/Life Technologies

2.3.2 Xenopus oocyte expression system

2.3.2.1 mRNA preparation and GluN1/GluN2A receptor expression

Glutamate ionotropic receptor NMDA subunit 1/2A (GRIN1/GRIN2A) constructs coding for GluN1 and GluN2A were generated by Genscript (Piscataway, NJ) using restriction sites BamHI and PmeI respectively. Linearization of GRIN1/GRIN2A plasmids were performed using the same restriction enzymes as above. Once linearized, plasmids were used for *in vitro* transcription using mScript (Cellscript, Madison, WI). Transcripts were capped, polyA tailed and purified, and the size was confirmed by gel electrophoresis. mRNA preparation for oocyte injections were performed by RD_Biotech (Besancon, France). GRIN1/GRIN2A human mRNA (0.15ng solution, total volume 40nl ratio 1:5) was injected into the cytoplasm of Xenopus oocytes (stage V-VI) previously dissected and de-folliculated (provided by EcoCyte Bioscience, Castrop-Rauxel, Germany) via an automated micro-injector (Robocyte, MCS, Reutlingen, Germany) using a glass micropipette (5.5µm diameter, MCS). Oocytes were left to express receptors for 72 h at 17°C in a Barth's solution (pH 7.4, comprising 88mM NaCl, 1mM KCl, 2.4mM $NaHCO_3$, 0.33mM $Ca(NO_3)_2$, 0.41mM $CaCl_2$, 0.82mM $MgSO_4$, 5mM Tris-HCl, supplemented with penicillin/streptomycin (100IU/mL), with solution changed daily.

2.4 Electrophysiology

Electrophysiology is an essential tool in the study of single cells and ultimately neuronal networks within the brain. The cell membrane controls the exchange of electrically charged ions across the membrane, such as Na^+, K^+, Cl^- and Ca^{2+}. Distribution of ions produces an electrical potential across the cell membrane (which is measured as voltage), where the inside of the cell is more negatively charged than the outside. Changes in this electrical potential can be measured electrophysiologically in a number of ways; either extracellularly or

intracellularly (Carter and Shieh, 2015). The methods outlined below use an example of both extracellular (MEAs) and intracellular (TEVC/whole cell patch clamp).

2.4.1 Multi-electrode array (MEA) electrophysiology

Electrical activity is essential for neuronal communication, which occurs across an inter-connected network. Therefore, it is useful to record neuronal activity as such in order to further understand not only normal brain functions, but also diseased states. MEAs are a frequently used *in vitro* models as extracellular recordings can be performed using multiple electrodes across a large area. MEAs are also useful in terms of their ability to stimulate presynaptic pathways whilst simultaneously recording their postsynaptic response (Steidl *et al.*, 2006; Hill *et al.*, 2010).

2.4.1.1 MEA recordings and long-term potentiation

Evoked electrical activity across hippocampal slices was monitored and recorded using titanium nitrate MEAs (MCS, GmbH, Reutlingen, Germany); 64 electrodes in an 8x8 layout (including one reference electrode), each electrode measuring 30µm in diameter with a 200µm spacing between electrodes. Prior to recording, MEAs were cleaned with 5% (w/v) Terg-A-Zyme (Cole-Palmer, UK) for a minimum of 20 min, rinsed with tap water followed by distilled water and allowed to air-dry. MEAs were subjected to 100% methanol using a cotton bud to gently remove any grease or dirt from the electrodes and pads, and finally plasma cleaned (Harrick Plasma, New York, USA) to make the electrode surface more hydrophilic. Slices were placed and positioned on MEAs in aCSF using a Leitz Diavert microscope, with images of the slice and electrode position being acquired via a camera connected to a PC. Slices were positioned so that the Schaffer collateral and CA1 areas were covering the electrodes (Figure 2.2B) and weighed down with a slice harp (Harvard Apparatus, UK) to ensure constant contact

with the electrodes. MEAs were carefully placed into the head stage (MEA1060-Inv-BC, MCS, Germany), continually perfused with carboxygenated aCSF (~3mL/min) and maintained at 32°C in order to maximise slice viability. Slices were allowed to equilibrate in the head stage for at least 10 min before any stimulation was applied. Following this, bi-phasic voltage pulses were applied to one electrode (STG2008 stimulator, MCS; 100µs biphasic pulses, ± 0.5-2.0V, every 30 s) to evoke field excitatory postsynaptic potentials (fEPSPs) (Hill *et al.*, 2010). Signals were amplified by a 60-channel head-stage amplifier (MEA60 System, MCS, Germany), and simultaneously sampled at 10kHz per channel and amplified at 1200x gain. Data acquisition to a computer was carried out using the software MC_Rack which monitored and recorded data for offline analysis at a later date.

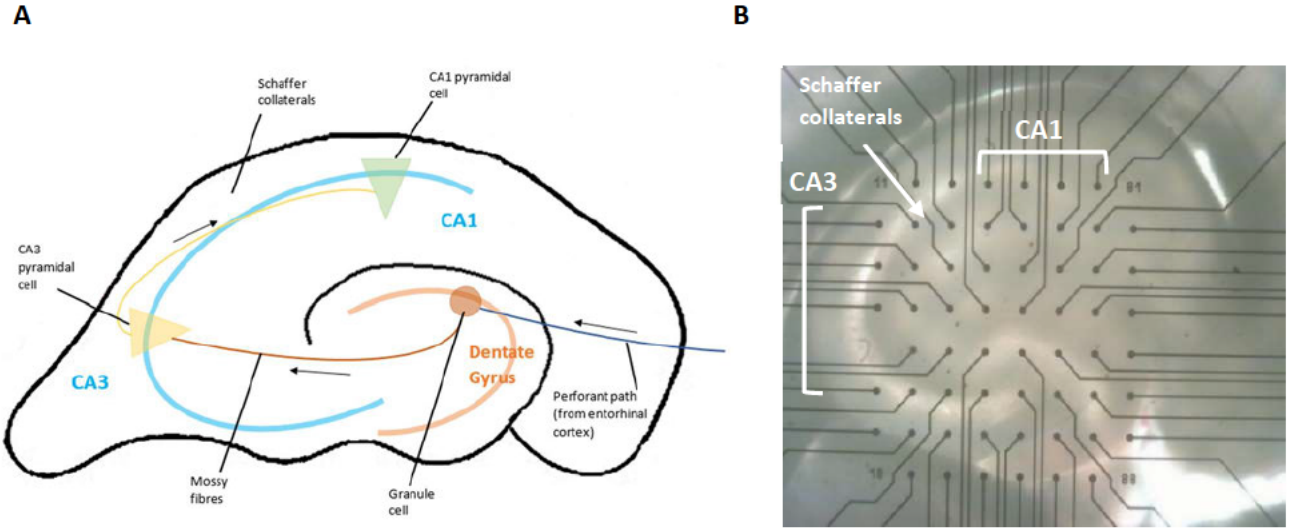

Figure 2.2: Schaffer collaterals within hippocampal slice. A: Schematic of the hippocampus within the brain, identifying the Schaffer collaterals pathway running from CA3 region to CA1 region (pathway indicated in yellow). **B:** Representative image of an acute hippocampal brain slice laying on 64 channel MEA (8x8 array), indicating both CA3 and CA1 areas, as well as the Schaffer collaterals pathway.

Using a captured image of the slice over the MEA (Figure 2.2B), an appropriate stimulation electrode was selected using MEA_Select. Paired-pulse recordings were carried out with an inter-stimulus interval of 50ms, and long-term potentiation (LTP) induction was carried out on Schaffer collateral-CA1 pathway (as shown in Figure 2.2A) using high frequency stimulation (HFS; 100Hz) to identify NMDAR activation and functionality. Paired pulse fEPSPs were evoked every 30 s both pre- and post-LTP induction, being recorded for 30 min pre-LTP induction to establish a steady baseline and for 60 min post-LTP induction to establish whether any long-lasting potentiation had been evoked. The fEPSPs could be isolated into separate glutamatergic components; either AMPARs and kainate receptors, or NMDARs. AMPAR/kainate receptors or NMDAR were blocked by addition of glutamatergic antagonists 6-cyano-7-nitroquinoxaline-2,3-dione (CNQX; Abcam, UK) or DL-2-Amino-5-phosphonopentanoic acid (DL-APV; Abcam, UK), respectively, to the perfusing aCSF. CNQX was dissolved in ddH20 and used at a final concentration of 5μM, and DL-APV was dissolved in ddH20 and used at a final concentration of 50μM. To determine any functional effect of generated Aabs on NMDARs and neuronal networks, slices were pre-incubated for 1 h in aCSF containing Aabs (1:1000 dilution) with continuous carboxygenation. Slices were incubated with either mNMDAR/rNMDAR or mIgG2b/rIgG antibodies as positive and negative controls respectively (1:1000 dilution). These slices were then subjected to the protocols as described above. One slice per animal was used per condition.

2.4.2 Patch clamp electrophysiology

Patch clamp is a method of measuring intracellular signals from a single cell. It can measure the amount of current across the cell membrane at a fixed voltage (voltage-clamp). A glass micropipette is used to make tight contact with a ‘patch’ of neuronal membrane. Following a

small amount of suction, a tight seal is formed between the two. If further suction is applied, the membrane patch within the pipette is disrupted, causing the interior of the pipette to become continuous with the cytoplasm of the cells (whole-cell configuration). This allows measurements of electrical potentials and currents from the entire cell (Hill and Stephens, 2021). Other configurations of patch clamp exist; inside-out and outside-out recordings which are beneficial to measure single channel currents and the influence of intracellular/extracellular molecules (Hamill *et al.*, 1981).

2.4.3 TEVC in Xenopus oocytes

TEVC is a type of whole cell recording used on large cells (such as oocytes) as two recording electrodes are inserted into the cell. One electrode is used to measure voltage and the other is used to inject current (Figure 2.3) (Dascal, 2001).

TEVC recordings were performed using an automated platform (HiClamp, MCS). Electrodes (0.1-1MΩ resistance) were filled with potassium chloride (KCl 1.5M) and potassium acetate (KAc 1.5M). Oocytes were impaled, and voltage clamped at a holding potential of -60 mV. After the impalement, oocytes were rinsed with normal frog ringer buffer for 60 s followed by a stabilising period of 60 s (pH 7.85; containing 88mM NaCl, 2.5mM KCl, 1.8mM $CaCl_2$, 5mM HEPES, with EDTA (10µM) being added to chelate zinc ions Zn^{2+}). The cells were briefly exposed to 1µM glutamate/10µM glycine (10 s) every 3 min for 12 min to ensure the cells were expressing the NMDAR subunits and were responsive, as well as ensuring minimal leakage when clamped. The last 6 min of these test responses were considered as control amplitude responses to glutamate. Following this, cells were exposed to either NMDAR1 Aabs or rabbit IgG either acutely or chronically (1:1000 or 1:300 dilution), whilst being exposed to 1µM glutamate/10µM glycine (10 s) throughout in order to monitor NMDAR current. The NMDAR antagonist MK-801 and allosteric modulator TCN-201 were also applied in

increasing concentrations (ranging from 10nM to 1μM), acting as positive controls for the systems. To evaluate the cellular response, area under the curve (AUC) for each glutamate-evoked current was calculated and normalised to AUC of control responses.

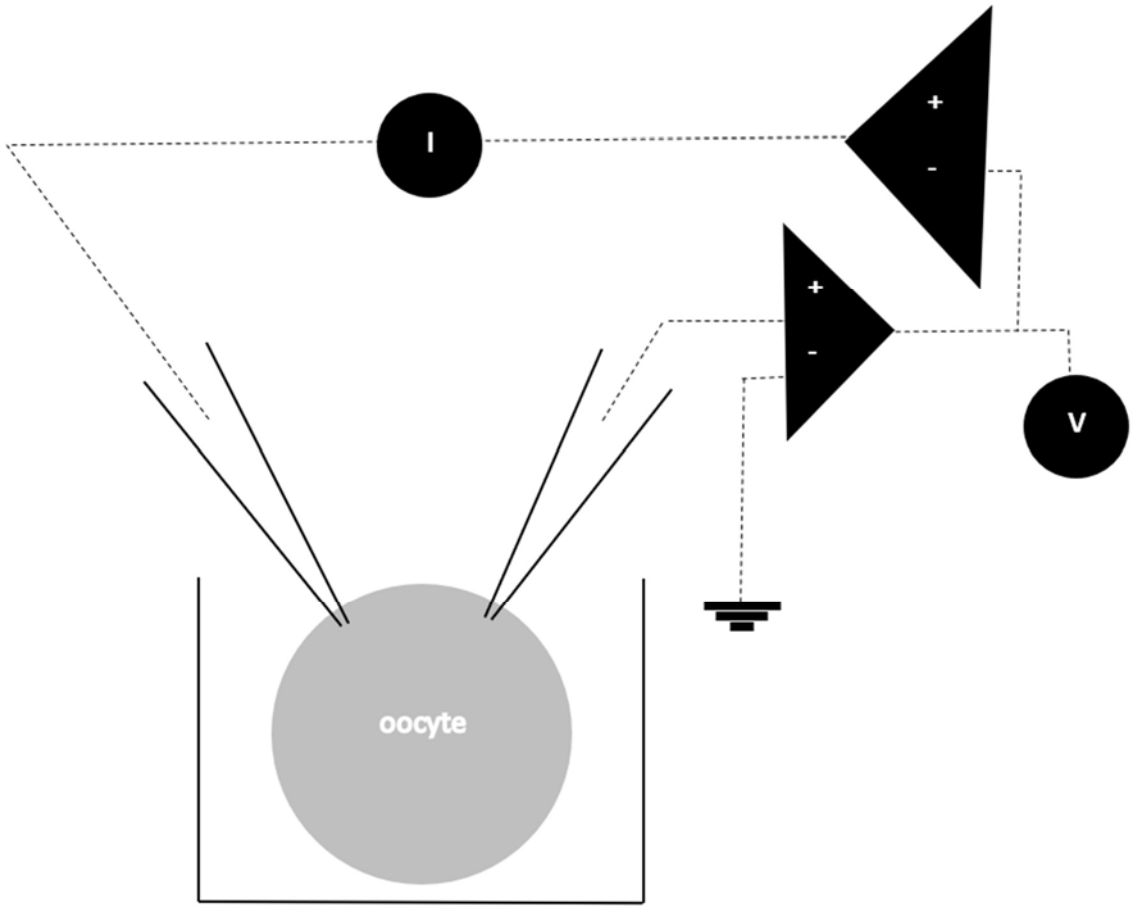

Figure 2.3: A schematic of two-electrode voltage clamp on Xenopus oocytes. This method utilises two pipettes, one for sensing voltage (V) and the other injecting current (I). The microelectrodes compare the membrane potential against a holding voltage (controlled via a computer), calculating the current flowing across the membrane.

2.4.4 Whole cell patch clamp and primary hippocampal cultures

Patch clamp can be performed in many different configurations, allowing the study of all ion channels within the cell membrane (whole-cell) (Purves *et al.*, 2004). The functionality of NMDAR and AMPAR Aabs were further investigated using whole-cell patch-clamp (voltage clamp) on primary hippocampal neurons. EPSCs were recorded from primary neurons from day *in vitro* (DIV) 7 onwards, at which point, either acute or chronic incubation with Aabs was carried out and any changes in spontaneous firing was recorded.

The intracellular solution was prepared using the recipe shown in Table 14. The buffer was adjusted to pH 7.3, and osmolarity to ~280 mOsm, and subsequently aliquoted and stored at –20°C until use. 1L of extracellular buffer was prepared using the recipe in Table 14, with pH being checked and adjusted to 7.4, and osmolarity checked and adjusted to ~300mOsm. This was stored at 4°C until use.

Table 14: Composition of intracellular and extracellular patch clamp solution. For intracellular buffer, KOH was used to adjust pH to 7.3 and aliquoted (0.5ml) and stored at -20. Extracellular solution, pH was adjusted with NaOH to pH 7.4 and stored at 4 degrees until use.

Intracellular solution		**Extracellular solution**	
Component	**Final Conc.**	**Component**	**Final Conc.**
K Gluconate	145	NaCl	130
NaCl	5	KCl	3
HEPES free	10	HEPES free	10
EGTA	0.2	$MgCl_2$	1
GTP – Na salt	0.3	$CaCl_2$	2
ATP – Mg salt	4	Glucose	30

2.4.4.1 Patch pipettes

Patch pipettes were pulled from borosilicate glass using horizontal electrode puller (P1000 Flaming/Brown micropipette puller) to make patch pipettes with a resistance of 3-10MΩ. Pipettes were backfilled with an intracellular solution (as detailed in Table 14). Multiple patch pipettes were prepared before experiments.

2.4.4.2 Whole-cell patch-clamp

Cells were initially transferred into the recording chamber, immersed in extracellular solution (without perfusion) and a single isolated cell was positioned at the centre of the microscope. Patch pipettes were inserted into the electrode holder, which was attached to the head-stage and connected to a patch clamp amplifier. Prior to entering the patch pipette into the bath solution, positive pressure (~1ml) was applied using a 1ml syringe connected to the electrode holder via plastic tubing. Using the 'coarse' setting, the micromanipulator was used to lower the pipette into the bath until it was just above the cell. A test pulse (50 ms, 5 mV) was applied to monitor the pipette resistance in Clampex 10.6 software (Molecular Devices, UK) and current flowing in this 'open' configuration, was monitored and offset to zero using the MultiClamp 700B commander software (Molecular Devices, UK). The pipette was then gradually lowered using the 'fine' setting of the micromanipulator until the tip was touching the cell. Positive pressure was released from the patch pipette, facilitating the formation of a 'gigaseal' i.e., a resistance > 10^9 ohms. To achieve whole cell configuration, sharp suction was applied to rupture the cell membrane under the pipette tip. This resulted in the production of fast and slow transients at the start and end, respectively, of the test pulse, which were electronically compensated for using the MultiClamp 700B commander (Molecular Devices). Cells were held at -70mV throughout the experiment, without any perfusion. The values for series resistance and membrane capacitance were recorded and monitored throughout the

experiment. Any significant deviations in these parameters resulted in the recording being discarded. Current signals were filtered at 2 kHz and sampled at 10 kHz using an Axon Digidata 1550B.

2.4.4.3 Spontaneous excitatory postsynaptic currents (sEPSCs)

Once a stable whole-cell configuration had been achieved, sEPSCs were recorded for 10 min to obtain a baseline. If AMPAR Aabs were being tested, pharmacological inhibitors bicuculline methiodide (BMI; 10µM; Abcam) and DL-APV (50µM) were added prior to baseline, whereas if NMDAR Aabs were being tested the pharmacological inhibitors BMI and 2,3-Dioxo-6-nitro-1,2,3,4-tetrahydrobenzo[f]quinoxaline-7-sulfonamide (NBQX; 5µM, Abcam, UK) were added prior to baseline to isolate events for the respective receptor being investigated. For 'acute' application experiments, following a 10 min baseline, Aabs were either directly added to the bath extracellular solution and incubated for 10 min or 30 min and sEPSCs were monitored throughout.

For 'chronic' application experiments, primary neurons were incubated with either Aabs for 24 h prior to patch clamp recording. Here, no baseline could be recorded, but 30 min of activity was monitored following the application of appropriate pharmacological inhibitors.

For both acute and chronic experiments, a negative control (rIgG) was used to ensure any effects observed was due to receptor specific Aabs, and not non-specific effects.

2.4.4.4 Miniature excitatory postsynaptic currents (mEPSCs)

To help assess whether any functional effects observed may be presynaptic in nature, the above experiments were carried out in the presence of tetrodotoxin (TTX; 1µM, Abcam, UK) to isolate mEPSCs, with the same parameters being measured.

An overview of all experiments performed for each Aab is detailed in Figure 2.4.

2.5 Statistical Analysis

All data are presented as mean ± standard deviation (SD) and analysed using GraphPad Prism 7.00 (GraphPad Software, Inc). MEA experiments were analysed via Mc_Rack (MultiChannel Systems) and patch clamp experiments were analysed using a template search function (Clampfit, Molecular Devices, UK) and exported to Microsoft Excel for sorting. All data were exported to Microsoft Excel and GraphPad Prism. All data sets were tested for normality using D'Agostino Pearson normality test, where all data passed and therefore was tested for significance using appropriate Student's t-tests or one-way analysis of variance (ANOVA). Two-way ANOVAs were also conducted, where F values are reported, and differences are considered as statistically significant when $p<0.05$. Finally, cumulative frequency plots were generated for AMPAR patch-clamp experiments, where inter-event intervals were compared between Aab-incubated cells and control. These plots were analysed statistically by performing Kolmogorov-Smirnov tests and considered significant when $p<0.05$.

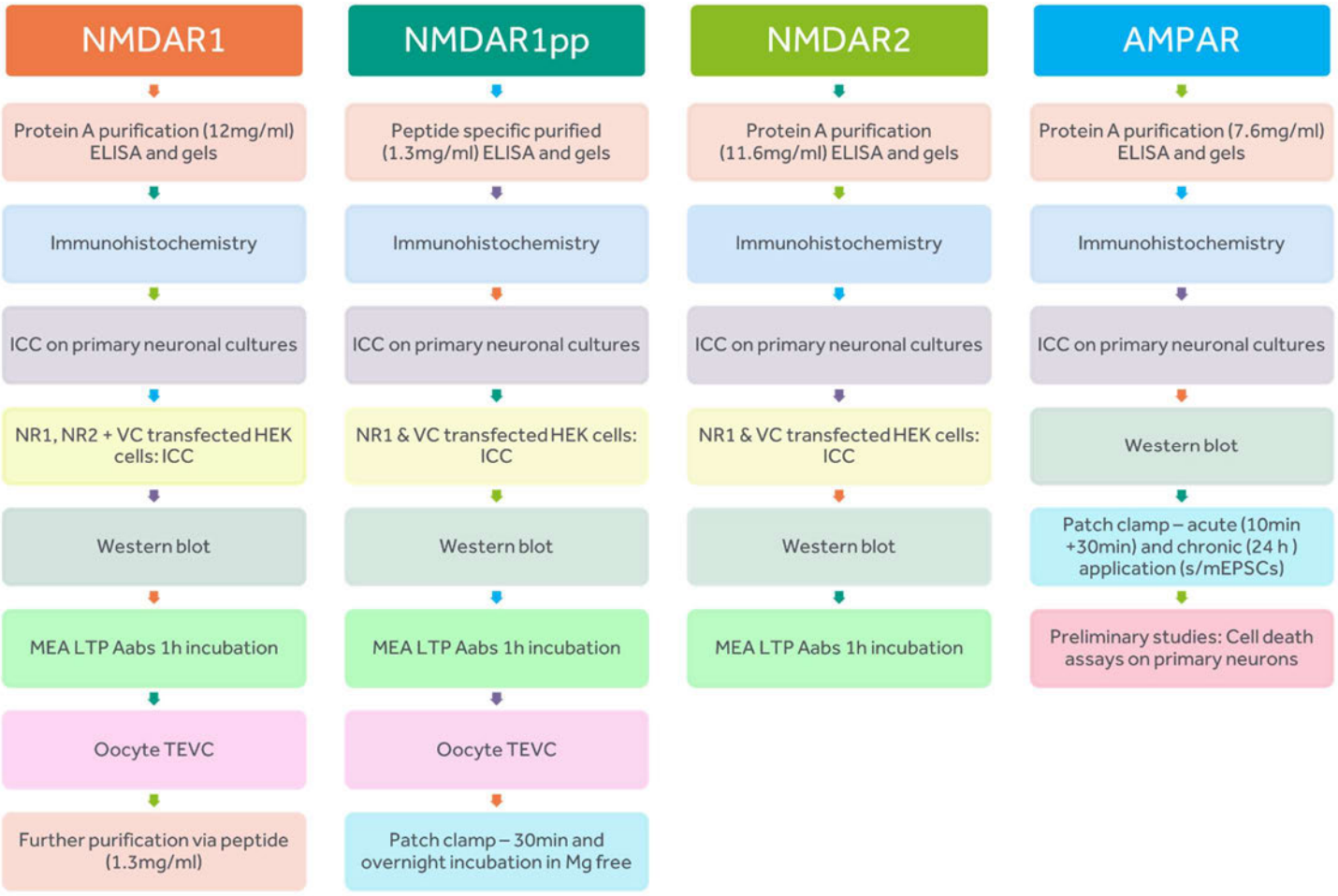

Figure 2.4: Schematic of all experiments performed throughout this thesis with each generated Aab.

3. Generation and characterisation of NMDAR Aabs

3.1. Introduction

NMDARs are members of the glutamate ionotropic receptor family, involved in excitatory neurotransmission. NMDAR Aabs have been found in patients with ANRE and autoimmune epilepsy. It is not fully understood whether these NMDAR Aabs are pathogenic or if they serve as a compensatory mechanism in response to seizures; however, it has been shown that *in vitro* application of patient Aabs to primary hippocampal neurons results in binding to NMDARs, cross-linking and subsequent internalisation (Hughes *et al.*, 2010). How these *in vitro* effects translate to *in vivo* behavioural changes is not fully understood. Previous studies have shown that infusion of patient NMDAR Aabs in mice resulted in epileptic seizures (Wright *et al.*, 2015), behavioural changes, and memory impairment (Planagumà *et al.*, 2015). Understanding if and how these Aabs may cause these behavioural changes is of huge importance and could lead to developing compounds which can intervene in this mechanism. In addition, understanding how these NMDAR Aabs act with regard to autoimmune epilepsy, whether acting pathogenically or as a compensatory mechanism in response to seizures, would aid in developing a therapy for people who have these Aabs in their serum. In order to investigate the potential pathogenicity of NMDAR Aabs, Aabs were generated using peptide immunisation, with peptides being based on the binding location of patient NMDAR Aabs. This chapter details the experiments used to generate and assess the specificity of anti-NMDAR Aabs.

3.2 Production of rabbit polyclonal NMDAR 1 Aabs (rabbit #1)

Regions of high immunogenicity as well as proximity to where patient anti-NMDAR Aabs bind (see section 2.1) were identified within the extracellular domains of NR1 subunit of NMDARs (regions chosen highlighted in Figure 3.1). Certain peptides (2, 4 and 5, sequences

detailed in Table 1 and illustrated in Figure 3.1) were cyclised via a thioester in an aim to better represent the natural conformation of these sequences, as well as to promote molecular stability (Purcell 2007). All peptides were subsequently conjugated to KLH, BSA and OVA externally (Peptide Synthetics). These conjugated peptides were combined and used to immunise one rabbit (see section 2.1.1) in order to elicit an immune response.

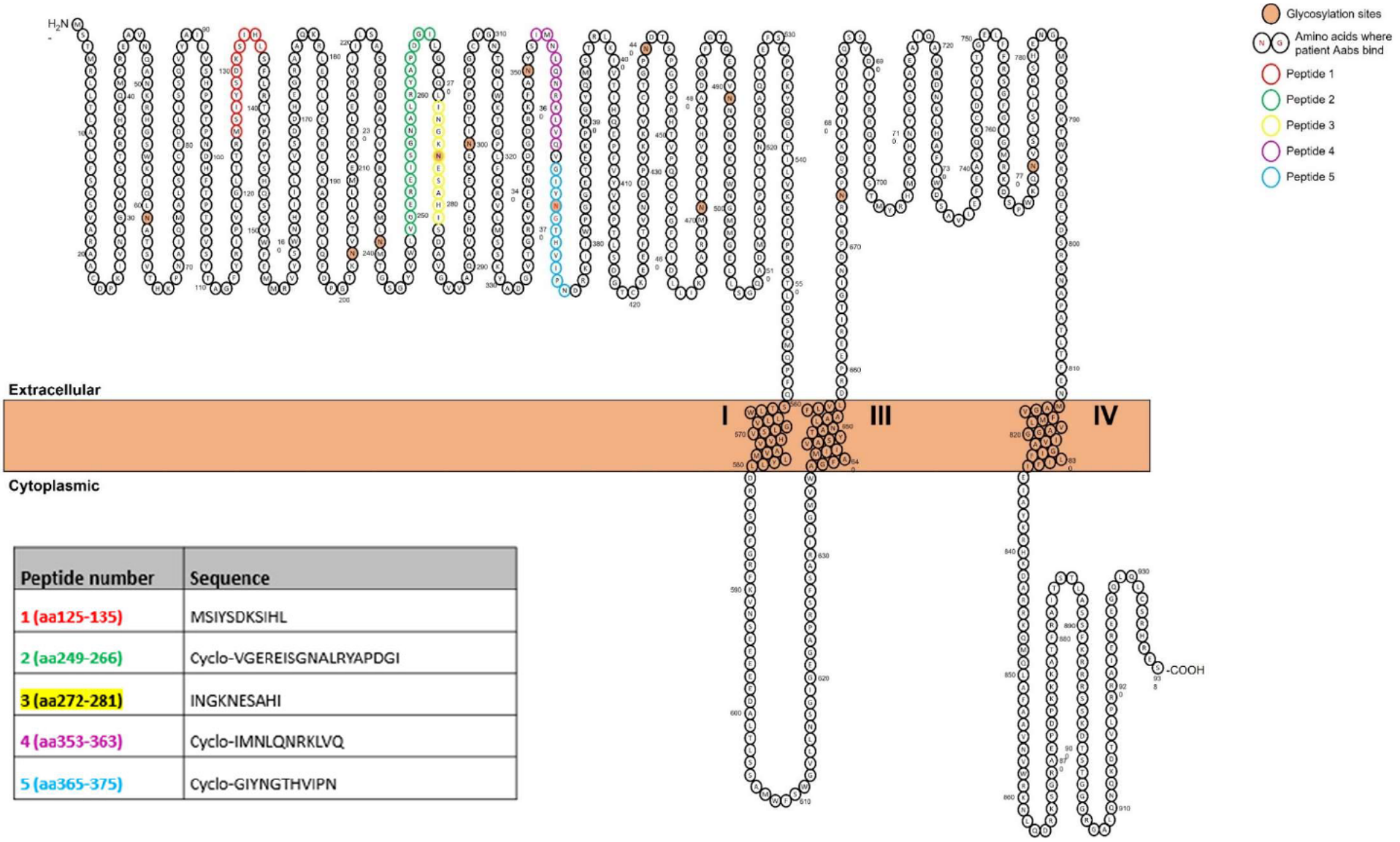

Peptide number	Sequence
1 (aa125-135)	MSIYSDKSIHL
2 (aa249-266)	Cyclo-VGEREISGNALRYAPDGI
3 (aa272-281)	INGKNESAHI
4 (aa353-363)	Cyclo-IMNLQNRKLVQ
5 (aa365-375)	Cyclo-GIYNGTHVIPN

Figure 3.1: NMDAR peptide sequences used for the immunisation of rabbit #1. All peptides were located within the amino terminal domain (ATD) of NR1 subunit and generated with the addition of a C residue and an Ac residue on either end. Peptides 2, 4 and 5 were cyclised via a thioester to help better represent the true epitope.

3.2.1 Titres and ELISA of antibody sera

The rabbit immunisation procedure was followed as described in section 2.1.1. Rabbit bleeds (BL) were taken 14 days after immunisation boosts, and 7 days after the final immunisation; serum titres were monitored using an ELISA to detect the presence of IgG antibodies against the peptides. The total number of immunisation boosts was determined based on ELISA results. As expected, no detectable immune response was observed against any peptide or the ATD at BL0 (pre-immunisation). Following the first immunisation (BL1), minimal binding to each peptide was detected, similar to that of BL0; however, following the second and third immunisation (BL2 and terminal bleed, respectively), an increase in binding was detected to peptides 2, 4 and 5, with the terminal bleed binding to these peptides being as low as 1:100,000 dilution (Figure 3.2B, D and E, respectively). Similar results were observed when binding of terminal bleed sera was tested against the ATD protein in its natural conformation, which was used to assess if the Aabs generated would bind to native ATD, as well as immunisation peptides. The ATD was detected, in particular following immunisations 2 and 3, detectable as low as 1:100,000 dilution (Figure 3.2F). In contrast, minimal binding was detected to peptides 1 and 3 following all immunisations boosts, where a slight increase in binding was detected by terminal bleed sera only at 1:100 dilution (Figure 3.2A and C).

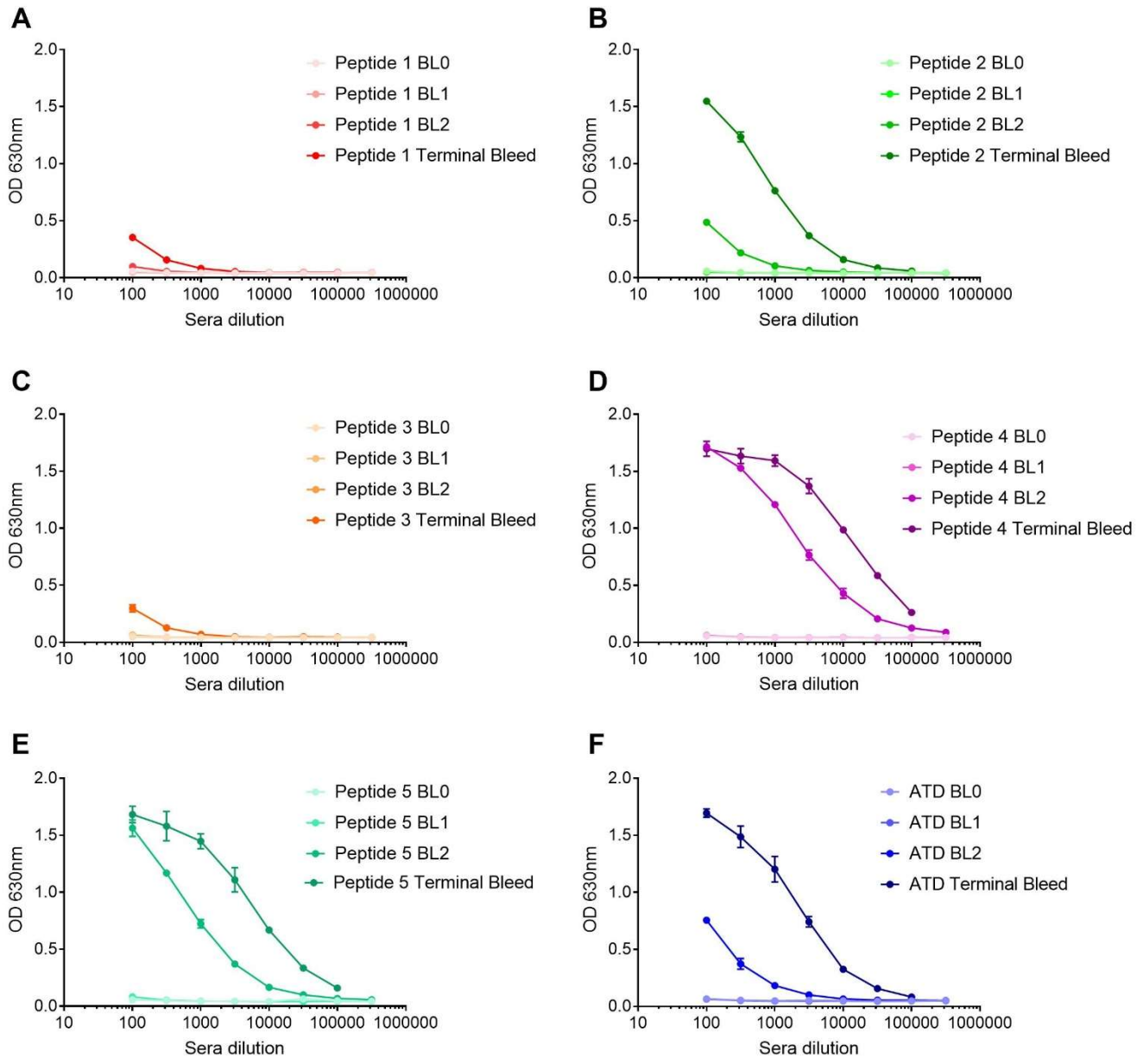

Figure 3.2: Rabbit anti-NMDAR1 immunogenicity response. Pre-immunisation bleed (BL0), bleed 1 (BL1), bleed 2 (BL2) and terminal bleed responses to peptides 1-5 (A-E respectively) used for immunisations. Binding of sera to native NR1 amino-terminal domain (ATD) in its natural conformation occurred, which increased with each immunisation boost **(F)**. An increase in response to the peptides was observed with each immunisation boost, with the largest responses against peptides 2, 4 and 5, as well as the ATD protein (panels B, D, E and F respectively). N=3 technical replicates per dilution, n=1 rabbit.

3.2.2 Purification and analysis of NMDAR1 Aabs

Terminal serum from the NMDAR1-immunised rabbit was purified using Protein A resin to isolate total IgG from final serum as described in section 2.1.3 (henceforth known as NMDAR1 Aabs). IgG was then quantified and analysed using SDS-PAGE and ELISA. Fractions from all steps within the purification process: pre-purification, wash 1, wash 2, eluates 1-6, and post-purification were analysed using SDS-PAGE and subsequent Coomassie staining. Proteins were detected in the pre-purification fraction at 150 kDa, 90 kDa, 50 kDa as well as 25 kDa, of which the band at 150 kDa is expected to be IgG (Figure 3.3A). The presence of a band at the expected IgG size of 150 kDa in eluates 1-4, and the absence of a band at this size in both wash 1 and 2, as well as the absence in 'post-purification' column, indicate successful purification of total IgG from terminal serum. All other proteins detected in the 'pre-purification' column at bands of 90 kDa, 50 kDa and 25 kDa, among others, were not detected in any eluates, but instead were present in the 'post-purification' fraction (Figure 3.3A) highlighting the specificity of the purification for IgG only.

Quantification of total IgG was performed using a protein A280 nanodrop, measuring absorbance at 280nm to determine protein concentration. This revealed 12mg/ml total IgG was acquired from NMDAR1 peptide immunisation, of which anywhere between 1-10% is predicted to be target (NMDAR) specific (Hnasko and McGarvey, 2015). To verify that the purification process had no negative effect on NMDAR1 Aab specificity to the immunisation peptides, a repeat ELISA was carried out using the total protein A-purified IgG (Figure 3.3B); this revealed increased binding to peptides 2, 4 and 5 and the ATD protein, with binding detected as low as 0.1µg/ml. Minimal binding was detected with peptides 1 and 3 (Figure 3.3B), even at the highest dilution of 10µg/ml. These data are in line with results seen pre-purification, with increased binding being detected against peptides 2, 4, 5 and the ATD, with minimal binding against peptides 1 and 3 (Figure 3.2A-F).

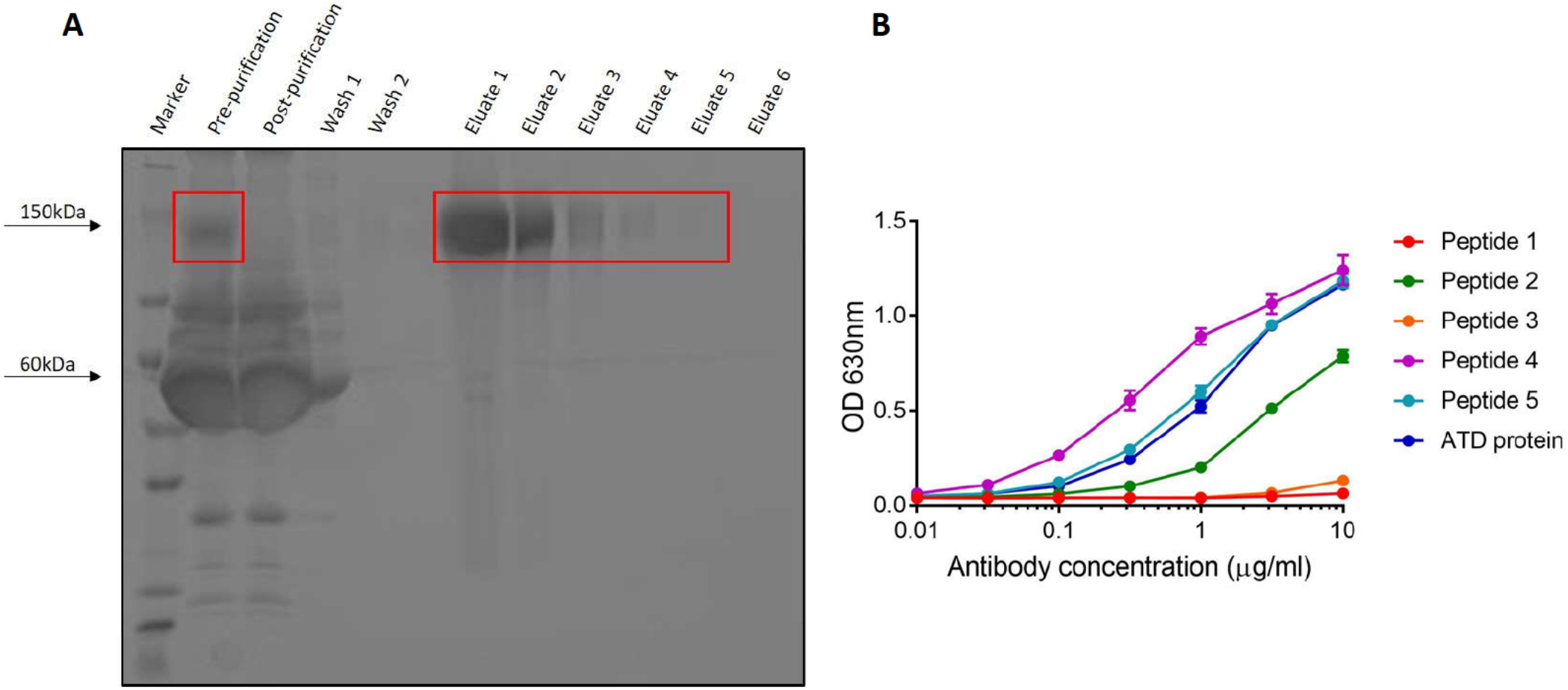

Figure 3.3: Protein A purification of NMDAR1 Aabs. (A) SDS-PAGE analysis of rabbit serum purified by protein A-sepharose resin. Analysis of all fractions revealed a specific band at 150kDa in pre-purification sample and all eluates, which is not present in the post-purification sample. **(B)** Protein A purified NMDAR1 Aabs revealed greater binding to peptides 2, 4 and 5 and ATD protein, comparable to pre-purification. N=3 technical replicates per concentration.

Further quantification was carried via SDS-PAGE and subsequent Coomassie staining. This was performed to validate the concentration of total IgG measured by comparison to a commercial rabbit total IgG of known concentration. A titration of both NMDAR1 Aabs and control rIgG concentrations was tested. Both antibodies produced bands at the expected size of 150 kDa; in addition, all bands produced were of comparable intensity and size at all dilutions tested (Figure 3.4).

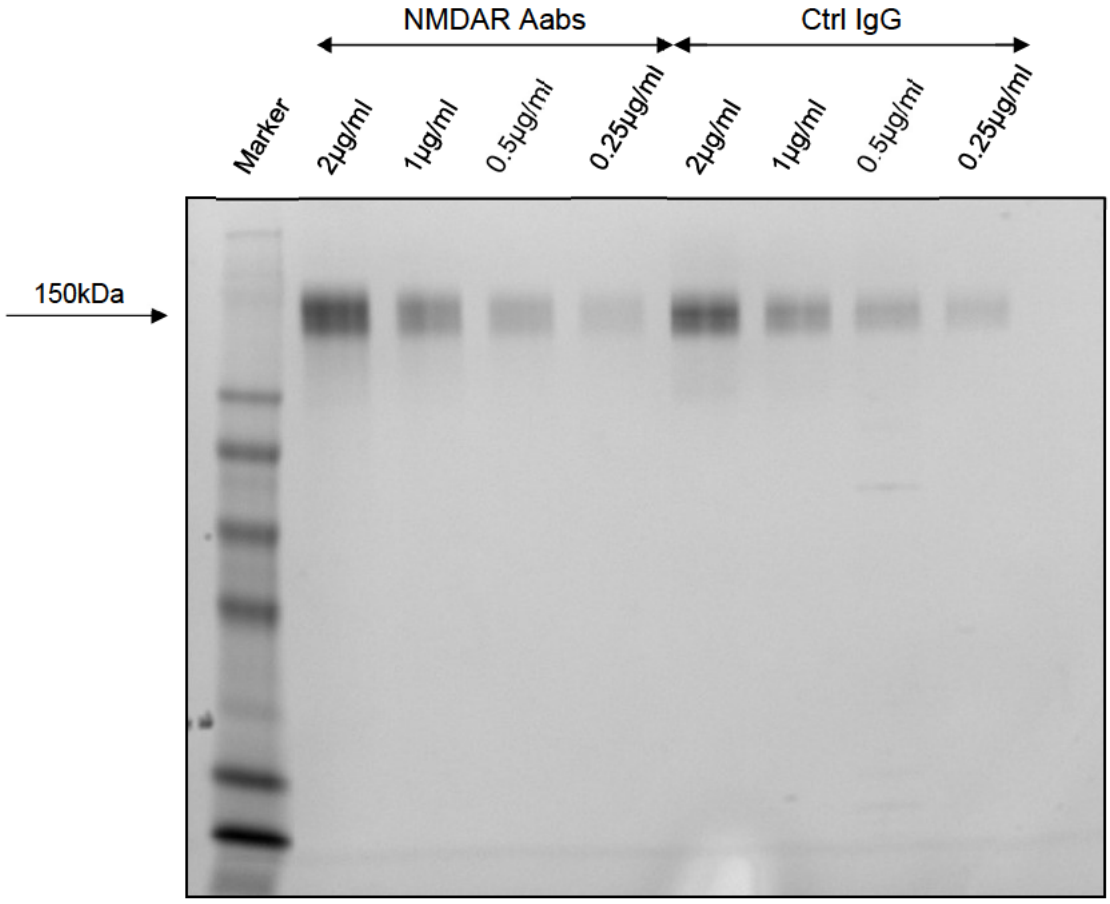

Figure 3.4: Protein A purified NMDAR1 Aabs are comparable to control rabbit IgG. Concentration of NMDAR Aabs determined via A280 measurement is comparable in band size and dilution as control IgG of known concentration (n=1 technical replicate).

3.3 Characterisation of NMDAR1 Aabs using *in vitro* models.

3.3.1 NMDAR1 Aab detection of NMDARs in NR1-transfected HEK cells

In order to analyse the specificity of NMDAR1 Aabs, HEK cells were transfected with either a vector encoding the NR1 subunit or an empty vector (see section 2.2.1). The day after transfection, cells were fixed with PFA in order to preserve cells by preventing degradation and autolysis and incubated with NMDAR1 Aabs and ICC performed (as described in section 2.2.1.1).

NMDAR1 Aabs positively stained NR1-transfected HEK cells (as shown by the white arrows Figure 3.5A), while also eliciting some low-level background staining (as shown by white arrowheads; Figure 3.5A). These positively stained cells co-localised with cells, which were also positively labelled with the commercial anti-NR1 antibody mNMDAR (as shown by white arrows; Figure 3.5A). A second commercial antibody was also tested; rNMDAR, which elicited similar staining to that of NMDAR1 Aabs, where positively stained cells were also co-labelled with another commercial antibody mNMDAR (white arrows; Figure 3.5B). Negative controls were also employed; class specific antibodies rIgG and mIgG2b, as well as a secondary-only antibody incubation. The class-specific negative control rIgG demonstrated low levels of background staining (as shown by white arrowheads; Figure 3.5C), as also seen with NMDAR1 Aabs, but importantly no clear, bright labelling of NR1-tranfected HEK cells was detected with rIgG incubated cells. The secondary-only control showed no labelling in NR1-transfected HEK cells (Figure 3.5D).

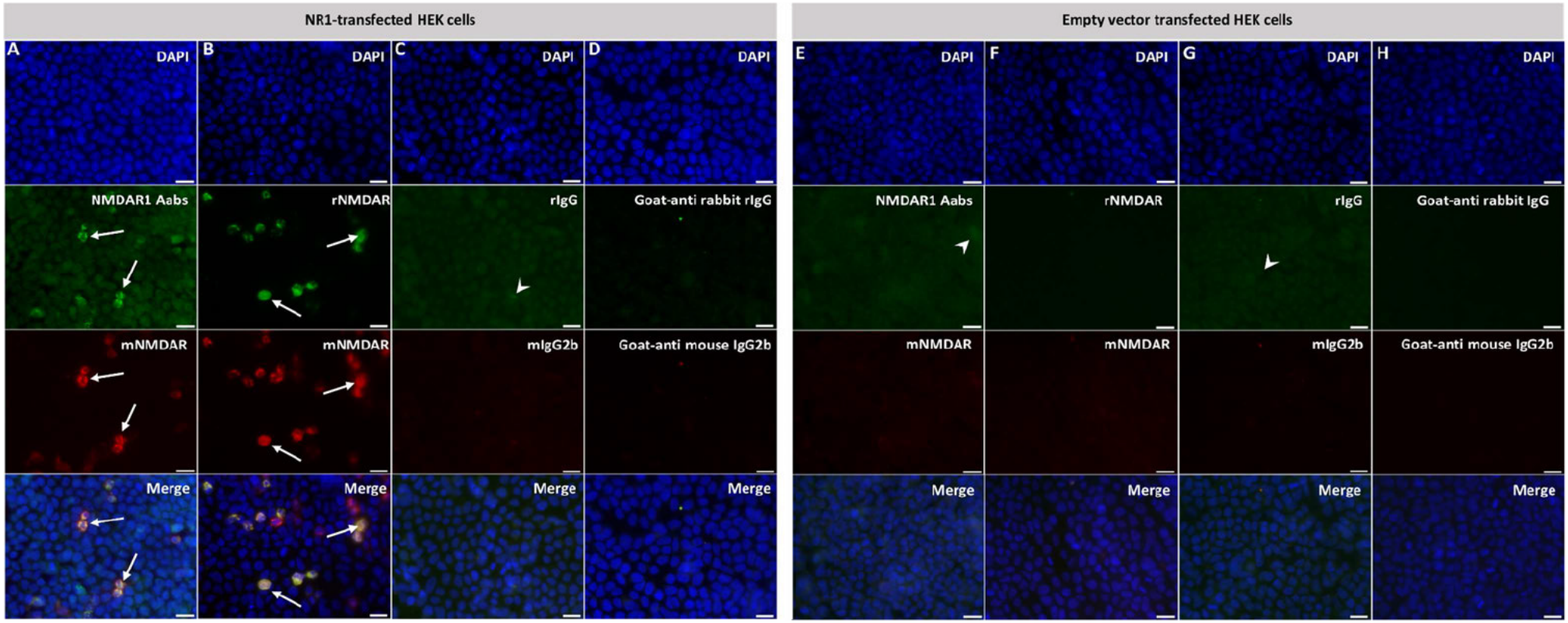

Figure 3.5: ICC staining of NR1 and empty vector transfected HEK cells. Representative images of NMDAR staining present in NR1-transfected HEK cells but absent in empty vector-transfected HEK cells. **(A)** Cells transfected with NR1 detected by NMDAR1 Aabs (green), and co-labelled by the commercial antibody mNMDAR (red) as indicated by white arrows. **(B)** Both commercial antibodies mNMDAR and rNMDAR co-labelled the same NR1-transfected cells (white arrows). **(C & D)** Cells incubated with the class-specific negative controls rIgG and mIgG2b, as well as a secondary-only control elicited no labelling. ICC staining of empty vector transfected HEK cells resulted in no clear staining when incubated with NMDAR1 Aabs (**E**), as well as two commercial anti-NR1 antibodies mNMDAR and rNMDAR **(F)**. **(G & H)** Cells incubated with the class-specific negative controls rIgG and mIgG2b, as well as a secondary-only control did not exhibit any positive staining. Representative images selected from n=3 replicates per condition. Scale = 20µm.

Empty vector transfected HEK cells were also subjected to ICC. NMDAR1 Aabs showed no specific labelling, with only low levels of background staining, as seen in NR1-transfected HEK cells (shown by white arrowheads; Figure 3.5E). Similarly, neither commercial NMDAR antibody positively labelled any cells (Figure 3.5F). As above, the cells were also incubated with class specific negative controls; rIgG and mIgG2b, both of which resulted in no bright labelling of any cells. Again, there was some background staining detected with rIgG (as shown by white arrowheads; Figure 3.5G), a similar level to that detected by those incubated with NMDAR1 Aabs and rIgG in both NR1- and empty vector-transfected HEK cells (Figure 3.5A, C & E respectively). The secondary-only control showed no labelling in empty vector-transfected HEK cells (Figure 3.5H).

3.3.2 NMDAR1 Aab detection of NMDARs to native NMDARs

Labelling of endogenous receptors in more physiologically relevant models was then carried out: primary mouse hippocampal cultures (DIV7-20, the age at which cultures were synaptically mature) and adult hippocampal brain sections.

Neuronal networks, which spontaneously develop within mouse cultures, provide a useful tool for the precise investigation of neuronal activity and synaptic transmission. For this purpose, hippocampal and cortical neuronal cultures were generated (see section 2.5.3), characterised, and subsequently used for the further testing of NMDAR1 Aab specificity. Primary hippocampal and cortical neurons were fixed at DIV7-20 and exposed to NMDAR1 Aabs, and co-labelled with the neuronal-specific marker, βIII tubulin, and astrocyte-specific marker, GFAP, to identify cell-type specificity within the culture.

NMDAR1 Aabs faintly detected cortical cells which were co-labelled by the neuronal marker βIII tubulin (as shown by the white arrows; Figure 3.6A), but not by the astrocyte marker GFAP. Cells were also subjected to a secondary-only control, whereby all primary antibodies were omitted. No labelling was detected in any of the channels (Figure 3.6B), indicating all of the labelling seen in Figure 3.6A is not due to any background staining caused by the secondary antibodies.

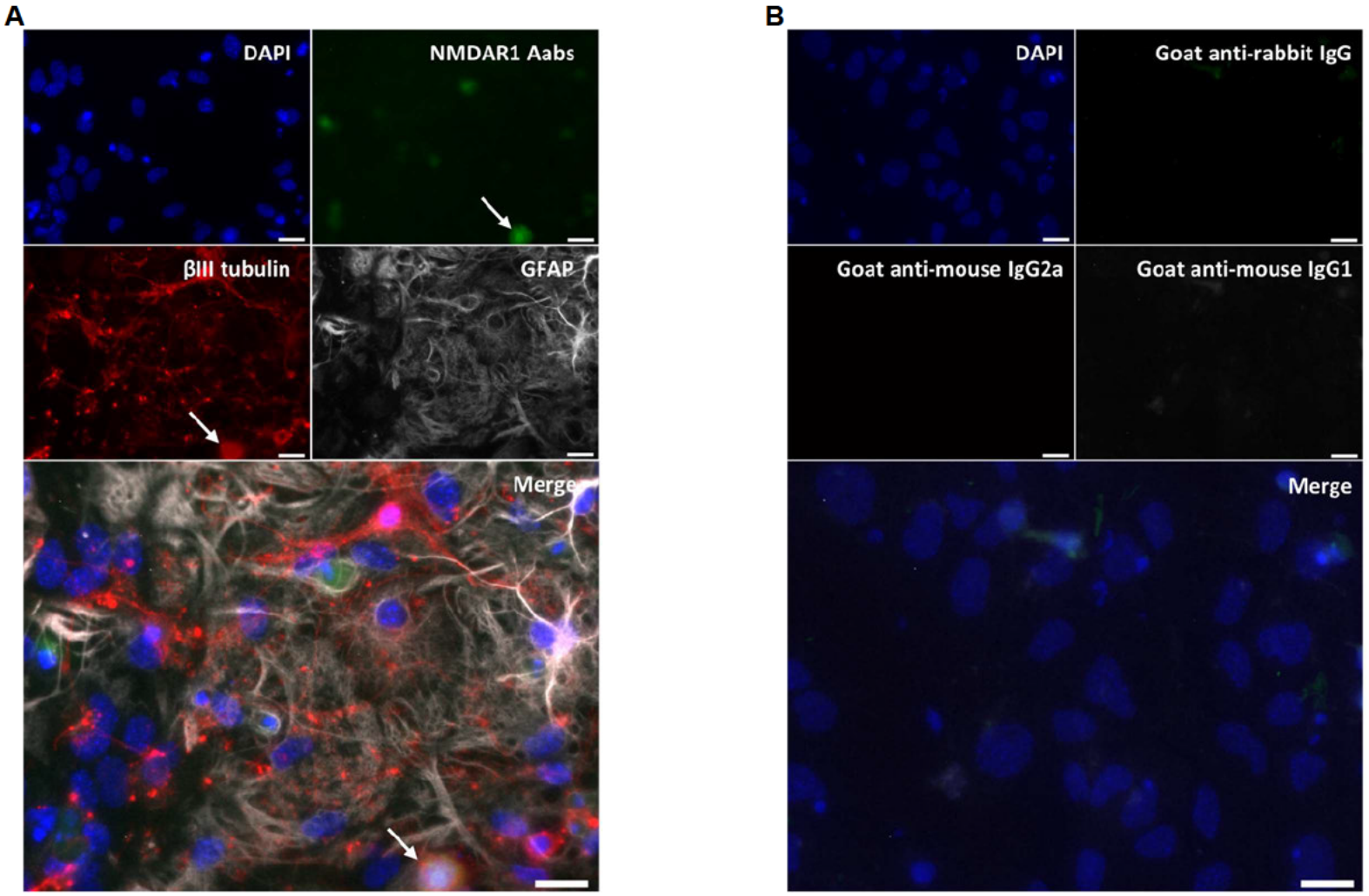

Figure 3.6: Immunocytochemical staining of fixed primary cortical neurons (DIV14). (A) Cells were stained with NMDAR1 Aabs (green), βIII tubulin; a neuronal marker (red), GFAP; an astrocyte marker (white) and a nuclear stain (DAPI: blue). NMDAR1 Aabs incubation elicited faint staining, which co-localised with βIII tubulin-stained cells, as indicated by the white arrows. **(B)** A secondary-only control was performed; anti-rabbit IgG (green), anti-mouse IgG2a (red) and anti-mouse IgG1 (white). No visible staining was detected in any channel. Representative image selected from n=5 technical replicates (across 3 biological replicates). Scale = 20μm.

The addition of an anti-NR1 commercial antibody (rNMDAR) resulted in clear staining (Figure 3.7A), again co-localising with βIII tubulin-stained cortical neurons, serving as a positive control for the protocol. Similarly, a class specific negative control (rIgG) was also used to ensure all staining observed with NMDAR1 Aabs was due exclusively to any NMDAR-specific IgG, and not from non-NMDAR specific IgG. Faint staining was seen with the negative control rIgG, however these rIgG labelled cells co-localised with cells labelled with the neuronal marker βIII tubulin (as shown by white arrows; Figure 3.7B), as well as the astrocyte marker GFAP (as shown by orange arrows; Figure 3.7B), indicating a lack of cell-type specificity. This is dissimilar to NMDAR1 Aabs, where any staining observed only co-localised with βIII tubulin positive cells, not GFAP positive cells (as shown above; Figure 3.6A).

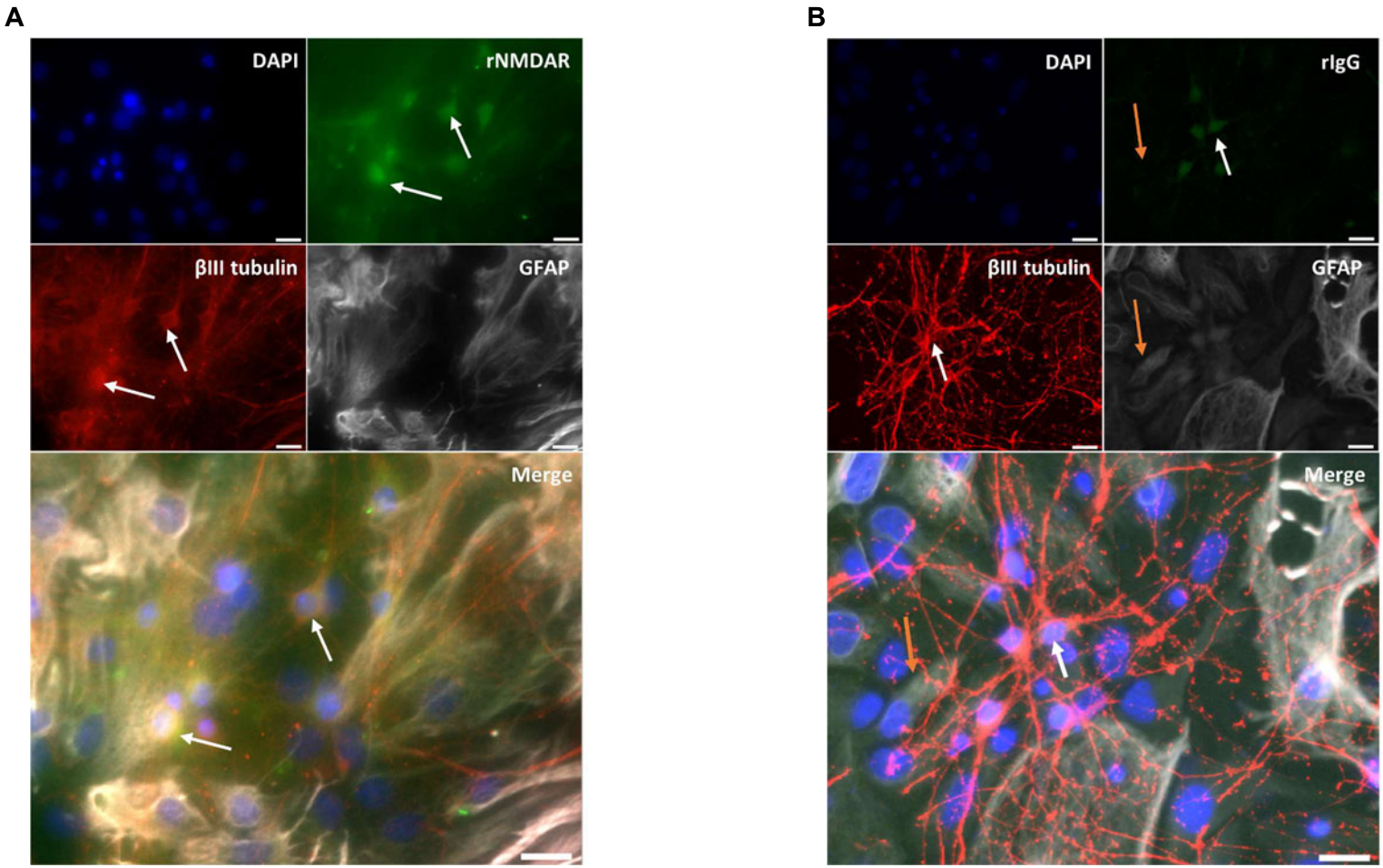

Figure 3.7: Immunocytochemical staining of fixed primary cortical neurons (DIV14). (A) Clear staining observed with a commercial anti-NR1 antibody (rNMDAR; green) co-localised with those labelled by the neuronal marker βIII tubulin (red, as shown by the white arrows), but did not co-localise with GFAP-labelled cells (white). **(B)** Faint staining detected with class-specific negative control rIgG (green), co-localised with βIII tubulin-stained cells (as indicated by white arrows), as well as cells labelled by GFAP (orange arrows). Representative image selected from n=6 technical replicates (across 3 biological replicates). Scale = 20µm.

IHC was carried out on adult mouse brain sections to determine cell-type specificity as well as spatial binding within the hippocampus. Using perfusion fixed and cryopreserved mouse brain sections (12µm), clear binding could be seen when NMDAR1 Aabs were applied (Figure 3.8). NMDAR1 Aab labelled cells could be seen throughout the hippocampus, in CA1, CA3 and DG regions, all of which co-labelled with the neuronal marker NeuN.

Similar binding and localisation could be seen with the commercial antibody rNMDAR, where co-labelling with NeuN was detected throughout all areas of the hippocampus (Figure 3.8). Class specific negative control rIgG showed faint binding throughout all areas of the hippocampus, co-labelling with NeuN (Figure 3.8). An additional secondary-only antibody control was also performed where the primary antibody was omitted prior to secondary antibody incubation to ensure any binding seen in all three antibody conditions above was not due to any non-specific binding caused by the secondary antibodies. Both secondary antibodies (anti-guinea pig IgG (green) and anti-rabbit IgG (red)) resulted in no staining in either channel (Figure 3.8).

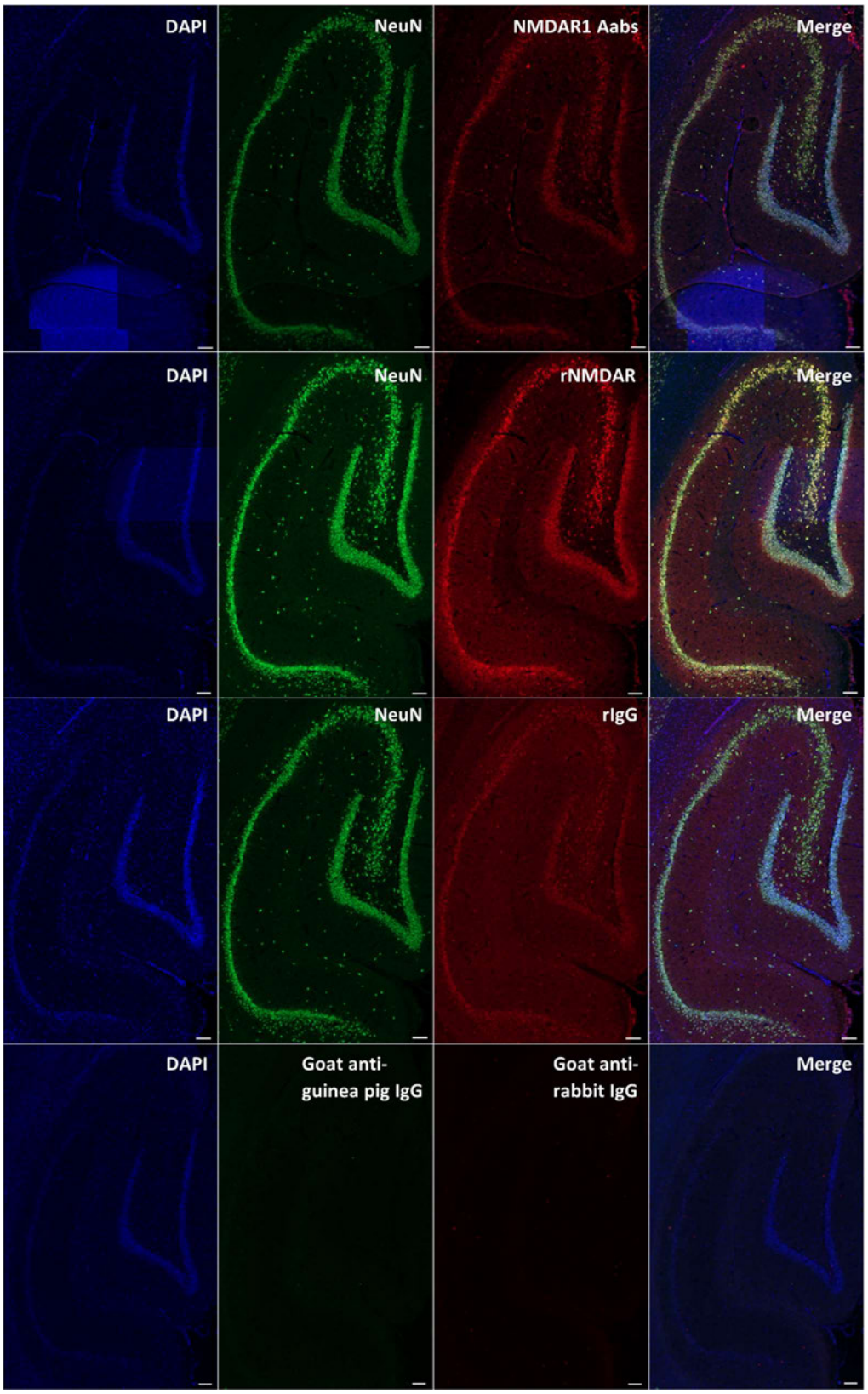

Figure 3.8: Immunohistochemical staining of fixed mouse brain sections. NMDAR staining in hippocampal mouse brain sections could be seen throughout the hippocampus. All sections were co-stained with NeuN (green) and DAPI. NMDAR1 Aabs displayed similar localisation and expression to commercial antibodies, with rIgG also eliciting some staining, highlighting some background binding from IgG. The secondary antibody only negative control showed no binding in either channel. Representative images selected from n=3 technical replicates per condition. Scale = 100µm.

However, when looking at these signals at a higher magnification a slightly different binding pattern of rIgG could be seen when compared to both NMDAR1 Aabs and rNMDAR (Figure 3.9). NMDAR1 Aabs appear to be binding to more membrane bound targets, with clearer labelling of neuronal structures and processes. This is as expected as NMDAR1 Aabs target an extracellular region of NMDARs, which are in themselves localised to the membrane. This is in contrast to the class specific rIgG where any labelling is less clear, with increased background. In addition, it is important to note that no labelling was observed in secondary antibody only control (Figure 3.9).

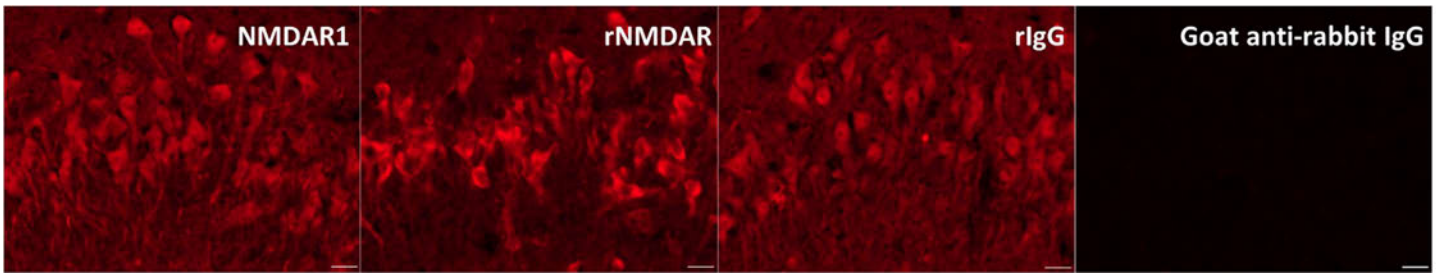

Figure 3.9: Immunohistochemical staining of fixed mouse brain. Representative images of higher magnification of Figure 3.10. The localisation of binding seen with NMDAR1 Aabs appears more membrane bound, of which similar binding can be seen with the commercial antibody rNMDAR. Staining observed with rIgG however appears less clear, with increased background. A secondary-only control was also employed as a negative control for the experiment, where no labelling was seen. Representative images selected from n=3 technical replicates per condition. Scale = 20μm.

The ATD of the NR1 subunit was used to assess the specificity of NMDAR1 Aabs by western blot. Purified human NR1 ATD was run on SDS-PAGE and probed with NMDAR1 Aabs. The blot probed with NMDAR1 Aabs detected a strong band at the predicted size of 60 kDa, indicating the ATD of the NR1 subunit is bound by NMDAR1 Aabs. A slightly smaller band just under 60 kDa can also be seen (Figure 3.10A), which may be due slight degradation of the sample or low levels of non-specific binding. These bands were also detected by the commercial anti-NR1 antibody rNMDAR, but not by commercial mNMDAR (Figure 3.10A).

Blots were also incubated with the class-specific negative controls rIgG and mIgG2b, a secondary antibody only, as well as an irrelevant antibody Equilibrative Nucleoside Transporter 1 (ENT1; a transporter which allows adenosine to transit cellular membranes by passive diffusion, which should not bind human NR1 ATD). No band was observed following incubation with rIgG, mIgG2b, secondary antibody only, or the irrelevant antibody ENT1 (Figure 3.10B).

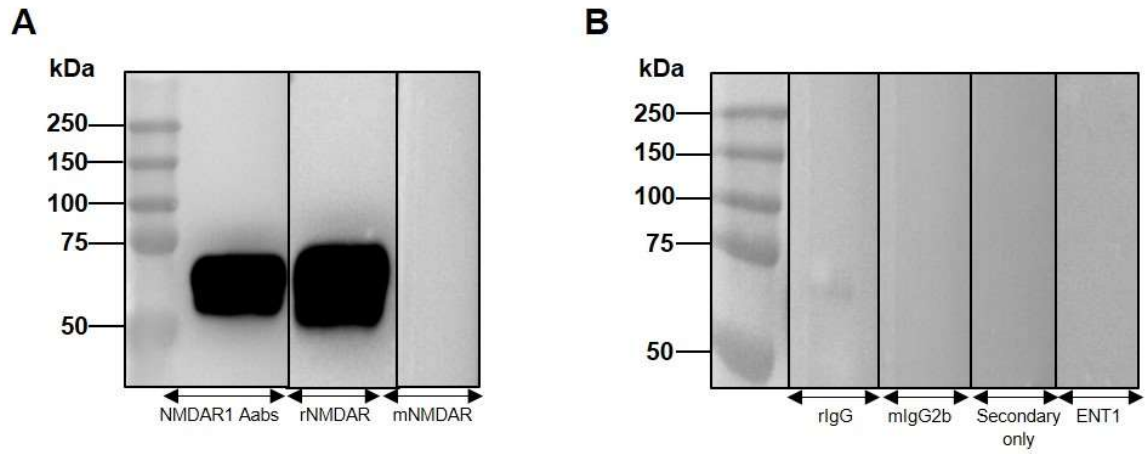

Figure 3.10: Human ATD of NR1 subunit probed with NMDAR1 Aabs. (A) Blots incubated with NMDAR1 Aabs and the commercial antibody rNMDAR detected strong bands at 60kDa, with mNMDAR not detecting any clear band. (B) Blots incubated with the negative controls; rIgG, mIgG2b, secondary antibody only and the irrelevant antibody ENT1 did not detect any bands at the expected molecular weight. Representative blots selected from n=3 technical replicates.

Subsequent western blots were carried out to assess if NMDAR1 Aabs detect full-length NR1 when in a denatured state. Lysates from NR1- and empty vector-transfected HEK cells, primary cortical neurons (mouse) and whole brain (mouse) were generated and run on SDS-PAGE and probed with NMDAR1 Aabs. No clear band was identified at the expected molecular weight of the NR1 subunit (105 kDa) in either HEK cell lysate, primary cortical cell lysate or whole brain lysate. However, multiple other bands were detected by NMDAR1 Aabs. A faint band was detected at ~110 kDa and strong bands at ~70 kDa across all four samples, with additional bands at 50 kDa and 60 kDa in primary cortical cell, whole brain and NR1 HEK cell lysates (Figure 3.11A). It is possible that further breakdown of the protein could be occurring and NMDAR1 Aabs are detecting the ATD of the NR1 subunit in different glycosylated states (7 glycosylation sites are present within the human ATD; see Figure 3.1) or, alternatively, these bands could be indicating degradation of the samples. However, as neither of these bands were detected with the positive control (commercial antibody; mNMDAR), where a single, clean

band is detected at the expected size of 105 kDa in NR1-HEK, whole brain and primary cortical lysates, both of these possibilities seem unlikely. It is more probable these bands are being caused by other non-NMDAR specific IgG within the composition; as only 1-10% is thought to be specific for NMDARs (Hnasko and McGarvey, 2015), other specific IgG could be binding to targets within these samples. In addition, it may be possible that our NMDAR1 Aabs do not detect NR1 subunit in the denatured state, as is also seen for the commercial antibody rNMDAR and, as such, is not suitable for use in western blots.

When blots were probed with commercial anti-NR1 antibodies, differing results were seen. The monoclonal antibody mNMDAR detected a band at the expected molecular weight of 105kDa in primary cortical cell, whole brain and NR1 HEK cell lysate (as shown by the red box), with no visible band in empty vector transfected HEK cell lysate (Figure 3.11A). By contrast, the polyclonal antibody rNMDAR detected multiple bands in whole brain lysate, one of which is at the expected size of 105 kDa (highlighted by the red box), with additional bands at 150 kDa and 70 kDa. No bands were detected in primary cortical cell lysate and only one band was detected in both NR1 and empty vector transfected HEK cell lysate at 50 kDa (Figure 3.11A). The differences in these results may be due to the different epitopes being targeted by each of the commercial antibodies, with mNMDAR targeting a region outside of the ATD (amino acids 660-811) and rNMDAR targeting amino acids 35-53 within the ATD. In addition, rNMDAR is polyclonal, and therefore contains a mixture of IgG targeting different epitopes within this region, whereas mNMDAR is a monoclonal antibody and therefore bind to a single epitope, which may explain the increased specificity for the expected band size of 105 kDa.

Blots probed with the class specific control rIgG detected similar bands to that seen with NMDAR1 Aabs, with bands at 100 kDa, 90 kDa, 60 kDa and 50 kDa, among others, across all four samples. Similar to NMDAR1 Aabs, total IgG is used, therefore there may be antibodies within this composition which target alternative proteins within our samples, which may

explain the multiple bands detected (Figure 3.11A). As expected, blots probed with the class specific negative control mIgG2b and the secondary antibody only, did not detect any bands across any of the four samples (Figure 3.11A). To ensure all lanes were loaded and transferred correctly, the housekeeping gene GAPDH was probed for and acted as an additional control for the protocol employed. This process revealed a single, clean band at the expected size of 37 kDa, note the different sizes of bands being caused by different amounts of protein being loaded (10µg cortical cell, HEK NR1 and HEK empty vector lysate, compared to 50µg protein of whole brain lysate; Figure 3.11B).

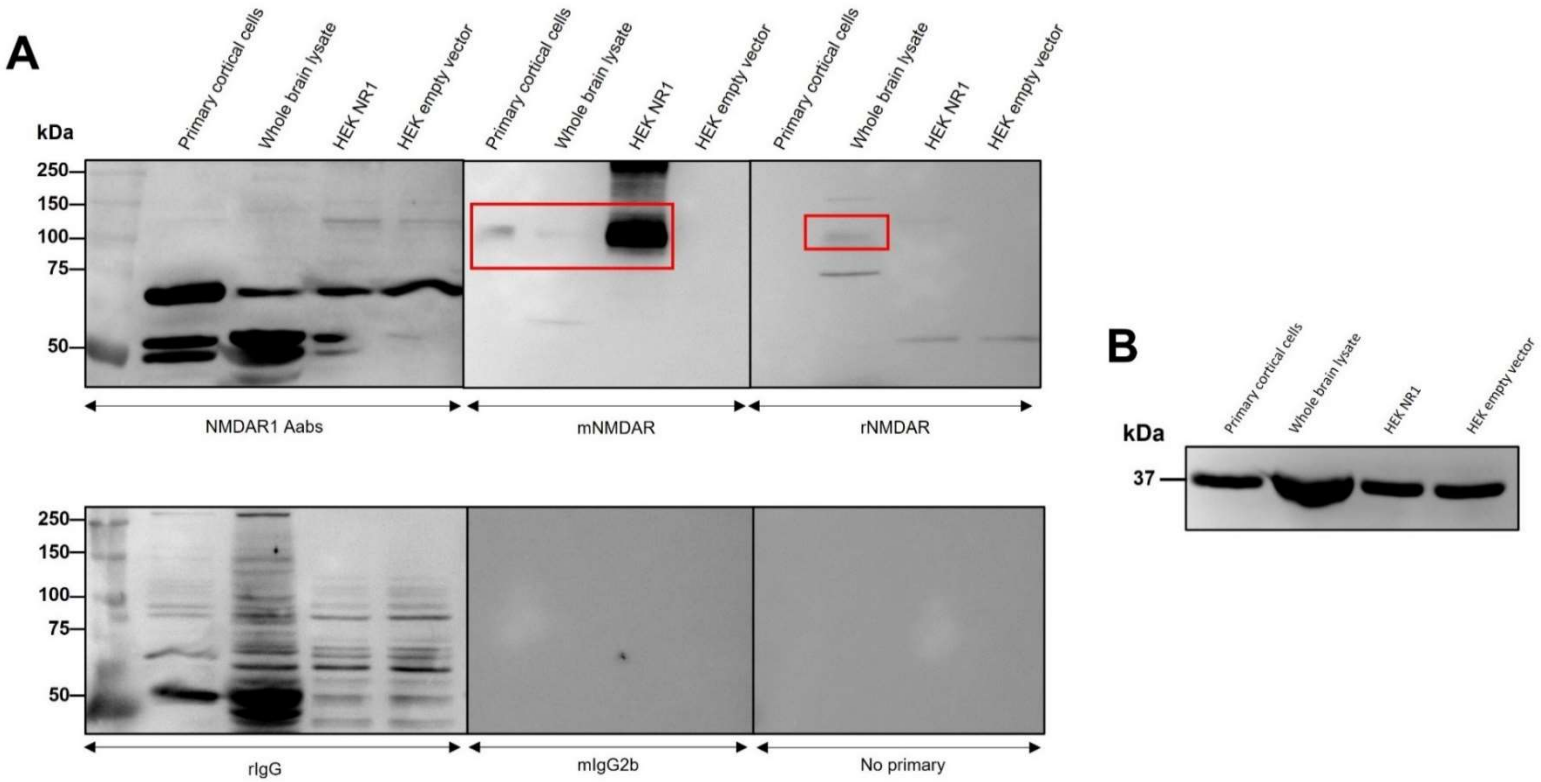

Figure 3.11: Western blot of primary cortical cells, whole brain and NR1- and empty vector-transfected HEK cells. (A) Lysates probed with NMDAR1 Aabs did not detect a band at the expected molecular weight of 105 kDa in any sample, however multiple other bands were detected at 60 kDa and 50 kDa in all cell lysates, and at 40 kDa in primary cortical cells, whole brain and NR1 HEK cell lysates. Commercial anti-NR1 antibody mNMDAR displayed bands at the expected size of ~105 kDa in primary cortical cells, whole brain and NR1-HEK cells (as shown by red box), with no band in empty vector transfected HEK cells, whereas the commercial antibody rNMDAR elicited a faint band at the expected molecular weight (indicated by red box), with other bands at 150 kDa and 60 kDa in whole brain lysate, and 50 kDa in NR1 and empty vector transfected HEK cells. The class specific control rIgG did not display a clear band at the correct size in any sample, but instead a multitude of bands were seen at other sizes, primarily 60 kDa and 50 kDa. The negative control mIgG2b and secondary-only control both showed no bands across all samples. **(B)** A single clean band was detected at the expected size of 37 kDa when probed with the loading control GAPDH. A larger band was detected in whole brain lysate as 50µg protein was loaded for this sample compared to only 10µg protein for all other samples. Representative blots selected from n=3 technical replicates.

3.4 Production of rabbit polyclonal anti-NMDAR2 Aabs (rabbit #2)

Due to the lack of functional effects seen with NMDAR1 Aabs (as described in section 4.3 and section 4.4.2) a second batch of anti-NMDAR Aabs was generated (as described in section 2.1) using alternative epitopes (as illustrated in both Figure 3.12).

As before, regions of high immunogenicity (see section 2.1) were identified within the extracellular domains of NR1 subunit of NMDARs, with peptides 6 and 7 being located within the ATD, and peptides 8 and 9 being located extracellularly outside of the ATD. In addition, peptide 8 was cyclised via a thioester in an attempt to better represent the natural conformation of this sequence, as well as to promote molecular stability (Purcell 2007). All peptides were subsequently conjugated to KLH, BSA and OVA externally (Peptide Synthetics). These conjugated peptides (locations of peptides within NR1 subunit are shown in Figure 3.12) were combined and used to immunise one rabbit (see section 2.1.1) in order to elicit an immune response.

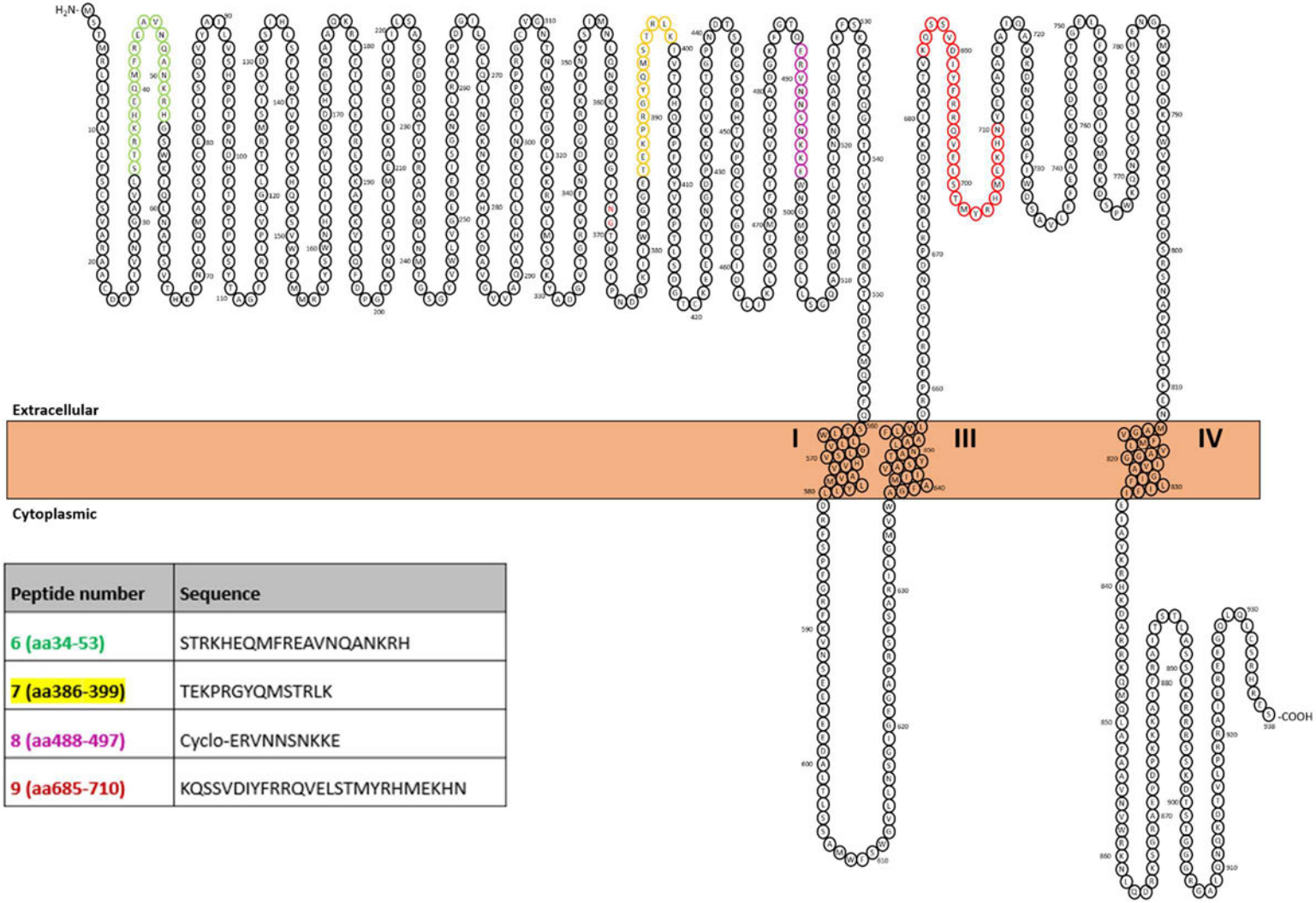

Peptide number	Sequence
6 (aa34-53)	STRKHEQMFREAVNQANKRH
7 (aa386-399)	TEKPRGYQMSTRLK
8 (aa488-497)	Cyclo-ERVNNSNKKE
9 (aa685-710)	KQSSVDIYFRRQVELSTMYRHMEKHN

Figure 3.12: NMDAR peptide sequences used for the immunisation of rabbit #2. Peptides were not limited to regions within the amino terminal domain (ATD), but instead at any extracellular protruding loop within the NR1 subunit. Peptides were generated with the addition of a C residue and an Ac residue on either end. Peptide 8 (shown in purple) was cyclised via a thioester to help better represent the true epitope.

3.4.1 Titres and ELISA of sera of NMDAR2 Aabs

The immunisation procedure was followed using peptides 6-9, as described in section 2.1.1 and serum titres were monitored using an ELISA to detect the presence of IgG antibodies against the peptides. The total number of immunisation boosts (4 immunisations) was determined based on the initial ELISA results. As expected, no detectable immune response was seen against any peptides at BL0 (pre-immunisation). In this case, no ELISA was performed following the first immunisation, as results from NMDAR1 Aabs indicated a lack of binding at this time point. Following the second and third immunisation boost (BL2 and BL3) an increase in binding to peptides 6, 7 and 9 was observed (Figure 3.13A, B and D respectively). Interestingly, minimal binding was observed against the cyclised peptide 8 (Figure 3.13C). The terminal sera did not appear to reach the same peak of binding as the previous BL3 for peptides 6, 7 and 9 (Figure 3.13A, B & D respectively), however, when EC_{50} values were calculated, the dilution of terminal sera required to reach half maximal binding was approximately the same, if not greater, than BL3 for peptides 6, 7 and 9 (shown by square symbols and solid/dotted lines; Figure 3.13A, B & D).

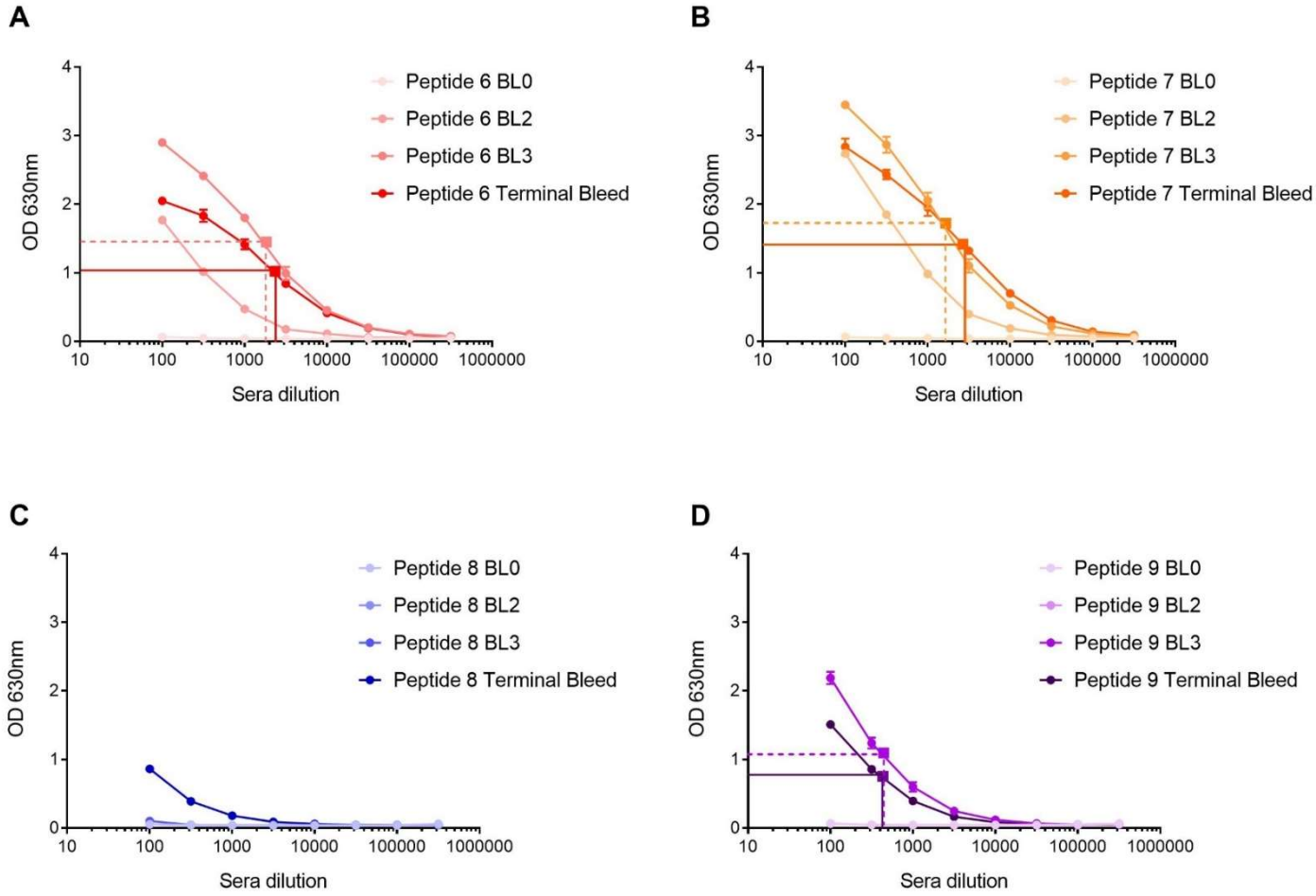

Figure 3.13: Rabbit anti-NMDAR2 Aab immunogenicity response. Pre-immunisation bleed (BL0), bleed 2 (BL2),3 (BL3) and terminal bleed responses to peptides 6-9 (**A-D** respectively) used for immunisations. An increase in response to the peptides was observed with each immunisation boost, with the largest responses against peptides 6, 7 and 9 (panels **A, B and D** respectively). EC_{50} values for BL3 and terminal sera (A, B and C) are represented by solid and dotted lines (terminal sera and BL3 respectively). N=3 technical replicates per dilution.

3.4.2 Purification and analysis of NMDAR2 Aabs

Terminal serum from NMDAR2 immunised rabbit was purified using Protein A resin to isolate total IgG from final serum as described in section 2.1.3 (hereby known as NMDAR2 Aabs, generated against sequence within NR1 subunit, from rabbit #2). These IgG antibodies were then quantified and analysed using further ELISA and SDS-PAGE. Fractions from all steps within the purification process were analysed using SDS-PAGE and Coomassie staining: pre-purification, wash 1, wash 2, eluates 1-6 and post-purification. Protein bands were detected at 150 kDa, 90 kDa, 60 kDa and 50 kDa as well as 25 kDa, among others, of which the band at 150 kDa is the expected size of IgG (Figure 3.14A). The presence of a band at 150 kDa in eluates 1 and 2 indicates most of total IgG was purified from the terminal serum. Faint bands can be seen at 150 kDa in both wash 1 and 2, indicating some IgG was removed from the column before elution, as well as a faint band being present at 150 kDa in the post-purification fraction, indicating not all IgG was purified. All other protein bands detected in the pre-purification fraction were also present in the post-purification fraction, indicating the specificity of the purification for IgG. Two additional faint bands could also be seen in eluate 1, at just above 50 kDa and at 25 kDa, which may represent the heavy and light chains of IgG respectively.

Quantification of total IgG was performed using a protein A280 nanodrop, measuring the absorbance at 280nm which determined the concentration of protein. This revealed 11.6mg/ml total IgG was acquired from the immunisation protocol, of which anywhere between 1-10% is predicted to be NMDAR specific (Hnasko and McGarvey, 2015). To verify that the purification process did not have any negative effect on NMDAR2 Aabs specificity to the immunised peptides, a further ELISA was carried out using total IgG (Figure 3.14B). This process revealed strong Aab binding to peptides 6, 7 and 9, similar to that seen by the terminal sera ELISA (Figure 3.13A, B & D), with binding detected as low as 0.316µg/ml. In contrast, minimal

binding was observed to peptide 8, consistent with those results prior to protein A purification (Figure 3.13C).

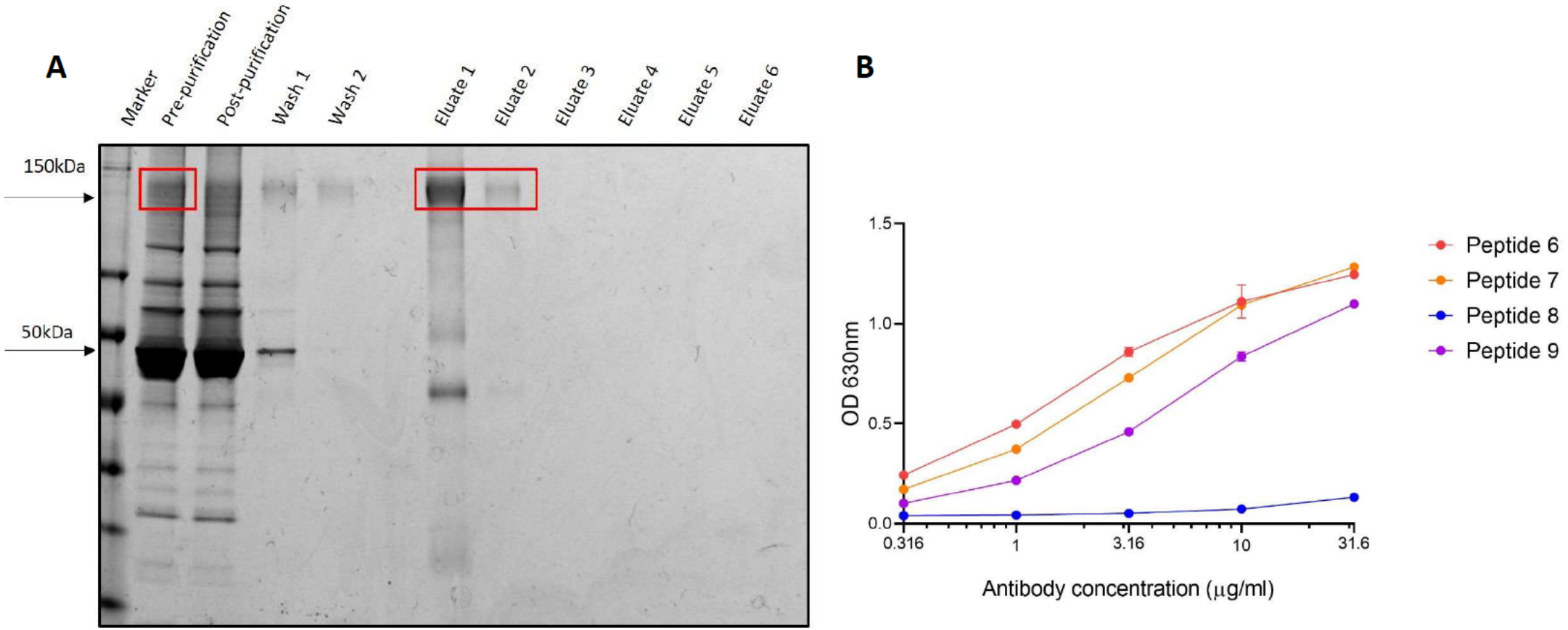

Figure 3.14: Protein A purification of NMDAR2 Aabs. (A) SDS-PAGE analysis of rabbit serum purified by protein A-sepharose resin. Analysis of all fractions revealed a specific band at 150 kDa in pre-purification sample and all eluates, which is not present in the post-purification sample. **(B)** Protein A purified NMDAR2 resulted in similar binding to immunisation peptides as pre-purification, indicating purification has not altered conformation or specificity of NMDAR Aabs within total IgG sample. N=3 technical replicates per concentration.

Further quantification using SDS-PAGE was carried out to validate the measured NMDAR2 Aab concentration. A commercial rabbit total IgG of known concentration was used as a control, whereby both antibodies were used at a titration of concentrations to compare size and intensity of any bands produced. Both antibodies produced bands at the expected size of 150 kDa, with all bands being of similar size and intensity (Figure 3.15). Additional bands can be seen just above and below 150 kDa across both antibodies at all dilutions, as well as an additional band of ~50 kDa, which may represent the heavy chain of IgG.

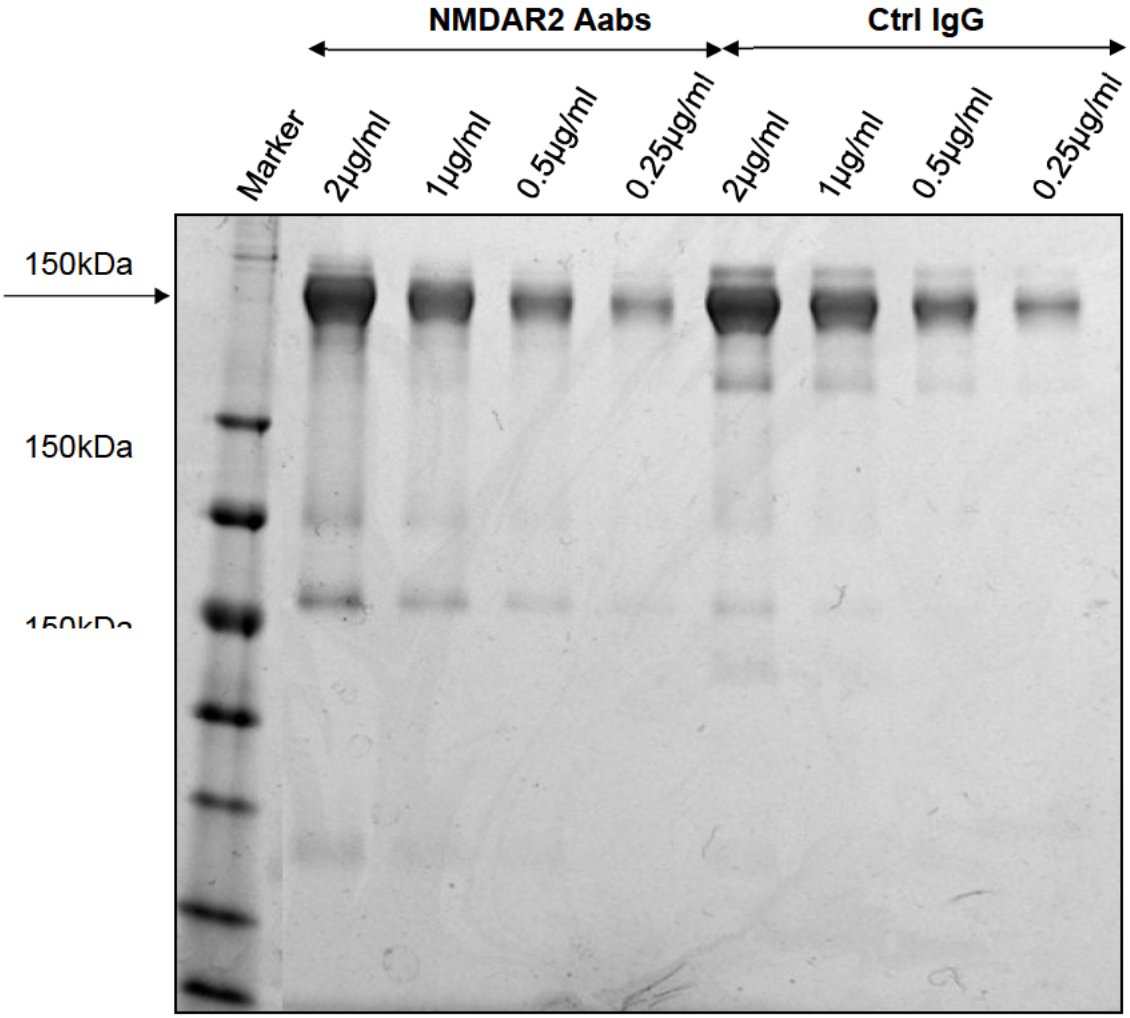

Figure 3.15: Protein A purified NMDAR Aabs are comparable to control rabbit IgG. Concentration of NMDAR Aabs determined via A280 measurement is comparable in band size and dilution as control IgG of known concentration (n=1 technical replicates).

3.5 Characterisation of NMDAR2 Aabs on *in vitro* systems

3.5.1 NMDAR2 Aab detection of NMDAR in NR1-transfected HEK cells

In order to analyse the specificity of NMDAR2 Aabs, HEK cells were transfected either with a vector encoding the NR1 subunit or an empty vector (see section 2.2.1). The day after transfection, cells were fixed and incubated with NMDAR2 Aabs, and ICC was performed (as described in section 2.2.1.1).

NMDAR2 Aabs positively stained NR1-transfected HEK cells (green; as shown by the white arrows; Figure 3.16A), while also eliciting some background staining (as shown by white arrowheads), which is likely to be caused by the presence of both NMDAR-specific and non-NMDAR specific IgG respectively. This is similar to the staining that was seen previously with NMDAR1 Aabs (see Figure 3.5A). These positively stained cells co-localised with cells which were positively labelled with the commercial anti-NR1 antibody mNMDAR (red; as shown by white arrows; Figure 3.16A). A second commercial antibody was also tested; rNMDAR, which elicited similar staining to that of NMDAR1 Aabs, where positively stained cells were also co-labelled by the commercial antibody mNMDAR (as shown by white arrows; Figure 3.16B). Negative controls were also employed: rIgG and mIgG2b, as well as a secondary-only antibody incubation. The class-specific negative control rIgG demonstrated low levels of background staining (as shown by white arrowheads; Figure 3.16C), similar to that seen with NMDAR2 Aabs, but no clear, bright labelling of NR1-tranfected HEK cells was detected. The secondary-only control also resulted in no positively stained cells (Figure 3.16D).

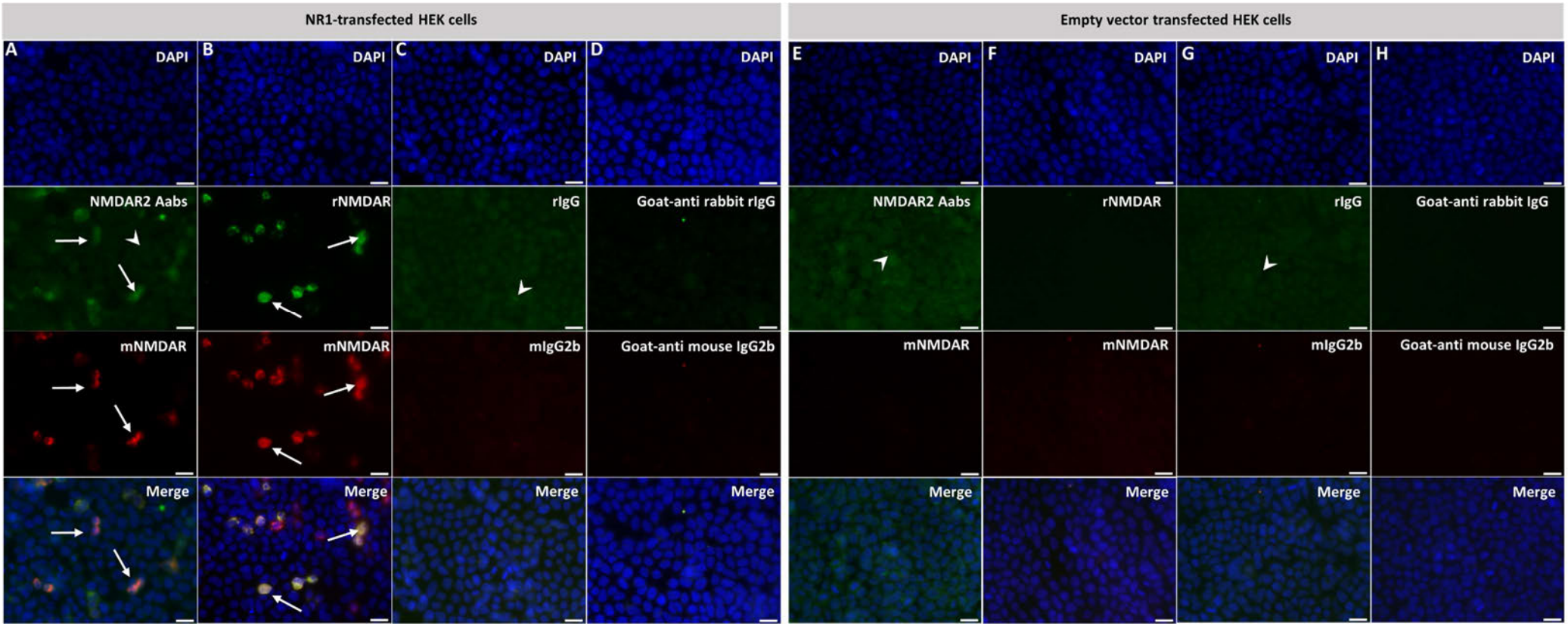

Figure 3.16: ICC staining of NR1 and empty vector transfected HEK cells. Cells were stained with NMDAR2 Aabs (**A**; 1:100), two commercial anti-NR1 antibodies: mouse anti-NR1 (**B**; mNMDAR; 1:1000), rabbit anti-NR1 (rNMDAR; 1:1000), as well as a nuclear stain (DAPI, blue). Cells transfected with NR1 were detected by NMDAR2 Aabs, which were co-labelled by the commercial antibody mNMDAR (as shown by white arrows). Both commercial antibodies mNMDAR and rNMDAR co-labelled the same NR1-transfected cells (as shown by white arrows; **B**). Cells were also incubated with the class-specific negative controls rIgG and mIgG2b, as well as being subjected to a secondary-only control. Neither of these conditions elicited any positively stained cells **(C &D).** ICC staining of empty vector transfected HEK cells showed no clear staining when stained with NMDAR1 Aabs (1:100; **E**), as well as two commercial anti-NR1 antibodies **(F):** mouse anti-NR1 (mNMDAR; 1:1000), rabbit anti-NR1 (rNMDAR; 1:1000). **(G & H)** Cells incubated with the class-specific negative controls rIgG and mIgG2b, as well as a secondary-only control did not exhibit any positive staining. Representative images selected from n=3 replicates per condition. Scale = 20µm.

Empty vector transfected HEK cells were also subjected to ICC. NMDAR2 Aabs did not show any labelling, although a low level of background labelling was detected, similar to that seen with NMDAR2 Aabs in NR1-transfected HEK cells (shown by white arrowheads; Figure 3.16E), and similar to that seen previously with NMDAR1 Aabs in both NR1- and empty-vector-transfected HEK cells (Figure 3.5A and Figure 3.5E respectively). Similarly, neither commercial antibody positively labelled any cells (Figure 3.16F). As above, the cells were also incubated with class-specific negative controls: rIgG and mIgG2b, both of which resulted in no bright labelling of any cells. Again, there was some background staining detected with rIgG (as shown by white arrowheads; Figure 3.16G), a similar level to that detected by those incubated with NMDAR2 Aabs and rIgG in both NR1- and empty vector-transfected HEK cells (Figure 3.16A & C and Figure 3.16E respectively). The secondary-only control also resulted in no positively stained cells (Figure 3.16H).

3.5.2 NMDAR2 Aab detection of NMDAR to native NMDARs

Similar to NMDAR1 Aabs, labelling of NMDARs in more physiologically relevant models was carried out: primary mouse cortical cultures and adult hippocampal brain sections.

Primary cortical neurons were fixed at DIV7-20 and exposed to NMDAR2 Aabs, and co-labelled with the neuronal-specific marker, βIII tubulin, and astrocyte-specific marker, GFAP, to identify cell-type specificity within the culture.

NMDAR2 Aabs detected cells, which were co-labelled by the neuronal marker βIII tubulin (as shown by the white arrows; Figure 3.17A), but not by the astrocyte marker GFAP. Cells were also subjected to a secondary-only control, whereby all primary antibodies were omitted. This resulted in no labelling being detected in any of the channels (Figure 3.17B), indicating that all of the labelling seen in Figure 3.17A is not due to any background staining caused by the secondary antibodies.

Positive (commercial antibody rNMDAR) and additional negative controls (rIgG) were used as before (see Figure 3.7A & B respectively).

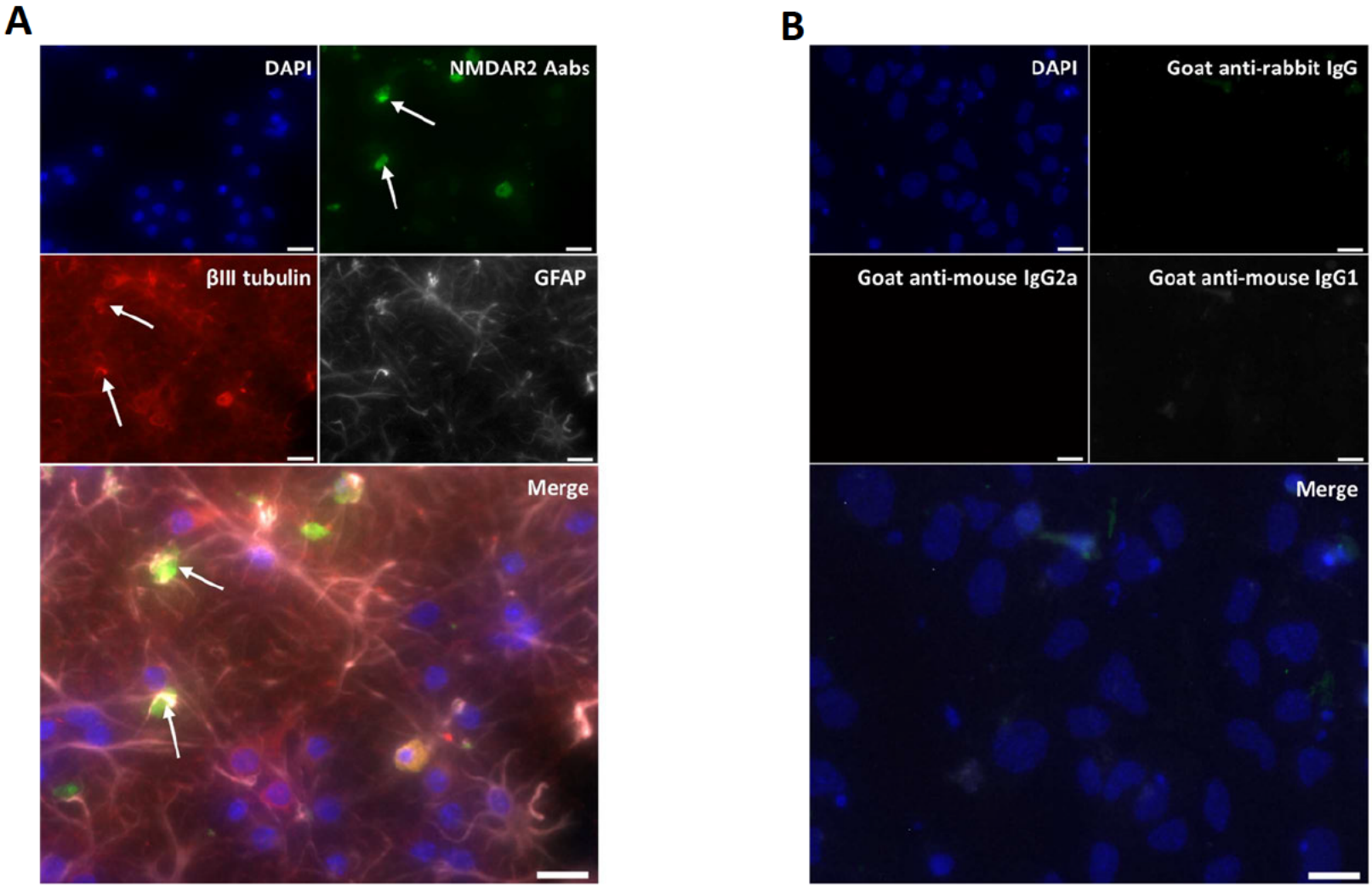

Figure 3.17: Immunocytochemical staining of fixed primary cortical neurons (DIV14). (A) Cells were stained with NMDAR2 Aabs (green), βIII tubulin; a neuronal marker (red), GFAP; an astrocyte marker (white) and a nuclear stain (DAPI: blue). Faint staining was seen with NMDAR2 Aabs (green) as indicated by the white arrows. **(B)** A secondary-only control was performed, where cells were incubated with the secondary antibodies: anti-rabbit IgG (green), anti-mouse IgG2a (red) and anti-mouse IgG1 (white). No visible staining was detected in any channel. Representative image selected from n=5 technical replicates (across 3 biological replicates). Scale = 20µm.

IHC was carried out on adult mouse brain sections to determine cell-type specificity as well as spatial binding. Using perfusion fixed and cryopreserved mouse brain sections (12μm), minimal binding could be seen when sections were incubated with NMDAR2 Aabs (Figure 3.18). Sections were co-labelled with βIII tubulin and NeuN (neuronal markers), of which only NeuN elicited some faint staining within the dentate gyrus. Therefore, it is hard to distinguish the spatial binding and cell-type specificity of NMDAR2 Aabs within the hippocampus; the lack of binding observed by both NMDAR2 Aabs and βIII tubulin could indicate an issue with the quality of sections used or could indicate simply a lack of binding. Therefore, further optimisation of fixation and antibody incubation is required to fully determine the binding of NMDAR2 Aabs within the hippocampus.

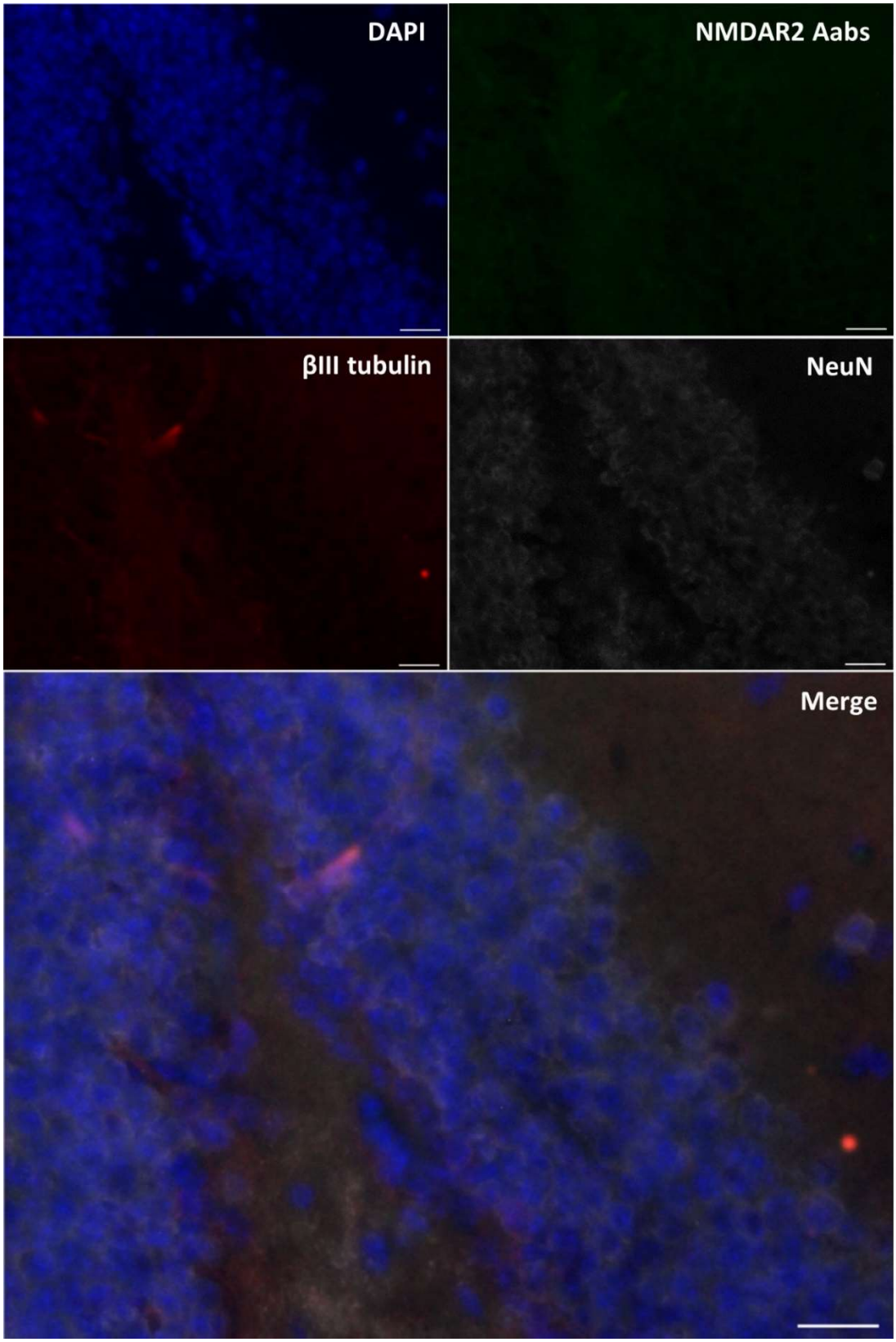

Figure 3.18: Representative image of immunohistochemical staining of dentate gyrus of fixed hippocampal brain slice. Stained with NMDAR2 Aabs, co-stained with NeuN and βIII tubulin. All three antibodies demonstrated minimal binding, highlighting a higher magnification for visualisation is required. Representative image selected from n=4 replicates. Scale = 20μm.

The ATD of the NR1 subunit was used to assess the specificity of NMDAR2 Aabs by western blot. Purified human NR1 ATD was run on SDS-PAGE and probed with NMDAR2 Aabs. NMDAR2 Aabs detected a strong band at the predicted size of 60 kDa, indicating the ATD of the NR1 subunit is bound by NMDAR2 Aabs. A slightly smaller band just under 60 kDa can also be seen (Figure 3.19), which may be due to a different glycosylated state of the ATD or slight degradation of the sample. This band could also be detected with commercial antibodies directed against a region within the NR1 ATD (rNMDAR), but not with class-specific negative controls (as shown in Figure 3.10)

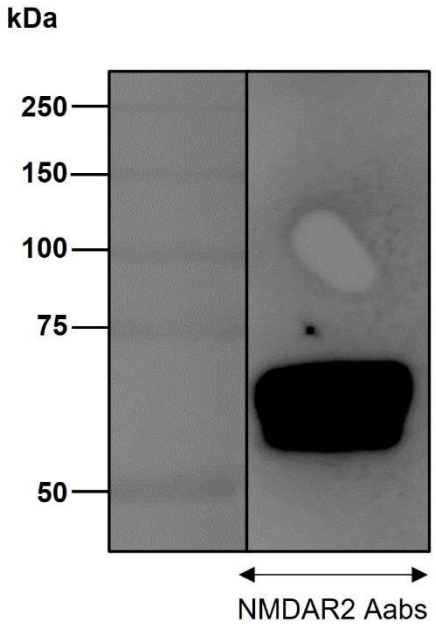

Figure 3.19: Human ATD of NR1 subunit probed with NMDAR2 Aabs. Blots incubated with NMDAR2 Aabs detected a strong band at 60kDa. Representative blot selected from n=3 technical replicates.

Subsequent western blots were carried out to assess if NMDAR2 Aabs detect full-length NR1 when in a denatured state. Lysates from NR1-transfected HEK cells, primary cortical neurons (mouse) and whole brain (mouse) were generated and run on SDS-PAGE and probed with NMDAR2 Aabs (Figure 3.20A). No clear band was identified at the expected molecular weight of the NR1 subunit (105 kDa) in either HEK cell lysate, primary cortical cell lysate or whole brain lysate. However, multiple other bands were detected by NMDAR2 Aabs; strong bands

were detected at 70 kDa across all four samples, with additional bands at 250 kDa and 150 kDa in primary cortical cells, 90 kDa, 80 kDa, and 60 kDa among others in whole brain lysate and faint bands at 90 kDa, 95 kDa and 100 kDa in NR1 HEK cell lysates (Figure 3.20A). These bands may represent the ATD of the NR1 subunit at different glycosylated states or could be indicating degradation of the samples. However, as the commercial antibody (mNMDAR) only detected a clear single band at the expected size of 105 kDa (shown previously in section 3.3.2; Figure 3.11A) without detecting any bands, which may indicate sample degradation, it is more likely that the multiple bands seen with NMDAR2 Aabs are caused by non-NMDAR specific IgG within the composition. Alternatively, as the Aabs are generated against a mixture of both linear and cyclised peptides, it may be the case that Aabs have been generated which bind to epitopes which are present in the natural conformation, but not detectable once in a denatured state.

As before, a loading control, GAPDH was used to ensure correct loading and transfer of proteins was carried out. This revealed a single, clean band at the expected size of 37 kDa, with differences in band sizes caused by different amounts of protein loaded for samples (10µg of cortical cell, HEK NR1 and HEK empty vector lysate, compared to 50µg protein of whole brain lysate; Figure 3.20B).

.

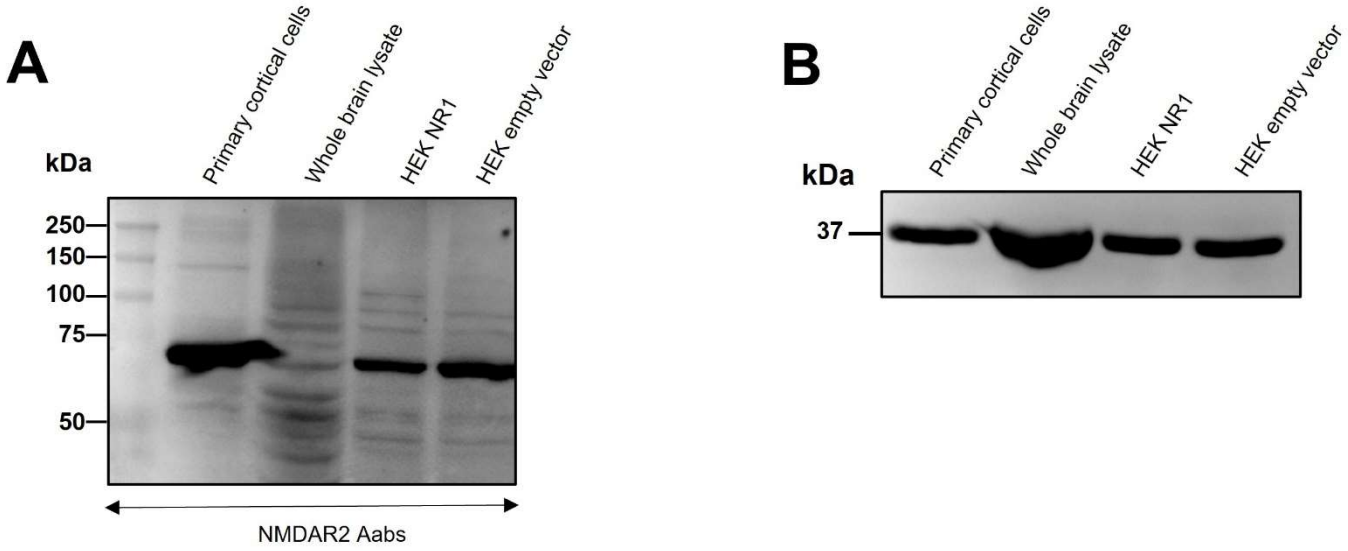

Figure 3.20: Representative western blot assessing binding specificity of protein A purified NMDAR2 Aabs to NR1 transfected HEK cells, whole brain and NR1- and empty vector-transfected HEK cells. (A) NMDAR2 Aabs did not elicit a band at the correct size in any sample but did show a myriad of other bands across all samples. **(B)** GAPDH probed blots resulted in a single, clean band at the expected size of 37 kDa. Representative blots selected from n=3 technical replicates.

3.6 Peptide purification of NMDAR1 Aabs

Based upon the lack of clear functional effects observed with both NMDAR1 & 2 Aabs (as described later in section 4.3, 4.4.1 and 4.4.2), further purification was carried out. As before, quantification of total IgG was performed by measuring absorbance at 280nm, which revealed 1.3mg/ml NMDAR-specific IgG was acquired from NMDAR1 Aabs. SDS-PAGE comparing the protein purified Aabs (henceforth, NMDAR1pp) to a control commercial IgG antibody, revealed bands of similar size and intensity at all dilutions, indicating an accurate measurement of NMDAR1pp Aabs concentration (Figure 3.21A). An additional faint band was seen at ~50 kDa across both antibodies at all dilutions, which may be detecting the heavy chain of IgG.

To verify the additional purification had not had any detrimental effect of NMDAR1pp Aabs binding to the immunised peptides, an ELISA was carried out using the peptide purified

material (Figure 3.21B). This revealed increased binding to peptides 2, 4 and 5 and minimal binding to peptide 1, similar to that seen pre-purification (Figure 3.2A-F) and following protein A purification (Figure 3.3A). Further purification resulted in an apparent increase in binding to peptide 3, which had not been seen in previous purification states (Figure 3.21B). An additional ELISA was performed to assess if an increase in the binding to the ATD protein could be seen post peptide-purification compared to post-protein A purification. As all of the NMDAR-specific IgG should have been concentrated out by the peptide purification process, binding to the ATD protein should be more readily detected when compared to the protein A purified sample. The ELISA results support this, whereby the peptide purified material required 0.51µg/ml to elicit a 50% maximal concentration response (as shown by red dotted line; Figure 3.21C), whereas the protein A purified material required 2.36µg/ml to elicit a 50% maximal response (as shown by blue dotted line; Figure 3.21C).

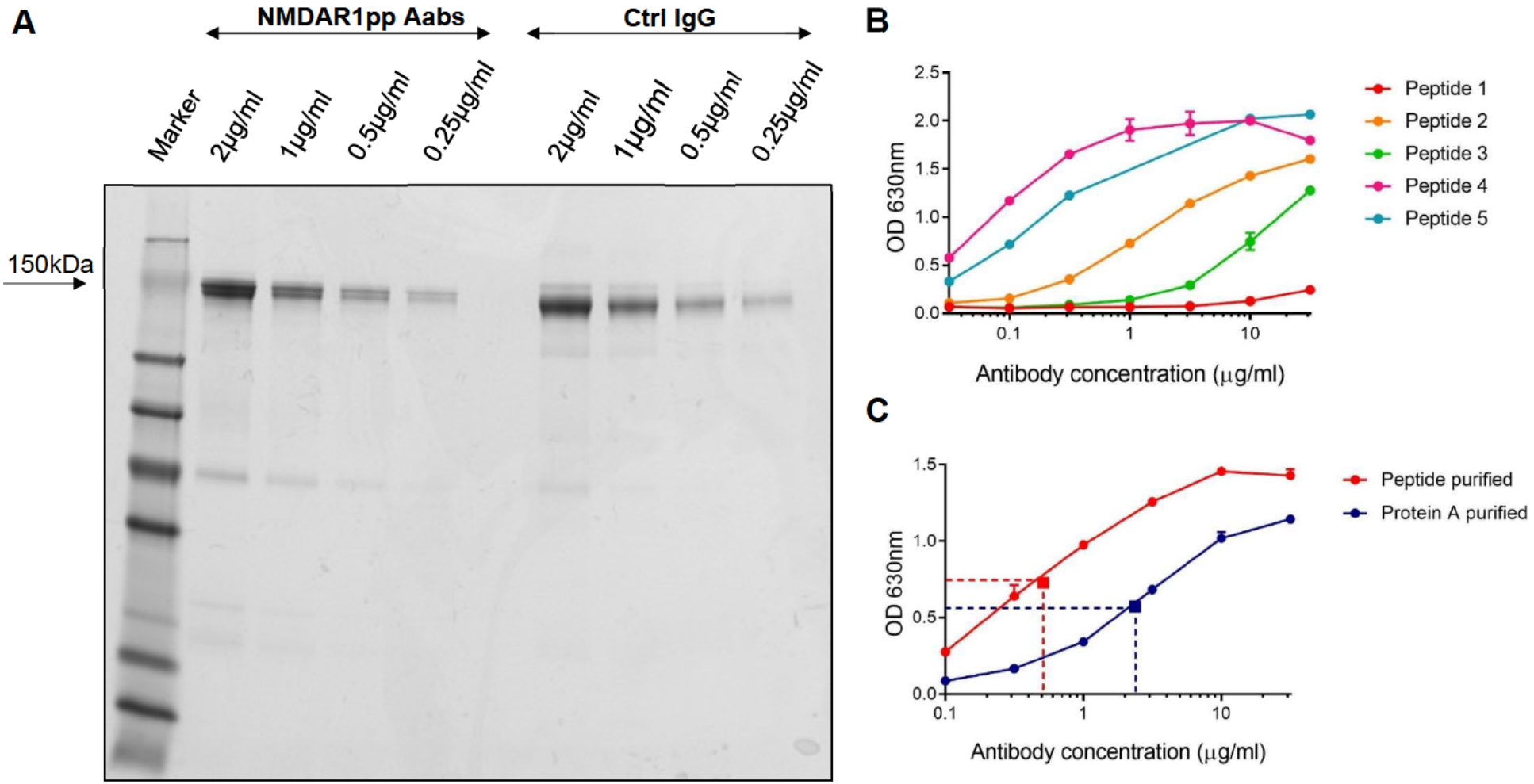

Figure 3.21: Peptide purification of NMDAR1 Aabs. (A) SDS-PAGE analysis of rabbit serum purified by immunisation peptides compared with control rabbit IgG of known concentration showed a band at the expected size of 150 kDa across all dilutions. **(B)** Peptide purified NMDAR1 Aabs revealed peptides 2, 4 and 5 remain the strongest binding, similar to that seen by protein A purified NMDAR1 Aabs, with an increase in binding to peptides 3 and 1. **(C)** Peptide purified material resulted in an increase in binding to ATD protein due to a more concentrated specific material, dotted lies represent EC_{50} values. N=3 technical replicates per concentration.

3.7 Characterisation of NMDAR1pp Aabs on *in vitro* systems

3.7.1 NMDAR1pp Aab detection of NMDAR in NR1-transfected HEK cells

In order to analyse the specificity of NMDAR1pp Aabs, HEK cells were transfected with either a vector encoding the NR1 subunit or an empty vector (see section 2.2.1). The day after transfection, cells were fixed and incubated with NMDAR1pp Aabs, and ICC performed (as described in section 2.2.1.1).

NMDAR1pp Aabs positively stained NR1-transfected HEK cells (as shown by the white arrows; Figure 3.22A), while eliciting less background staining than that seen with NMDAR1 Aabs and NMDAR2 (as shown by white arrowheads), most likely due to most of the non-NMDAR specific IgG being removed in the further purification. These positively stained cells co-localised with cells which were also positively labelled with the commercial anti-NR1 antibody mNMDAR (as shown by white arrows; Figure 3.22A). A second commercial antibody was also tested: rNMDAR, which elicited similar staining to all NMDAR Aabs, whereby positively stained cells were also co-labelled by the commercial antibody mNMDAR (as shown by white arrows; Figure 3.22B). Negative controls were also employed; class specific antibodies rIgG and mIgG2b, as well as a secondary-only antibody incubation. The class-specific negative control rIgG demonstrated low levels of background staining (as shown by white arrowheads; Figure 3.22C), as seen with NMDAR1 (Figure 3.5A) and NMDAR2 Aabs (Figure 3.16A), but no clear, bright labelling of NR1-tranfected HEK cells was detected. The secondary only control also showed no labelling of NR1-transfected HEK cells (Figure 3.22D).

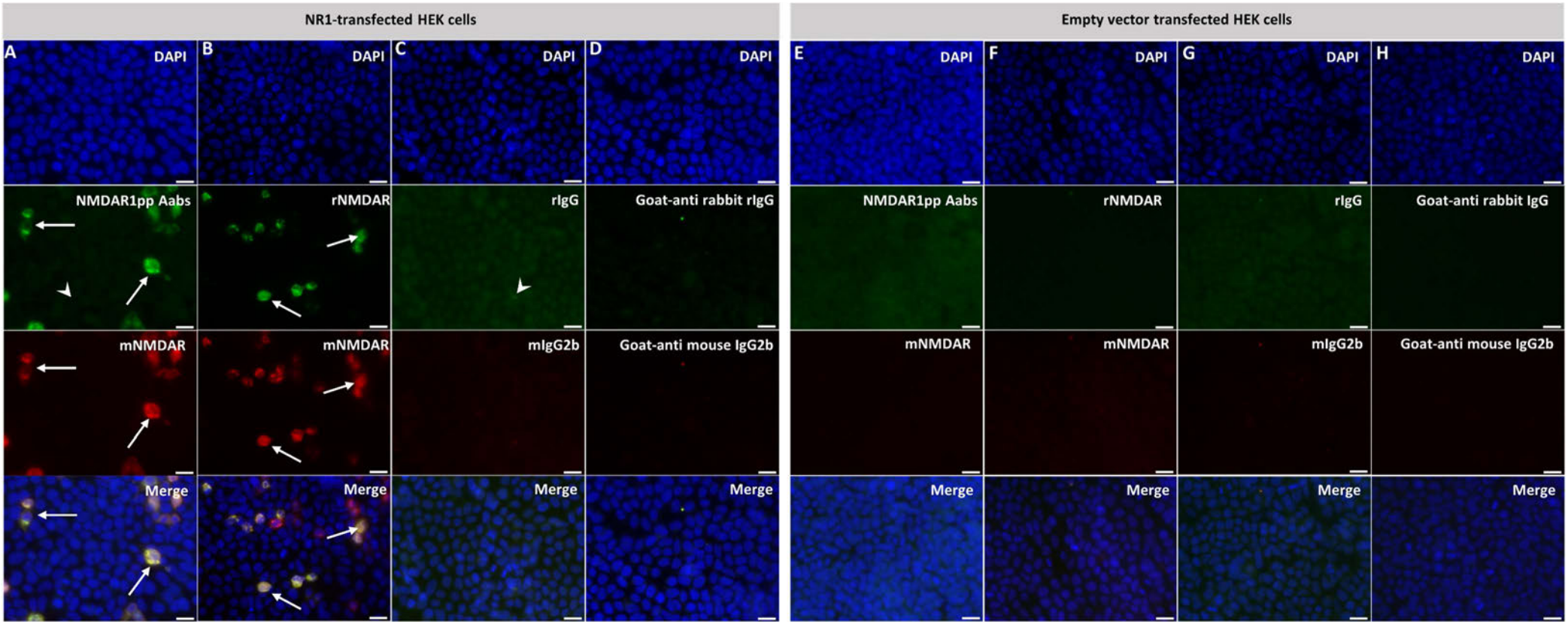

Figure 3.22: ICC staining of NR1 and empty vector transfected HEK cells. Cells were stained with NMDAR1pp Aabs, two commercial anti-NR1 antibodies: mouse anti-NR1 (mNMDAR), rabbit anti-NR1 (rNMDAR) and a nuclear stain (DAPI, blue). Cells transfected with NR1 were detected by NMDAR1pp Aabs, which were co-labelled by the commercial antibody mNMDAR (**A;** as shown by white arrows). Both commercial antibodies mNMDAR and rNMDAR co-labelled the same NR1-transfected cells (**B;** as shown by white arrows). Cells were incubated with the class-specific negative controls rIgG and mIgG2b, as well as being subjected to a secondary-only control. Neither of these conditions elicited any positively stained cells **(C & D).** ICC staining of empty vector transfected HEK cells showed no clear staining when stained with NMDAR1 Aabs (1:100; **E**), as well as two commercial anti-NR1 antibodies **(F)**. **(G & H)** Cells incubated with the class-specific negative controls rIgG and mIgG2b, as well as a secondary-only control did not exhibit any positive staining. Representative images selected from n=3 replicates per condition. Scale = 20µm.

Empty vector transfected HEK cells were also subjected to ICC. NMDAR1pp Aabs did not brightly stain any cells, there was however low levels of background labelling, as seen in NR1-transfected HEK cells (shown by white arrowheads; Figure 3.22E). Similarly, neither commercial antibody positively labelled any cells (Figure 3.22F). As above, the cells were also incubated with class specific negative controls; rIgG and mIgG2b, both of which gave no bright labelling of any cells. Again, there was some background staining detected with rIgG (as shown by white arrowheads; Figure 3.22G), a similar level to that detected by those incubated with NMDAR1 & 2 Aabs and rIgG in both NR1- and empty vector-transfected HEK cells (Figure 3.5A, C, E & G and Figure 3.16A & C respectively).

3.7.1.1 NMDAR Aab detection of NMDAR to native NMDARs

ICC was carried out to determine cell-type specificity of NMDAR1pp Aabs in primary cortical neurons to determine the labelling of endogenous receptors in a more physiological relevant model. Primary cortical neurons were fixed at DIV7-20 and exposed to NMDAR1pp Aabs, and co-labelled with the neuronal-specific marker, βIII tubulin, and astrocyte-specific marker, GFAP, to identify cell-type specificity within the culture.

NMDAR1pp Aabs stained cells were co-labelled by the neuronal marker βIII tubulin (as shown by the white arrows; Figure 3.23A), but not by the astrocyte marker GFAP. Cells were also subjected to a secondary-only control, whereby no binding was detected due to the lack of primary antibody incubation (Figure 3.23B), indicating all of the labelling seen in Figure 3.23A occurred as a result of primary antibody binding, not due to background staining caused by the secondary antibodies.

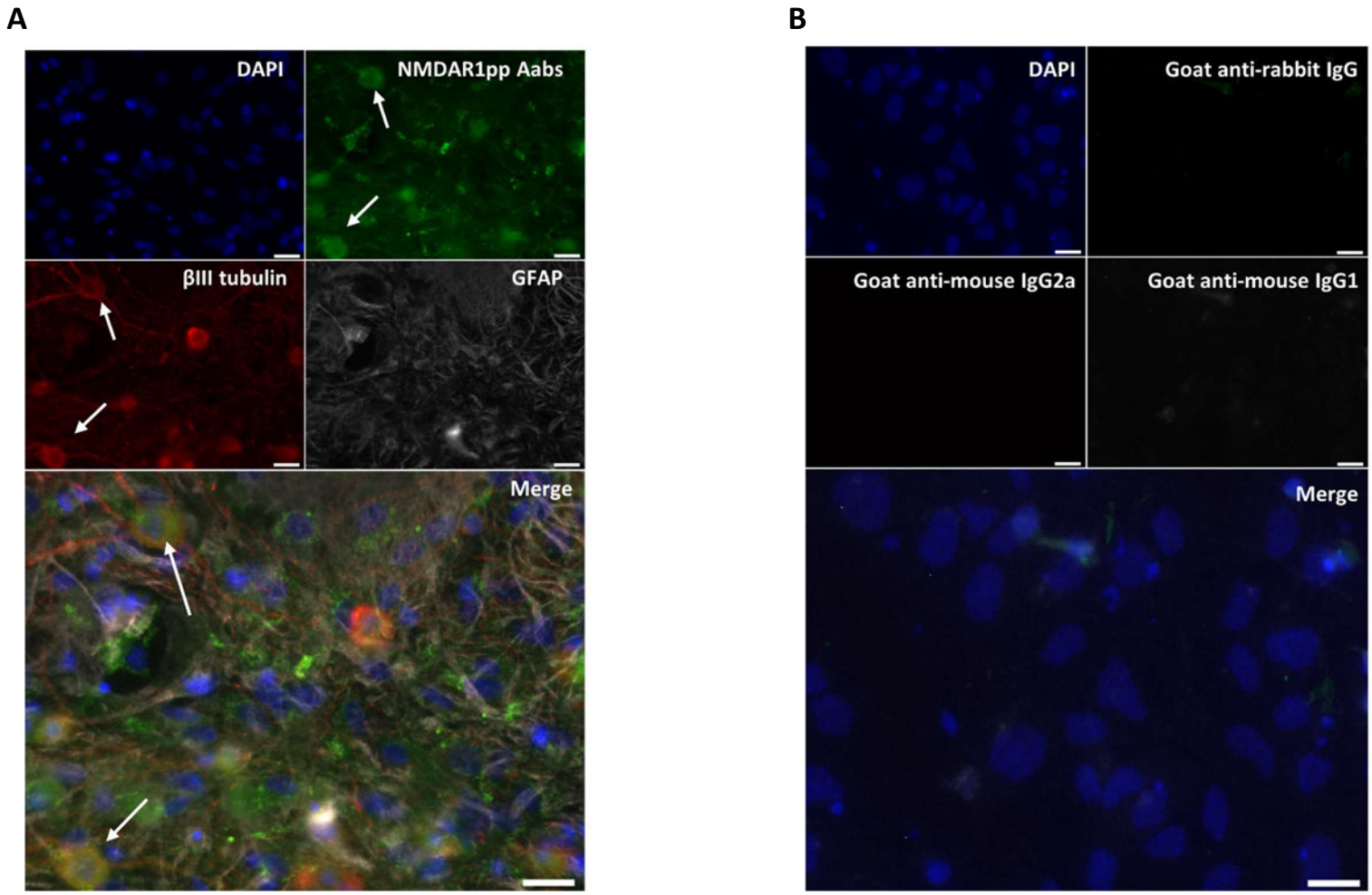

Figure 3.23: ICC staining of primary cortical neuronal cells (DIV14). (A) Cells stained with NMDAR1pp Aabs (green), co-stained with βIII tubulin; a neuronal marker (red), and a nuclear stain (DAPI: blue). **(B)** Secondary antibody only control resulted in no staining in any channel. Representative image selected from n=4 technical replicates (across 3 biological replicates). Scale = 20µm.

IHC was also carried out on mouse hippocampal brain sections to determine spatial binding within the brain as well as cell-type specificity. Using perfusion fixed and cryopreserved mouse brain sections (12µm), minimal binding was observed with NMDAR1pp Aabs (Figure 3.24). Only faint staining was detected with co-labels βIII tubulin (neuronal cells) and GFAP (astrocytes), which have been validated and optimised previously, suggesting this staining is likely due to an issue relating to the quality of sections used, which is possible due to immersion fixation. Alternatively, a higher magnification may be required to detect the staining pattern of all antibodies (as shown for NMDAR1 Aabs in Figure 3.8). Overall, although it is hard to distinguish the specificity of NMDAR1pp Aabs for different cell types using IHC, as well as spatial binding within the hippocampus, clear specific staining can be seen with NMDAR1pp Aabs when staining primary cortical neurons (as shown in Figure 3.23A).

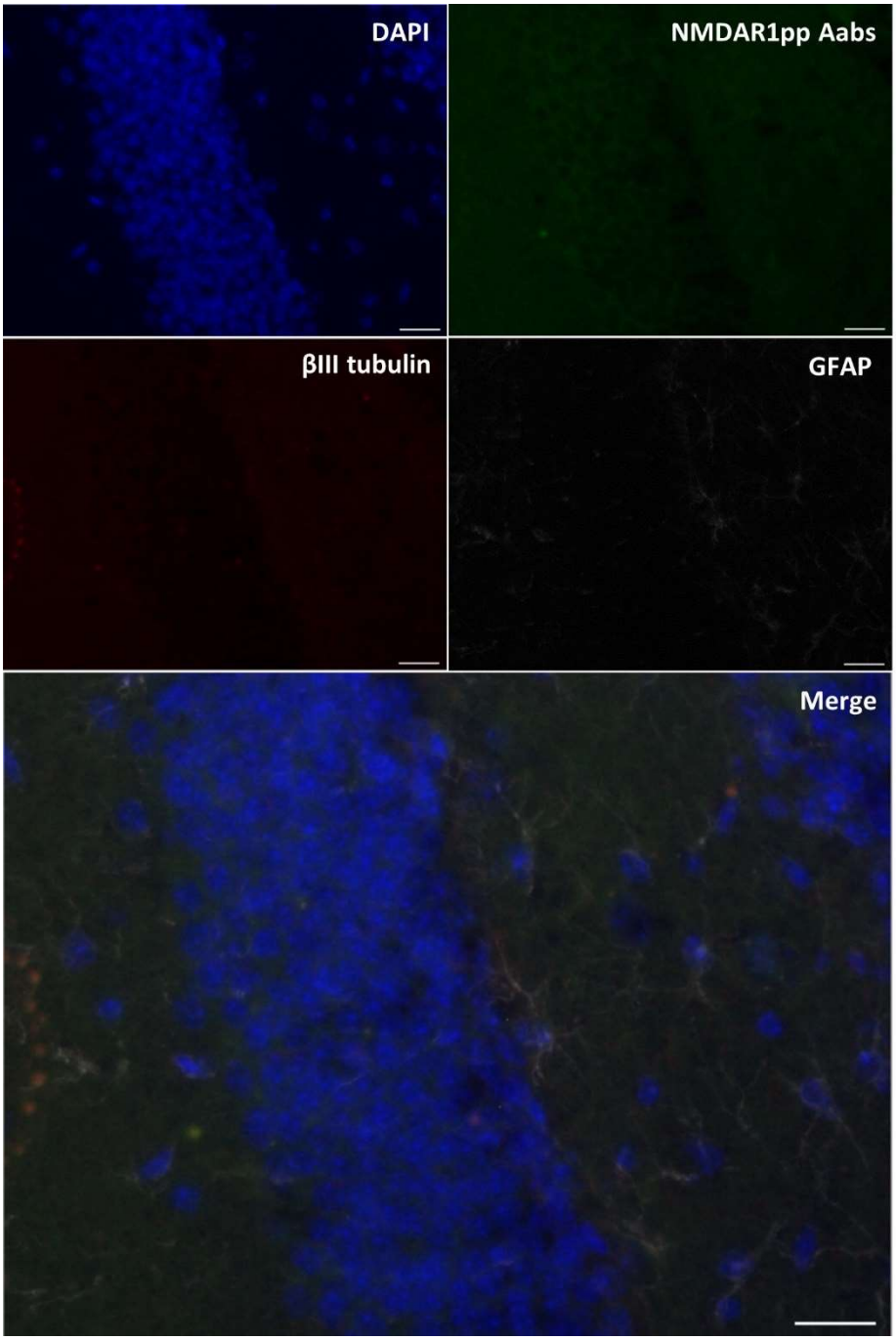

Figure 3.24: Representative image of immunohistochemical staining of dentate gyrus of fixed hippocampal brain slice. Cells incubated with NMDAR1pp Aabs, and co-stained with βIII tubulin and GFAP demonstrated minimal binding, highlighting a higher magnification for visualisation is required. Representative image selected from n=3 replicates. Scale = 20μm.

The ATD of the NR1 subunit was used to assess the specificity of NMDAR1pp Aabs by western blot. Purified human NR1 ATD was run on SDS-PAGE and probed with NMDAR1pp Aabs. The blot probed with NMDAR1pp Aabs detected a strong band at the predicted size of 60 kDa, indicating the ATD of the NR1 subunit is bound by NMDAR1pp Aabs. A slightly smaller band just under 60 kDa can also be seen (Figure 3.25), which may be due to a different glycosylated state of the ATD (7 glycosylation sites within the ATD: Figure 3.1), or slight degradation of the sample.

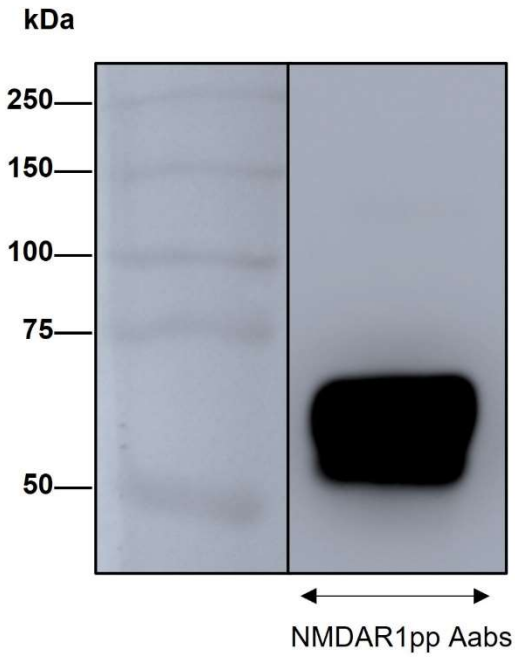

Figure 3.25: Human ATD of NR1 subunit probed with NMDAR1pp Aabs. Blots incubated with NMDAR1pp Aabs detected a strong band at 60 kDa. Representative blot selected from n=3 technical replicates.

Subsequent western blots were carried out to assess if NMDAR1pp Aabs detect full-length NR1 when in a denatured state. Lysates from NR1-transfected HEK cells, primary cortical neurons (mouse) and whole brain (mouse) were generated and run on SDS-PAGE and probed with NMDAR1pp Aabs. No clear band was identified at the expected molecular weight of the NR1 subunit (105 kDa) in either HEK cell lysate, primary cortical cell lysate or whole brain lysate. However, a single band was detected at 70 kDa across all four samples, with additional bands at 50 kDa in primary cortical cells and whole brain lysate and a faint band just above 100 kDa NR1 HEK cell lysate (Figure 3.26A). Despite this lack of a clear band at the expected size of 105 kDa, several of the 'non-specific' bands seen previously with NMDAR1 and NMDAR2, as well as rIgG were not seen here. As with NMDAR1 and NMDAR2 Aabs, these non-NMDAR-related bands are likely to be caused by the Aabs not being able to detect full length NR1 subunit when in the denatured state. Thus, as the Aabs are generated against a

mixture of both linear and cyclised peptides, it may be the case that Aabs have been generated which bind to epitopes which are present in the natural conformation, but not detectable once in a denatured state.

As before, a loading control, GAPDH was used to ensure correct loading and transfer of proteins was carried out. This revealed a single, clean band at the expected size of 37 kDa, with differences in band sizes caused by different amounts of protein loaded for samples (10µg of cortical cell, HEK NR1 and HEK empty vector lysate, compared to 50µg protein of whole brain lysate; Figure 3.26B), confirming the validity of the experimental approach.

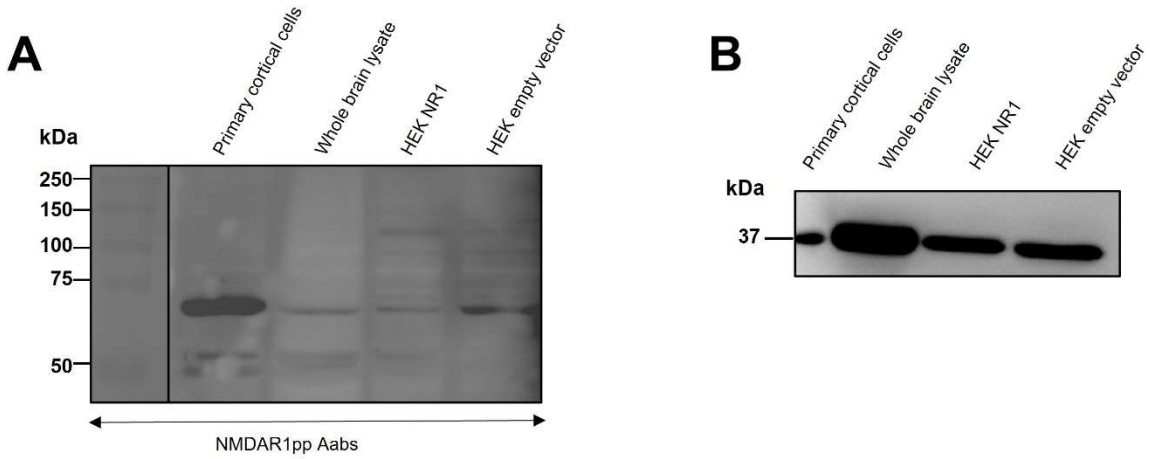

Figure 3.26: Binding specificity of NMDAR1pp Aabs in western blot. (A) Representative gel bands for NMDAR1pp Aabs against primary cortical cell lysate (10µg protein), whole mouse brain lysate (50µg protein), and NR1- and empty vector-transfected HEK cell lysates (10µg protein). No specific band was detected at the expected size of 105 kDa in any sample. **(B)** GAPDH probed blots resulted in a single, clean band at the expected size of 37 kDa. Representative blots selected from n=3 technical replicates.

3.8 Discussion

NMDAR Aabs have been increasingly identified as pathogenic entities in patients with autoimmune NMDAR encephalopathy, while more recently these Aabs have been identified in sera of patients with autoimmune epilepsy. Here we immunised rabbits with peptides based on sequences identified from patient sera to produce a series of NMDAR Aabs, purified total IgG and subsequently examined the specificity for NMDARs. The results of these characterisation experiments are summarised below:

- Strong binding against immunisation peptides was detected following immunisation of both rabbits 1 and 2. This was maintained following protein-A purification.
- NMDAR1 and 2 Aabs displayed specific staining in NR1-transfected HEK cells.
- NMDAR1 and 2 Aabs show specific staining in primary neurons, although, less specificity was observed in western blots.
- Further purification of NMDAR1 Aabs by peptide (NMDAR1pp Aabs) resulted in a more concentrated sample of NMDAR-targeted Aabs, as measured by ELISA results, whereby less peptide purified material than Protein A purified material was required to elicit a 50% maximal response.
- NMDAR1pp Aabs showed increased specific staining in both NR1-transfected HEK cells and primary neurons, as well as detecting the NMDAR ATD in western blots.

A series of NMDAR Aabs were produced, of which NMDAR1pp Aabs demonstrated clearer binding and reduced background providing a strong basis for further functional studies detailed in Chapter 4.

3.8.1 Peptide immunisation generates NMDAR Aabs

Synthetic peptides have numerous applications in research, one of which is the production of antibodies through peptide immunisation. This method has been carried out extensively and used successfully for disease diagnosis (Trier and Houen, 2017) as well as research into pathological mechanisms of native Aabs in patients (Pan *et al.*, 2018; Wagnon *et al.*, 2020). Design of immunisation peptides is crucial to successful antibody generation, with optimal length being between 8-25 amino acids targeting protruding regions, often yielding antibodies with good specificity (Trier and Houen, 2017; Trier *et al.*, 2019). As our study involved generating peptide immunised Aabs against NMDARs to determine any pathogenic potential, the epitopes and peptides used were determined based on knowledge from patient anti-NR1 Aabs that had been previously identified in the literature (as illustrated in Figure 3.1). A study conducted by Gleichman *et al* showed that patient anti-NR1 Aabs bind to two amino acids within the NR1 ATD; N368/G369 (as illustrated in Figure 3.1) (Gleichman *et al.*, 2012), these patient Aabs have been shown to cross-link and cause internalisation of NMDARs when applied to primary hippocampal neurons (Hughes *et al.*, 2010). Therefore, a region encompassing these two amino acids (N368/G369) was designed (peptide 5; Figure 3.1). Other regions within the NR1 subunit which were deemed immunogenic due to their extracellular location and protruding loops were used to design other peptides used for immunisation. Immunisation peptides were split over two animals, peptides 1-5 immunising rabbit #1, and peptides 6-9 immunising rabbit #2.

In an attempt to better mimic the natural conformation of NR1 regions, several peptides were cyclised via a thioester. Peptides 2, 4 and 5 were cyclised for NMDAR1 Aabs, which following immunisations gave the best immunogenic response as shown by the ELISAs (Figure 3.2B, D and E respectively), whereby each immunisation boost resulted in increased concentration of NMDAR specific Aabs and hence increased binding. This is in contrast to peptides 1 and 3,

which failed to generate a strong immunogenic response throughout each immunisation boost (Figure 3.2A and C respectively), which were non-cyclised and linear in nature (Purcell *et al.*, 2007).

Following immunisation, antibody specificity was tested via ELISA to ensure an immunogenic response specific to the immunised peptides had been developed, a methodology used routinely following peptide immunisation (Lee *et al.*, 2010; Pan *et al.*, 2018). The presented data show an increased binding to three out of five peptides used for immunisation in rabbit #1, the three peptides which were cyclised prior to immunisation. Increased binding was also detected against the ATD protein via ELISA (Figure 3.2A-F), giving a promising indication that these Aabs will also bind to native NMDARs effectively. Protein A purification of the terminal serum produced substantial total IgG (12mg/ml), where approximately 1-10% is typically expected to be NMDAR specific (Hnasko and McGarvey, 2015).

Similarly, immunisation of rabbit #2 with peptides 6-9 (Table 2) generated a strong immunogenic response to three out of the four peptides used for immunisation (Figure 3.13A, B & D). These results are in contrast to peptides 1-5, whereby the linear peptides (6, 7 and 9) were bound to the most by terminal sera, with peptide 8, the cyclised peptide eliciting a minimal immunogenic response. Similar to NMDAR1 Aabs, protein A purification of the terminal serum from rabbit #2 produced 11.4mg/ml total IgG.

A direct comparison to other peptide immunised anti-NMDAR Aabs in the literature cannot be easily made. Some recent studies have generated NMDAR Aabs following peptide immunisation, although different peptides/epitopes were used. In addition, other studies have not performed or documented protein A purification and quantification of total IgG, hence minimal comparisons in antibody purification and concentration can be made (Pan *et al.*, 2018; Wagnon *et al.*, 2020). Furthermore, many studies investigating the pathogenic potential of

NMDAR Aabs typically obtain patient CSF or patient sera which has been tested for the presence/absence of NMDAR Aabs and use these to assess binding and functional properties of Aabs (Hughes *et al.*, 2010; Planagumà *et al.*, 2015; Taraschenko *et al.*, 2019). These data have thus far yielded conflicting results with regard to functional effects (i.e., epileptic potential of Aabs, with some mouse models exhibiting spontaneous seizures following infusion of patient CSF/sera, while others do not). Conflicting functional activity may be as a result of the type of Aabs used, whereby other components within CSF or sera may be altering the functional effects of NMDAR Aabs.

3.8.2 Anti-NMDAR Aabs bind to native NMDARs

To test the binding of our NMDAR Aabs, a range of techniques such as ICC, IHC and Western blot were employed, as detailed in other studies generating peptide immunised Aabs/testing Aab positive patient CSF (Trier *et al.*, 2012; Jones *et al.*, 2019; Wagnon *et al.*, 2020). Similar to results seen in Wagnon *et al* and Jones *et al,* when our NMDAR Aabs were applied to NR1 transfected HEK cells binding was observed, similar to that of commercial anti-NR1 antibodies. Moreover, when applied to empty-vector transfected HEK cells, no staining was identified. Furthermore, class specific negative controls rIgG and mIgG2b did not elicit any staining on either NR1- or empty vector-transfected HEK cells. Despite different peptides/immunisation protocols being carried out between our study and those in the literature, similar specificity was seen to native NR1. All immunisation peptides used both in this thesis and previous studies contained the sequence to which patient Aabs have been shown to bind (N368, G369) (Gleichman *et al.*, 2012), whether it be immunisation of whole receptor complex (Jones *et al.*, 2019), one 19 amino acid long peptide (Wagnon *et al.*, 2020) or a mixture of five peptides as carried out in our study, all generated NMDAR Aabs appear to interact with NR1 transfected HEK cells in a similar manner.

This specificity was also identified when NMDAR Aabs were applied to primary hippocampal and cortical neurons. Specific binding of neuronal cells was seen with NMDAR1 and NMDAR2 Aabs, which co-localised with βIII tubulin-stained neurons. A stronger signal was observed following further peptide purification of NMDAR1 Aabs. Our data are in keeping with findings in previous studies where Aabs from patient CSF demonstrate NMDAR staining in hippocampal neurons (Hughes *et al.*, 2010). One significant difference is that we have demonstrated these similar findings using NMDAR Aabs which have been generated following peptide immunisation, rather than from patient CSF. This is of huge value as these are able to be utilised as a tool in order to investigate binding and functional properties more readily than NMDAR Aabs from patient CSF.

Clear signals within the CA1, CA3 and DG regions of the hippocampus could also be seen when NMDAR1 Aabs were applied to mouse brain sections, a result which was comparable to commercial anti-NR1 antibodies. Specific labelling, albeit to a lesser extent could also be seen with the class specific rIgG, a phenomenon which has been noted previously and is hypothesised to be due to Fc binding to Fc receptors within the tissue (Hewitt *et al.*, 2014). Therefore, conclusions about the specificity of NMDAR Aabs for use in IHC are ambiguous.

The lack of specificity shown by our NMDAR Aabs in western blotting experiments as shown by the multiple non-specific bands may be explained by the fact that this Aab is polyclonal and therefore contains Aabs against multiple epitopes, as well as 'non-NMDAR specific' antibodies specific for other proteins in the lysate (Lipman *et al.*, 2005), which could be confirmed in further experiments by pre-incubating Aab with immunisation peptide to see which bands remain and are therefore caused by non-NMDAR specific antibodies. This was also seen for the commercial rNMDAR antibody, a polyclonal antibody. As polyclonal antibodies represent a pool of antibodies against the immunogen there is a greater chance of

cross-reactivity (Bordeaux *et al.*, 2010). In addition, the lack of specific band at the correct size in NMDAR Aab incubated blots may also be due to the conformation of protein present. As NMDAR Aabs were generated against a mixture of linear and cyclised peptides (cyclised in order to better represent the 3D structure), it is possible that the majority of Aabs generated recognise epitopes in the native conformation and therefore cannot bind the protein of interest after it is fully denatured (Bordeaux *et al.*, 2010). This is supported by the ATD western blot experiments, where native NR1 ATD was probed and clearly detected with NMDAR Aabs.

In addition, it is not uncommon for antibodies to work in certain assays and not in others, where the epitopes they target may be more readily available depending on the present conformation (Lipman *et al.*, 2005; Saper, 2009). This is shown by the two anti-NR1 commercial antibodies used in this chapter, whereby one anti-NR1 commercial antibody is recommended for the use in western blot (mNMDAR; Synaptic Systems), and the other is not (rNMDAR; Synaptic Systems), due to the different epitopes they target and in which conformation they preferentially bind (with rNMDAR targeting amino acids 35-53 within the ATD of NR1 and mNMDAR targeting amino acids 660-811 within the NR1 subunit, which lies within an extracellular loop between transmembrane domains 3 and 4, outside of the ATD). The commercial antibody rNMDAR, when used in western blot identified a multitude of bands, similar to that of our Aabs and rIgG, highlighting the need to determine the correct use of different antibodies for selected assays. Despite the ambiguity surrounding NMDAR specificity following IHC and western blot experiments, ICC on primary cortical neurons and in particular NR1-transfected HEK cells resulted in very clear, specific binding of NMDAR Aabs. Similarly, no labelling in empty vector transfected HEK cells gives confidence that these Aabs were not binding to native components of HEK cells, but instead are binding to the transfected material; in this case NR1 subunit. However, as shown by some data in this chapter,

these Aabs may be better suited to characterisation techniques whereby the target protein is in its natural conformation, as opposed to in a denatured state.

Further investigation into the binding specificity and functionality of NMDAR Aabs could be determined via the use of confocal microscopy on NR1-transfected HEK cells, primary neurons as well as brain slices. Performing this imaging at higher magnification and resolution would help elucidate the specific binding location of these NMDAR Aabs, as well as whether any Aab-induced internalisation of NR1 subunit was taking place. Furthermore, performing co-labelling with antibodies which target other subunits of NMDARs, as well as other glutamate receptors such as AMPAR, would help determine the specificity of our generated Aabs for NMDARs.

3.8.3 Conclusions

It can be concluded that specific NMDAR Aabs directed against the NR1 subunit can be generated following immunisation with peptides against specific epitopes. These Aabs in both the protein A- (NMDAR1 and NMDAR2) and peptide purified (NMDAR1pp) form showed increased binding to immunisation peptides, as well as the native ATD protein, with NMDAR1pp Aabs requiring only 0.51µg/ml to elicit a 50% maximal response compared to NMDAR1 Aabs requiring 2.36µg/ml to elicit a 50% maximal response. NMDAR1 and 2 Aabs, as well as NMDAR1pp Aabs demonstrated NMDAR-specific staining in both NR1-transfected HEK cells and primary hippocampal neurons. Although the western blots showed many non-specific bands in whole brain lysate, cortical cell lysate and HEK lysate when probed with NMDAR1 and 2 Aabs and NMDAR1pp Aabs, all three specifically identified a strong clear band at the correct molecular weight when probed against native ATD protein.

Therefore, based on the evidence presented in this thesis NMDAR1pp Aabs resulted in increased binding to immunisation peptides, as shown by EC50s, as well as cleaner

immunostaining in both NR1-transfected HEK cells and primary neurons, where less background staining was observed. This specificity for NMDAR Aabs across a range of assays give a good foundation for subsequent testing in functional assays, as detailed in the next chapter.

4. Assessing the functionality of NMDAR Aabs

4.1 Introduction

Chapter 3 described the successful generation and characterisation of 3 distinct sets of NMDAR Aabs: NMDAR1 (protein A-purified and peptide-purified) and NMDAR2 (protein A-purified). This chapter will describe the results from the experiments using different electrophysiological systems to identify functional effects of anti-NMDAR Aabs on NMDARs and associated networks. Three main electrophysiological techniques were utilised throughout this chapter: TEVC using *Xenopus* oocytes, MEAs recording from acute mouse hippocampal brain slices, and whole-cell patch-clamp on primary hippocampal neurons.

Xenopus oocytes were used as an expression system, whereby NR1/NR2A subunits of NMDARs could be overexpressed in isolation. Due to the large diameter of oocytes (~1.1mm), it is relatively easy to inject cDNA, resulting in efficient translation of ion channels. Currents from these channels can be subsequently recorded via TEVC (Tammaro *et al.*, 2008). A brief co-application of glutamate and glycine was used to assay NR1/NR2A expression, glutamate and glycine were then applied at regular time points throughout each experiment. Data were quantified as AUC. NMDAR1 Aabs or control rIgG were applied to the oocytes and incubated for both 'acute' and 'chronic' time periods. The effects of NMDAR1 Aabs were compared to negative control rIgG to determine that any other 'non-NMDAR specific' IgG was not producing any electrophysiological effects. The second electrophysiological technique performed utilised MEA recordings from acute hippocampal brain slices. This method allowed a more physiological approach to be taken where the effect of NMDAR Aabs on NMDARs could be assessed at the network level. Stimulation of the Schaffer collaterals was used to evoke a post-synaptic response in the CA1 region. Using a specific stimulation pattern, LTP can be induced which, in this area, is NMDAR-dependent (Bliss and Collingridge, 1993). Successful

LTP results in a potentiation of the post-synaptic signal, which is a result of NMDAR channel activation and AMPAR recruitment to the post-synaptic membrane. The third electrophysiological technique used utilised whole-cell patch-clamp recording from primary hippocampal neurons. This method again allowed a more physiological approach whereby NMDAR currents could be investigated in isolation via application of pharmacological inhibitors.

Thus, we aimed to assess any changes in NMDAR current following NMDAR Aab application using these three electrophysiological paradigms. Results from these approaches aimed to provide insights into any potential involvement of NMDAR Aabs in cell signalling which has potential to be correlated with seizure activity.

4.2 Xenopus oocytes experimental setup

To investigate the effects of NMDAR1 protein A purified Aabs (NMDAR1 Aabs) on NMDAR activity, *Xenopus* oocytes were injected with human NR1/NR2A cDNA and left for 3-5 days to allow expression (as illustrated in Figure 4.1). Oocytes were recorded electrophysiologically using TEVC, whereby NMDAR current was evoked using the NR1/NR2 agonists glycine and glutamate respectively (as shown in Figure 4.1).

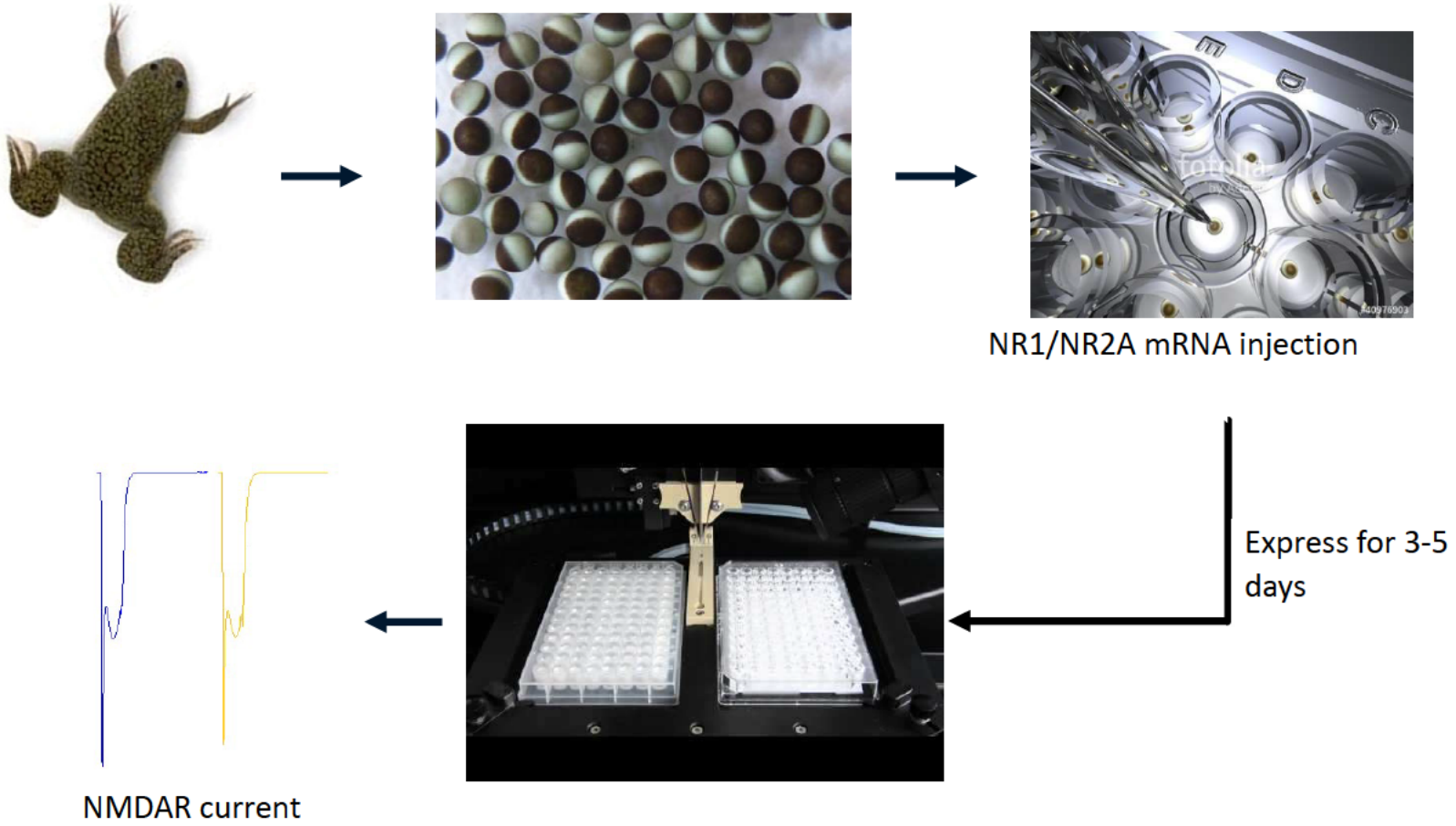

Figure 4.1: Schematic of oocyte experimental setup. Oocytes obtained from Xenopus Laevis and GluN1/2A mRNA injected into the cytoplasm, left for 3-5 days to allow the receptors to be expressed before being subjected to two-electrode voltage-clamp. NMDAR currents were measured following application of agonists glutamate and glycine.

4.2.1 Known NMDAR antagonists reduce NMDAR current

NMDAR Aabs are hypothesised to have an inhibitory effect on NMDAR current, via internalisation of the receptor (Hughes *et al.*, 2010). Therefore, two NMDAR inhibitors (non-competitive NMDAR antagonist MK-801 and an allosteric modulator TCN-201) were employed as positive controls. Oocytes were incubated in increasing concentrations of NMDAR inhibitor (10nM – 3.16μM), with NMDAR currents being evoked via application of glutamate/glycine at regular intervals throughout (Figure 4.2C).

Increasing concentrations of MK-801 were applied to oocytes, where the highest concentration used (1μM) significantly reduced the AUC of the evoked NMDAR current (0.1 ± 0.05) when compared to equimolar DMSO-incubated oocytes (vehicle control; 1.2 ± 0.09; Figure 4.2A). Using a two-way ANOVA, a significant effect of MK-801 was identified when compared to DMSO ($F(1,4) = 237.7$, $p = 0.0001$, n = 3 per group). In addition, a significant effect of drug concentration was observed ($F(8,32) = 26.51$, $p<0.0001$, n = 3 per group). The interaction between time and drug concentration was also significant ($F(8,32) = 75.88$, $p<0.0001$, n = 3 per group).

Similar to MK-801, the NR1 allosteric modulator TCN-201 was also applied in increasing concentrations to identify any effects on NMDAR current. The highest concentration used (3.16μM) significantly reduced the AUC of the evoked NMDAR current (0.2 ± 0.05) when compared to equimolar DMSO (1.5 ± 0.2; Figure 4.2B). A significant effect of TCN-201 was identified when compared to DMSO ($F(1,11) = 102.2$, $p <0.0001$, n = 6-7 per group). A significant effect of drug concentration was also observed ($F(7,77) =26.9$, $p<0.0001$, n = 6-7 per group). A significant interaction between time and drug concentration was also seen; ($F(7,77) = 104.2$, $p<0.0001$, n = 6-7 per group). The addition of these pharmacological inhibitors acted as positive controls for the model system.

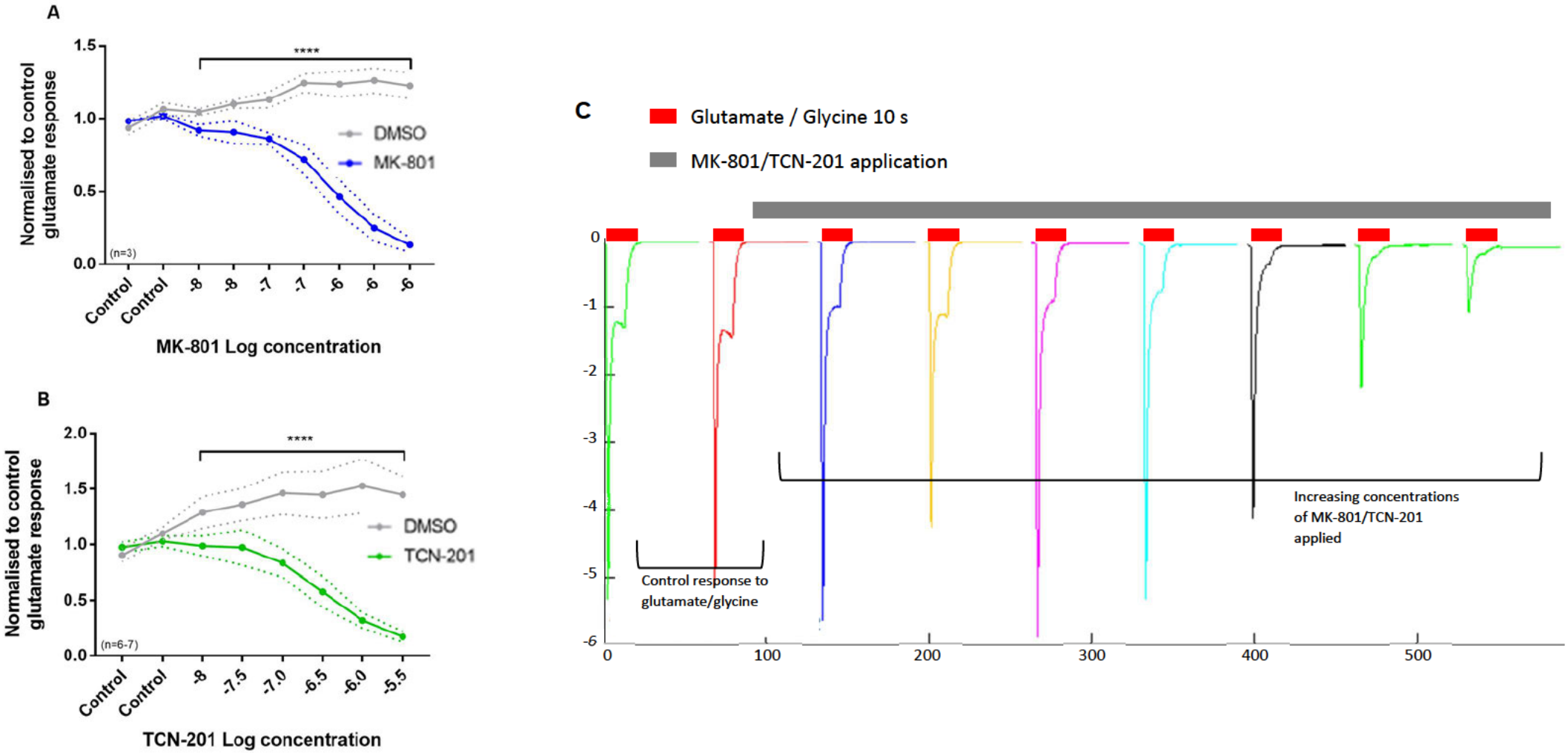

Figure 4.2: Known NMDAR antagonists significantly reduce NMDAR current. (A) A significant reduction in area under the curve of the glutamate-evoked response was seen with increasing concentration of MK-801; a non-competitive NMDAR antagonist when compared to its vehicle control; DMSO. A two-way ANOVA revealed a significant effect of drug vs vehicle ($p = 0.0001$, $n = 3$ per group), and also a significant effect of drug concentration used ($p < 0.0001$, $n = 3$ per group). **(B)** Similarly, a significant reduction in glutamate-evoked response was seen with increasing concentration of TCN-201; a NR1 allosteric modulator. Again, a two-way ANOVA revealed both a significant effect of drug vs vehicle ($p < 0.0001$, $n = 6$-7 per group), and drug concentration used ($p < 0.0001$, $n = 6$-7 per group) respectively). Data are represented as mean ± SD, ****: $p < 0.0001$. **(C)** Overview of protocol used for acute application of NMDAR antagonists on Xenopus oocytes. Control responses were used to normalise all subsequent evoked current responses. MK-801 and TCN-201 were applied in increasing concentration, evoking NMDAR current regularly throughout to monitor any changes in area under the curve.

4.2.2 NMDAR1 Aabs have no functional effects on NMDAR expressing oocytes following acute incubation

Acute effects of NMDAR1 Aabs (protein A purified) were tested by incubation with oocytes for either 21 mins, or 60 mins. To ensure the oocytes were expressing NR1/2A and responsive to glutamate/glycine, four control measurements were performed every 3 min prior to any antibody application. Any oocytes that were unresponsive were not used in the experiment.

To test effects of NMDAR1 Aabs over a 21 min incubation, oocytes were incubated with either NMDAR1 Aabs or control rIgG for a total of 21 min with glutamate/glycine applied every 3 min for 10 s, to evaluate any changes in NMDAR current, as shown in Figure 4.3A (based on the protocol described in (Castillo-Gomez *et al.*, 2016)). To test effects of Aabs over a 60 min period, oocytes were incubated with either NMDAR1 Aabs or rIgG for a total of 60 min with glutamate/glycine applied every 15 min (10 s each) to evaluate any changes in NMDAR current. Both NMDAR1 Aabs and control rIgG were tested at two dilutions; 1:1000 and 1:300 (12µg/ml and 40µg/ml respectively). These dilutions were chosen based on ELISA data (see section 3.2), where greater than 50% binding was seen to most peptides at both 1:300 and 1:1000 (Figure 3.2 & Figure 3.3B). All data for acute experiments were normalised to the last two control glutamate responses (as shown in Figure 4.1), as per methodology in (Mullier *et al.*, 2017).

No significant differences in AUC were observed following a 21 min incubation with either NMDAR1 Aabs or rIgG (1:1000 dilution), as shown by representative traces in Figure 4.3B. Oocytes incubated with NMDAR1 Aabs generated a similar AUC (1.1 ± 0.03) to those incubated with rIgG (1.2 ± 0.09; Figure 4.3C). A two-way ANOVA found no significant differences between NMDAR1 Aabs or rIgG incubated oocytes ($F(1,9) = 1.81$, $p = 0.2118$, n = 5-6 per group) but a significant effect of time on AUC ($F(7,63) = 5.64$, $p<0.0001$, n = 5-6

per group). As a result, the interaction between time and antibody incubation was also identified as significant ($F(7,63) = 2.92$, $p = 0.0103$, n = 5-6 per group) (Figure 4.3C). Therefore, NMDAR1 Aabs had no effect on NMDAR current following acute incubation at 1:1000 dilution. This experiment was repeated using 1:300 dilution to assess if higher concentrations of Aab was required to elicit a functional effect. However, no differences in AUC were observed between NMDAR1 Aab incubated oocytes (0.9 ± 0.09) and those oocytes incubated with rIgG (0.9 ± 0.06; Figure 4.3D). Similar to 1:1000 dilution results, a two-way ANOVA found a significant effect of time ($F(7,63) = 7.40$, $p<0.0001$, n = 5-6 per group), with no significant effect identified between NMDAR1 Aabs and rIgG incubated oocytes ($F(1,9) = 0.03$, $p = 0.8613$, n=5-6 per group). The interaction between time and antibody incubation was not identified as significant ($F(7,63) = 0.98$, $p = 0.4557$, n = 5-6 per group). Therefore, there was a lack of functional effects of NMDAR1 Aabs acutely on NMDA current in oocyte experiments, even at a higher concentration.

Since no functional effect was observed following 21 min incubation at either dilution of NMDAR1 Aabs, a longer, albeit still 'acute' incubation of 60 min was carried out to assess if more time was required for e.g., NMDAR internalisation to occur. This incubation was carried out at 1:300 dilution, according to effective dilutions in ELISA experiments (see Section 3-2). No significant differences in AUC were identified between those oocytes incubated with NMDAR1 Aabs (0.9 ± 0.1) to those incubated in rIgG (0.9 ± 0.1; Figure 4.3E). A two-way ANOVA identified a significant effect of time on area under the curve ($F(4,72) = 13.91$, $p<0.0001$, n = 9-11 per group), with no significance detected between NMDAR1 Aabs and rIgG incubated oocytes ($F(1,18) = 0.44$, $p = 0.5150$, n = 9-11 per group). The interaction between time and antibody incubation was not significant ($F(4,72) = 0.78$, $p = 0.5396$, n = 9-11 per group).

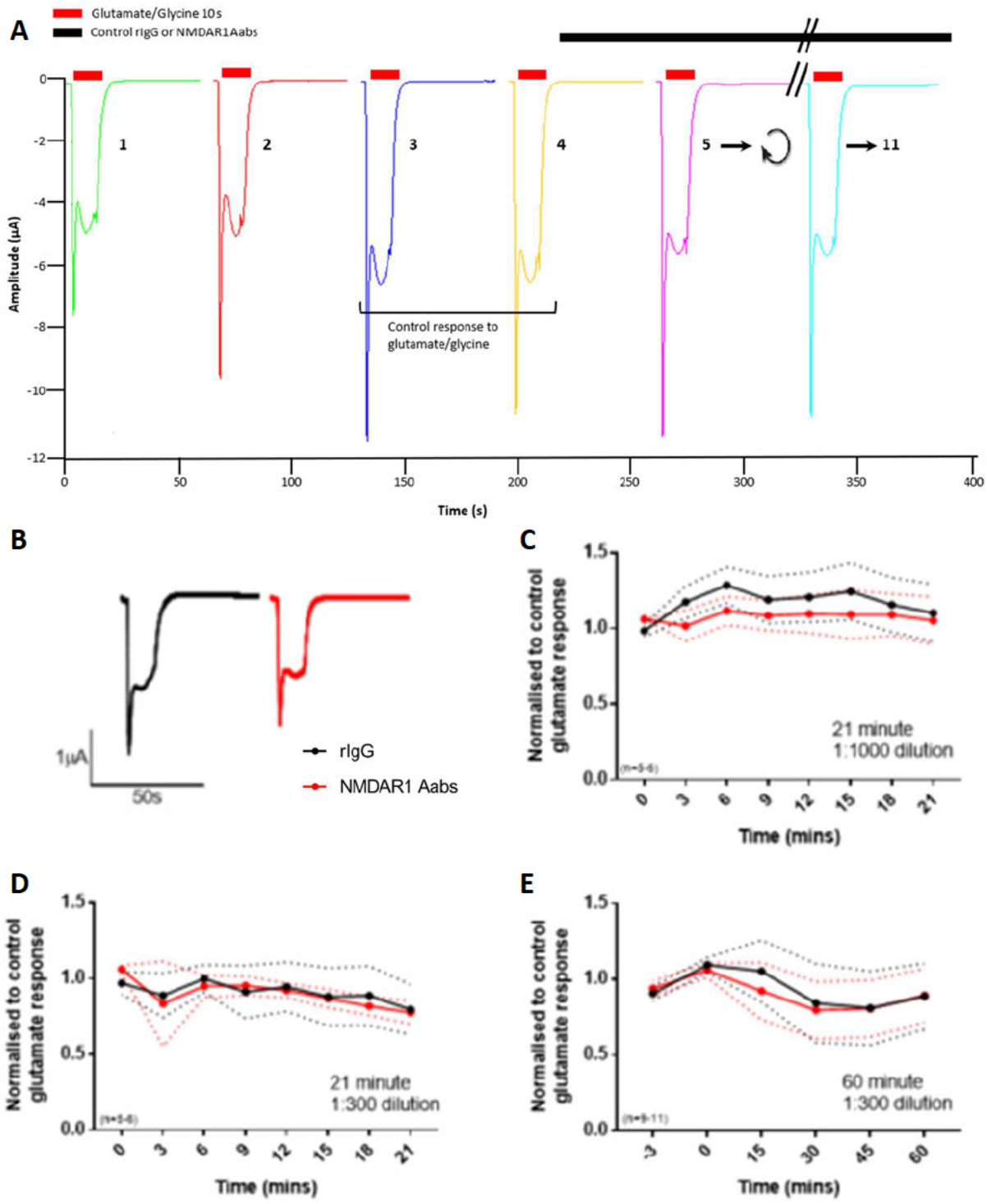

Figure 4.3: No significant change in NMDAR current is seen following acute NMDAR1 Aabs incubation. (A) Overview of protocol used for acute application of NMDAR1 Aabs on Xenopus oocytes. **(B)** Representative traces of NMDAR currents at 21min following application with NMDAR1 Aabs or rIgG. **(C)** No change in area under the curve of the glutamate-evoked response was seen in NMDAR1 Aab incubated oocytes compared to those incubated with IgG at the lowest dilution (1:1000) over a 21 min period. A significant effect of time was found ($p<0.0001$, n = 5-6 per group), but no significant effect of antibody ($p = 0.2118$, n = 5-6 per group). **(D)** Similarly, no significance was found when oocytes were incubated with NMDAR1 Aabs at a higher dilution (1:300) for a total of 21 min ($p = 0.8613$, n = 5-6 per group), only a significance of time was observed ($p<0.0001$, n = 5-6 per group). **(E)** Longer incubation of 60 min of NMDAR1 Aabs and IgG at 1:300 dilution also elicited no changes in NMDAR current between the two antibody applications ($p = 0.5150$, n = 9-11 per group) but did elicit a significant effect of time ($p <0.0001$, n = 9-11 per group). All data are represented as mean ± SD.

4.2.3 NMDAR1 Aabs have no functional effects on NMDAR expressing oocytes following chronic incubation

NMDAR1 Aabs in epilepsy patients are constantly produced and present in both the blood and CSF (Vincent and Bien, 2008). If these Aabs are pathogenic, native NMDARs would be subjected to chronic exposure to Aabs. Therefore, longer incubations of NMDAR1 Aabs and rIgG were performed to model a chronic *in vivo* exposure, where any functional effect may require e.g., downregulation of gene expression. These were performed by way of an overnight (24 h) incubation and a three-day (72 h) incubation. This experimental setup differed slightly to acute experiments as the oocytes were incubated with NMDAR1 Aabs/rIgG prior to being subjected to TEVC, therefore no baseline responses could be performed for each oocyte. Instead, four glutamate/glycine responses were measured, and any differences in NMDAR currents between those incubated with NMDAR1 Aabs or rIgG were measured (Figure 4.4A).

Overnight incubation (24 h) at 1:1000 dilution did not result in any significant changes in AUC of evoked NMDAR currents (representative traces are shown in Figure 4.4B). Oocytes incubated with NMDAR1 Aabs, generated a similar AUC of evoked NMDAR currents (-40.1 ± 14.0) to those oocytes incubated with rIgG (-49.2 ± 16.7; Figure 4.4C). When tested for significance using a two-way ANOVA, similar to acute exposure, a significant effect of time was identified ($F(3,51) = 27.64$, $p<0.0001$ n = 9-10 per group), but no significant effect of antibody ($F(1,17) = 1.88$, $p = 0.1886$, n = 9-10 per group). The interaction between time and antibody incubation was not significant ($F(3,51) = 0.59$, $p = 0.6222$, n = 9-10 per group).

Overnight incubation was repeated using a 1:300 dilution, where NMDAR1 Aab incubated oocytes produced a similar AUC of evoked NMDAR currents (-38.6 ± 7.8) to those incubated with rIgG (-37.9 ± 11.7; Figure 4.4D). A two-way ANOVA was used to test for significance, where again a significant effect of time was identified ($F(3,54) = 17.34$, $p<0.0001$, n = 10 per

group), but no significance was identified with respect to antibody incubation ($F(1,18) = 0.26$, $p = 0.6167$, n = 10 per group). The interaction between time and antibody incubation was not significant $F(3,54) = 1.12$, $p = 0.3488$, n = 10 per group).

To further test the chronic effects of NMDAR1 Aabs on NMDAR current, 72 h incubation was performed at both 1:1000 and 1:300 dilutions, incubating oocytes with either NMDAR1 Aabs or rIgG. As before, NMDAR1 Aab incubated oocytes (1:1000) generated similar AUC values following glutamate/glycine application, as shown by representative traces (Figure 4.4E). NMDAR1 Aab incubated oocytes resulted in similar AUC values (-12.4 ± 8.2) to those incubated with rIgG (-9.5 ± 7.1; Figure 4.4E). A two-way ANOVA was performed, with a significant effect of time identified ($F(3,30) = 12.35$, $p<0.0001$, n = 6 per group), however, no significant effect of antibody was observed ($F(1,10) = 0.20$, $p = 0.6612$, n = 6 per group). No significance for the interaction between time and antibody incubation was seen ($F(3,30) = 1.04$, $p = 0.3903$, n = 6 per group).

Similar to above, 72 h incubation was repeated at 1:300 dilution. NMDAR1 Aab incubated oocytes resulted in an AUC of NMDAR current (-12.8 ± 8.9), similar to that of rIgG incubated oocytes (-6.7 ± 3.2; Figure 4.4F). A two-way ANOVA was performed, with a significant effect of time observed ($F(3,36) = 14.5$, $p<0.0001$, n = 7 per group). No significance was seen with regards to antibody incubation ($F(1,12) = 3.19$, $p = 0.0995$, n = 7 per group). No significant interaction was observed between time and antibody incubation ($F(3,36) = 1.2$, $p = 0.3254$, n = 7 per group).

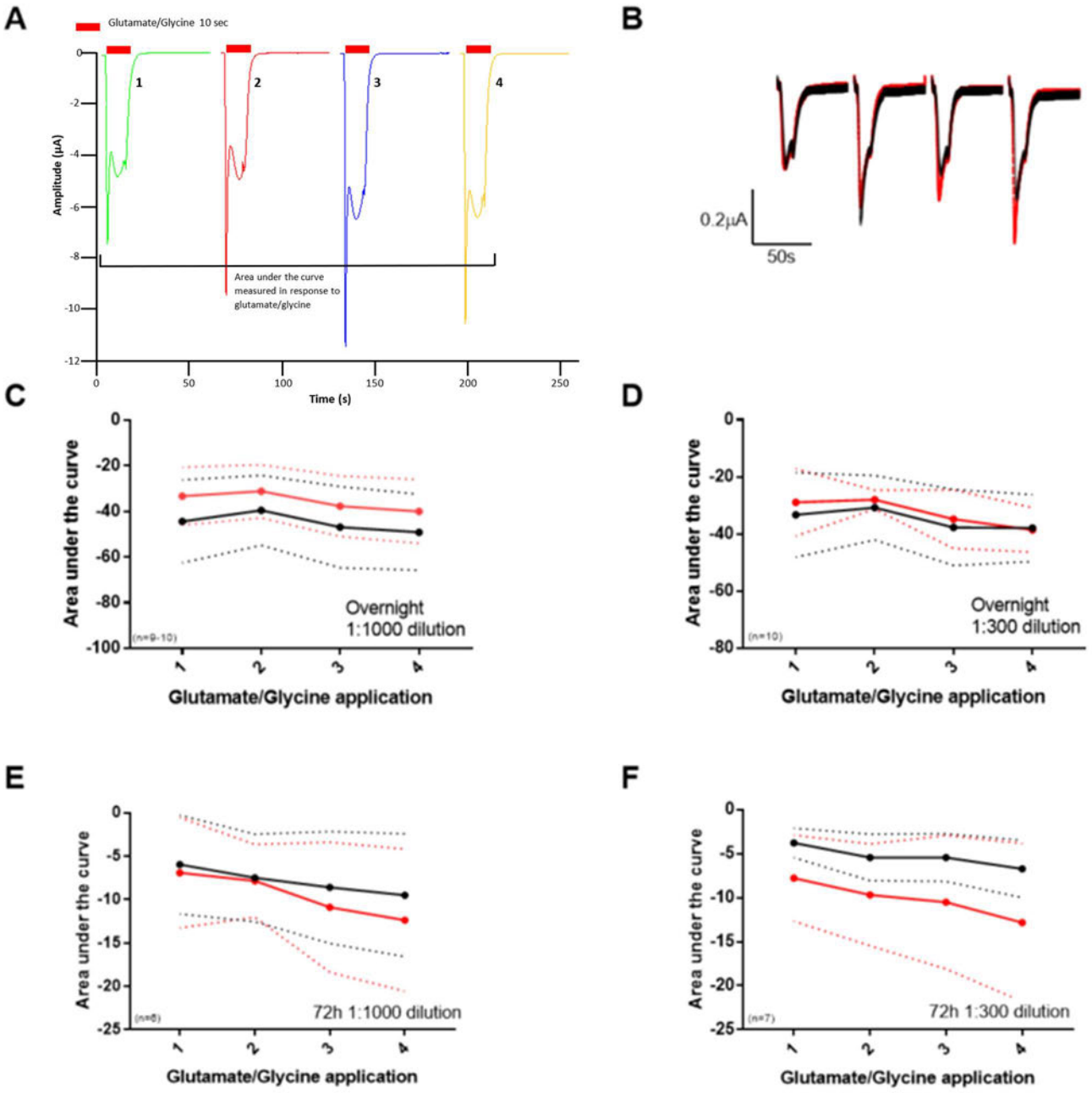

Figure 4.4: No significant change in NMDAR current is seen following chronic Aab incubation. (A) Overview of protocol used for chronic application of Aabs on Xenopus oocytes. (B) Representative traces of NMDAR1 Aabs and rIgG incubated oocytes. (C) No change in area under the curve of the glutamate-evoked response was observed in NMDAR1 Aab incubated oocytes compared to those incubated with IgG at the lowest dilution (1:1000) overnight. A significant effect of time was found ($p<0.0001$, n = 9-10 per group), but no significant effect of antibody $p = 0.1886$, n = 9-10 per group). **(D)** Similarly, no significance was found when oocytes were incubated overnight with NMDAR1 Aabs at a higher dilution (1:300; $p = 0.6167$, n = 10 per group), only a significance of time was observed ($p<0.0001$, n = 10 per group). **(E)** Longer incubation of 72 h of NMDAR1 Aabs and IgG at 1:1000 dilution also elicited no changes in NMDAR current between the two antibody applications ($p = 0.6612$, n = 6 per group), but did elicit a significant effect of time ($p <0.0001$, n = 6 per group). **(F)** Once again, a higher dilution of 1:300 did not elicit any changes in NMDAR current between NMDAR1 Aabs and IgG incubated oocytes ($p = 0.0995$, n = 7 per group), only a significant effect of time was observed ($p<0.0001$, n = 7 per group) All data are represented as mean ± SD.

4.2.4 NMDAR1 Aabs do not alter NMDAR current via allosteric modulation

As NMDAR1 Aabs did not elicit any functional effects following either acute or chronic incubation, co-application of NMDAR1 Aabs with the allosteric modulator TCN-201 was carried out to assess whether NMDAR1 Aabs might have an inhibitory functional effect via an allosteric mechanism of action. If so, we would expect a shift in the concentration response curve, where less TCN-201 is required to elicit a similar level of inhibition. To test this hypothesis, NMDAR1 Aabs or rIgG were incubated for a total of 21 min, in the presence of increasing concentrations of the allosteric modulator TCN-201, with glutamate/glycine applications occurring every 3 min throughout this incubation for 10 s each to monitor changes to NMDAR current. The highest concentration of TCN-201 used (3.16μM) alone significantly reduced the AUC of the evoked NMDAR current (0.2 ± 0.06), similar to previous TCN-201 effects (Figure 4.2B). Those oocytes incubated with TCN-201 plus NMDAR1 Aabs reduced the AUC of the evoked NMDAR currents in a similar manner to TCN-201 alone (0.1 ± 0.03), also similar to those incubated with TCN-201 plus rIgG (0.2 ± 0.07; Figure 4.5). There were no significant differences between those oocytes incubated with TCN-201 alone, TCN-201 plus NMDAR1 Aabs or TCN-201 plus rIgG ($F(2,20) = 1.24$, $p = 0.3090$, n = 7-8 per group). However, a significant effect of increasing TCN-201 concentration was identified ($F(7,140) = 429.1$, $p<0.0001$, n = 7-8 per group). The interaction between time and TCN-201 concentration was considered significant ($F(14,40) = 2.33$, $p = 0.0064$, n = 7-8 per group). Therefore, TCN-201 was capable of reducing NMDAR current, but NMDAR1 Aabs did not alter NMDAR current via an allosteric mechanism of action.

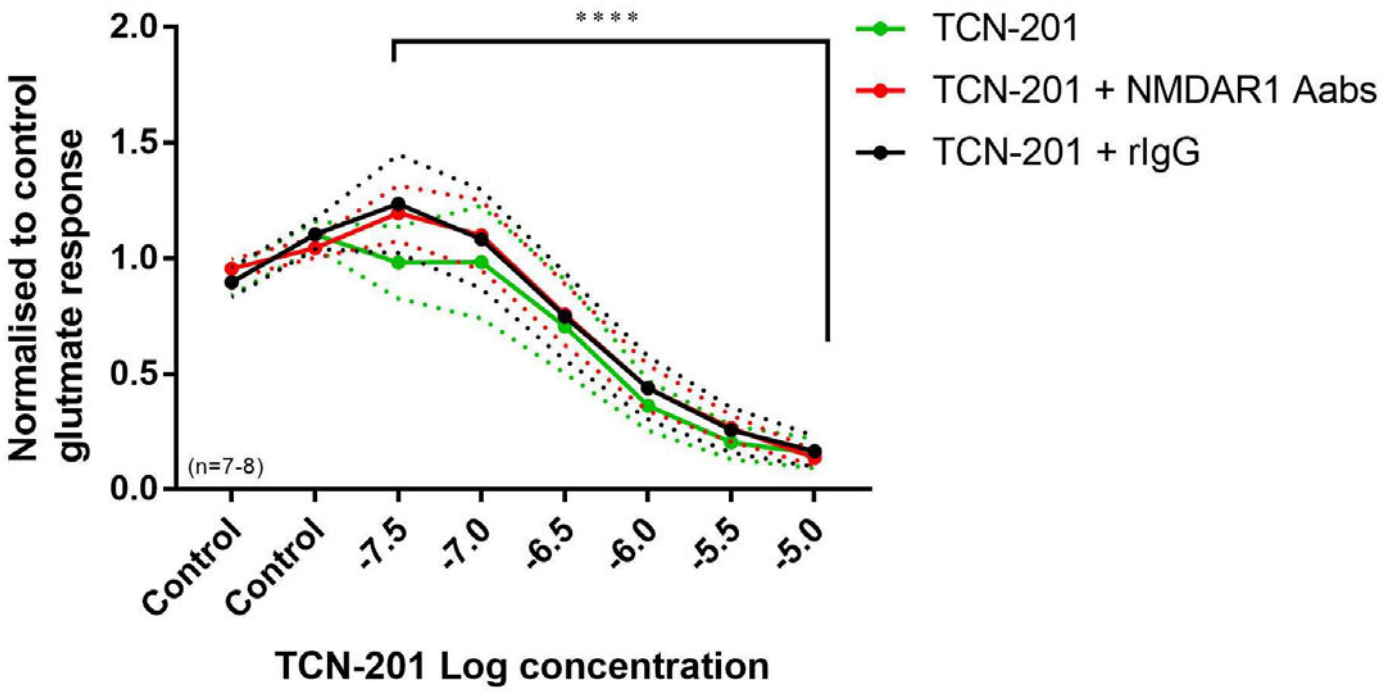

Figure 4.5: No significant effect of NMDAR1 Aab incubation was observed when co-incubated with increasing concentrations of the NR1 allosteric modulator TCN-201. A two-way ANOVA, as before revealed a significant effect of TCN-201 concentration on all three groups ($p < 0.0001$, n = 7-8 per group), but no effect of antibody was observed ($p = 0.3090$, n = 7-8 per group). Data are represented as mean ± SD, ****: $p < 0.0001$.

Overall, the results demonstrate that NMDAR1 Aabs have no significant effect on NMDAR current of NR1/NR2A expressing oocytes, following either acute or chronic incubation. Of interest, anti-NR1 commercial antibodies also had no significant effect in oocyte experiments (Brice Mullier, UCB, personal communication (data not shown)). Both MK-801 and TCN-201 however, did result in a significant, concentration dependent reduction in NMDAR current, and therefore acted as positive controls for these experiments.

4.2.5 NMDAR1pp Aabs have no functional effects on NMDAR expressing oocytes following acute incubation

As detailed in Chapter 3, NMDAR1 Aabs were subjected to further purification as a result of a lack of significant functional effect observed in both oocyte experiments (as described above), and MEA LTP experiments (see section 4.3), generating NMDAR1pp Aabs. These Aabs had been purified by peptide immunisation, removing all non-NMDAR specific IgG, therefore generating a more target-specific composition. As above (section 4.2.2), oocytes expressing NR1 and NR2A subunits were subjected to four control measurements of glutamate/glycine. These were performed every 3 min prior to any antibody application, of which the 3rd and 4th control responses were used to normalise all subsequent responses (see Figure 4.6A). Any oocytes which were unresponsive were not used in the experiments. Oocytes were then incubated acutely (60 min) with NMDAR1pp Aabs or rIgG, while being exposed to glutamate/glycine every 15min (10 s each) to determine any changes in NMDAR current. Both NMDAR1pp Aabs and control rIgG were tested at 1:300 dilution (4µg/ml), which was determined based on ELISA data (see section 3.6), where greater than 50% binding was seen to peptides 2, 4 and 5 as well as the ATD (see Figure 3.21B-C). No significant differences in area under the curve were observed following a 60 min incubation with either NMDAR1pp Aabs or rIgG (1:300 dilution). Oocytes incubated with NMDAR1pp Aabs generated a similar AUC (0.6 ± 0.26) to those incubated with rIgG (0.7 ± 0.23; Figure 4.6B). A two-way ANOVA found no significant differences between NMDAR1 Aabs or rIgG incubated oocytes ($F(1,21) = 3.58$, $p = 0.07$, n = 11-12 per group), but a significant effect of time on area under the curve ($F(5,105) = 192.5$, $p<0.0001$, n = 11-12 per group). The interaction between the effect of time and antibody incubation was not identified as significant ($F(5,105) = 1.62$, $p = 0.16$, n = 11-12 per group) (Figure 4.6B). Therefore, NMDAR1pp Aabs had no effect on NMDAR current

following 60 min incubation at 1:300 dilution when compared to control rIgG in oocyte experiments.

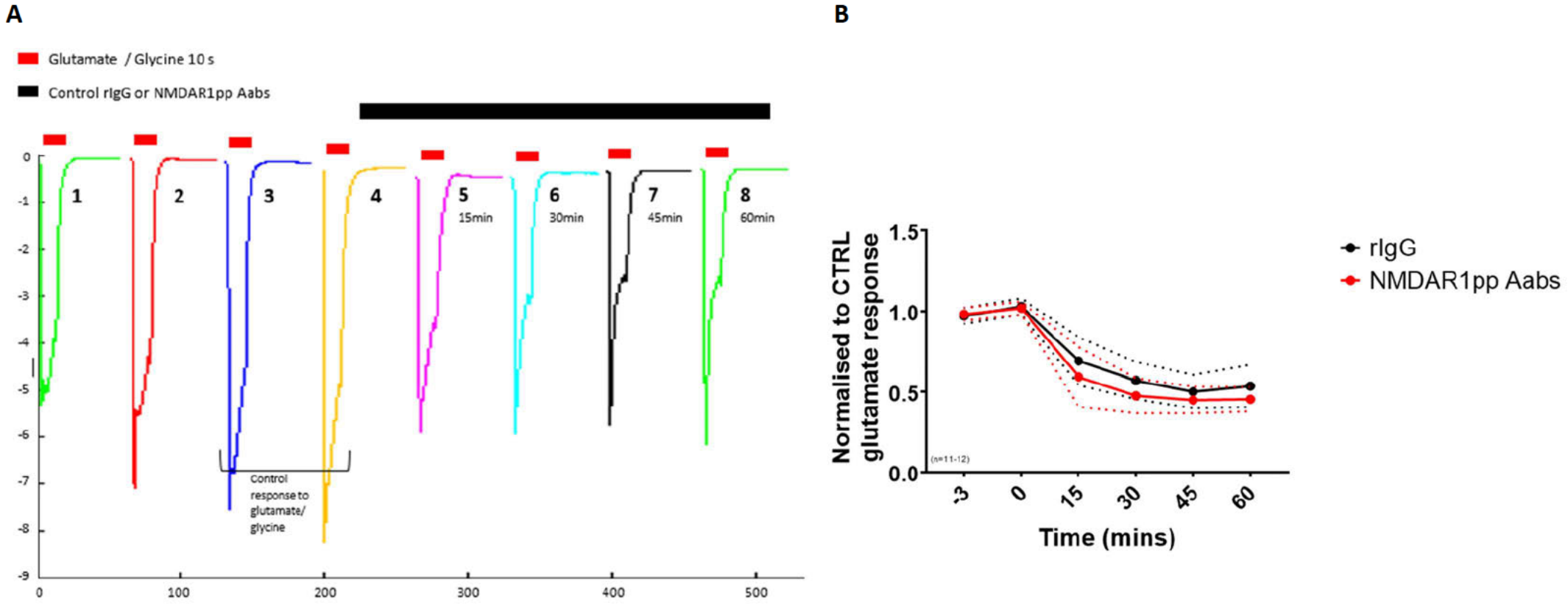

Figure 4.6: No significant changes in NMDAR current was seen following acute NMDAR1pp Aab incubation. (A) An overview of the protocol used for 60 min incubation of NMDAR1pp Aabs on Xenopus oocytes, whereby NR1/NR2A expressing oocytes displayed NMDAR current when evoked with the agonists glutamate/glycine. Control responses 3 and 4 were used to normalise all subsequent evoked current responses. NMDAR1pp Aabs and rIgG were applied for 60 min, evoking NMDAR current regularly throughout to monitor any changes in area under the curve. **(B)** No change in area under the curve of the glutamate-evoked response was seen in NMDAR1pp Aab incubated oocytes compared to those incubated with rIgG at 1:300 dilution over a 60 min period. A significant effect of time was found when analysed with two-way ANOVA, but no significant effect of antibody ($p<0.0001$ and $p = 0.07$ respectively, $n = 11$-12 per group). All data are represented as mean ± SD.

4.3 Effects of Aabs on NMDAR-dependent LTP

4.3.1 Schaffer collateral long-term potentiation (LTP)

Within the hippocampus, the most commonly studied synapse is the Schaffer collateral input to CA1 pyramidal neurons. Axon collaterals from CA3 pyramidal cells project to CA1, transferring information, the process of which is proposed to underlie memories (Bliss and Collingridge, 1993). Certain patterns of synaptic activity produce LTP; this is a long-lasting increase in synaptic strength, a process that in the Schaffer collaterals-CA1 pathway is NMDAR-dependent (Bliss and Collingridge, 1993). LTP is widely considered to be one of the major cellular mechanisms underlying learning and memory, both of which are impacted in patients who present with anti-NMDAR Aabs (Dalmau *et al.*, 2007). LTP can be recapitulated *in vitro* using different patterns of stimulation, such as high frequency stimulation (HFS) or theta burst stimulation (TBS). Therefore, this pathway can be used as a method of analysing changes in NMDAR channel function and assessing functional effects of NMDAR Aabs.

4.3.2 Commercial anti-NMDAR antibodies and class specific negative controls have no significant effect on NMDAR-dependent LTP

MEA recordings from acute hippocampal brain slices were used to assess the effects of NMDAR Aabs in a more physiological setup. Stimulation of the Schaffer collaterals is a method evoking a post-synaptic response in the CA1, using the stimulation pattern HFS, LTP can be induced which, in this area, is NMDAR-dependent.

Vehicle experiments (in the absence of antibody/pharmacological inhibitor) were carried out, with HFS being delivered after a 30 min stable baseline of evoked fEPSPs with minimal fluctuations in fEPSP slope and amplitude. This HFS caused an induction of LTP as shown by ~150% potentiation in fEPSP slope for at least 1 h post HFS (as shown by black line; Figure

4.7A). The addition of the AMPAR blocker CNQX (5μM) at 90 min caused a rapid reduction in fEPSP amplitude. Subsequent addition of the general voltage-gated sodium channel blocker, TTX (1μM), abolished any remaining signal. To confirm that this process is NMDAR-dependent, inhibition of LTP was performed by the addition of an NMDAR antagonist (DL-APV; 50μM) as a positive control. Application of DL-APV, inhibited HFS-induced LTP (as shown in green; Figure 4.7A), verifying that the potentiation induced in this pathway was NMDAR-dependent.

Several commercial antibodies were tested using the above protocol, including two commercial anti-NR1 antibodies (rNMDAR and mNMDAR (shown in Figure 4.7 in blue and orange respectively)), and two class specific IgG negative controls (rIgG and mIgG2b (shown in Figure 4.7 in pink and purple respectively)). Commercial anti-NR1 antibodies which had been used as positive controls for characterisation of NMDAR Aabs (see Chapter 3) were used in functional studies to identify whether these were able to generate an effect on NMDAR-dependent LTP. Class specific negative controls were also used to ensure any effects seen with NMDAR Aabs, were NMDAR-specific effects and not due to 'non-NMDAR specific' IgG. The same protocol as described above was used, with slices being incubated for 1 h with each antibody prior to the experimental protocol. All vehicle and antibody incubated slices generated a ~130-160% potentiation following HFS when normalised against the pre-LTP baseline as shown in Figure 4.7A. All data represented are mean ± SD.

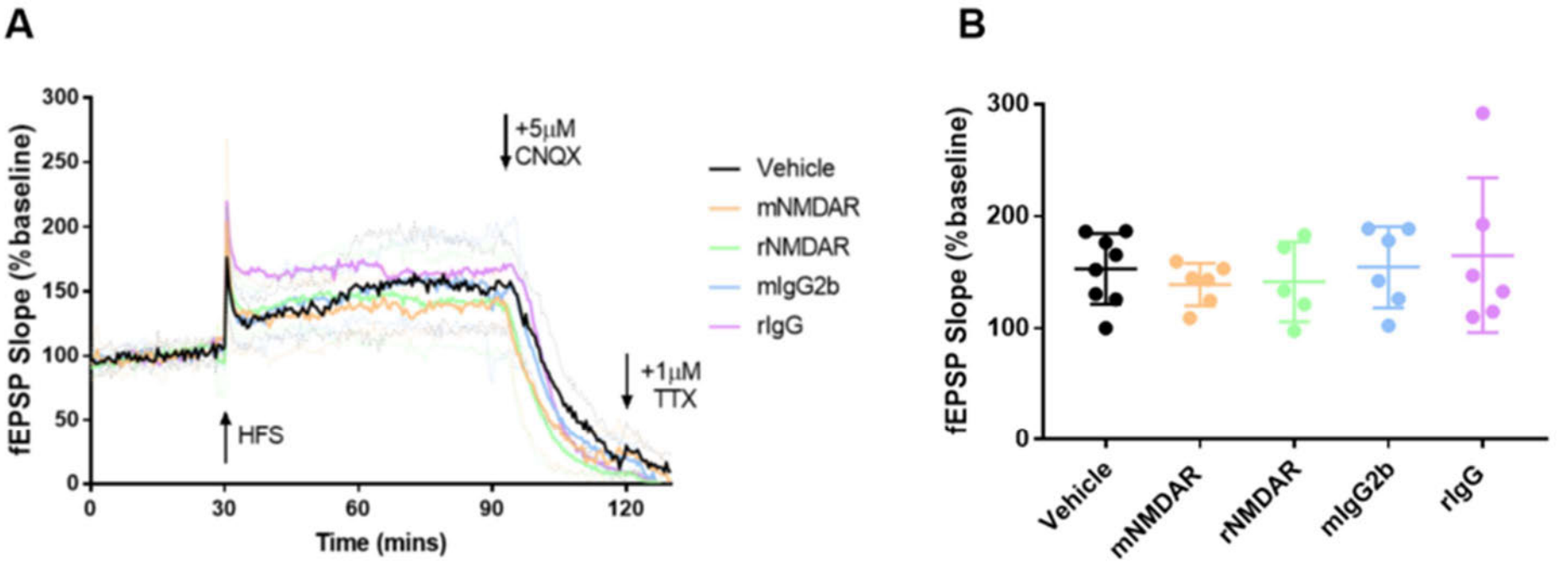

Figure 4.7: Normalised traces of HFS induced LTP for vehicle, as well as both positive (mNMDAR and rNMDAR) and negative controls (mIgG2b and rIgG). **(A)** Normalised mean traces of vehicle, mNMDAR, rNMDAR, mIgG2b and rIgG treated slices undergoing LTP induction. Vehicle experiments typically elicited a potentiation of ~150% post-HFS, which was maintained for at least 1 h. The addition of both positive and negative controls also elicited a potentiation following HFS, varying from 140%-160%. All signals were reduced after 1 h by the addition of the AMPAR antagonist CNQX, leaving only the NMDAR signal. This remaining signal was then inhibited by the addition of TTX at the end of the experiments. **(B)** Comparison of LTP magnitude (mean fEPSP slope during 80-90min of experiment) revealed no significant changes in potentiation of any condition when compared to vehicle slices (mNMDAR $p = 0.9238$, rNMDAR $p = 0.9676$, mIgG2b $p = 0.9999$, rIgG $p = 0.9543$, $n = 5$-9 per group). Data represented as mean ± SD.

Data were normalised to pre-LTP baseline and analysed statistically using one-way ANOVA tests to compare 1 h post-LTP mean values of two commercial anti-NR1 antibodies (mNMDAR and rNMDAR) and two class-specific negative controls (mIgG2b and rIgG) to that of vehicle. Vehicle slices generated a potentiation at 1 h post-LTP: 153.1 ± 31.6%. Commercial anti-NR1 antibodies mNMDAR and rNMDAR elicited similar levels of potentiation following HFS; 136.3 ± 19.7% and 141.7± 35.7% respectively ($p = 0.9238$ and $p = 0.9676$, n = 5-9 per group), similar to that of NMDAR1 Aabs. Slices incubated in class specific negative controls (mIgG2b and rIgG) also generated potentiated fEPSPs following HFS, similar to that of vehicle slices: 154.6 ± 36.3% and 159.4 ± 75.5 ($p = 0.9999$ and $p = 0.9543$ respectively, n = 5-9 per group; Figure 4.7A-B).

These data confirm that non-NMDAR specific IgG within the protein A purified sample have no effect on NMDAR-dependent LTP, as demonstrated by the lack of significant effect of mIgG2b and rIgG negative controls on 1 h post-LTP potentiation levels. The two commercial anti-NR1 antibodies also demonstrated no significant functional effect on NMDAR current, unlike our NMDAR1pp Aab. These commercial antibodies have different target epitopes, with mNMDAR targeting a linear region outside of the ATD within the NR1 subunit (amino acids 660 to 811), whereas rNMDAR targets a linear sequence of amino acids 35 to 53 within the ATD of NR1 subunit. It was of interest that neither of these antibodies have functional effects in any system used here, nor did we detect any functional effect of rNMDAR in oocyte experiments (data not shown; performed previously at UCB).

4.3.3 NMDAR1 protein A purified Aabs do not inhibit NMDAR-dependent LTP

To test NMDAR Aabs (both protein A and peptide purified Aabs) using this protocol, a 1 h pre-incubation of hippocampal brain slices was carried out (1:1000 dilution). This pre-

incubation was followed by the same protocol described above, with a 30 min stable baseline of fEPSPs, LTP induction via HFS, and 1 h monitoring of fEPSP slope following LTP induction (Figure 4.8A, as shown in red).

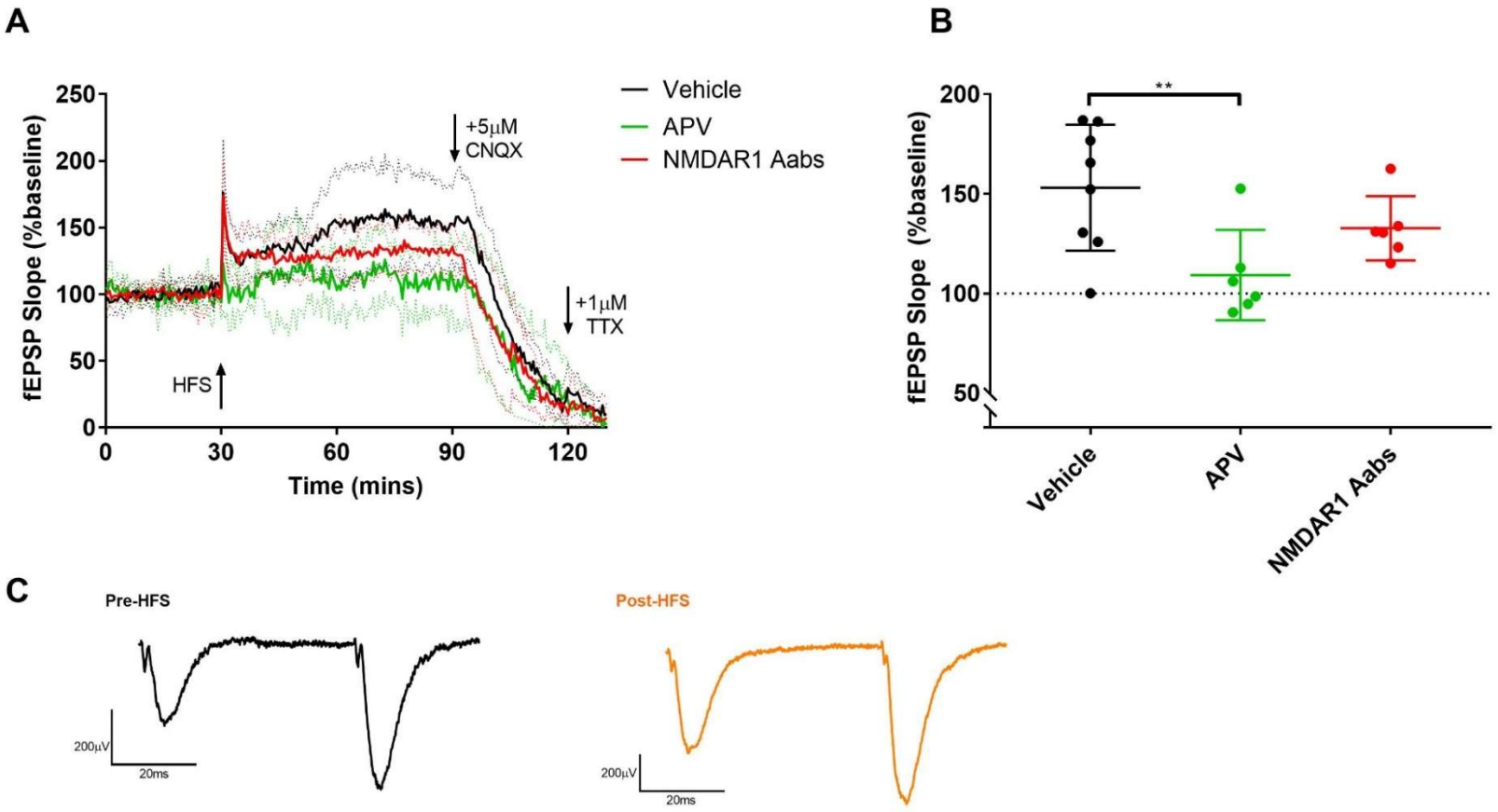

Figure 4.8: Normalised traces of HFS induced LTP for vehicle, NMDAR1 Aabs incubated and APV treated. (A) Normalised mean traces of vehicle, APV and NMDAR1 Aabs treated slices undergoing LTP induction. Vehicle experiments typically elicited a potentiation of 150% post-HFS, which was maintained for at least 1 h. The addition of APV almost completely inhibited any HFS-induced LTP (shown in green), whereas a 1 h pre-incubation with NMDAR1 Aabs elicited a potentiation of 130-140% post-HFS. **(B)** Comparison of LTP magnitudes (mean fEPSP slope during 80-90min of experiment), revealed a significant reduction in potentiation of APV treated slices compared to vehicle ($p = 0.0046$, $n = 6$-9 per group), but NMDAR1 Aabs treated slices were not significantly different to vehicle slices ($p = 0.3013$, $n = 6$-9 per group). **(C)** Representative traces of paired pulse recordings pre-HFS (black) and post-HFS (orange) in vehicle recordings. Data represented as mean ± SD, **: $p < 0.01$.

Data were normalised to pre-LTP baseline, data passed normality testing (D'Agostino & Pearsons test) and were analysed statistically using one-way ANOVA to compare 1 h post-LTP mean values of APV and NMDAR1 Aabs to that of vehicle. Vehicle-treated slices generated a potentiation at 1 h post-LTP: 153.1 ± 31.6%, whilst NMDAR1 Aab-treated slices generated a potentiation of 132.7 ± 16.1% (Figure 4.8B). No significant effect was identified in those slices pre-incubated with NMDAR1 Aabs (n=6-9 per group (1 slice per animal), p = 0.3013; Figure 4.8B).

The addition of the non-competitive NMDAR antagonist DL-APV (50μM) effectively prevented HFS-induced potentiation, eliciting potentiation of 109.2 ± 22.7% as shown in Figure 4.8B. A one-way ANOVA with Dunnett's multiple comparisons test identified significantly less LTP in APV-treated slices when compared to vehicle-treated slices (n=6-9 per group, p = 0.0046). These results demonstrate that NMDAR1 Aabs had no significant effect on NMDAR function with regard to LTP.

These data, together with the negative oocyte TEVC data (detailed in section 3.0) led to the development of a second, independent preparation of protein A purified NMDAR Aabs raised against different epitopes (NMDAR2 Aabs) as described in Chapter 3.

4.3.4 NMDAR2 Aabs do no alter NMDAR-dependent LTP

Experiments in 4.3.2 were repeated with NMDAR2 Aabs. Data were normalised to pre-LTP baseline, data passed normality testing (D'Agostino & Pearsons test) and were analysed statistically using one-way ANOVA tests to compare 1 h post-LTP mean values from APV-treated and NMDAR2 Aab-treated slices to vehicle-treated slices. Vehicle slices generated a significant potentiation at 1 h post-LTP of 153.1 ± 31.6% (as shown in black; Figure 4.9A). Similar to vehicle, NMDAR2 Protein A purified Aabs elicited a post-HFS potentiation of 148 ± 21.7% (as shown by blue line; Figure 4.9A). In these experiments NMDAR2 Aabs did not have any significant effects on levels of potentiation when compared to vehicle (n=6-9 per group, $p = 0.9820$; Figure 4.9B). The addition of the non-competitive NMDAR antagonist DL-APV prevented the HFS-induced potentiation, eliciting a potentiation of 109.2 ± 22.7% (as shown in green; Figure 4.9A); this represented significantly less potentiation in APV slices compared to vehicle (n=6-9 per group, $p = 0.0046$).

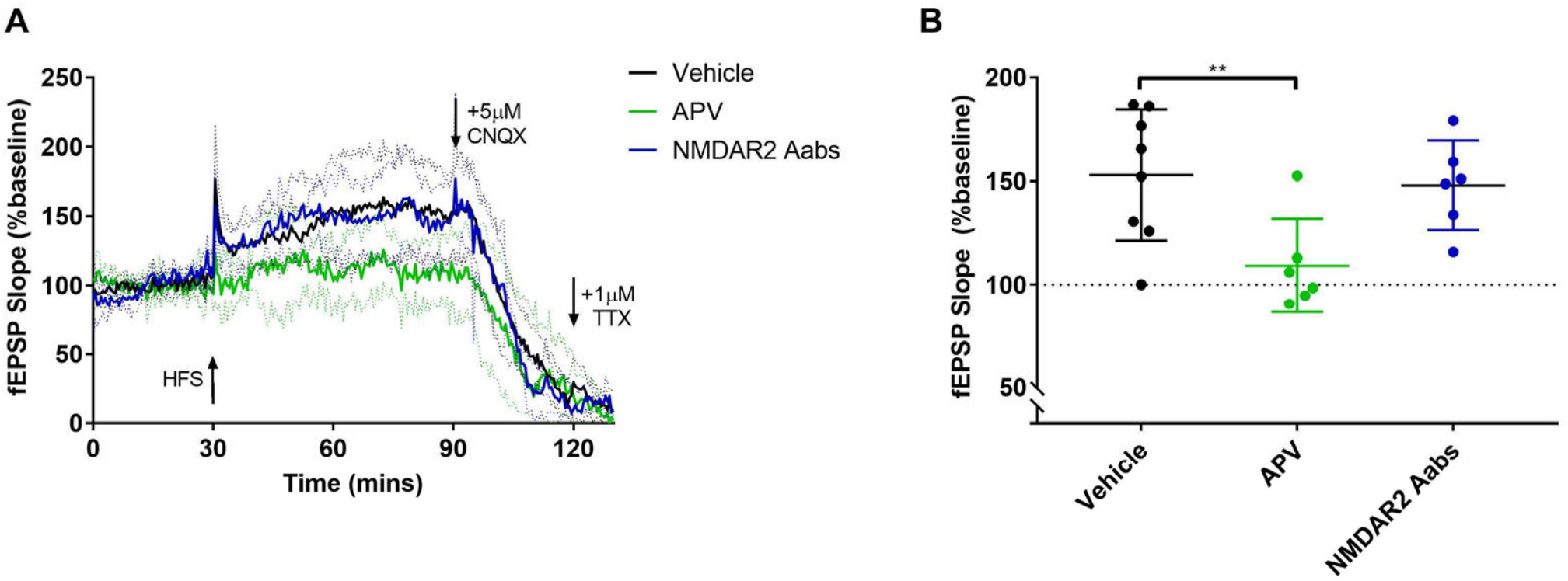

Figure 4.9: Normalised traces of HFS induced LTP for vehicle, NMDAR2 Aabs incubated and APV treated. (A) Normalised mean traces of vehicle, APV and NMDAR2 Aabs treated slices undergoing LTP induction. Vehicle experiments typically elicited a potentiation of 150% post-HFS, which was maintained for at least 1 h. The addition of APV almost completely inhibited any HFS-induced LTP (shown in green), whereas a 1 h pre-incubation with NMDAR2 Protein A purified Aabs elicited a potentiation of 150% post-HFS (shown in blue). **(B)** Comparison of LTP magnitudes (mean fEPSP slope during 80-90min of experiment) revealed a significant reduction in potentiation of APV treated slices compared to vehicle ($p = 0.0046$, $n = 6$-9 per group), where NMDAR2 Aabs treated slices were not significantly different to vehicle slices ($p = 0.98$, $n = 6$-9 per group). Data represented as mean ± SD, **: $p < 0.01$.

Overall, these results demonstrate that NMDAR2 Aabs had no significant effect on NMDAR function with regard to LTP experiments on mouse hippocampal brain slices on MEAs. As neither NMDAR1 or NMDAR2 Aabs generated a significant functional effect in either oocyte experiments (NMDAR1 Aabs only; section 4.1) or MEA-LTP experiments (both NMDAR1 and NMDAR2 Aabs; sections 4.3.3 and 4.3.4), it was decided to further purify NMDAR1 Aabs. Although pre-incubation of both NMDAR1 and 2 Aabs led to no significant changes in potentiation levels following LTP induction, NMDAR1 Aabs showed a numerical, although not significant reduction in potentiation; 132.7 ± 16.1% (Figure 4.8B; $p = 0.3013$, $n = 6$-9 per group), compared to no reduction in potentiation seen by NMDAR2 Aabs slices; 148 ± 21.7% (Figure 4.9B; $p=0.98$), with the post-HFS values of NMDAR1 Aabs being closer to that of APV (green trace; Figure 4.8B). Therefore, NMDAR1 Aabs were selected for further purification, designed to purify NMDAR specific IgG (see section 2.2).

4.3.5 NMDAR1pp reduces NMDAR-dependent LTP

As both NMDAR Aabs were protein A purified, it may be that only a small percentage of antibodies within the sample are specific for NMDARs; therefore, further purification was carried out. This was performed by isolating only the Aabs which were specific for the NR1 immunisation peptides (NMDAR1pp Aabs). As detailed in Chapter 3, these peptide purified Aabs (NMDAR1pp) demonstrated increased specificity and reduced background staining in ICC with NR1-transfected HEK cells and primary neurons. As above, vehicle experiments were carried out (in the absence of antibodies/pharmacological inhibitors), with HFS inducing potentiation after a 30 min stable baseline of evoked fEPSPs with minimal fluctuations in amplitude and slope. NMDAR1pp Aabs were pre-incubated for 1 h with hippocampal brain slices (1:1000 dilution) prior to MEA recording. This pre-incubation was followed by the same protocol described above: a 30 min stable baseline of fEPSPs, LTP induction via HFS, and 1 h

monitoring of fEPSP slope (Figure 4.10A shown in purple), similar to of the effects of the NMDAR antagonist APV (as shown in green).

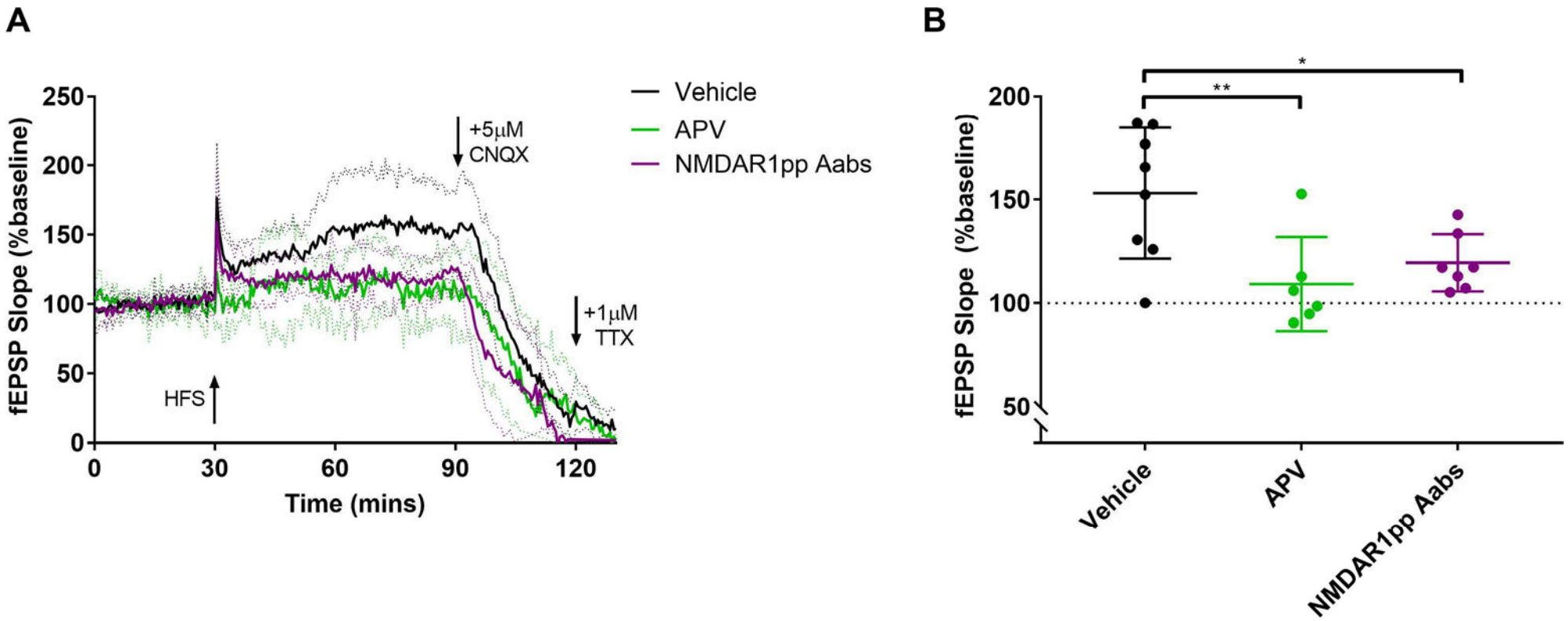

Figure 4.10: Normalised traces of HFS induced long term potentiation (LTP) for vehicle, NMDAR1pp Aabs incubated and APV treated. (A) Normalised mean traces of vehicle, APV and NMDAR1pp Aabs treated slices undergoing LTP induction. Vehicle experiments typically elicited a potentiation of 150% post-HFS, which was maintained for at least 1 h. The addition of APV almost completely inhibited any HFS-induced LTP (shown in green), whereas a 1 h pre-incubation with NMDAR1pp Aabs elicited a potentiation of 110-120% post-HFS (shown in purple). **(B)** LTP magnitude (mean fEPSP slope during 80-90min of experiment) revealed a significant reduction in potentiation of APV treated slices compared to vehicle ($p = 0.0046$, $n = 6$-9 per group), with NMDAR1pp Aabs treated slices demonstrating a similar significant reduction when compared to vehicle ($p = 0.0271$, $n = 6$-9 per group). Data represented as mean ± SD, *: $p < 0.05$, **: $p < 0.01$.

Data were normalised to pre-LTP baseline and passed normality testing and were analysed statistically using one-way ANOVA tests to compare 1 h post-LTP mean values of APV and NMDAR1pp Aabs to that of vehicle. Data were compared with vehicle and APV (50µM) incubated data used above. Thus, vehicle slices generated a significant potentiation at 1 h post-LTP of 153.1 ± 31.6%. The addition of the non-competitive NMDAR antagonist DL-APV prevented HFS-induced potentiation, reducing potentiation to 109.2 ± 22.7%. NMDAR1pp Aabs reduced HFS-induced potentiation to similar levels as APV: 119.5 ± 13.8%. There was a significant difference in potentiation in comparison to vehicle for both APV (n=6-9 per group, p = 0.0046) and NMDAR1pp Aabs (n=6-9 per group, p = 0.0271; Figure 4.10B). These data demonstrate a significant effect of the final peptide purified NMDAR Aabs (NMDAR1pp) on NMDAR function.

These data confirm that NMDAR1pp Aabs have a significant inhibitory effect on NMDAR-dependent LTP, where NMDAR1 and NMDAR2 Aabs do not. This is likely due to the removal of non-NMDAR specific IgG from NMDAR1pp Aabs, resulting in a more concentrated sample of NMDAR specific Aabs.

4.4 Effects of NMDAR1pp Aabs on hippocampal neurons

4.4.1 Spontaneous excitatory postsynaptic currents

Whole-cell patch-clamp and primary hippocampal neurons (DIV14-21) were used to measure sEPSCs in the absence and presence of NMDAR1pp Aabs to investigate any functional pre-/post-synaptic effects. Cells were recorded in Mg^{2+}-free external solution without perfusion and held at -70mV throughout. $GABA_AR$ and AMPAR antagonists, BMI (10µM) and NBQX (5µM) respectively, were added via bath application and left to equilibrate while a suitable cell was identified. This cell was patched and ‘broken into’, obtaining a whole-cell configuration,

resulting in long events which were large in amplitude (Figure 4.11C), these were recorded and monitored, obtaining a 10 min baseline, whereby parameters such as amplitude and frequency could be analysed.

4.4.2 NMDAR1pp Aabs do not affect sEPSC frequency or amplitude

To test the effects of acute NMDAR1pp Aab application, a 10 min baseline of sEPSCs was recorded, and subsequently NMDAR1pp Aabs or rIgG (1:1000) were added to the cells via bath application and sEPSCs recorded for a further 30 min. At the end of the experiment, the NMDAR antagonist DL-APV was added to the bath to confirm that all observed events were NMDAR-driven.

Acute bath application (30min) of NMDAR1pp Aabs resulted in no significant changes in sEPSC frequency when compared to pre-treatment baselines (representative traces shown in Figure 4.11C). Following 30 min application of NMDAR1pp Aabs, cells generated sEPSC frequency 0.03 ± 0.03 Hz compared to its pre-treatment baseline sEPSC frequency 0.05 ± 0.04 Hz. When analysed using a paired t-test, no significance was identified (n=9 per group, $p = 0.1051$, Figure 4.11A). Similarly, when rIgG-treated cells were compared to their own baseline, no changes in sEPSC frequency were observed. rIgG incubated cells generated a mean ± SD sEPSC frequency of 0.06 ± 0.04 Hz, compared to that of its own baseline 0.08 ± 0.05 Hz. When analysed using a paired t-test, no significance was identified (n=9 per group, $p = 0.2257$; Figure 4.11B).

In addition, no significant changes in sEPSC amplitude were observed between NMDAR1pp Aabs and their pre-treated baseline following 30min incubation (n=9 per group, $p = 0.1427$; Figure 4.12A). Similarly, no significant effect was observed when comparing rIgG treated cells to their pre-incubation baselines (n=9 per group, $p = 0.6260$; Figure 4.12B).

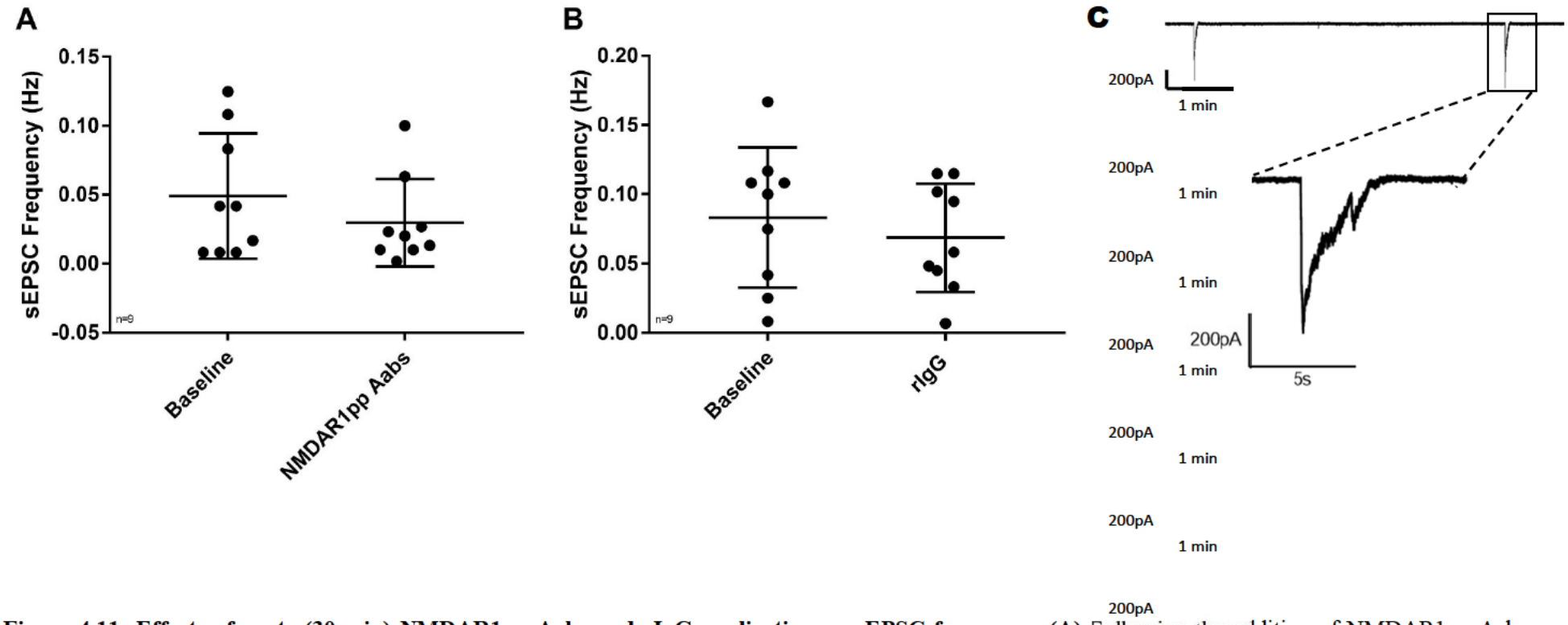

Figure 4.11: Effects of acute (30 min) NMDAR1pp Aabs and rIgG application on sEPSC frequency. (A) Following the addition of NMDAR1pp Aabs, no significant reduction in sEPSC frequency was identified in those primary neurons applied with NMDAR1pp Aabs when compared to its respective baseline ($p = 0.1051$, $n = 9$ per group). **(B)** In addition, no significance was identified between rIgG incubated cells compared to its own pre-application baseline ($p = 0.2257$, $n = 9$ per group). **(C)** Representative traces of sEPSCs in the presence of Mg^{2+} free external solution, BMI and NBQX. Data was collected over three separate neuronal cultures and presented as mean ± SD.

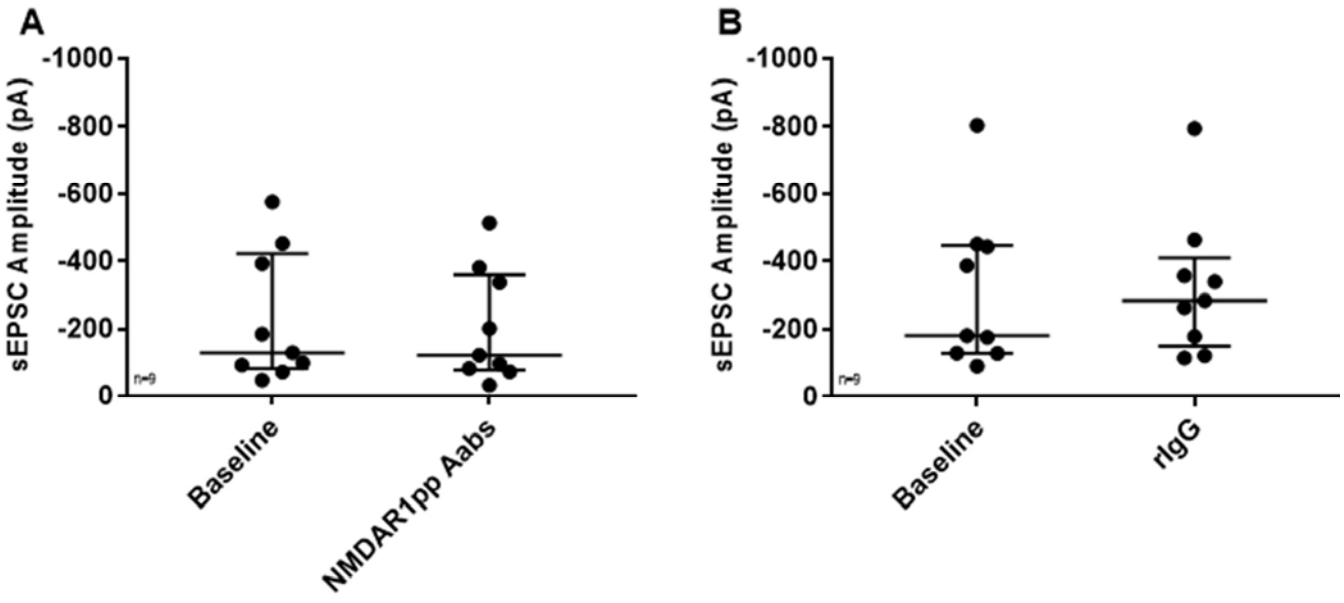

Figure 4.12: Effects of acute (30 min) NMDAR1pp Aabs and rIgG application on sEPSC amplitude. **(A)** Following addition of NMDAR1pp Aabs, no significant reduction in sEPSC amplitude was identified when compared to their pre-treatment baseline ($p = 0.1427$, $n = 9$ cells per group). **(B)** Similarly, cells incubated with rIgG showed no significant changes in sEPSC amplitude when compared to their respective pre-incubation baselines ($p = 0.6260$, $n = 9$ cells per group). Data was collected over three separate neuronal cultures and presented as mean ± SD.

To determine whether longer, chronic exposure to NMDAR1pp Aabs had any effects on sEPSCs, experiments were repeated using a 24 h pre-treatment. Both NMDAR1pp Aabs and rIgG were applied to hippocampal neurons in culture the day before patching. Once removed from culture, cells were placed in Mg^{2+} free external solution containing antagonists BMI (10μM) and NBQX (10μM) and allowed to equilibrate. Once whole-cell configuration had been achieved, 30 min of sEPSCs were recorded where both frequency and amplitude were measured. At the end of the experiment, the NMDAR antagonist DL-APV was added to the bath to confirm that all observed events were NMDAR driven.

Interestingly, the NMDAR1pp Aabs incubated cells showed no significant changes in sEPSC frequency compared to rIgG incubated cells, from a mean value of 0.04 ± 0.04 Hz for NMDAR1pp Aab treated cells, to a mean value of 0.04 ± 0.05 Hz for rIgG treated cells. This did not yield any significance when analysed statistically (n=8-10 per group, unpaired t-test, p = 0.8902; Figure 4.13A). Similarly, changes in amplitude were monitored, where as with 30 min application, no significant changes in sEPSC amplitude following NMDAR1pp Aabs (n=8-10 per group, unpaired t-test, p = 0.3567; Figure 4.13B).

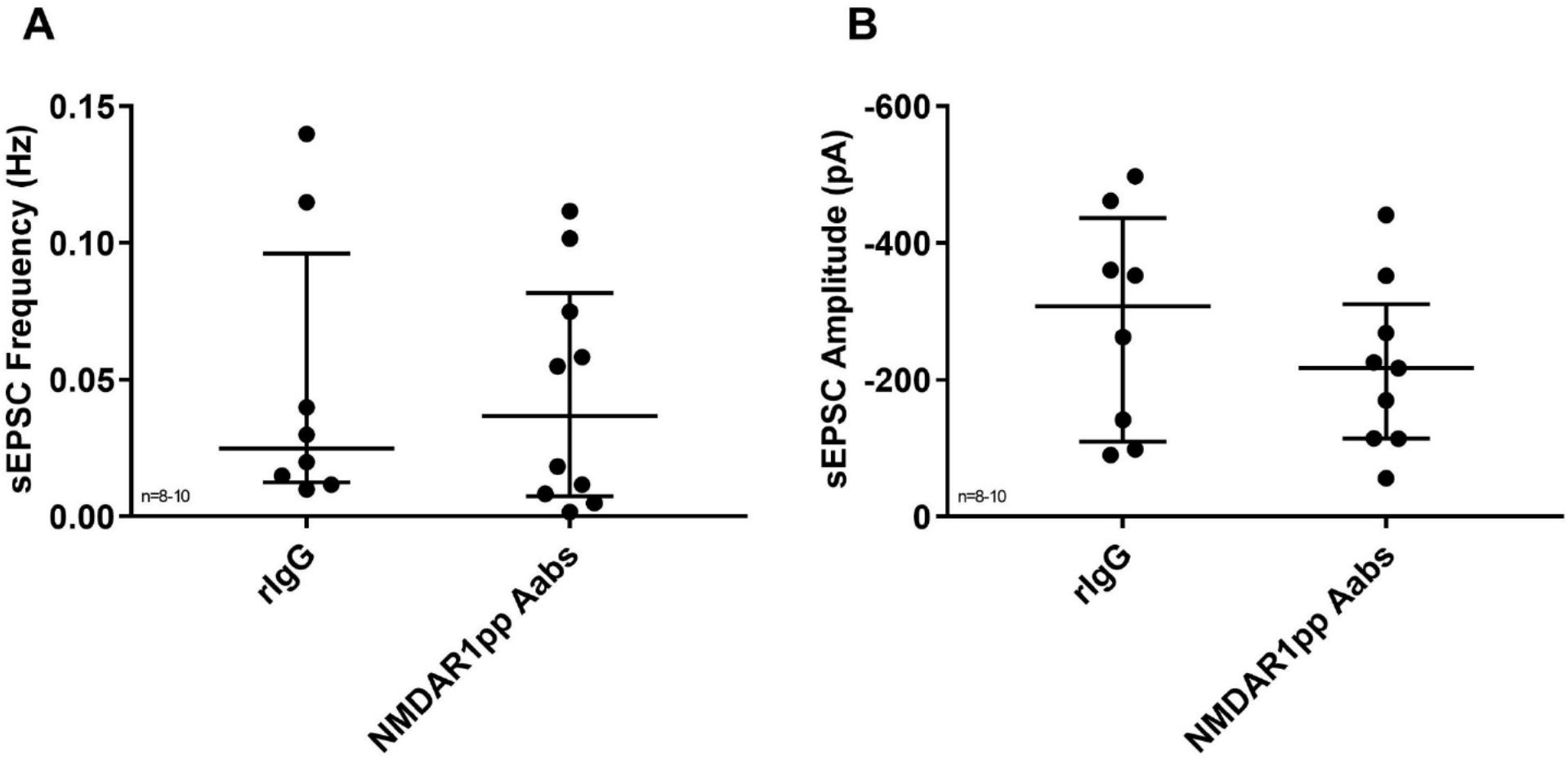

Figure 4.13: Effects of chronic (overnight) NMDAR1pp Aabs and rIgG application on sEPSC frequency and amplitude. Following addition of NMDAR1pp Aabs, no significant changes in sEPSC frequency ($p = 0.8902$, n = 8-10 cells per group) **(A)** or amplitude ($p = 0.3567$, n = 8-10 cells per group) **(B)** were identified in those applied with NMDAR1pp Aabs compared to those with rIgG. Data was collected over two separate neuronal cultures and presented as mean ± SD.

4.5 Discussion

Our results thus far have demonstrated that we are able to generate Aabs specifically targeted to the NR1 subunit of NMDARs (see section 3.2) which bind specifically to native NMDARs (see sections 3.3). The results of the experiments carried out in this chapter are summarised below:

- NMDAR1 Aabs and NMDAR1pp Aabs display no functional effect on NMDAR current in NR1/NR2A expressing oocytes.
- NMDAR1 and NMDAR2 Aabs do not show any significant reduction in HFS-induced potentiation in hippocampal brain slices following 1 h pre-incubation.
- NMDAR1pp Aabs, produced by further peptide purification of NMDAR1 Aabs, caused a significant reduction in HFS-induced LTP following 1 h pre-incubation.
- NMDAR1pp Aabs had no effect on sEPSC frequency or amplitude on whole-cell patch-clamp.
- Commercial NMDAR Abs had no effect in oocytes or on LTP under the same experimental conditions.

4.5.1 NMDAR1 Aabs do not display any functional effects in NR1/NR2A expressing Xenopus oocytes

Previous investigations have used the *Xenopus* oocyte model to characterise novel drug compounds, as well as antibodies against NMDARs, via assessing their effects on NMDAR current (Castillo-Gomez *et al.*, 2016; Mullier *et al.*, 2017). One such study demonstrated that patient anti-NMDAR Aabs and a commercial anti-NR1 antibody (mNMDAR; Synaptic Systems) had significantly lower NMDAR current compared to negative controls (Castillo-Gomez *et al.*, 2016). Based upon these data, the same commercial antibody was added to our NR1/NR2A expressing oocytes to attempt to confirm these results, whereby if similar results were produced, this commercial antibody could be used as a functional positive control throughout all experiments. However, no inhibition in NMDAR current was observed with mNMDAR in our oocyte system (Brice Mullier UCB, personal communication, data not shown), contrasting those results shown by Castillo-Gomez. This difference may be due to a difference in statistical analysis; the study performed by Castillo-Gomez analysed differences in current between seropositive and seronegative treated oocytes, whilst we compared NMDAR current of antibody-treated oocytes to their pre-treatment baseline. To account for this lack of positive antibody control, NMDAR antagonists/allosteric modulators were utilised in the current protocols to ensure NR1/NR2A expressing oocytes were generating an NMDAR current that could be inhibited. The non-competitive NMDAR antagonist MK-801 inhibited NMDAR current in a concentration-dependent manner, as also observed by Mullier *et al* (Mullier *et al*., 2017). This shows pharmacological modulators can produce changes in NMDAR current in our hands; therefore, the lack of effect seen by NMDAR Aabs is possibly due to a lack of their functionality in this system. TCN-201, an allosteric modulator whose action is dependent on the occupancy of the NR1 binding domain, but not the NR2 (Zhu and Paoletti, 2015), also reduced NMDAR current, further validating the experimental system.

To test our Aabs, NMDAR1 Aabs (and control rIgG) were applied both acutely and chronically, at two different concentrations. However, acute and chronic incubations at both concentrations had no significant effect on NMDAR current. This lack of functional effect by NMDAR Aabs could be attributed to the fact that oocytes are known to have high turnover rates of proteins. Since, unlike standard pharmacological agents, anti-NMDAR Aabs are hypothesised to exert their effects via cross-linking and subsequent internalisation of synaptic NMDARs (Hughes *et al.*, 2010), this high turnover rate of proteins in oocytes may conceal any subtle changes in NMDAR level at the surface caused by the presence and subsequent binding of NMDAR Aabs. In addition, only 1-10% of antibodies are estimated to be targeting NMDARs (Hnasko and McGarvey, 2015), meaning any subtle changes in NMDAR level at the surface and consequently minimal changes in NMDAR current are being overlooked in this system (as also seen with commercial antibodies). Therefore, as discussed in Chapter 3, further purification of NMDAR1 Aabs was carried out using immunisation peptides, generating a more NMDAR-specific composition of IgG (NMDAR1pp). Despite this, no significant differences were identified between those oocytes incubated with NMDAR1pp Aabs and those with control IgG, indicating the absence of functional effect seen both here and previously with NMDAR Aabs is not due to a lack of specific IgG. There was, however, evidence of 'rundown' of the NMDAR current in both treatment groups, generating a significant effect of time in most experiments. It is possible that this run-down may have also contributed to the lack of measurable effect of NMDAR Aabs.

An alternative possibility for the lack of measurable effects of NMDAR Aabs in oocytes is that NMDAR Aabs may interact with auxiliary subunits or scaffolding proteins which are not present in the current oocyte system, but which are present in native neurons. One current hypothesised mechanism of action for anti-NMDAR Aabs involves binding to and crosslinking of NMDARs and subsequent internalisation (Hughes *et al.*, 2010), with a possible interaction

with the protein EPHRB2, which normally stabilises NMDARs at the membrane surface (Planaguma *et al.*, 2016). Therefore, oocytes may not have the mechanistic capabilities to reproduce the protein complexes required for the internalisation process (Goldin, 2006). To assess if either a high turnover rate of oocyte proteins, or a lack of necessary proteins in oocytes may be the cause of a lack of functional effects seen with NMDAR Aabs, an alternative model system may be tested with NMDAR Aabs to identify any functionality of Aabs. With this in mind, functionality of NMDAR Aabs on NMDARs was investigated in a more physiologically relevant system; namely, using MEAs and patch-clamp to record NMDAR-dependent LTP in hippocampal brain slices and sEPSCs in primary hippocampal neurons respectively.

4.5.2 Schaffer collaterals-CA1 LTP is NMDAR dependent, but NMDAR1 & 2 Aabs have no significant effect

LTP is a persistent strengthening of synapses underlying synaptic plasticity which, dependent on brain area, can be NMDAR-dependent, such areas include the Schaffer collateral pathway within the hippocampus (Malenka, 1994). Several studies have used Schaffer collateral-CA1 LTP to study the effects of patient anti-NMDAR Aabs on NMDAR function and hence network activity within the native brain (Zhang *et al.*, 2012).

We have shown LTP can be effectively induced in acute brain slices using HFS, where ~150% potentiation in evoked fEPSP signal was achieved under vehicle conditions. This potentiation could be inhibited by the addition of 50µM DL-APV. Acute hippocampal mouse brain sections pre-incubated with either class specific negative controls (mIgG2b or rIgG), or NMDAR1 and NMDAR2 Aabs for 1 h all continued to elicit a similar significant potentiation following LTP induction, to that of vehicle. These results differ to experiments using patient CSF containing NMDAR Aabs (Zhang *et al.*, 2012) where an acute 5 min pre-incubation was reported to cause a significant inhibition of LTP (Zhang et al., 2012). In addition, a significant inhibition of LTP

was observed in hippocampal brain slices from rats which had patient CSF-containing NMDAR Aabs stereotactically infused 1-8 days prior (Würdemann *et al.*, 2016; Blome *et al.*, 2018; Kersten *et al.*, 2019). The difference between our results and those of previous studies could be attributed to patient CSF being used, whereas our studies used peptide immunised generated Aabs, where a mixture of 5 immunisation peptides were used. Therefore, our Aabs may be targeting different epitopes, some of which do not contribute to this functional effect. In addition, previous studies primarily use NMDAR Aabs from patient CSF where higher titres and other components may be present which contribute to such effects (Zhang *et al.*, 2012; Würdemann *et al.*, 2016).

Despite the fact no significant effect was found following NMDAR1 and NMDAR2 Aabs pre-incubation, a numerical reduction in the data that failed to reach significance (Figure 4.8A), suggested a small effect may be occurring in the late phase of LTP in NMDAR1 Aab incubated slices when compared to vehicle and control antibody incubated slices. This is heightened by the fact that IgG controls did not have any effect in these experiments, therefore, further purification of NMDAR1 Aabs was carried out to generate a more specific sample of Aabs.

4.5.3 Peptide purification of NMDAR Aabs elicited a significant reduction in LTP

The further purification of NMDAR1 Aabs via immunisation peptide generated a sample of NMDAR specific Aabs (NMDAR1pp Aabs). Application of NMDAR1pp Aabs to acute hippocampal brain slices for 1 h prior to adding to MEAs significantly reduced HFS-induced potentiation; this effect was of similar magnitude to that seen in APV-treated hippocampal slices.

Specific patterns of activity are able to induce LTP in postsynaptic neurons via concurrent depolarisation of the postsynaptic neuron and relief of the Mg^{2+} block from NMDARs, resulting in an influx in Ca^{2+} in the postsynaptic neuron. This increase in Ca^{2+} concentration

activates CaMKII - phosphorylating proteins, including AMPARs. CaMKII activation also leads to the insertion of additional AMPARs into the synapse, thus increasing EPSP amplitude (Malenka, 2003). The maintenance of the potentiated EPSP (late phase LTP) is a protein-synthesis dependent mechanism, initiated by a number of protein kinases (Luscher and Malenka, 2012). Therefore, inhibiting NMDARs may inhibit Ca^{2+} influx and subsequent AMPAR insertion into the synapse. This is in keeping with results described in Chapter 4, whereby NMDAR1pp Aab incubation resulted in a significant inhibition of HFS-induced potentiation. This coincides with a previous study, where patient anti-NMDAR Aabs are thought to exhibit binding to, and cross-linking of NMDARs, leading to internalisation of these receptors (Hughes *et al.*, 2010). This mechanism has been confirmed by modifying Aabs to create Fabs, where the Fc region of the antibody is removed; and when these were applied, no crosslinking or internalisation occurred, identifying the Fc region of the Aabs as necessary for this mechanism (Hughes *et al.*, 2010). Therefore, as both early- and late-phase LTP are dependent on the initial activation of NMDARs, any NMDAR Aab-dependent internalisation of NMDARs prior to LTP induction would account for the lack of LTP observed.

The effects seen in this chapter are also in line with similar experiments conducted by others previously, despite different compositions of Aabs used between our study and those in the literature (Zhang *et al.*, 2012; Würdemann *et al.*, 2016; Blome *et al.*, 2018; Kersten *et al.*, 2019), whereby a reduction in LTP was observed following varying incubation periods with NMDAR Aabs obtained from patient sera. As previous studies have documented an internalisation of NMDARS (Hughes *et al.*, 2010), it can be hypothesised that reduced NMDAR number at the synapse on particularly inhibitory neurons would disrupt the negative feedback onto excitatory neurons, and therefore impact the excitatory/inhibitory balance; an effect which is in line with other animal models, such as an NR1 hypo-morphic mouse model of schizophrenia (Gandal *et al.*, 2012). These mice express approximately 15% of normal levels

of the NR1 subunit of NMDARs (Gandal *et al.*, 2012) which was associated with a disrupted excitatory/inhibitory network (Gandal *et al.*, 2012), and as such exhibit lethal seizures when induced with a subthreshold dose of kainic acid, while their wild type counterparts did not (Duncan *et al.*, 2010).

4.5.4 NMDAR1pp Aabs have no significant effect on sEPSC frequency following acute exposure

Since further purification of NMDAR1 Aabs exhibited a significant reduction in LTP following pre-incubation, further functional studies were carried out using whole-cell patch-clamp on hippocampal neurons to assess their activity on single cell activity. Hippocampal neurons were recorded in Mg^{2+} free external solution in order to remove the magnesium block from NMDARs which are present under physiological baseline neurotransmission. Antagonists to $GABA_A$Rs and AMPARs were added to isolate any NMDAR response and NMDAR1pp Aabs were added via bath application for 30 min. No significant changes in sEPSC frequency or amplitude were observed when compared to those treated with rIgG, or when compared to their pre-treatment baselines. This lack of presynaptic effect coincides with previous studies in the literature (Hughes *et al.*, 2010), where NMDAR Aabs demonstrated a lack of effect on mEPSC frequency and amplitude of primary hippocampal neurons. Further experiments were carried out to isolate out miniature EPSC (mEPSC) events, whereby TTX was added to remove any action potential mediated events. However, all events were inhibited following the addition of TTX, suggesting the miniature EPSC population was too small to record any changes in NMDAR activity. Future studies could be optimised and performed to investigate this further, whereby primary culture density, age of cultures and conditions primary neurons were grown in could be altered to improve the activity recorded both in the presence and absence of pharmacological inhibitors.

4.5.5 Limitations of techniques used in this chapter

The evidence presented in this chapter suggests that one limitation of these functional studies is the purification state of NMDAR Aabs. Initial oocyte and MEA-LTP experiments were carried out with protein A purified NMDAR Aabs, both of which showed no functional effect. This could simply be due to a lack of functional effect of our NMDAR Aabs, or instead not enough Aab being present to display an effect in these studies, as only 1-10% of total IgG are thought to be target specific (Hnasko and McGarvey, 2015). Importantly, further purification of NMDAR1 Aabs by immunisation peptides resulted in a greater percentage of NMDAR-specific IgG which gave positive effects in MEA-LTP experiments, whereby a functional reduction in LTP was proven.

Xenopus oocytes were used as an isolated overexpression system, whereby NMDARs could be expressed, and their currents measured in response to the addition of both antibodies and pharmacological modulators. Although used by many previous studies to characterise novel drug compounds, including NMDAR Aabs effect on NMDAR current (Castillo-Gomez *et al.*, 2016), this system was found not to generate measurable functional effects for our NMDAR Aabs. Previous studies conducted by Castillo-Gomez noted a significant difference in NMDAR current following oocyte incubation with patient-CSF as well as an anti-NR1 commercial antibody, when compared to those oocytes incubated with control CSF. The presence of control CSF showed an increase in NMDAR current, which may be the cause of reported significance between control and NMDAR Aab and commercial antibody incubated oocytes. This difference may also be due to the fact that patient CSF was used, which may contain other antibodies against different epitopes as well as other components which may contribute to the significant effect observed by this study, an effect which was not observed with our NMDAR Aabs.

This system also has its limitations which may make it unsuitable for investigating functional effects of our NMDAR Aabs. As mentioned in section 4.1, oocytes have a rapid turnover rate of proteins, and thus any subtle changes in NMDAR level at the surface may go unnoticed. Furthermore, due to experimental constraints, oocyte experiments could not be repeated with NMDAR2 Aabs to assess if any functional effects were observed in this system with these Aabs.

The whole-cell patch-clamp experiments detailed in this chapter resulted in large events which were long in duration, unusual to those documented previously in the literature (Hughes *et al.*, 2010). When TTX was bath applied, to isolate mEPSCs, all events were inhibited, suggesting the mEPSC population was too small to record. Further studies optimising this setup would be useful to investigate the effect of NMDAR Aabs on NMDAR currents and networks of primary neurons. Factors such as primary culture density, age of cultures and recording conditions could be altered to improve the activity recorded both in the presence and absence of pharmacological inhibitors.

4.5.6 Conclusions

This chapter has shown that NMDAR1pp showed a significant inhibitory effect on HFS-induced LTP but that NMDAR1 and NMDAR1pp Aabs had no functional effects in oocyte experiments. Similarly, NMDAR1 and NMDAR2 had no clear effect in MEA-LTP experiments. contrasting previous studies, (Zhang *et al.*, 2012; Würdemann *et al.*, 2016; Blome *et al.*, 2018; Kersten *et al.*, 2019). Thus, these data argue that the purification state of NMDAR Aabs is of fundamental importance. Following further purification of NMDAR1 Aabs via immunisation peptide a significant functional effect was observed in MEA-LTP experiments, where a significant reduction in HFS-induced potentiation was shown, in a similar manner to the effect of the NMDAR competitive antagonist APV. This effect is more in line with the

current hypothesis in the literature, where patient Aabs cause a reduction in NMDARs at the synapse via internalisation (Hughes *et al.*, 2010), which may be the mechanism underlying the inhibition of LTP. This is also in line with previous studies, where LTP inhibition has been observed following incubation/infusion of patient CSF containing NMDAR Aabs (Zhang *et al.*, 2012; Würdemann *et al.*, 2016; Blome *et al.*, 2018; Kersten *et al.*, 2019).

Here we have shown one of the first studies using NMDAR Aabs generated through peptide immunisation which have a functional effect similar to those studies using patient Aabs. This is vital as these Aabs can serve as an experimental tool, enabling further investigation into the exact mechanism of action, how this relates to neuronal excitability and, potentially, the seizures reported in conditions characterized by the presence of NMDAR Aabs. In addition, as NMDAR Aabs may serve as a biomarker of disease, they can be used as a diagnostic tool; therefore, increased knowledge of their mechanism of action will be vital.

5 Generation and characterisation of AMPAR Aabs

5.1 Introduction

AMPARs are members of the glutamate ionotropic receptor family, which are important mediators of excitatory neurotransmission and, by extension, potential epileptogenic targets within the human CNS. Previous studies have been conflicting with regard to the functional effects of anti-AMPAR Aabs, whereby some studies identify an increase in seizures in rabbits following immunisation of GluR3 protein (Rogers *et al.*, 1994); others, a death in primary hippocampal neurons following 24 h incubation with peptide-immunised generated anti-GluR3 Aabs (Levite *et al.*, 1999), and others reporting no functional effect following application of patient anti-GluR3 Aabs to primary cortical neurons (Frassoni *et al.*, 2001). Understanding the effects of GluR3 Aabs would be of benefit, especially in autoimmune epilepsy where there is little and/or conflicting evidence of their mechanisms of action. Gaining an insight into whether GluR3 Aabs are involved in pathogenicity, or alternatively if these Aabs are generated as a compensatory mechanism to reduce seizure activity, could aid in the development of novel AEDs for patients with autoimmune epilepsy. To investigate the effects of AMPAR Aabs, rabbits were immunised with a single peptide against the GluR3 subunit in order to generate anti-AMPAR polyclonal antibodies. This short chapter details the generation and experimental characterisation used to assess the specificity of anti-AMPAR Aabs.

5.2 Production of rabbit polyclonal antibodies

Patient Aabs have been shown to bind to a particular epitope within the extracellular domain of the GluR3 subunit of AMPARs, named the GluR3B peptide (sequence illustrated in Figure 5.1). As this peptide sequence is located on a hinge region within the ATD of GluR3 subunit, it is deemed a region of high immunogenicity and a 24 amino acid long peptide (non-cyclised)

was generated and subsequently conjugated to KLH, BSA and OVA externally (Peptide Synthetics). These conjugated peptides were used to immunise a rabbit (see section 2.1.1) in order to elicit an immune response.

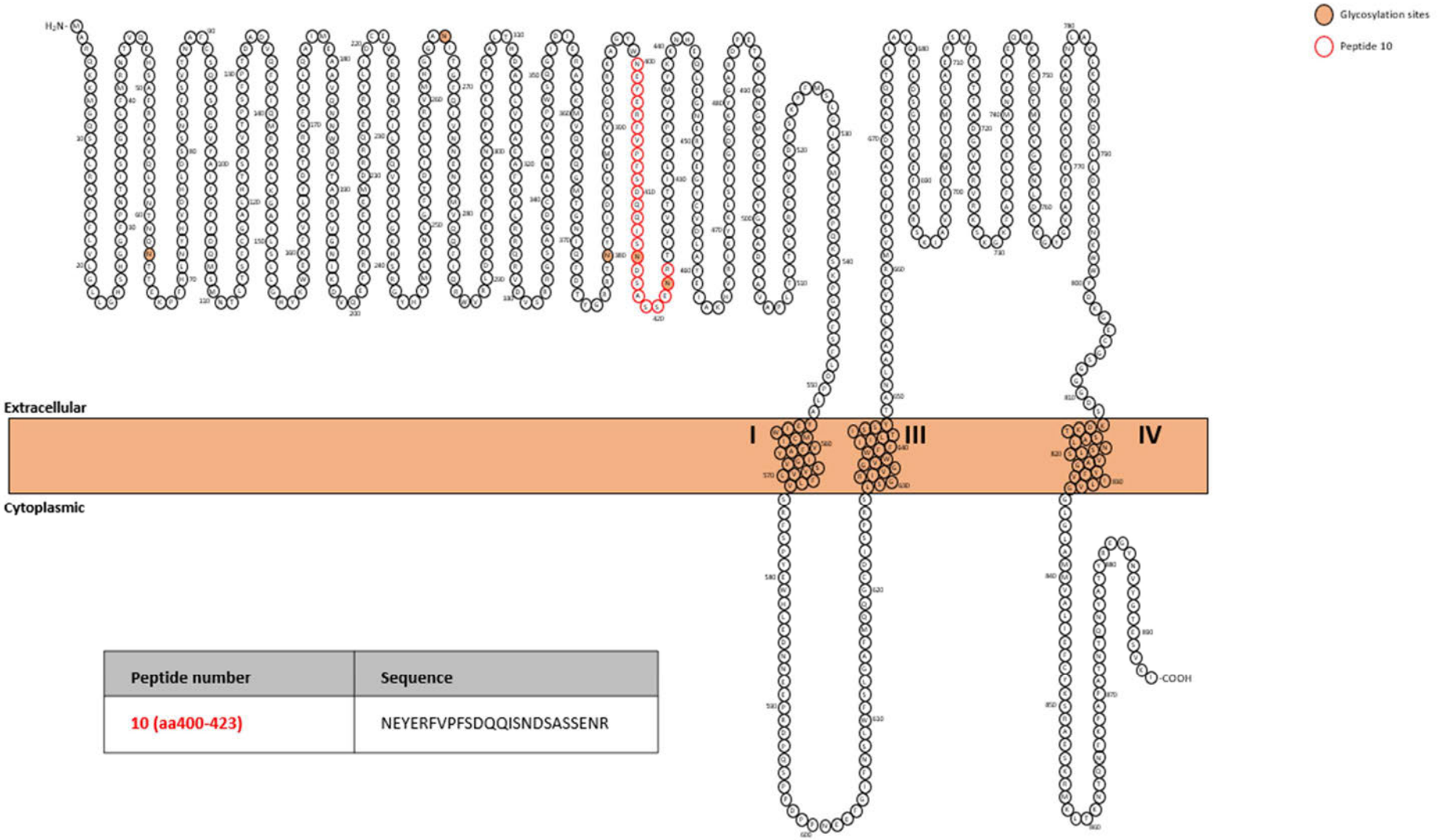

Peptide number	Sequence
10 (aa400-423)	NEYERFVPFSDQQISNDSASSENR

Figure 5.1: AMPAR peptide sequence used for the immunisation of rabbit #3. The peptide was generated and modified with N-terminal acetylation and C-terminal amidation.

5.2.1 Titres and ELISA of antibody sera

The rabbit immunisation procedure was followed as described in section 2.1.1. Rabbit bleeds were taken 14 days after immunisation boosts, and 7 days after the final immunisation, where serum titres were monitored using an ELISA to detect the presence of IgG antibodies against the immunisation peptide (Figure 5.2). The total number of immunisation boosts given was determined based on these ELISA results. As expected, no detectable immune response was seen against the peptide at bleed 0 (pre-immunisation). In this case, no ELISA was carried out following the first immunisation due to the minimal binding seen previously for BL1 during NMDAR immunisations (see section 3.1). Following the second and third immunisations (BL2 and BL3, respectively) an increase in binding to the AMPAR immunisation peptide was detected. The terminal sera curves as shown in Figure 5.2 did not seem to reach the same peak of binding as the previous BL3, however when the 'EC_{50}' values were calculated, the dilution of sera required to reach half-maximal binding of the terminal sera was greater than that of BL3 (1:19,459 dilution for terminal sera (as shown by square symbols and solid line, compared to 1:7,987 dilution for BL3 (values shown by square symbols and dotted lines; Figure 5.2). These data indicate a greater immune response and hence more antibody produced following the final immunisation boost when compared to BL3, resulting in an increased binding to immunisation peptide and hence more substrate breakdown and higher absorbance measured. Binding of the terminal sera to the immunisation peptide was detected as low as 1:100,000 (Figure 5.2).

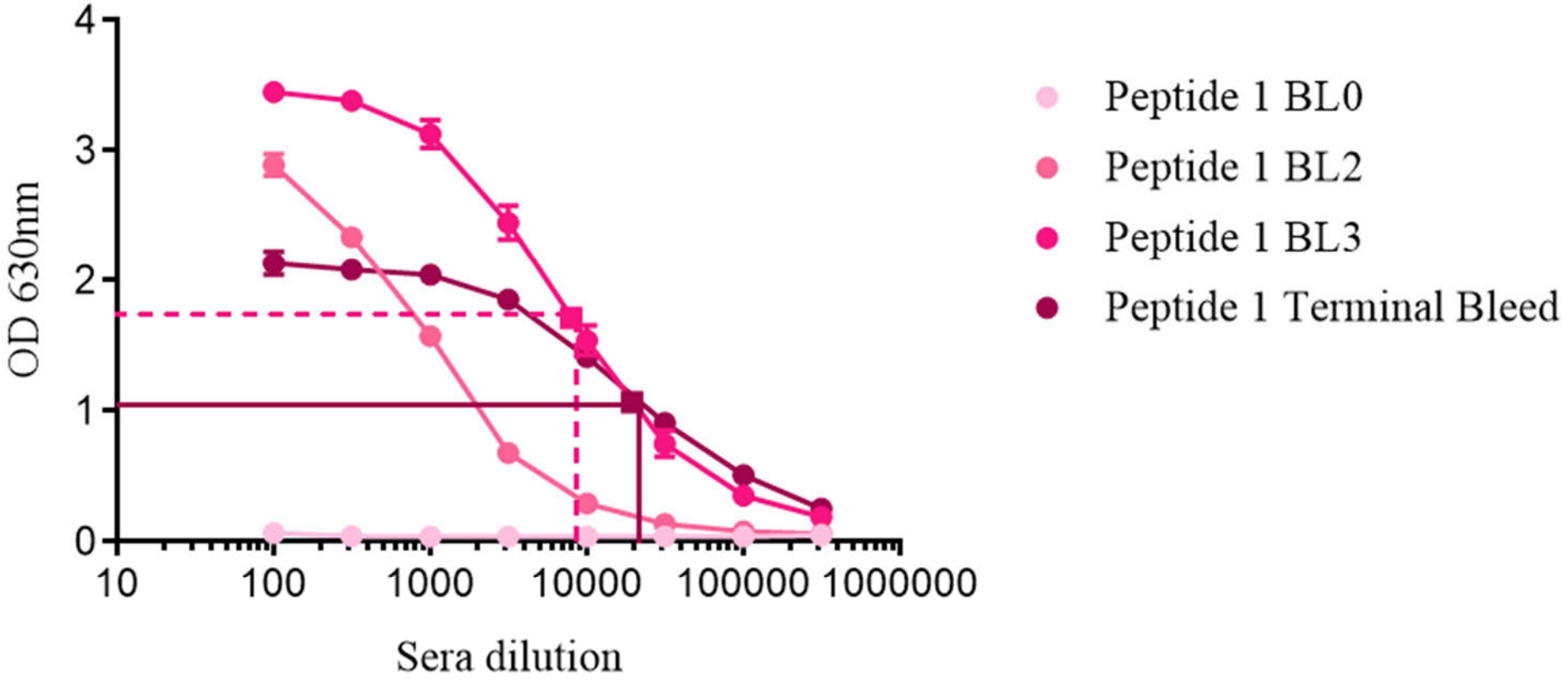

Figure 5.2: Rabbit anti-AMPAR immunogenicity response. Pre-immunisation bleed (BL0), bleed 2 (BL2), 3 (BL3) and terminal bleed responses to AMPAR peptide used for immunisations. An increase in response to the peptide was observed with each immunisation boost. Dotted lines show EC_{50} values for BL3 and Terminal bleed. N=3 technical replicates.

5.2.2 Purification and analysis of AMPAR Aabs

Terminal serum from the AMPAR-immunised rabbit was purified using Protein A resin to isolate total IgG. Total IgG was then quantified and analysed using further ELISA and SDS-PAGE.

Fractions from all steps within the purification process were analysed using SDS-PAGE and subsequent Coomassie staining. Proteins were detected at multiple sizes including 150 kDa, 90 kDa, 60 kDa and 30 kDa, of which the band at 150 kDa is the expected size of IgG (Figure 5.3A). The presence of a band at 150 kDa in eluates 1 and 2 indicates that most of the IgG was purified from the terminal serum. Fainter bands at 150 kDa can also be seen in wash 1 and wash 2, indicating some IgG was lost from the column before eluting, as well as a faint band in the post-purification fraction suggesting a small amount of IgG remained in the terminal serum following purification. All other bands detected in the pre-purification fraction were also present in the post-purification fraction, indicating the specificity of the purification for IgG only. However, faint bands can be seen in eluate 1 at 50 kDa and 25 kDa, which may represent the heavy and light chains of IgG respectively (Figure 5.3A).

Quantification of total IgG was performed using an A280 nanodrop, where protein concentration was determined by measuring the absorbance at 280nm. This revealed 7.6mg/ml total IgG was purified, of which anywhere between 1-10% is predicted to be AMPAR-specific (Hnasko and McGarvey, 2015). To verify the purification process had not altered AMPAR Aab specificity to the immunised peptide, a further ELISA was performed using the total IgG material. This revealed greater binding to the immunisation peptide, with minimal binding to an irrelevant peptide (a peptide not related in amino acid sequence, or function) (Figure 5.3B), similar to that seen pre-purification (Figure 5.2).

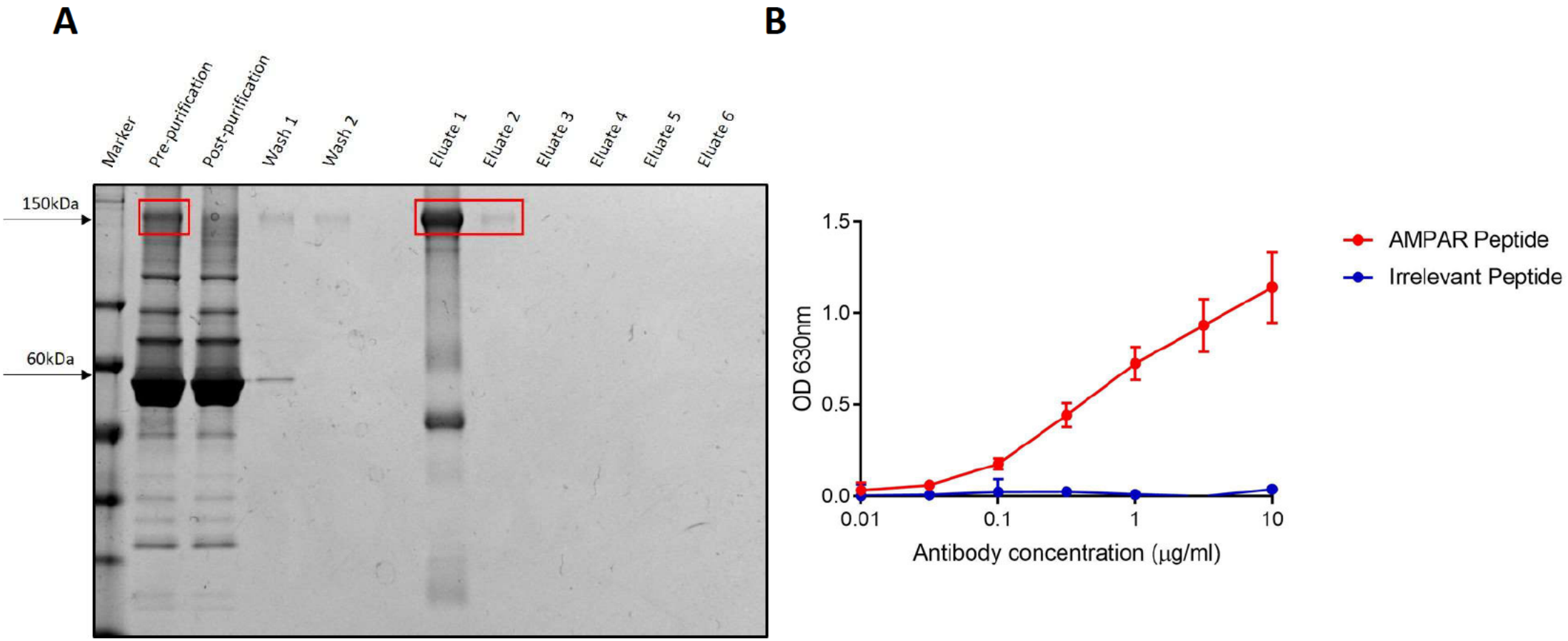

Figure 5.3: Protein A purification of AMPAR Aabs. (A) SDS-PAGE analysis of rabbit serum purified by protein A-sepharose resin. (A) Analysis of all fractions revealed a specific band at 150 kDa in pre-purification sample and eluates 1-2 (as indicated by the red boxes), which is not present in the post-purification sample. **(B)** ELISA of protein A purified AMPAR Aabs revealed a similar binding to the immunisation peptide as pre-purification, while minimal binding to an irrelevant peptide was retained. N=3 technical replicates.

Further quantification using SDS-PAGE was carried out to validate the concentration of total IgG measured. A commercial rabbit IgG of known concentration was used as a control, where concentrations of both AMPAR Aabs and control IgG were titrated and analysed via SDS-PAGE and Coomassie staining. Uniform bands were seen at 150 kDa across both AMPAR Aabs and control rIgG at all dilutions (Figure 5.4), faint bands could also be detected at 50 kDa (in AMPAR Aabs and rIgG) and 25 kDa (AMPAR Aabs only), which may be due to heavy and light chains of IgG. Additional bands just over 150 kDa and at ~120 kDa could be seen in control IgG dilutions.

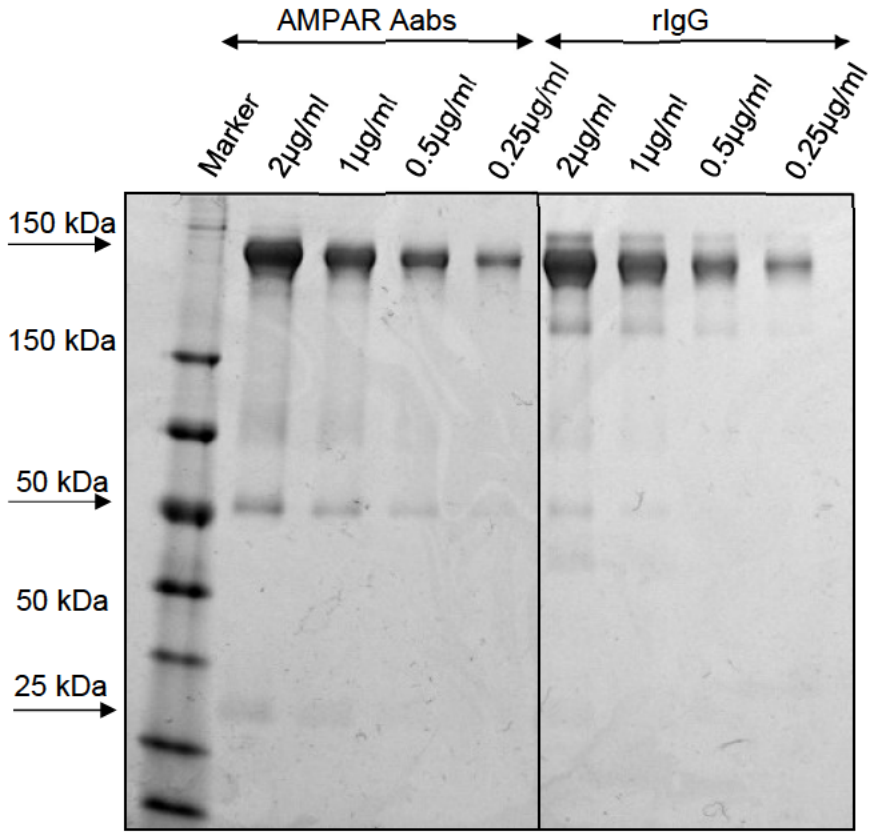

Figure 5.4: Protein A purification of AMPAR Aabs. SDS-PAGE analysis of rabbit serum purified by protein A-sepharose resin compared with control rabbit IgG of known concentrations. Analysis revealed a single band at the expected size of 150 kDa across all dilutions for both AMPAR Aabs and the control rIgG

5.3 Characterisation of AMPAR Aabs on *in vitro* systems

5.3.1 AMPAR Aab detection of native AMPAR

ICC, IHC and Western blot techniques were utilised to determine the specificity of AMPAR Aabs against the GluR3 subunit. Primary neuronal cortical cultures were fixed with PFA, preserving and stabilising cell morphology, and incubated with anti-AMPAR Aabs or a commercial anti-AMPAR antibody, with negative controls rIgG and secondary antibody-only controls also being used.

Cells stained with AMPAR Aabs were also co-labelled with the neuronal marker βIII tubulin (as shown by the white arrows), but not with the astrocyte marker GFAP (Figure 5.5A). This staining was similar to that exhibited by the commercial anti-AMPAR antibody (cAMPAR), which also labelled cells which co-localised with βIII tubulin, but not GFAP (Figure 5.6A). Cells which were incubated with the class-specific negative control rIgG elicited some faint staining, however this staining co-localised with both βIII tubulin and GFAP stained cells, indicating a lack of specificity for any cell-type (Figure 5.6B). This latter staining may be due to the presence of non-AMPAR specific IgG which could be binding to its respective target with similar location to AMPARs, similar to that seen for NMDAR Aabs (see Chapter 3). In addition, a secondary-only control was performed, where cells were incubated with secondary antibodies without primary antibody. No staining was detected in any channel indicating no background binding caused by secondary antibodies (Figure 5.5B).

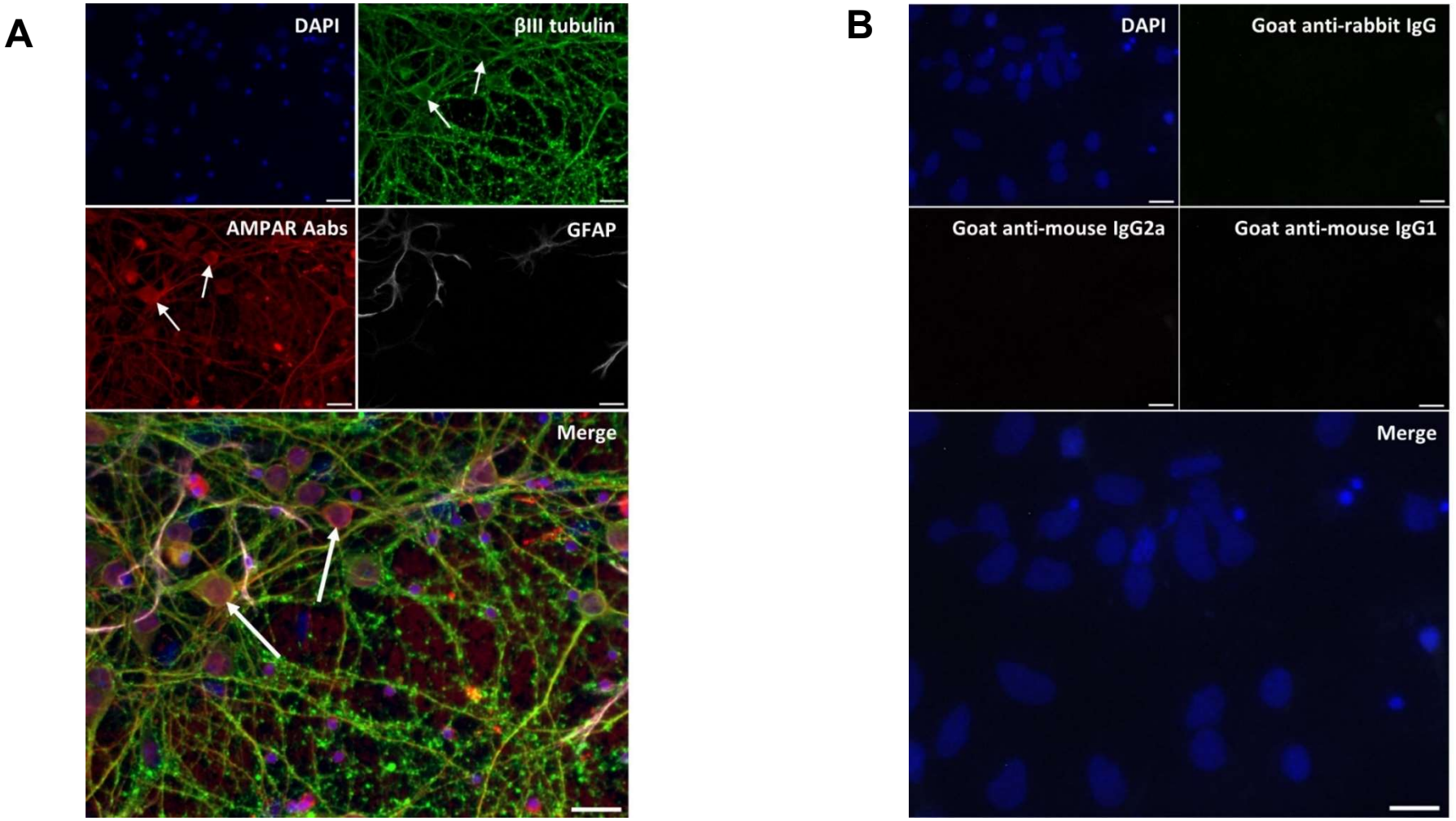

Figure 5.5: Immunocytochemical staining of fixed primary cortical neurons (DIV8). (A) Cells were stained with AMPAR Aabs (red), βIII tubulin; a neuronal marker (green), GFAP; an astrocyte marker (white) and a nuclear stain (DAPI: blue). Clear staining was seen with AMPAR Aabs as indicated by the white arrows. **(B)** Cells were stained with secondary antibodies only. Goat anti-rabbit IgG (green), goat anti-mouse IgG2a (red) and goat anti-mouse IgG1 (white). No labelling was detected in any of these channels. Scale = 20μm. Representative images selected from n=3 technical replicates.

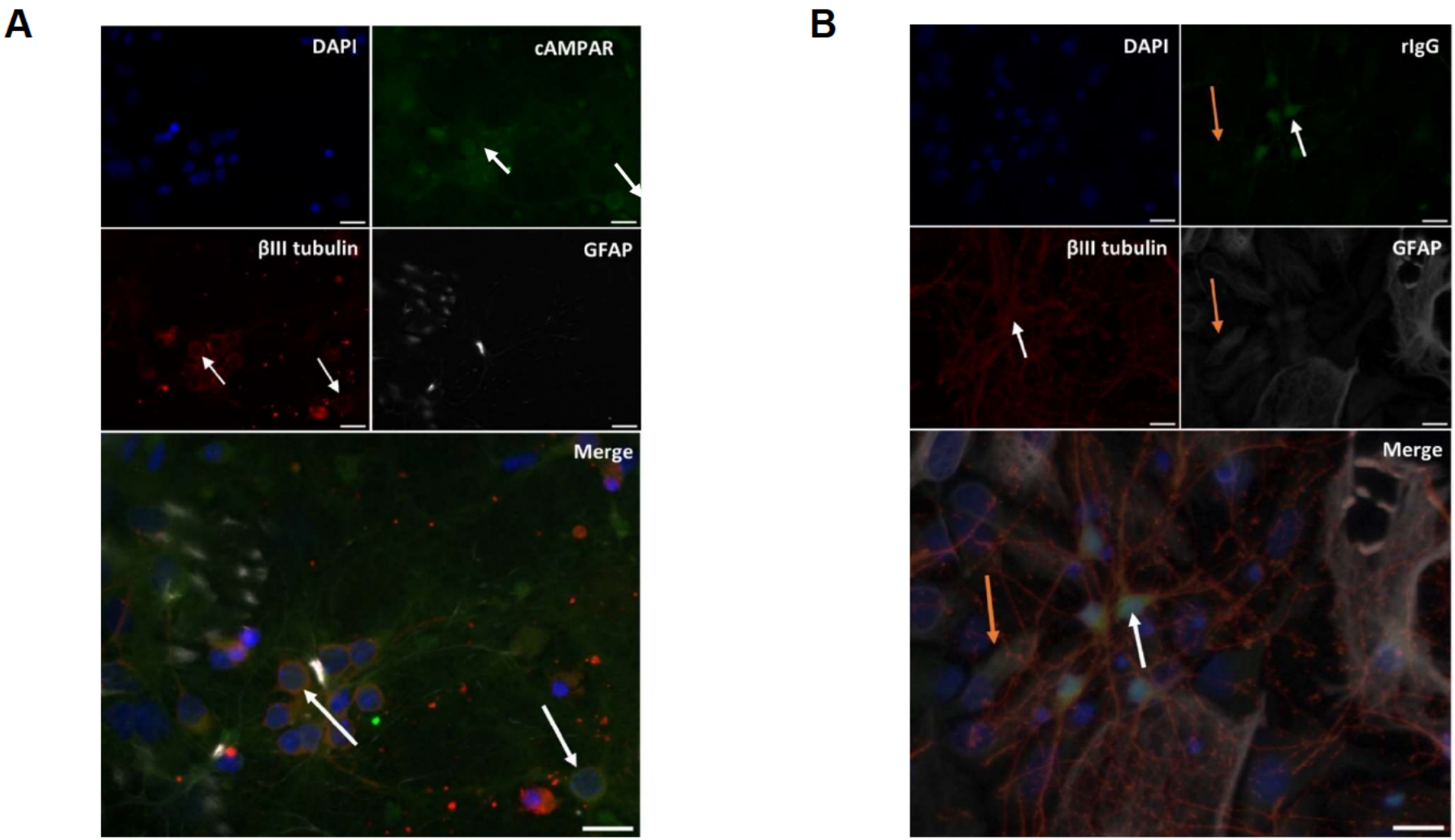

Figure 5.6: Immunocytochemical staining of fixed primary cortical neurons (DIV7). (A) Cells were stained with commercial AMPAR antibodies (cAMPAR; green), βIII tubulin; a neuronal marker (red), GFAP; an astrocyte marker (white) and a nuclear stain DAPI (blue). Clear staining was seen with cAMPAR as indicated by the white arrows. **(B)** Cells were stained with rIgG (green), βIII tubulin, GFAP and DAPI. Faint staining was detected with rIgG, which co-localised with βIII tubulin-stained cells (as indicated by white arrows), as well as cells labelled by GFAP (orange arrows). Scale = 20μm. Representative images selected from n=3 technical replicates.

IHC was carried out using mouse hippocampal brain sections to assess spatial binding within the hippocampus, as well as to distinguish cell-type specificity within whole brain sections. Using perfusion fixed and cryopreserved mouse brain sections (12μm), AMPARs were stained by AMPAR Aabs as well as commercial anti-AMPAR antibodies. Cells were co-labelled with βIII tubulin and NeuN as markers for neurons. Minimal binding was seen throughout the hippocampus with AMPAR Aabs; however, this was also the case for βIII tubulin, and to some extent NeuN (Figure 5.7). This raises difficulty in distinguishing the specificity of AMPAR Aabs within the hippocampus, as the lack of binding observed with the co-labels, which have been validated and optimised previously, may be indicating an issue with the protocols employed.

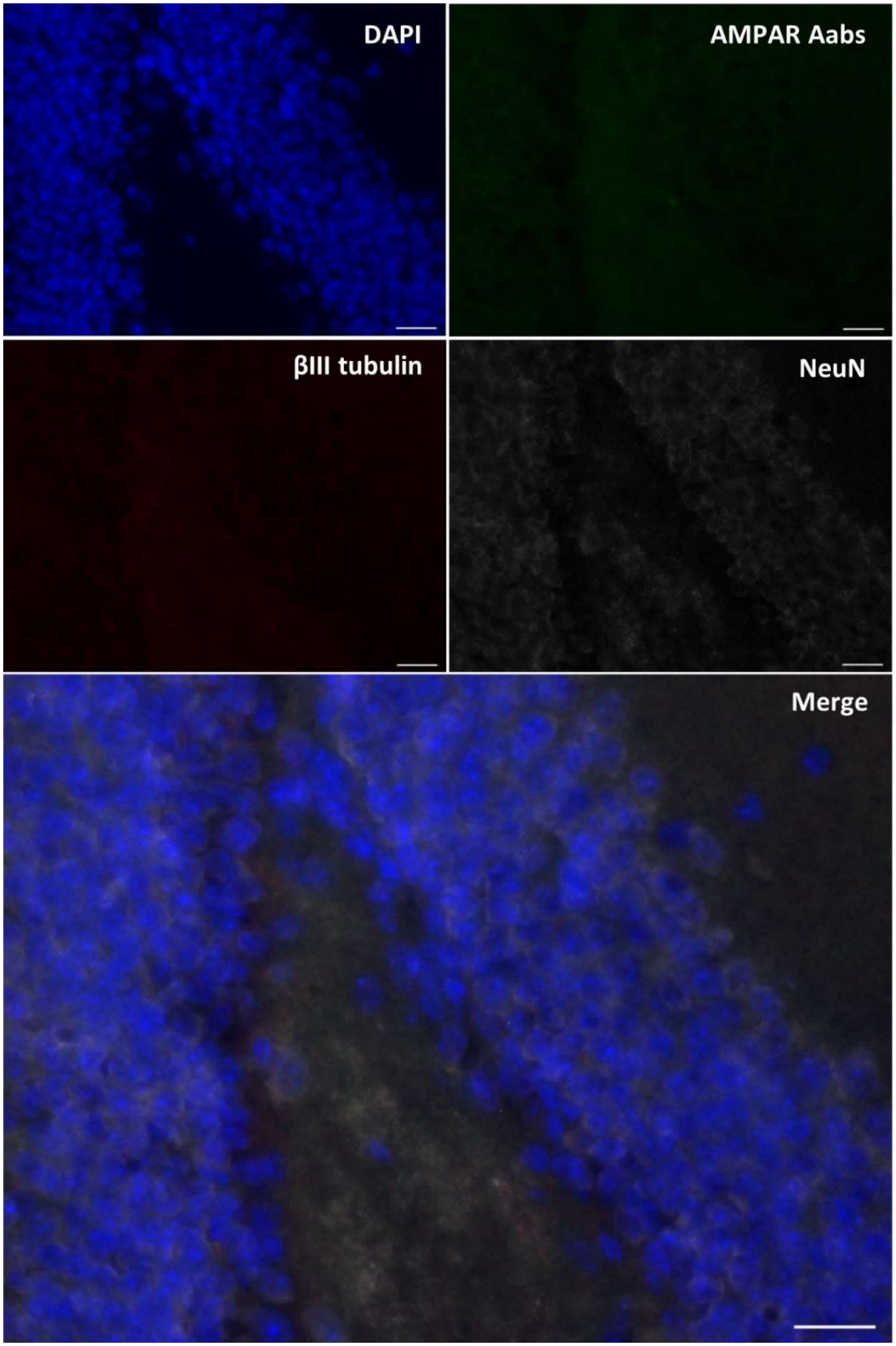

Figure 5.7: Immunohistochemical staining of fixed hippocampal brain slice. Stained with AMPAR Aabs (green), co-stained with NeuN (white) and βIII tubulin (red), as well as a nuclear stain (DAPI; blue). All three antibodies demonstrated minimal binding, highlighting a higher magnification for visualisation is required. Scale = 20μm. Representative image selected from n=3 technical replicates.

Western blots were performed as described in Section 2.2.1.2, with whole brain lysates being run on SDS-PAGE and subsequently probed with AMPAR Aabs, cAMPAR, rIgG (negative) control as well as a secondary antibody only (negative) control. AMPAR Aabs detected a single clear band at just above 100 kDa (as expected, GluR3 molecular weight 101 kDa; Figure 5.8) in whole brain lysate, as well as a slightly fainter band at just above 150 kDa and at ~90 kDa (Figure 5.8), which may represent different glycosylated states of the protein, or alternatively may be caused by non-AMPAR specific IgG binding, as seen with our generated NMDAR Aabs (see section 3.3.2). The commercial anti-AMPAR antibody, detected two prominent bands at 100 kDa and 70 kDa, with an additional band just above 100 kDa (Figure 5.8). Lysates from primary cortical neurons were also run on SDS-PAGE and probed with AMPAR Aabs, cAMPAR, rIgG and secondary antibody only. These detected similar bands, with the exception of AMPAR Aabs detecting a few additional bands at ~60 kDa (data shown in Appendix 9.4), which may represent some non-AMPAR specific IgG binding.

Secondary-only controls resulted in no bands being detected (Figure 5.8), whereas the class-specific negative control rIgG consistently detected multiple bands at different molecular weights (Figure 5.8). This may be due to the nature of control used; as it is from a naïve non-immunised rabbit, it will likely contain other antibodies, some of which may be binding to targets within our lysates. A final loading control (GAPDH) was also tested, which resulted in clean blots with a single band at the expected molecular weight of 37 kDa (data shown in Appendix 9.4).

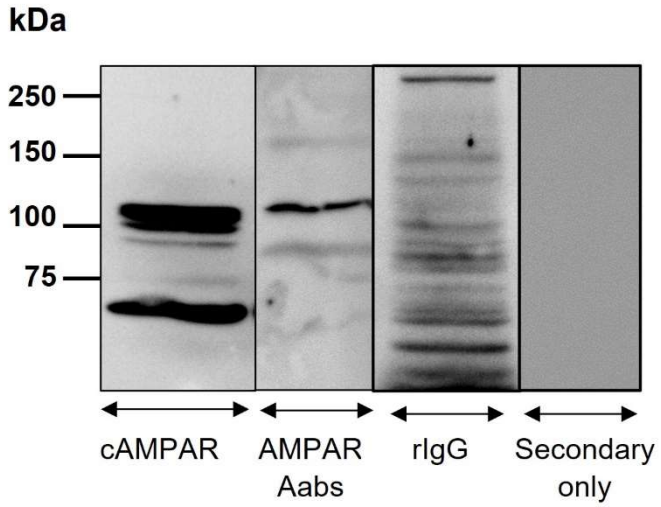

Figure 5.8: Western blot assessing binding specificity of protein A purified AMPAR Aabs to mouse whole brain lysate. AMPAR Aabs elicited a band at the correct size (101 kDa), similar to that of cAMPAR; a commercial anti-AMPAR antibody. The class-specific negative control rIgG elicited a multitude of bands in whole brain lysate, whereas the secondary only control did not elicit any bands. Representative blots selected from n=3 technical replicates.

5.4 Discussion

AMPAR Aabs have been increasingly identified as pathogenic, not only in patients with autoimmune epilepsy, but also in encephalitis and FTD. While previous studies have detailed pathogenic effects of Aabs using both patient Aabs and peptide immunised generated Aabs, such as the development of seizures (Rogers *et al.*, 1994), neuronal cell death (Levite and Hermelin, 1999) and memory impairment (Borroni *et al.*, 2017), little work has been done to determine the mechanistic involvement of AMPAR Aabs on seizure generation. Here, we targeted an immunogenic region of the GluR3 subunit of the AMPAR to produce anti-AMPAR Aabs similar to those reported in patients. Total IgG was purified via protein A purification and specificity for native AMPARs was subsequently examined via an array of assays. The results of this characterisation are summarised below:

- A strong immune response was generated in response to peptide immunisation, measured by ELISA both pre- and post-purification with protein A.
- Neuron-specific labelling with Aabs was observed in primary cortical neurons.
- Aabs detected a band at the predicted size of the GluR3 subunit in whole brain lysate, along with other non-specific bands.

5.4.1 Peptide immunisation generates a strong immune response

Synthetic peptides have numerous applications in research, one of which is the production of antibodies through peptide immunisation. This method has been carried out extensively and used successfully for disease diagnosis (Trier and Houen, 2017) as well as research into pathological mechanisms of native Aabs in patients (Ganor *et al.*, 2014; Palese *et al.*, 2020). Design of immunisation peptides is crucial to successful antibody generation, with optimal

length being between 8-25 amino acids targeting protruding regions to yield antibodies with good specificity (Trier and Houen, 2017; Trier *et al.*, 2019).

The human sequence corresponding to the GluR3B peptide (a 24 amino acid sequence positioned as a hinge region within the GluR3 subunit, linking two modular domains within the extracellular region; NEYERFVPFSDQQISNDSASSENR; see Figure 5.1), was used as the immunisation peptide to generate anti-AMPAR Aabs in this study. Rabbit and mouse (species used for Aab generation and functional testing - see Chapter 6) share 96% sequence homology, with only one amino acid differing in each (Uniprot; Gria3). Following immunisation, antibody specificity was tested via ELISA to ensure an immunogenic response specific to the immunised peptide had been developed, a methodology used routinely following peptide immunisation (Lee *et al.*, 2010; Pan *et al.*, 2018). We have shown a strong immunogenic response to this peptide, with a minimal response shown against an irrelevant peptide (Figure 5.2). Protein A purification of the terminal serum produced substantial total IgG (7.6mg/ml). Recent studies have used this peptide sequence to generate anti-GluR3 Aabs successfully, which have been shown to bind specifically to AMPAR, and also to exhibit functional pathogenic effects both *in vitro* (Levite et al., 1999) and *in vivo* (Ganor et al., 2005; Malina et al., 2006; Ganor et al., 2014).

Unlike NMDAR Aabs where the majority of studies have used patient Aabs to study pathogenic effects (Hughes *et al.*, 2010; Planagumà *et al.*, 2015), most studies investigating AMPAR Aabs typically generate anti-GluR3 Aabs via peptide immunisation (Levite *et al.*, 1999; Ganor *et al.*, 2005). These studies have immunised animals with the 24 amino acid sequence as in our study, and subsequently used either sera or total IgG (Levite and Hermelin, 1999; Ganor *et al.*, 2005; Malina *et al.*, 2006; Ganor *et al.*, 2014). These studies have investigated both *in vitro* and *in vivo* effects, whereby GluR3 Aabs *in vitro* have been shown

to activate AMPARs (Malina *et al.*, 2006) leading to neuronal death (Levite *et al.*, 1999). However, recent studies investigating GluR3B Aabs found in patients with FTD, show a reduction in GluR3-containing AMPARs following incubation of primary neurons with patient Aabs (Borroni *et al.*, 2017), as well as a reduction in glutamate release from synaptosomes (Palese *et al.*, 2020). These alternative *in vitro* effects demonstrate the necessity for further studies investigating the specificity of these Aabs and the potential pathogenicity (explored later in Chapter 6).

In vivo studies have yielded even more conflicting results, where some studies have shown an increase in spontaneous seizures following peptide immunisation in rabbits (Rogers et al., 1994) and an increase in PTZ-induced seizures in mice (Rogers *et al.*, 1994; Ganor *et al.*, 2014), with others showing partial protection from PTZ-induced seizures (Ganor *et al.*, 2005). As above, these conflicting results demonstrate the need for further investigation into these GluR3 Aabs to determine the specificity of these Aabs for the target receptor, and how these may exhibit any functional effects.

5.4.2 Anti-AMPAR Aabs bind to native AMPARs

To test the specificity of our AMPAR Aabs, ICC, IHC and Western blot were further employed. These assays are commonly used in combination with ELISA to validate the specificity of an antibody (Bordeaux *et al.*, 2010).

Following immunisation with GluR3B peptide and total IgG purification, specific binding to cortical neurons was seen following application of anti-AMPAR Aabs, staining which was comparable to commercial anti-AMPARs (targeting amino acids 60-73 of GluR3 ATD). These results are similar to those seen previously, where primary neurons have been successfully labelled using peptide derived AMPAR Aabs (Levite *et al.*, 1999), as well as GluR3 transfected COS7 cells being successfully labelled by patient-derived GluR3 Aabs (Borroni *et al.*, 2017).

Further investigation into the binding specificity and functionality of AMPAR Aabs could further be determined via the use of confocal microscopy on primary neurons as well as brain slices. Performing this imaging at higher magnification and resolution would help determine the specific binding location of AMPAR Aabs, as well as whether any Aab-induced internalisation of AMPARs occurs. In addition, performing co-labelling with antibodies which target other subunits of AMPARs, as well as other glutamate receptors would help determine the specificity of our generated Aabs for AMPARs.

As with NMDAR Aabs in Chapter 3, our AMPAR Aabs and negative control rIgG comprise total IgG, and it is therefore possible that there are also non-AMPAR specific antibodies which may bind specifically to proteins within the lysates used in western blotting. This may explain the presence of non-specific bands in addition to a band of expected size, in particular with rIgG incubated blots. These results are not comparable to any seen in the literature thus far as most studies do not use a class-specific total IgG as a control for their studies, with either a control immunisation peptide or control patient CSF being used (Levite *et al.*, 1999; Borroni *et al.*, 2017).

5.4.3 Conclusions

Specific Aabs directed against the GluR3 subunit of the AMPAR were successfully generated following immunisation with a peptide representing a specific ATD-epitope within the GluR3 subunit, termed the GluR3B peptide. Protein A-purified Aabs were specific for native AMPARs, as shown via ELISA, ICC and Western blot. In particular, the specificity of AMPAR Aabs for GluR3-containing neurons was demonstrated by the co-localisation of AMPAR Aabs with βIII tubulin-labelled cells, but not GFAP-labelled cells, indicating a neuron-specific labelling. The characterisation and specificity of AMPAR Aabs detailed in this chapter are vital to understanding the potential effects of patient Aabs. The immunisation peptide used in this

thesis, as well as in previous data, generated specific GluR3-directed Aabs. Knowing the specificity of these Aabs for GluR3-expressing neurons enabled functional studies to be performed, as detailed in the next chapter.

6. Assessing the functionality of AMPAR Aabs

6.1 Introduction

Based on the results described in Chapter 5, anti-AMPAR Aabs were next used in *in vitro* systems to determine any functional effects on neuronal activity, and hence postulate how these Aabs may be implicated in excitatory neurotransmission.

The findings presented in the previous chapter indicate that the generated AMPAR Aabs successfully bind to AMPARs *in vitro,* as shown in ICC and Western blot. The main electrophysiological technique used throughout this chapter is whole-cell patch-clamp on primary hippocampal neuronal cells. These cells display sEPSCs consisting of both action potential (AP)-dependent and AP-independent currents; the latter are typically termed mEPSCs. EPSCs are comprised of both AMPAR and NMDAR glutamatergic currents depending on the holding voltage, both of which can each be inhibited or isolated using different pharmacological blockers. Baseline sEPSC activity was recorded in the presence of $GABA_AR$ and NMDAR antagonists (bicuculline (BMI; 10µM) and DL-APV (50µM), respectively) in order to isolate AMPAR currents. Either AMPAR Aabs (1:1000 dilution) or the selective AMPAR antagonist NBQX (5µM) were added acutely in order to assess any effect on AMPAR current. Chronic (24 h) Aab incubations were also performed.

Prevention of the generation of action potentials with the potent voltage-gated Na^+ channel blocker TTX isolates mEPSCs, which occur in response to spontaneous, action potential-independent release of glutamate from the presynaptic terminal. Observing a change in mEPSC amplitude is indicative of altered postsynaptic sensitivity to glutamate, such as an alteration in the number and composition of AMPARs, whereas a change in mEPSC frequency is consistent with presynaptic loci of action which affects glutamate release (Zucker and Regehr, 2002).

Both acute and chronic Aab applications were repeated in the presence of TTX to fully elucidate any effects on AMPAR-mediated mEPSCs.

6.2 Aab effects on spontaneous excitatory postsynaptic currents

Whole-cell patch-clamp and primary hippocampal neurons (DIV7-14) were used to measure sEPSCs in the presence and absence of AMPAR Aabs to elucidate any functional pre-/post-synaptic effects. BMI (10 µM) and DL-APV (50µM) were added via bath application and equilibrated while a suitable cell was identified. Cells were recorded in the whole-cell patch-clamp configuration. sEPSCs were recorded and monitored, whereby parameters such as amplitude and frequency could be analysed (example traces shown in Figure 6.1C).

6.2.1 Acute 10min AMPAR Aab incubation

To test the effects of acute AMPAR Aabs application, a 10 min baseline of sEPSCs was recorded, and subsequently AMPAR Aabs or rIgG (1:1000 dilution) were added to the cells via bath application and sEPSCs recorded for a further 10 min. At the end of the experiment, the AMPAR antagonist NBQX (10µM) was added to the bath to confirm that all observed events were mediated by AMPARs.

Acute bath application (10 min) of AMPAR Aabs resulted in a significant reduction in sEPSC frequency. Cells incubated with AMPAR Aabs had a significantly lower sEPSC frequency (0.8 ± 0.4 Hz) compared to those incubated with rIgG (1.3 ± 1.0 Hz; n=21-23 per group, $p = 0.0396$ unpaired t-test, Figure 6.1A). Significant differences in cumulative inter-event interval distributions were also observed following 10 min incubation of AMPAR Aabs when compared to IgG incubated cells ($p<0.0001$; Kolmogorov-Smirnov test; Figure 6.1B).

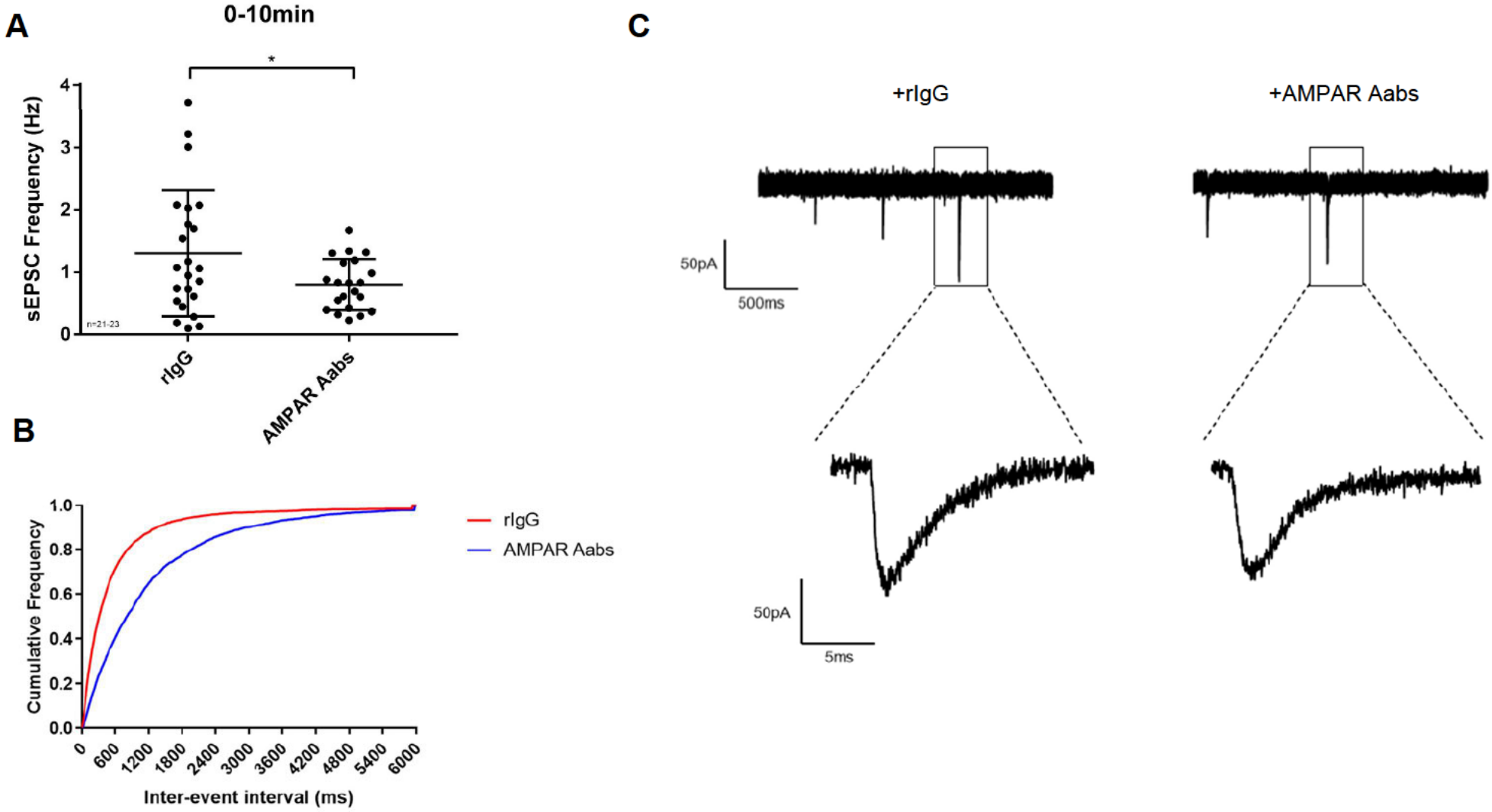

Figure 6.1 Effects of acute (10 min) AMPAR Aabs (1:1000 dilution) and rIgG application (1:1000 dilution) on sEPSC frequency. (A) Following addition of AMPAR Aabs, significant differences between AMPAR Aabs and rIgG treated cells over the 10 min period was detected (A; $p = 0.0396$, $n = 21$-23 per group). **(B)** Significant differences in cumulative inter-event interval were also observed following AMPAR Aabs 10min incubation when compared to IgG incubated cells ($p<0.0001$). **(C)** Representative traces of sEPSCs from rIgG and AMPAR treated cells. Data were collected over three separate neuronal cultures and presented as mean ± SD *: $p < 0.05$.

No significant effect on sEPSC amplitude was observed following application of AMPAR Aabs over 0-10 min, whereby cells incubated with AMPAR Aabs generated sEPSCs of similar amplitude (-22.3 ± 7.3 pA) to those incubated with rIgG (-20.4 ± 7.2 pA, n=24 per group, unpaired t-test, p = 0.364; Figure 6.2A). However, significant differences in cumulative frequency of sEPSC amplitude were observed following 10 min incubation of AMPAR Aabs when compared to IgG incubated cells (p<0.0001; Kolmogorov-Smirnov test; Figure 6.2B).

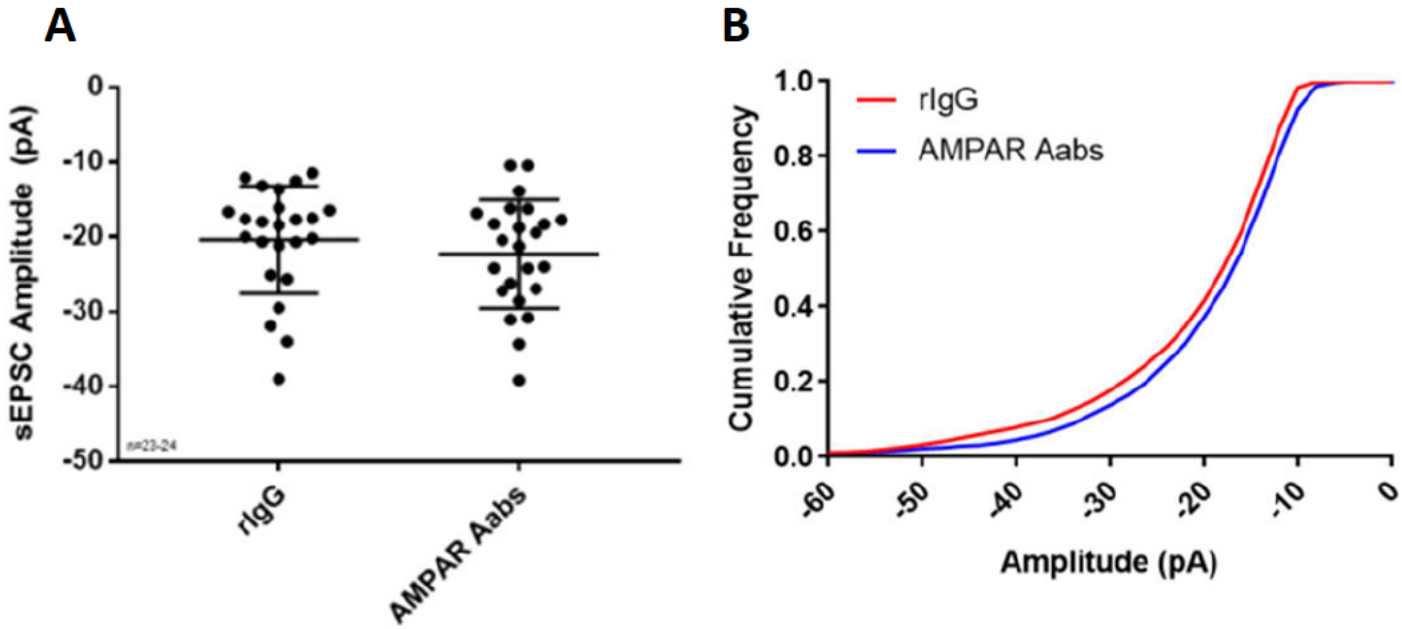

Figure 6.2 Effects of acute (10 min) AMPAR Aabs (1:1000 dilution) and rIgG application (1:1000 dilution) on sEPSC amplitude. (A) Following addition of AMPAR Aabs, no significant differences were observed between AMPAR Aabs and rIgG treated cells over the 10 min period (A; p = 0.364, n = 23-24 cells per group). **(B)** Significant differences in cumulative frequency of sEPSC amplitude were observed following AMPAR Aabs 10min incubation when compared to IgG incubated cells (p<0.0001). Data were collected over three separate neuronal cultures and presented as mean ± SD.

6.2.2 Acute 30 min AMPAR Aab incubation

To assess if a significant reduction in sEPSC frequency could still be observed following a longer, but still 'acute', AMPAR Aab incubation, both AMPAR Aabs and rIgG (1:1000 dilution) were bath applied for 30 min, and amplitude and frequency of sEPSCs were montiored throughout. At the end of the experiment, the AMPAR antagonist NBQX was added to the bath to confirm that all observed events were AMPAR-mediated.

30 min acute bath application of AMPAR Aabs resulted in a significant reduction in sEPSC frequency. Cells incubated with AMPAR Aabs had a significantly lower sEPSC frequency (0.7 ± 0.4 Hz) compared to those cells incubated with rIgG (1.3 ± 0.8 Hz, n=15 per group, p = 0.0318; unpaired t-test, Figure 6.3D). When this effect was further divided into 10 min bins, a significant reduction was observed for all time bins: 0-10 min (n=21-22 per group, p = 0.0192, unpaired t-test; Figure 6.3A), 10-20 min (n= 14-15 per group, p = 0.0294, unpaired t-test; Figure 6.3B) and 20-30 min (n=14-15 per group, p = 0.0387, unpaired t-test; Figure 6.3C). Significant differences in cumulative inter-event interval distributions were also observed following AMPAR Aabs 30min incubation when compared to IgG incubated cells ($p<0.0001$; Kolmogorov-Smirnov test; Figure 6.3E).

No significant effect was identified on sEPSC amplitude following application of AMPAR Aabs at 0-30 min (n=15 per group, p = 0.889, unpaired t-test; Figure 6.4A) or at any 10 min bin (Figure 6.4B-D).

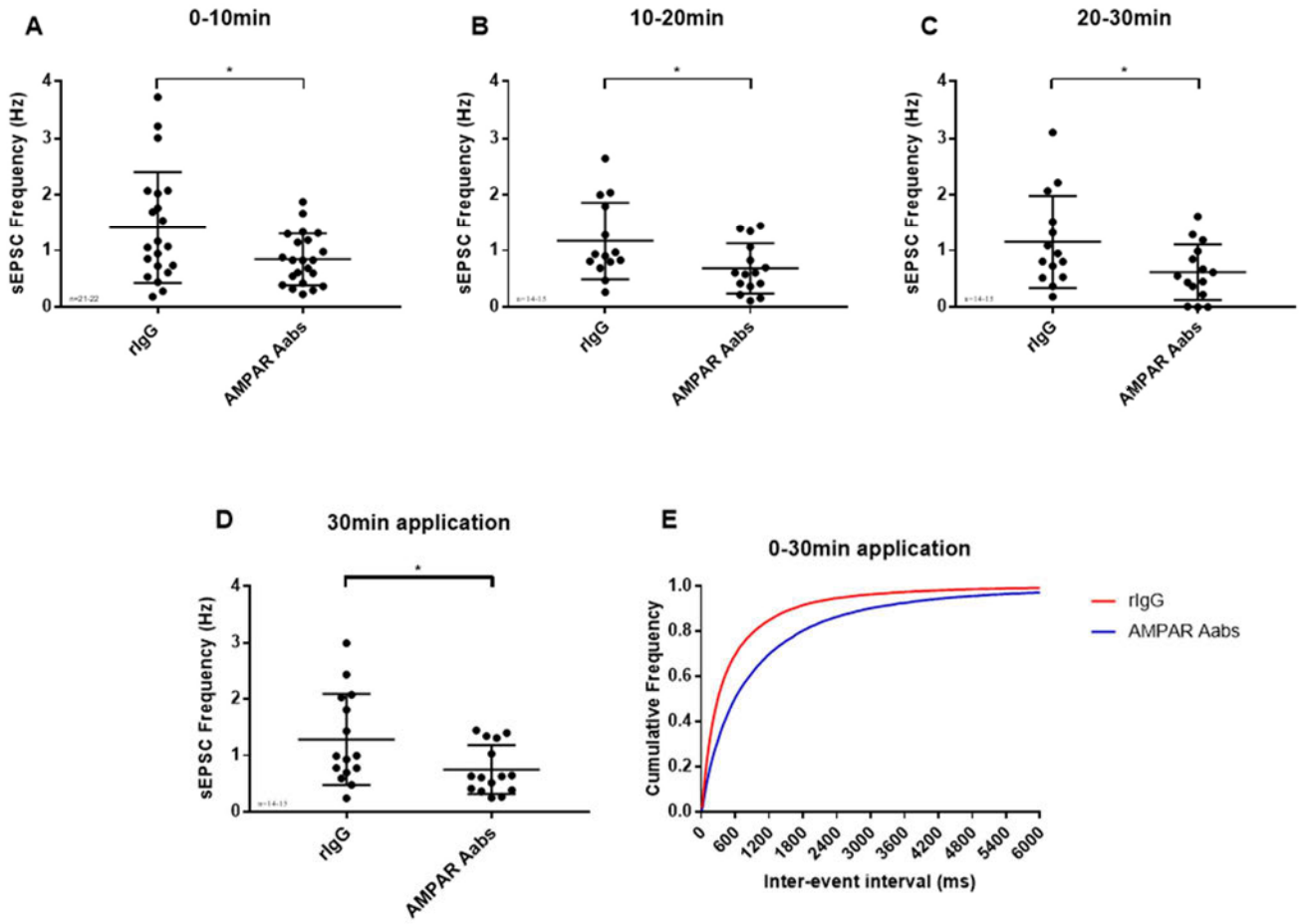

Figure 6.3: Effects of acute (30 min) AMPAR Aabs and rIgG application on sEPSC frequency. Following addition of AMPAR Aabs (1:1000 dilution), significant reductions were seen at each 10 min increment (**A**; 0-10 min; p = 0.0192. **B**; 10-20 min; p = 0.0294 and **C**; 20-30 min; p = 0.0387, n = 14-22 cells per group). Overall, a significant reduction in sEPSC frequency at 0-30 min was also detected (**D**; p = 0.0318, n = 14-15 cells per group). Significant differences in cumulative inter-event interval were also observed following AMPAR Aabs 30min incubation when compared to IgG incubated cells (**E**; p<0.0001) Data were collected over three separate neuronal cultures and presented as mean ± SD, *: p <0.05.

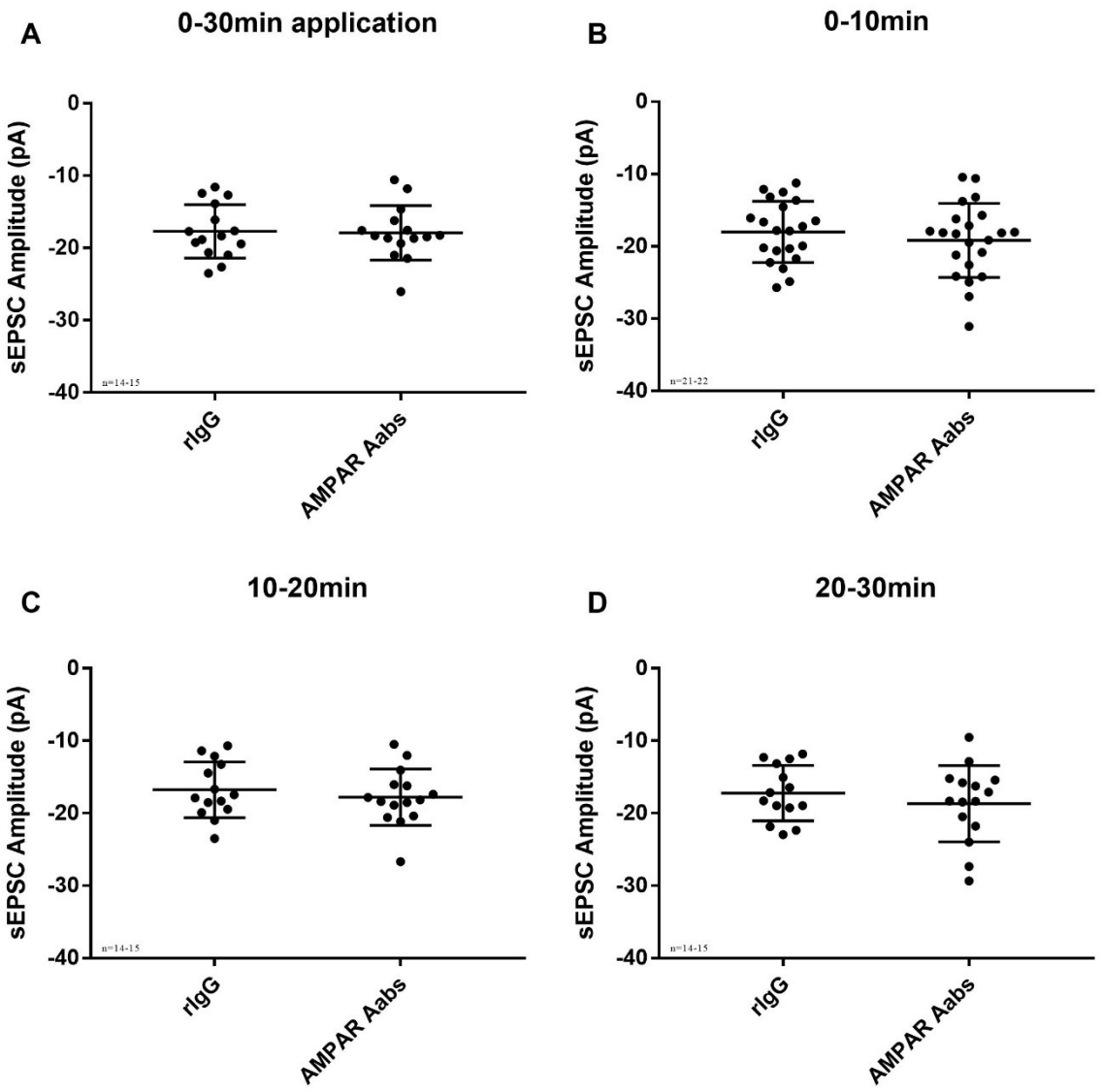

Figure 6.4: Effects of acute (30 min) AMPAR Aabs and rIgG application on sEPSC amplitude. No significant reduction in sEPSC amplitude was observed at 0-30 min, or 10 min intervals. Data were collected from 14-22 cells over three separate neuronal cultures and presented as mean ± SD.

Following acute application of either AMPAR Aabs or rIgG, frequency and amplitude of sEPSCs were compared to pre-incubation baselines. Acute, 30 min application of AMPAR Aabs resulted in a numerical but non-significant reduction in sEPSC frequency at 0-10 min bins (0.8 ± 0.4 Hz) compared to pre-incubation baseline (1.1 ± 0.5 Hz, n=22 per group, p = 0.0814, paired t-test; Figure 6.5A). At 10-20 min, cells incubated with AMPAR Aabs had a significantly lower sEPSC frequency (0.7 ± 0.4 Hz), compared to pre-incubation baseline (1.1 ± 0.6 Hz, n=15 per group, p = 0.0041, paired t-test; Figure 6.5B). Similarly, at 20-30 min, cells incubated with AMPAR Aabs had a significantly lower sEPSC frequency (0.7 ± 0.4 Hz), compared to pre-incubation baseline (1.1 ± 0.6 Hz, n=13 per group, p = 0.0072, paired t-test; Figure 6.5C). Cells incubated with rIgG showed no significant changes in sEPSC frequency at 0-10 min, 10-20 min or 20-30 min when compared to their pre-incubation baselines (n=16-17 per group, p = 0.891, p = 0.375 and p = 0.397 respectively, paired t-tests; Figure 6.5D-F).

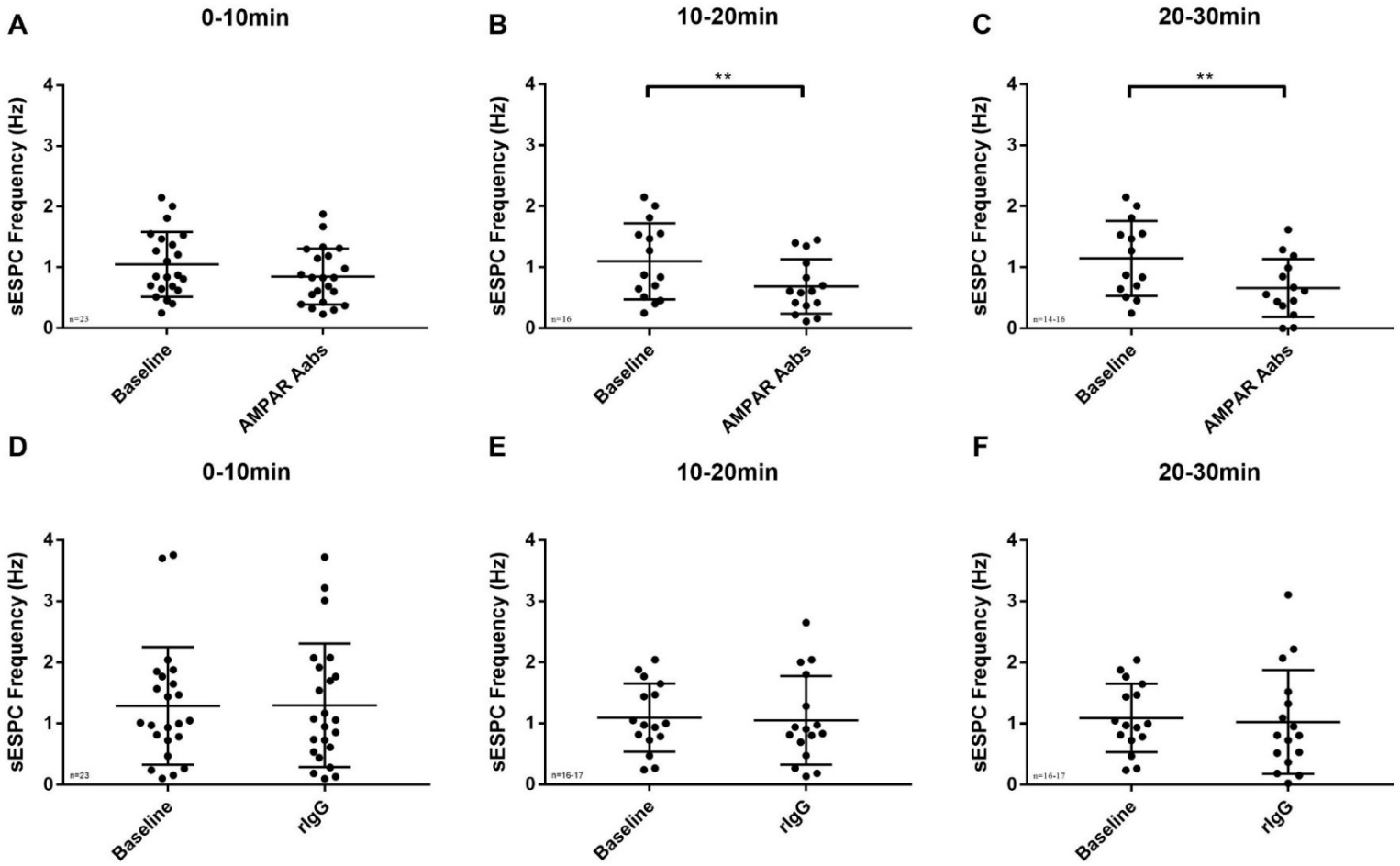

Figure 6.5: sEPSC frequency of AMPAR Aabs and rIgG incubated cells compared to their respective baselines. (A-C) AMPAR Aabs incubation (1:1000 dilution) resulted in a significant reduction in sEPSC frequency when compared to their own baseline at 10-20 and 20-30 min ($p = 0.0041$ and $p = 0.0072$ respectively, n = 14-24 cells per group). **(D-F)** Application of rIgG (1:1000 dilution) did not significantly alter sEPSC frequency when compared to own baseline ($p = 0.891$, $p = 0.375$ and $p = 0.397$ respectively, n = 16-23 cells per group). Data were collected over three separate neuronal cultures, presented as mean ± SD, *: $p < 0.05$, **: $p < 0.01$.

6.2.3 Effects of chronic (24 h) AMPAR Aab incubation

Exposure of native AMPARs to AMPAR Aabs in patients is typically chronic in nature due to their presence in CSF via intrathecal production (Levite, 2014). Therefore, a more chronic incubation was tested to determine whether this significant reduction in sEPSC frequency observed from acute application were maintained, or alternatively if any differing significant effects could be observed. Both AMPAR Aabs and rIgG (1:1000 dilution) were applied to hippocampal neurons in culture 24 h prior to recording. Cells were placed in external solution containing $GABA_AR$ and NMDAR antagonists (BMI (10µM) and APV (50µM) respectively) as well as the respective antibody and allowed to equilibrate. Once the whole-cell configuration had been achieved, 30 min of sEPSCs were recorded where both frequency and amplitude were measured. At the end of the experiment, the AMPAR antagonist NBQX was added to the bath to confirm that all observed events were mediated by AMPARs.

AMPAR Aab-incubated cells showed a significant reduction in sEPSC frequency (0.4 ± 0.3 Hz) compared to rIgG incubated cells (1.2 ± 0.9 Hz, n=11-13 per group, $p = 0.0113$, unpaired t-test; Figure 6.6A). Significant differences in cumulative inter-event interval distributions were also observed following 24 h incubation of AMPAR Aabs when compared to IgG incubated cells ($p<0.0001$; Kolmogorov-Smirnov test; Figure 6.6B). No difference in sEPSC amplitude was observed; cells incubated with AMPAR Aabs showed sEPSCs of similar amplitude (-27.1 ± 8.1 pA) to those cells incubated with rIgG (-21.8 ± 8.9 pA, n=12 per group, $p = 0.142$, unpaired t-test; Figure 6.6C).

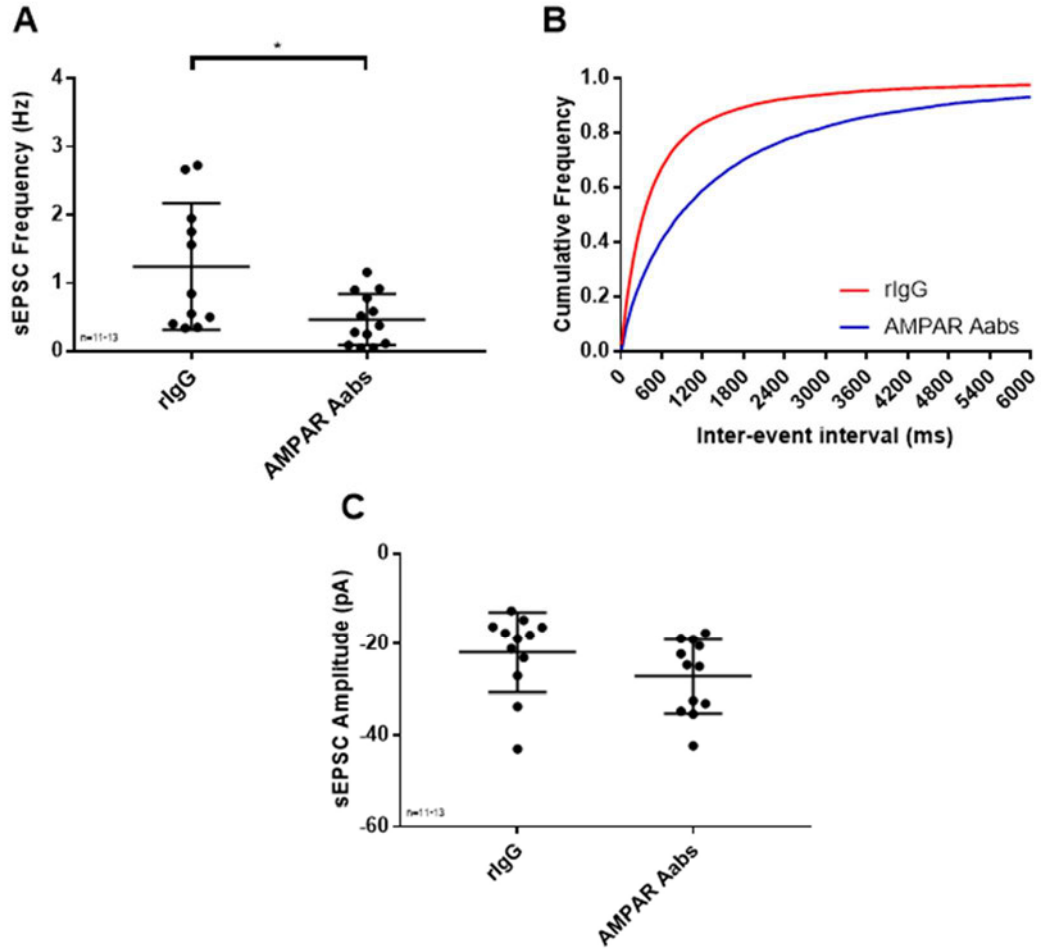

Figure 6.6: Effects of chronic (24 h) AMPAR Aabs and rIgG (1:1000 dilution) application on sEPSC frequency and amplitude. (A) Following addition of AMPAR Aabs, a significant reduction in sEPSC frequency was observed ($p = 0.0113$, $n = 11$-13 cells per group), **(B)** Significant differences in cumulative inter-event interval were also observed following 24 h incubation ($p<0.0001$). **(C)** No significant effect on amplitude was observed. Data were collected over three separate neuronal cultures and presented as mean ± SD, *: $p < 0.05$.

Significant effects on sEPSC frequency observed with acute and chronic exposure to Aabs were suggestive of either a presynaptic mechanism of action, or a reduction in the number of postsynaptic AMPARs.

To further test for potential presynaptic effects, acute (30 min) and chronic incubation experiments were repeated in the presence of TTX, to measure mEPSCs, whereby action potential-independent events, consistent with effects on presynaptic release of glutamate, could be measured.

6.3 Miniature excitatory postsynaptic currents (mEPSCs)

Whole-cell patch-clamp was used to measure mEPSCs via the bath application of TTX (1µM), while also isolating AMPAR currents via the bath application of BMI (10 µM) and DL-APV (50µM). Cells were incubated with AMPAR Aabs both acutely (30 min) and chronically (24 h), and parameters such as amplitude and frequency analysed, to help indicate any potential presynaptic functional effects of Aabs.

6.3.1 Effect of AMPAR Aabs application on mEPSCs

Following a 30 min application of either AMPARs Aabs or rIgG, frequency of mEPSCs were compared to their pre-incubation baselines (representative traces of mEPSC are illustrated in Figure 6.7C). Acute, 30 min application of AMPAR Aabs resulted in a significant reduction in frequency (0.4 ± 0.2 Hz) when compared to its pre-incubation baseline (0.5 ± 0.4 Hz, n=12 per group, $p = 0.0419$; paired t-test; Figure 6.7A). Cells incubated with rIgG showed no significant changes in mEPSC frequency (1.1 ± 1.0 Hz), compared to that of its pre-incubation baseline (130 ± 1.2 Hz, n=12-14 per group, $p = 0.205$, paired t-test; Figure 6.7B).

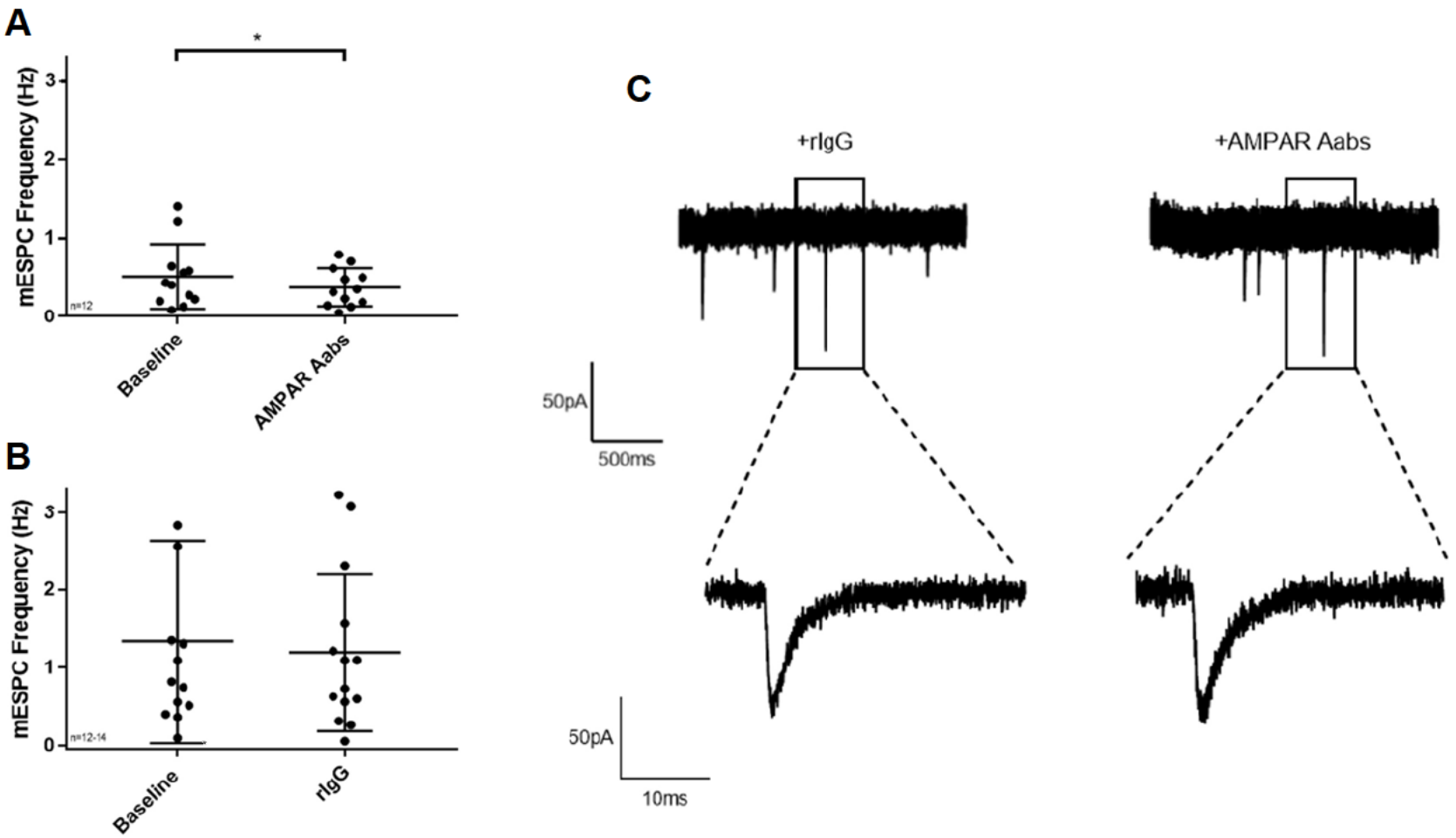

Figure 6.7: mEPSC frequency following 30 min AMPAR Aabs and rIgG incubation (1:1000 dilution) compared to their respective baselines. (A) AMPAR Aab incubation resulted in a significant reduction in mEPSC frequency when compared to their own baseline ($p = 0.0419$, $n = 12$ cells per group). **(B)** Application of rIgG did not significantly alter mEPSC frequency when compared to own baseline ($p = 0.205$, $n = 12$-14 per group). **(C)** Representative mEPSC traces of both rIgG and AMPAR treated cells. Data were collected over three separate neuronal cultures, presented as mean ± SD, *: $p < 0.05$.

Acute bath application (30 min) of AMPAR Aabs also resulted in a significant reduction in mEPSC frequency when compared to cells incubated with rIgG. Cells incubated with AMPAR Aabs had significantly less frequent mEPSCs (0.4 ± 0.2 Hz) when compared to those incubated with rIgG (1.1 ± 1.0 Hz, n=12-14 per group, p = 0.0109, unpaired t-test; Figure 6.8A). This effect was also seen following 24 h incubation, with those incubated with AMPAR Aabs generating less frequent mEPSCs (0.4 ± 0.2 Hz) when compared to rIgG following 24 h incubation (0.9 ± 0.6 Hz, n=8 per group, p = 0.0377, unpaired t-test; Figure 6.8B). As with sEPSC experiments, significant differences in cumulative inter-event intervals were also observed following both 30 min and 24 h incubation of AMPAR Aabs when compared to IgG incubated cells ($p<0.0001$; Kolmogorov-Smirnov test; Figure 6.8C-D).

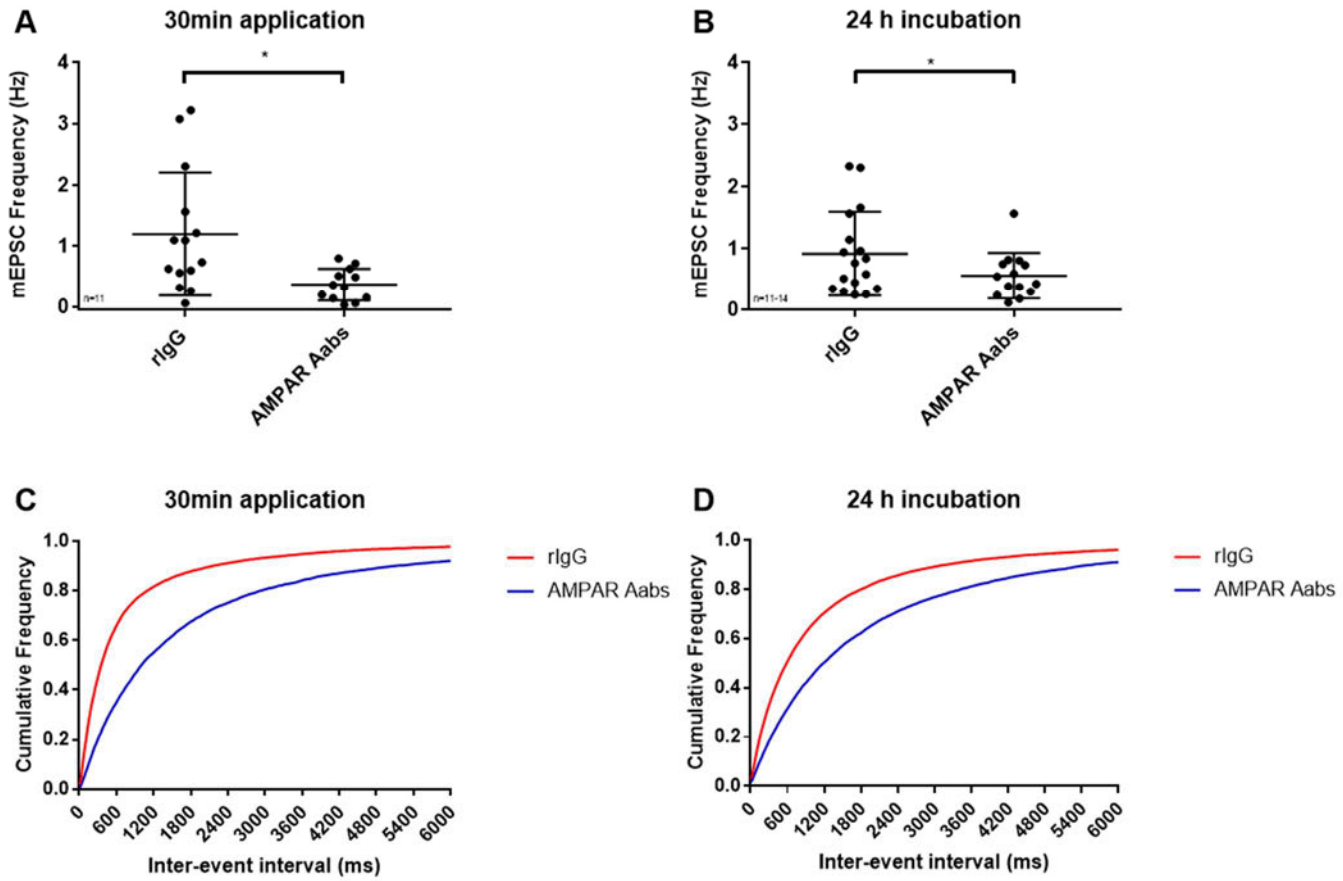

Figure 6.8: Effects of acute (30 min) and chronic (24 h) AMPAR Aabs and rIgG application on mEPSC frequency. Following addition of AMPAR Aabs, a significant reduction was seen in mEPSC frequency at 0-30 min (**A**; $p = 0.01$, $n = 11$ cells per group), as well as following 24 h incubation (**B**; $p = 0.0377$, $n = 11$-14 cells per group). Significant differences in cumulative frequency inter-event interval were observed following both 30 min application **(C)** and 24 h incubation **(D)** of AMPAR Aabs when compared to control IgG incubated cells. Data were collected over three separate neuronal cultures and presented as mean ± SD, *: $p < 0.05$.

Overall, these data demonstrate a significant reduction in sEPSC frequency following both acute and chronic AMPAR Aab exposure. This effect was reproduced when experiments were repeated in the presence of TTX, generating mEPSC, where a significant reduction in mEPSC frequency was observed following both acute and chronic Aab incubation. No changes in amplitude were seen following acute AMPAR Aab application (Figure 6.9A; unpaired t-test, $p = 0.27$, $n = 12\text{-}14$ per group) or chronic AMPAR Aab incubation (Figure 6.9B; unpaired t-test, $p = 0.87$, $n = 14\text{-}17$ per group).

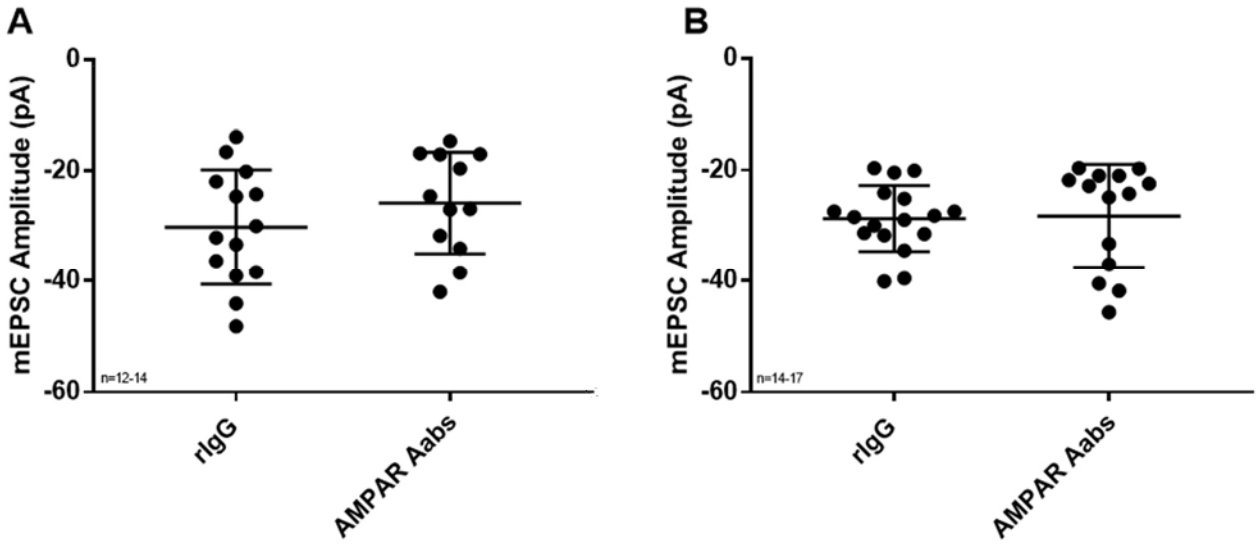

Figure 6.9: Effects of acute (30 min) and chronic (24 h) AMPAR Aabs and rIgG application on mEPSC amplitude. (A) Following addition of AMPAR Aabs, no significant changes were seen in mEPSC amplitude at 0-30 min ($p = 0.27$, $n = 12\text{-}14$ cells per group). **(B)** No effect was also seen following 24 h incubation ($p = 0.87$, $n = 14\text{-}17$ cells per group). Data were collected over three separate neuronal cultures and presented as mean ± SD, *: $p < 0.05$.

6.4 Discussion

While AMPAR Aabs have been extensively investigated using patient sera with regard to RE, there have been conflicting results regarding their mechanism of action with respect to seizure development (Rogers *et al.*, 1994; Ganor *et al.*, 2005; Ganor *et al.*, 2014). To further explore their possible mechanism of action, Aabs generated to specifically target the GluR3 subunit of AMPARs (see section 5.2), and which bind specifically to native AMPARs (section 5.3), were used in whole-cell patch-clamp experiments in which EPSCs were recorded from primary hippocampal neurons. The findings are summarised below:

- AMPAR Aabs significantly reduced sEPSC frequency following both acute (10 min and 30 min), and chronic (24 h) application.
- AMPAR Aabs significantly reduced mEPSC frequency following both acute (30 min) and chronic (24 h) application.
- Both AMPAR Aabs and rIgG had no effect on sEPSC or mEPSC amplitude.

6.4.1 AMPAR Aabs exhibit an inhibitory functional effect

The results of both sEPSC and mEPSC acute experiments demonstrate that hippocampal neurons incubated with AMPAR Aabs have a significant reduction in EPSC frequency. As sEPSCs are comprised of both AP-dependent and AP-independent events, TTX was added and experiments repeated to isolate AP-independent mEPSCs; here, any reductions in frequency are typically related more directly to a presynaptic effect (Zucker and Regehr, 2002). Acute application of AMPAR Aabs caused a reduction in mEPSC frequency, consistent with a reduction in presynaptic glutamate release, an alteration in the density of synaptic vesicles, (Zucker and Regehr, 2002) or an increase in postsynaptic internalisation of AMPARs (Gardoni et al., 2021). Further experiments utilising MEAs on hippocampal brain slices as detailed in

Chapter 4 could help elucidate the mechanism of AMPAR Aabs further. Applying a paired pulse stimulation to the Schaffer collateral pathway in hippocampal brain slices in the presence of AMPAR Aabs would help determine further whether these Aabs are affecting neurotransmitter release presynaptically. Under normal conditions in the CA1 region of hippocampus, healthy cells exhibit paired pulse facilitation, which are thought to occur due to an accumulation of calcium in the presynaptic terminal, residual from the first pulse at the time of the second pulse. In addition, paired pulse facilitation is often observed at synapses with a low initial probability of release, where a low fraction of vesicles are released following the first action potential, meaning many vesicles are still readily available at the time of the second pulse (Jackman and Regehr, 2017). Therefore, to test further the presynaptic effects of AMPAR Aabs, hippocampal brain slices could be incubated, and paired pulse ratio (PPR) measured. If these Aabs are having a presynaptic effect, we would expect to see a reduction in the amplitude of the first pulse, due to reducing the probability of the presynaptic vesicular release, paired with an increase in the amplitude of the second pulse, due to an increase in the amount of residual calcium and the number of vesicles ready to be released.

An alternative possibility is this could be due to a reduction in the number of functional presynaptic neurons following AMPAR Aabs application; in this regard, it has been reported that patient Aabs directed against GluR3 subunit of AMPARs cause neuronal death via activation of apoptosis (Levite *et al.*, 1999). By contrast, mEPSC amplitude was completely unaffected by the addition of AMPAR Aabs, suggesting minimal effect on the expression, distribution, or responsiveness of postsynaptic AMPARs on hippocampal neurons. However, it is also possible that GluR3 expressed presynaptically may be affected; the presynaptic expression of GluR3 subunits in the hippocampus is now well documented, as is their potential contribution to pathophysiology (Zanetti *et al.*, 2021).

Previous studies have tested both recombinant AMPAR Aabs or those from patients CSF and identified an agonistic-like effect following acute Aab application. This effect was identified by recording whole-cell membrane currents from rat neocortical slices, whereby a large inward current was produced following local Aab application (via puffer pipette) (Levite *et al.*, 1999). This differs from our results, where no changes in amplitude of sEPSCs or mEPSCs were observed following either acute or chronic AMPAR Aab application. The reported agonistic effect also resulted in increased neuronal death in those cells treated with AMPAR Aabs, which was proposed to occur via complement-independent excitotoxicity, mediated via activation of the AMPAR. Preliminary studies have been performed to investigate whether AMPAR Aab incubation of primary neuronal cells resulted in increased neuronal death. Following incubation of primary hippocampal neurons with AMPAR Aabs or control IgG, cells were labelled to detect cleaved caspase 3: a key mediator of neuronal cell death (Lavrik *et al.*, 2005). No obvious differences between those cells incubated with AMPAR Aabs and those with control IgG was seen (data shown in Appendix 9.6). However, as these were preliminary studies, no quantification has yet been carried out and hence, further studies are required to confirm this result.

More recent studies investigating the functional effects of GluR3 Aabs in FTD identified a decrease in GluR3 subunit synaptic localisation and a loss of dendritic spines following acute application of GluR3 Aabs (Borroni *et al.*, 2017). An increase in endocytosis of GluR3-containing AMPARs was accompanied by an increase in protein interacting with C kinase-1 / glutamate receptor-interacting protein-1 (PICK1/GRIP1) ratio (proteins necessary for AMPAR internalisation and insertion respectively) (Palese *et al.*, 2020; Gardoni *et al.*, 2021), effects similar to those seen with NR1-Aabs (Hughes *et al.*, 2010). Moreover, a decrease in AMPAR-evoked glutamate exocytosis was observed from synaptosomes following acute GluR3 Aabs application (Palese *et al.*, 2020). These more recent studies (Borroni *et al.*, 2017; Palese *et al.*,

2020) are more in keeping with our results, where an inhibitory effect was identified following both acute and chronic application of AMPAR Aabs, however whether this is occurring via an overall reduction in the number of synaptic AMPARs (for example, via endocytosis/internalisation), or via a presynaptic mechanism of action resulting in reduced glutamate release is unknown. Experiments that have implicated internalization typical involve 'chronic' (~24 h) incubation, whether such processes could occur over the shorter timeframes investigated here is unclear. One study using anti-GluA2 Aabs has reported similar effects to those reported here on mEPSC frequency, but not amplitude, in hippocampal neurons when Aabs were incubated for 24 h and also ~1 h; however, such effects were absent for Aabs incubations of ~30 min (Haselmann *et al.*, 2018). This study further showed that Aab effects were due to receptor internalisation. Overall, internalisation is more likely to contribute to the effects seen at 24 h here but cannot be fully ruled out for 'acute' applications. There has been some investigation regarding presynaptic ionotropic glutamate receptor controlling glutamate release (Lee *et al.*, 2002; Negrete-Diaz *et al.*, 2018), however, at present this evidence is sparse and requires further investigation into this before any conclusion can be made.

6.4.2 Conclusions

Data presented here provides evidence to support that AMPAR Aabs are exerting an inhibitory functional effect on neuronal AMPARs. However, further investigation is required to identify whether this effect is due to a reduction in the number of available AMPARs on the postsynaptic membrane (due to Aab-induced internalisation of AMPARs), or due to an inhibition of presynaptic glutamate release, an effect which is consistent with previous studies which have used patient derived GluR3 Aabs on mouse synaptosomes (Palese *et al.*, 2020). Preliminary studies assessing levels of cell death following AMPAR Aab incubation did not result in any obvious differences between AMPAR Aab- and IgG-incubated cell (either 30 min

or 24 h; Appendix 9.6), contrasting previous results whereby GluR3 Aab application to primary neurons resulted in increased neuronal death (Levite *et al.*, 1999; Ganor *et al.*, 2005). Further studies are required to confirm the preliminary findings detailed in Appendix 9.6 to further clarify the downstream mechanisms of these AMPAR Aabs, as well as confirming how the effects detailed in this chapter are implicated in a hyper-excitable network, such as in epilepsy patients.

7. General discussion and final conclusions

Aabs directed against subunits of NMDARs and AMPARs have been increasingly identified in patients with encephalitis, epilepsy, schizophrenia and dementia, with their mechanisms of action still not fully understood. Therefore, we aimed to generate both anti-AMPAR and anti-NMDAR Aabs to explore any functional effects that these Aabs may be having on their respective targets using several *in vitro* models. This study has demonstrated the successful generation of both anti-NR1 (NMDAR) and anti-GluR3 (AMPAR) Aabs following peptide immunisation. Characterisation of these Aabs was performed to determine cell-type specificity, followed by use in a range of functional *in vitro* models. Results demonstrated that anti-NMDARs Aabs, generated from immunisation with peptides known to be of immunogenic importance and specific for native NMDARs, significantly inhibited NMDAR-dependent LTP. AMPARs Aabs, generated by peptide immunisation were shown to be highly specific for native AMPARs and elicited a significant functional inhibitory effect on primary hippocampal neurons. How these findings may link to seizures and autoimmune epilepsy, as well as the implications of this are discussed below.

7.1. Can inhibitory functional effects of Aabs lead to seizures?

To date, it has been generally accepted that NMDAR Aabs are pathogenic in nature, and contribute to seizures, along with memory and cognitive impairment (Hughes *et al.*, 2010; Wright *et al.*, 2015; Planagumà *et al.*, 2015). These Aabs are thought to act generally via inhibitory mechanisms, which may appear counter-intuitive as seizures are often associated with hyper-excitability, with many studies both past and present exploring the use of NMDAR antagonists as novel AEDs, in an attempt to reduce network excitation (Barker-Haliski and White, 2015). Inhibition of NMDARs, as observed in MEA experiments with NMDAR1pp Aabs, may contribute to seizure generation via internalisation of NMDARs on GABAergic

neurons, resulting in a reduction in network inhibition and subsequently an excitatory/inhibitory imbalance, leading to hyper-excitation (as illustrated in Figure 7.1). This is consistent with previous findings, where application of NMDAR Aabs on primary hippocampal neurons were shown to result in cross-linking and internalisation of synaptic NMDARs (Hughes *et al.*, 2010; Moscato *et al.*, 2014). This is supported further by one study identifying disruptions in synaptic protein-protein interactions. Under normal conditions, NMDARs are anchored and stabilised at the synapse via protein-protein interactions with EPHB2Rs (Washburn *et al.*, 2020). However, previous studies have shown that upon application of NMDAR Aabs to primary neurons this interaction is disrupted, leaving NMDARs less stable at the synapse, and therefore promoting their internalisation (Mikasova *et al.*, 2012; Planaguma *et al.*, 2016). These alterations in synaptic expression of NMDARs were also shown via a reduction in synaptic plasticity following NMDAR Aab application (Zhang *et al.*, 2012; Würdemann *et al.*, 2016; Blome *et al.*, 2018; Kersten *et al.*, 2019). These findings have been confirmed in a study using post-mortem hippocampus from human patients with ANRE, who expressed significantly less synaptic NMDARs than age-matched controls (Hughes *et al.*, 2010).

Taken together, it can be hypothesised that NMDAR Aabs may result in seizures by decreasing the number of NMDARs via internalisation on both excitatory and inhibitory neurons and hence disrupting the excitatory/inhibitory balance. Under normal conditions, an excitatory signal arrives at the presynaptic neuron, causing glutamate release onto post-synaptic neurons (containing both NMDARs and AMPARs), which propagates throughout the network, as well as binding to NMDARs on inhibitory neurons, which provide negative feedback onto the presynaptic neuron via $GABA_A$Rs (Figure 7.1A). However, when NMDAR Aabs are present, binding and internalisation of NMDARs occurs, feedback inhibition from the inhibitory neuron is lost, thus resulting in an increased excitatory output, disrupting the balance and causing a

hyper-excitable network (Wright and Vincent, 2016) may result in compensatory changes in intrinsic excitability (Fitzgerald, 2012) (as shown in Figure 7.1B). These effects are also consistent with one recent study, whereby NMDAR Aabs increase the excitability of CA3 pyramidal neurons, making them more susceptible to seizures (Wright *et al.*, 2021).

The hypothesis that NMDAR Aabs act by disrupting the excitatory/inhibitory balance is consistent with a mouse model of schizophrenia, where mice express approximately 15% of the normal levels of the NR1 subunit of NMDARs (Gandal *et al.*, 2012). This reduced NMDAR expression led to a compensatory increase in $GABA_A$Rs *in vivo* and increased intrinsic excitability, resulting in a disrupted excitatory/inhibitory network. Mice with reduced NMDARs also demonstrate increased sensitivity to kainic acid and hence suffered more lethal seizures than wild type mice, suggesting a compensatory increased intrinsic excitability or increased sensitivity of AMPARs (Duncan *et al.*, 2010). Similarly, a reduction in NMDAR activity via the addition of a competitive NMDAR antagonist, D-CPP-ene, worsened seizures in 3 out of 8 patients with epilepsy (Sveinbjornsdottir *et al.*, 1993), suggesting that acute reduction of NMDAR function may lead to an imbalance of excitation and inhibition. Furthermore, infusion of Aabs purified from patients with NMDAR encephalitis significantly increased extracellular glutamate levels in rat hippocampus (Manto *et al.*, 2010), suggesting NMDAR Aabs induce a hyper-glutamatergic state, in line with the hypothesis described above. Finally, one recent study has shown that treatment with the neurosteroid pregnenolone sulphate upregulates NMDARs and reduced NMDAR-Aab induced seizure activity (Wright *et al.*, 2021).

Preliminary whole-cell patch-clamp experiments were also performed to investigate effects of NMDAR Aab on sEPSCs in primary neurons. Interestingly, no clear changes in sEPSC amplitude or frequency were seen following NMDAR Aab application. These data are in

contrast to recent previous findings who report a reduction in sEPSC amplitude and frequency in hippocampal neurons in *ex vivo* brain slices (Wright *et al.*, 2021), which may be due to conditions of the primary cultures vs brain slice used. Further optimisation of these cultures by altering density of neurons plated, as well as the level of glia within the culture could lead to cultures with denser inter-network connections and increased NMDAR-dependent activity, both in the presence and absence of TTX.

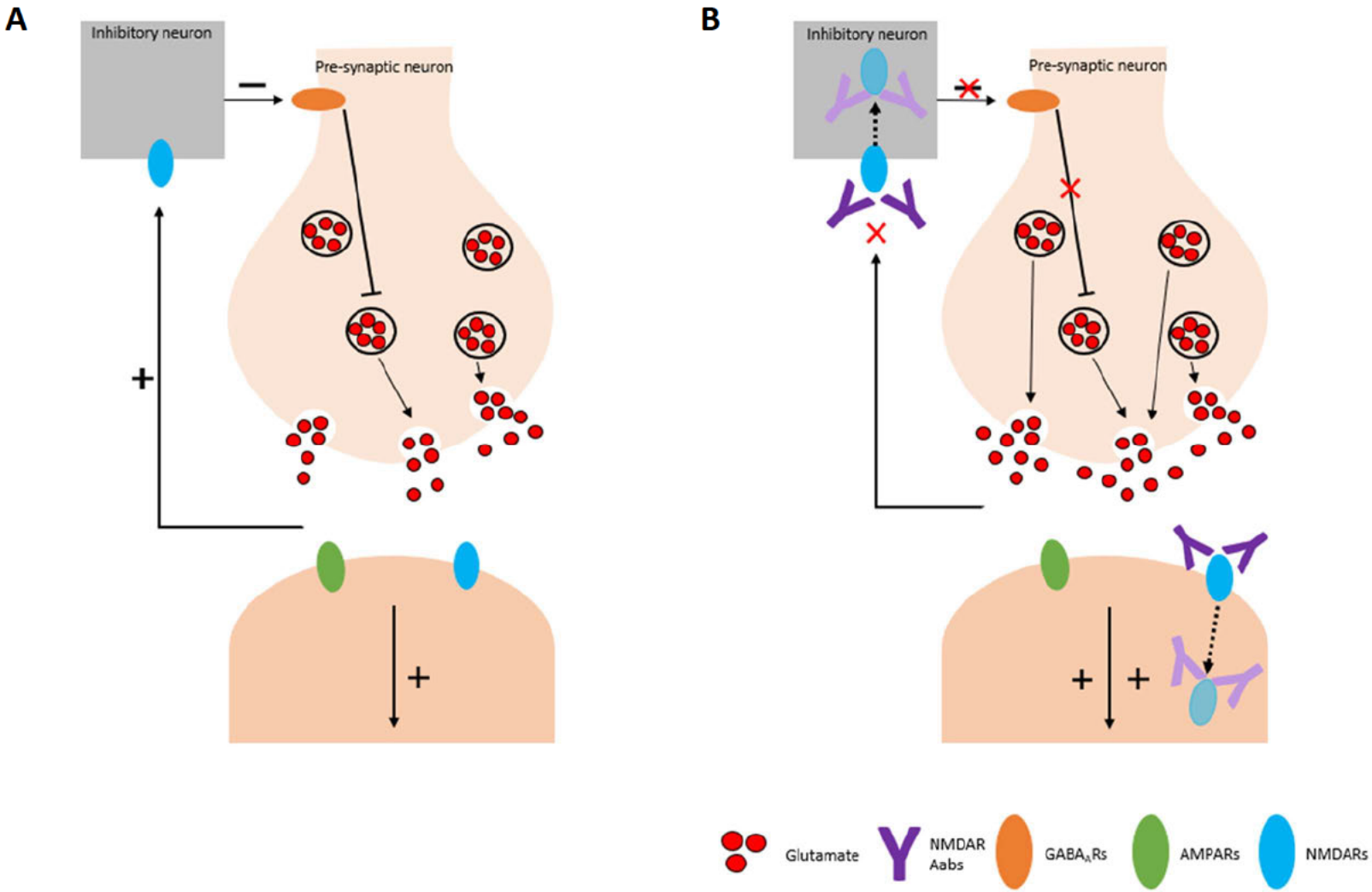

Figure 7.1: Schematic of how NMDAR Aabs may cause seizures. (A) Following Na^+ influx and depolarisation of the presynaptic neuron, glutamate is released, binding to both AMPARs and NMDARs on the postsynaptic membrane and propagating the signal throughout the network. Inhibitory neurons are also stimulated via glutamate binding to NMDARs, which feedback onto the presynaptic neuron via $GABA_AR$s, inhibiting further glutamate release. **(B)** In the presence of NMDAR Aabs, internalisation of NMDARs occurs on both the postsynaptic membrane as well as the inhibitory neuron, resulting in a loss of inhibition and hence increased presynaptic glutamate release, and subsequent increased excitatory output propagated throughout the network.

Less is understood regarding the mechanisms by which AMPAR Aabs are thought to act with regard to neuronal excitability and seizures/epilepsy. There is much conflicting evidence as to whether these Aabs are pathogenic and a cause of seizures (Levite *et al.*, 1999; Ganor *et al.*, 2014), or whether AMPAR Aabs may be protective against seizure generation (Ganor *et al.*, 2005). As detailed in Chapter 6, AMPAR Aabs elicited a reduction in sEPSC and mEPSC frequency but not amplitude, following both acute and chronic application in the presence and absence of TTX. Together, these data may be explained by AMPAR Aabs having a presynaptic inhibitory mechanism of action, which coincides with growing evidence in the literature of presynaptic GluR3 containing AMPAR expression (Lee *et al.*, 2002; Zanetti *et al.*, 2021). This proposed presynaptic mechanism of action of AMPAR Aabs is in line with recent *in vitro* studies, which have shown that acute treatment of GluR3 Aabs in synaptosomes obtained from mouse hippocampus resulted in a dose-dependent decrease in glutamate release (Palese *et al.*, 2020). However, an alternative explanation for the results described in Chapter 6 would be an Aab-induced internalisation of AMPARs on the postsynaptic membrane. Fewer receptors on the postsynaptic membrane would ultimately result in less availability for glutamate to bind and exert a response to, which would show experimentally as a reduction in EPSC frequency. Recent studies have demonstrated evidence to support this, where an increase in PICK1/GRIP1 ratio was observed following GluR3 Aab application (Palese *et al.*, 2020). These proteins are necessary for normal cycling of AMPARs, where PICK1 mediates the removal of GluR2/3 AMPARs from synapses, while GRIP1 stabilises the receptors in the postsynaptic density (Diering and Huganir, 2018; Gardoni *et al.*, 2021). Thus, an increase in the PICK1/GRIP1 ratio indicates an increase in endocytosis of GluR3-containing AMPARs (Palese *et al.*, 2020), an effect which has also been shown in rat hippocampal neurons (Borroni *et al.*, 2017) and prefrontal cortex neurons (Scheggia *et al.*, 2021). This has also been shown as a result of both GluR2 Aabs (Haselmann *et al.*, 2018) and NR1 targeting Aabs (Hughes *et al.*, 2010).

These more recent results suggesting an inhibitory effect of AMPAR Aabs (Palese *et al.*, 2020; Scheggia *et al.*, 2021) are generally in contrast with older studies. Thus, incubation of AMPAR Aabs resulted in a rapid inward current in GluR3-expressing oocytes (Malina *et al.*, 2006). Moreover, when AMPAR Aabs were co-applied with the AMPAR antagonist CNQX, a partial blockade in the current was observed. Together, these data suggested that AMPAR Aabs bind to GluR3-containing AMPARs and act as an agonist. It has been hypothesised that AMPAR Aabs binding to the GluR3B region causes the closure of the S1-S2 agonist binding domain, a conformational change which leads to channel activation (Armstrong *et al.*, 2003) . A similar AMPAR Aab 'agonist' effect was seen when GluR3 Aabs were added to rat neocortical brain slices and whole-cell membrane currents recorded, this effect was blocked by CNQX, but not by DL-APV, suggesting these Aabs act specifically on AMPARs (Levite *et al.*, 1999). More chronic (24 h) application of GluR3B Aabs in primary hippocampal neurons resulted in a significant increase in cell death (Levite *et al.*, 1999); incubation of cells with Annexin V and PI, revealed positive labelling with Annexin V only, confirming that cell death following Aab incubation was due to apoptosis rather than necrosis (Levite *et al.*, 1999). These findings support the hypothesis that GluR3B Aabs kill neurons via a non-classical complement-independent manner, namely, via activation of AMPARs, mimicking the effects of excess glutamate. This effect was not observed in our preliminary experiments of Aab-induced cell death (see Appendix 9.6); however, follow-up studies are required to fully quantify these results.

Overall, the data shown in this thesis are consistent with AMPAR Aab potential presynaptic effects and/or postsynaptic AMPAR internalisation, whereby a reduction in the overall number of receptors would lead to a decrease in the number of events recorded, a result which is in line with previous studies (Borroni *et al.*, 2017; Palese *et al.*, 2020; Scheggia *et al.*, 2021). These AMPAR Aab-induced changes may lead to a homeostatic decrease in the strength

of inhibitory response in the postsynaptic neuron, while also increasing the intrinsic excitability (as illustrated in Figure 7.2). This may result in a disruption to the excitatory/inhibitory network and promote seizure generation, an effect also previously shown for GluA1/2 Aabs (Peng *et al.*, 2015).

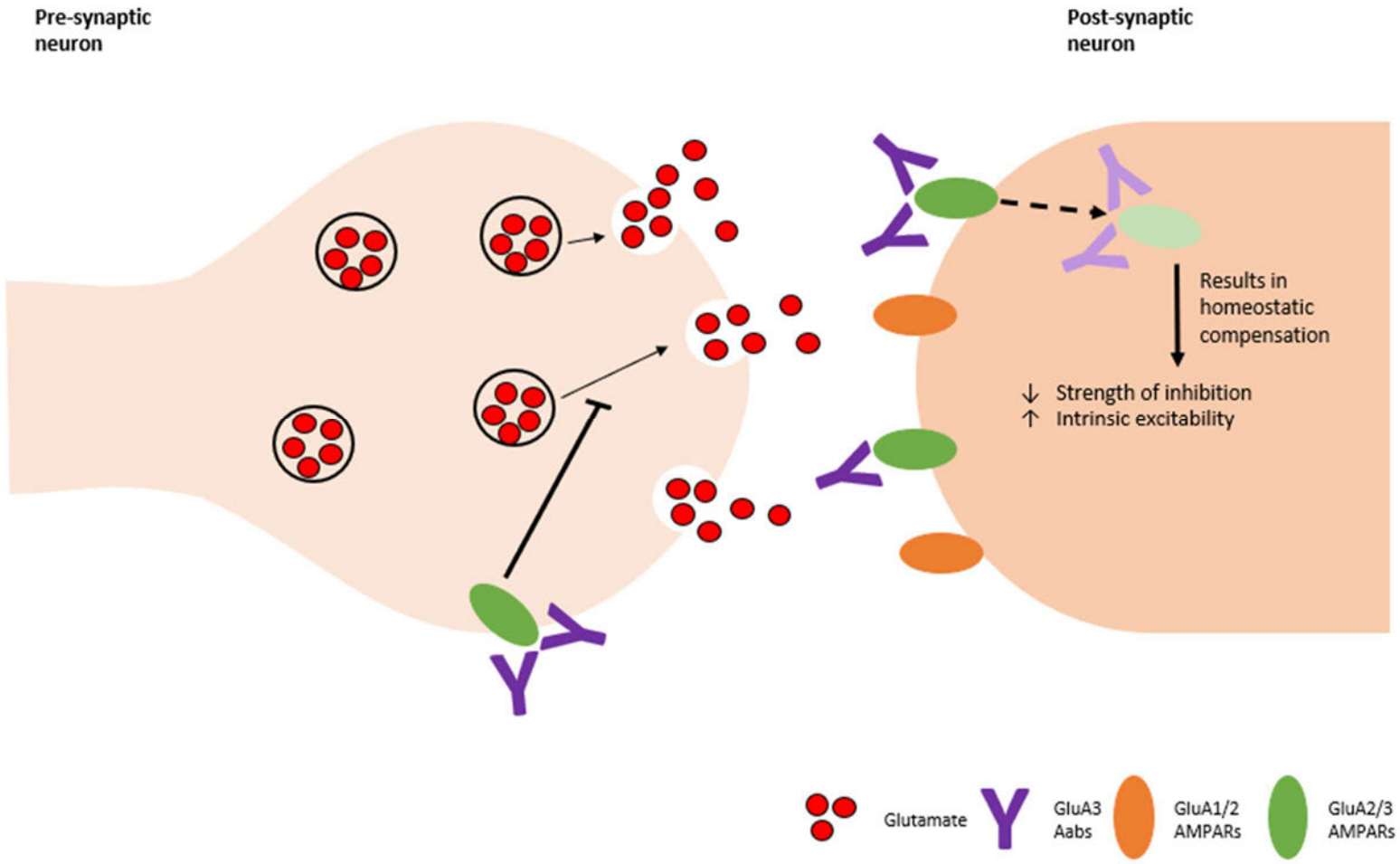

Figure 7.2 Schematic of potential mechanisms of AMPAR Aabs. AMPAR Aabs may exert their inhibitory effect on pre-synaptic glutamate release via presynaptic AMPARs. However, a more likely mechanisms is that AMPAR Aabs may cause antibody-induced internalisation of postsynaptic AMPARs resulting in homeostatic changes in post-synaptic responses to inhibitory signals, as well as a homeostatic increase in intrinsic excitability, resulting in an imbalance of the excitatory/inhibitory network.

7.2 NMDAR and AMPAR Aabs: causative or compensatory?

Pathogenic mechanisms of both NMDAR and AMPAR Aabs have been explored at length. However, less-well explored is the possibility of NMDAR and AMPAR Aabs being generated as a compensatory mechanism in response to seizures; for example, in an attempt to counteract the hyper-excitable network. This possibility at a synaptic level is supported by data presented in this thesis; other studies show Aabs may act overall within the network to dampen down hyper-excitability (Hughes *et al.*, 2010; Peng *et al.*, 2015; Palese *et al.*, 2020). Several *in vivo* studies assessing pathogenic effects of Aabs have shown conflicting results, especially regarding the epileptogenic effects (Rogers *et al.*, 1994; Planagumà *et al.*, 2015; Wright *et al.*, 2015), with one study describing AMPAR Aabs as having a seizure protective effect in female Lewis rats (Ganor *et al.*, 2005). A closer look at these Aabs in epileptiform states, such as 4-AP/Mg^{2+}-free models, and eventually *in vivo* models of epilepsy, would help to shed some light on the role of Aabs within an epileptic network and determine whether effects are causative in seizure or are generated as a result of compensation by the network.

7.3 Conclusions and future work

The original aims of this work were to generate, characterise and test the functional effects of both NMDAR and AMPAR Aabs in order to identify any potential pathogenic effects these may be having on neuronal networks. The data presented throughout this thesis have shown that NMDAR and AMPAR Aabs generated following peptide immunisation are specific for their respective targets and display significant functional effects on neuronal networks. Following peptide purification, NMDAR Aabs elicited a significant reduction in NMDAR-dependent LTP in acute hippocampal brain slices, while AMPAR Aabs demonstrated an

inhibitory effect on EPSC frequency on primary hippocampal neurons when measured via whole-cell patch-clamp. Future work can further address details on mechanisms, for example internalisation assays would help to determine whether NMDAR and AMPAR Aabs used in these experiments cause cross-linking and internalisation of their respective receptors, as has been previously suggested for NMDAR Aabs (Hughes *et al.*, 2010), AMPAR Aabs (Borroni *et al.*, 2017), and other Aabs such as GluA1/2 Aabs (Peng *et al.*, 2015). Furthermore, applying both NMDAR and AMPAR Aabs to an *in vitro* model of epileptiform activity, such as Mg^{2+}-free or 4-AP, or applying to organotypic hippocampal cultures (optimisation of which was performed and described in Appendix 9.2) would help to determine their roles on network activity and whether they are pro- or anti-epileptogenic.

The data presented in Chapter 6 are in keeping with a potential protective mechanism of neuronal Aabs at the level of the synapse, as shown by the inhibitory effect of AMPAR Aabs. This is supported by previous *in vivo* studies, where AMPAR Aabs have been shown to confer partial protection against PTZ-induced seizures (Ganor *et al.*, 2005). Despite this, it is generally accepted that neuronal Aabs are pathogenic in nature and contribute to seizure development (Wright *et al.*, 2015; Ganor *et al.*, 2014), despite mechanistically acting via an inhibitory mechanism of action, as seen with both NMDAR and AMPAR Aabs in this thesis, as well as in recent studies (Wright *et al.*, 2021). This is also the case with several other neuronal Aabs that have been identified in previous studies, including those targeting leucine-rich glioma inactivated-1 (LGI-1) (Binks *et al.*, 2018) and $GABA_B$Rs (Jain *et al.*, 2015). For example, LGI-1 Aabs have been shown to block the interaction of LGI-1 with its receptors ADAM22 and ADAM23 as well as induce internalisation of LG1-1 – ADAM22 complex, resulting in increased intrinsic excitability of neurons (Kornau *et al.*, 2020; Ramberger *et al.*, 2020). While clear pathogenic mechanisms of many neuronal Aabs have been identified, with many inducing internalisation of the target receptor (Hughes *et al.*, 2010; Borroni *et al.*, 2017), the exact

mechanism of actions and how these contribute to seizures is still relatively unclear. Having a deeper understanding of the mechanisms by which these Aabs exert their pathogenic effects at a synaptic level can aid in the development of more targeted treatments for seizure resolution. This has already been shown to be a viable avenue, where attenuated seizures were observed following the use of the IL-1 receptor antagonist anakinra in mice with NMDAR Aabs (Taraschenko *et al.*, 2021b), or reduced NMDAR Aab induced internalisation following incubation with EPHRB2 agonist (Planaguma *et al.*, 2016). Successful treatment of other Aab-mediated disorders such as myasthenia gravis have already been developed (Farmakidis *et al.*, 2018); thus, development of targeted therapies for seizures may be particularly useful when immunotherapies are not feasible, do not result in resolution of all symptoms or result in significant adverse effects (Dalmau *et al.*, 2011). In addition, it has been shown that epilepsy patients harbouring neuronal Aabs are typically resistant to the currently available AEDs, but respond well to treatments specifically targeting immunomodulation, such as corticosteroids, IVIg or plasma exchange (Toledano *et al.*, 2014), highlighting the need for quick diagnosis. Testing for some well-characterised Aabs has already been incorporated into epilepsy diagnosis, where incubation of patient's serum or CSF with HEK cells transfected with the antigen of interest is commonly performed (Ramanathan *et al.*, 2021). Hence, characterisation of these Aabs is vital to ensuring a quick diagnosis and subsequent treatment strategies.

To conclude, NMDAR and AMPAR Aabs generated in this thesis represent a useful tool for investigating the mechanism of action of these Aabs with regard to seizure generation. In addition, these can aid in the development of targeted therapies and novel AEDs.

8. References

Adamczyk, A., Mejias, R., Takamiya, K., Yocum, J., Krasnova, I. N., Calderon, J., Cadet, J. L., Huganir, R. L., Pletnikov, M. V. & Wang, T. (2012). GluA3-deficiency in mice is associated with increased social and aggressive behavior and elevated dopamine in striatum. *Behav Brain Res,* **229**(1), 265-72.

Alberts, B., Johnson, A., Lewis, J., Raff, M., Roberts, K. & Walter, P. (2014). Molecular Biology of the Cell. 6th ed. New York: Garland Science.

Alexopoulos, H., Akrivou, S., Mastroyanni, S., Antonopoulou, M., Dinopoulos, A., Giorgi, M., Konstantinou, K., Kouremenos, E., Lariou, M., Naoumis, D., Pavlidou, E., Pavlou, E., Voudris, K., Vlachoyiannopoulos, P. & Dalakas, M. C. (2018). Postherpes simplex encephalitis: a case series of viral-triggered autoimmunity, synaptic autoantibodies and response to therapy. *Ther Adv Neurol Disord,* **11**, 1756286418768778.

Amin, J. B., Salussolia, C. L., Chan, K., Regan, M. C., Dai, J., Zhou, H. X., Furukawa, H., Bowen, M. E. & Wollmuth, L. P. (2017). Divergent roles of a peripheral transmembrane segment in AMPA and NMDA receptors. *J Gen Physiol,* **149**(6), 661-680.

Anderson, C. M. & Swanson, R. A. (2000). Astrocyte glutamate transport: review of properties, regulation, and physiological functions. *Glia,* **32**(1), 1-14.

Armstrong, N., Jasti, J., Beich-Frandsen, M. & Gouaux, E. (2006). Measurement of conformational changes accompanying desensitization in an ionotropic glutamate receptor. *Cell,* **127**(1), 85-97.

Armstrong, N., Mayer, M. & Gouaux, E. (2003). Tuning activation of the AMPA-sensitive GluR2 ion channel by genetic adjustment of agonist-induced conformational changes. *Proc Natl Acad Sci U S A,* **100**(10), 5736-41.

Bapka, O. D., Reuber, M. & Irani, S. R. (2016). Antibody-associated epilepsies: Clinical features, evidence for immunotherapies and future research questions. *Seizure,* **41**, 26-41.

Barker-Haliski, M. & White, H. S. (2015). Glutamatergic Mechanisms Associated with Seizures and Epilepsy. *Cold Spring Harb Perspect Med,* **5**(8), a022863.

Bauer, J., Becker, A. J., Elyaman, W., Peltola, J., Rüegg, S., Titulaer, M. J., Varley, J. A. & Beghi, E. (2017). Innate and adaptive immunity in human epilepsies. *Epilepsia,* **58 Suppl 3**, 57-68.

Bauer, J., Bien, C. G. & Lassmann, H. (2002). Rasmussen's encephalitis: a role for autoimmune cytotoxic T lymphocytes. *Curr Opin Neurol,* **15**(2), 197-200.

Bazelot, M., Bocchio, M., Kasugai, Y., Fischer, D., Dodson, P. D., Ferraguti, F. & Capogna, M. (2015). Hippocampal Theta Input to the Amygdala Shapes Feedforward Inhibition to Gate Heterosynaptic Plasticity. *Neuron,* **87**(6), 1290-1303.

Bien, C. G. (2013). Value of autoantibodies for prediction of treatment response in patients with autoimmune epilepsy: review of the literature and suggestions for clinical management. *Epilepsia,* **54 Suppl 2**, 48-55.

Bien, C. G. & Holtkamp, M. (2017). "Autoimmune Epilepsy": Encephalitis With Autoantibodies for Epileptologists. *Epilepsy Curr,* **17**(3), 134-141.

Bien, C. G. & Schramm, J. (2009). Treatment of Rasmussen encephalitis half a century after its initial description: promising prospects and a dilemma. *Epilepsy Res,* **86**(2-3), 101-12.

Bien, C. G., Widman, G., Urbach, H., Sassen, R., Kuczaty, S., Wiestler, O. D., Schramm, J. & Elger, C. E. (2002). The natural history of Rasmussen's encephalitis. *Brain,* **125**(Pt 8), 1751-9.

Billiau, A. D., Wouters, C. H. & Lagae, L. G. (2005). Epilepsy and the immune system: is there a link? *Eur J Paediatr Neurol,* **9**(1), 29-42.

Binks, S. N. M., Klein, C. J., Waters, P., Pittock, S. J. & Irani, S. R. (2018). LGI1, CASPR2 and related antibodies: a molecular evolution of the phenotypes. *J Neurol Neurosurg Psychiatry,* **89**(5), 526-534.

Bliss, T. V. & Collingridge, G. L. (1993). A synaptic model of memory: long-term potentiation in the hippocampus. *Nature,* **361**(6407), 31-9.

Blome, R., Bach, W., Guli, X., Porath, K., Sellmann, T., Bien, C. G., Kohling, R. & Kirschstein, T. (2018). Differentially Altered NMDAR Dependent and Independent Long-Term Potentiation in the CA3 Subfield in a Model of Anti-NMDAR Encephalitis. *Front Synaptic Neurosci,* **10**, 26.

Blume, W. T., Lüders, H. O., Mizrahi, E., Tassinari, C., van Emde Boas, W. & Engel, J. (2001). Glossary of descriptive terminology for ictal semiology: report of the ILAE task force on classification and terminology. *Epilepsia,* **42**(9), 1212-8.

Bonilla, F. A. & Oettgen, H. C. (2010). Adaptive immunity. *J Allergy Clin Immunol,* **125**(2 Suppl 2), S33-40.

Bordeaux, J., Welsh, A., Agarwal, S., Killiam, E., Baquero, M., Hanna, J., Anagnostou, V. & Rimm, D. (2010). Antibody validation. *Biotechniques,* **48**(3), 197-209.

Borroni, B., Stanic, J., Verpelli, C., Mellone, M., Bonomi, E., Alberici, A., Bernasconi, P., Culotta, L., Zianni, E., Archetti, S., Manes, M., Gazzina, S., Ghidoni, R., Benussi, L., Stuani, C., Di Luca, M., Sala, C., Buratti, E., Padovani, A. & Gardoni, F. (2017). Anti-AMPA GluA3 antibodies in Frontotemporal dementia: a new molecular target. *Sci Rep,* **7**(1), 6723.

Boussif, O., Lezoualc'h, F., Zanta, M. A., Mergny, M. D., Scherman, D., Demeneix, B. & Behr, J. P. (1995). A versatile vector for gene and oligonucleotide transfer into cells in culture and in vivo: polyethylenimine. *Proc Natl Acad Sci U S A,* **92**(16), 7297-301.

Cantanelli, P., Sperduti, S., Ciavardelli, D., Stuppia, L., Gatta, V. & Sensi, S. L. (2014). Age-Dependent Modifications of AMPA Receptor Subunit Expression Levels and Related Cognitive Effects in 3xTg-AD Mice. *Front Aging Neurosci,* **6**, 200.

Carlson, N. G., Gahring, L. C., Twyman, R. E. & Rogers, S. W. (1997). Identification of amino acids in the glutamate receptor, GluR3, important for antibody-binding and receptor-specific activation. *J Biol Chem,* **272**(17), 11295-301.

Carter, M. & Shieh, J. (2015). Electrophysiology. *Guide to Research Techniques in Neuroscienceq.* 2nd ed.: Academic Press.

Castillo-Gomez, E., Oliveria, B., Tapken, D., Bertrand, S., Klein-Schmidt, C., Pan, H., Zafeiriou, P., Steiner, J., Jurek, B., Trippe, R., Prüss, H., Zimmerman, W.-H., Bertrand, D., Ehrenreich, H. & Hollman, M. (2016). All naturally occurring autoantibodies against the NMDA receptor subunit NR1 have pathogenic potential irrespective of epitope and immunoglobulin class. *Molecular Psychiatry*, 1-9.

Chater, T. E. & Goda, Y. (2014). The role of AMPA receptors in postsynaptic mechanisms of synaptic plasticity. *Front Cell Neurosci,* **8**, 401.

Chefdeville, A., Honnorat, J., Hampe, C. S. & Desestret, V. (2016). Neuronal central nervous system syndromes probably mediated by autoantibodies. *Eur J Neurosci,* **43**(12), 1535-52.

Dalmau, J. (2017). In vitro effects of a human monoclonal antibody against the N-methyl-d-aspartate receptor. *Brain,* **140**(2), e9.

Dalmau, J., Geis, C. & Graus, F. (2017). Autoantibodies to Synaptic Receptors and Neuronal Cell Surface Proteins in Autoimmune Diseases of the Central Nervous System. *Physiol Rev,* **97**(2), 839-887.

Dalmau, J., Gleichman, A. J., Hughes, E. G., Rossi, J. E., Peng, X., Lai, M., Dessain, S. K., Rosenfeld, M. R., Balice-Gordon, R. & Lynch, D. R. (2008). Anti-NMDA-receptor encephalitis: case series and analysis of the effects of antibodies. *Lancet Neurol,* **7**(12), 1091-8.

Dalmau, J., Lancaster, E., Martinez-Hernandez, E., Rosenfeld, M. R. & Balice-Gordon, R. (2011). Clinical experience and laboratory investigations in patients with anti-NMDAR encephalitis. *Lancet Neurol,* **10**(1), 63-74.

Dalmau, J., Tüzün, E., Wu, H. Y., Masjuan, J., Rossi, J. E., Voloschin, A., Baehring, J. M., Shimazaki, H., Koide, R., King, D., Mason, W., Sansing, L. H., Dichter, M. A., Rosenfeld, M. R. & Lynch, D. R. (2007). Paraneoplastic anti-N-methyl-D-aspartate receptor encephalitis associated with ovarian teratoma. *Ann Neurol,* **61**(1), 25-36.

Dascal, N. (2001). Voltage clamp recordings from Xenopus oocytes. *Curr Protoc Neurosci*.

Diering, G. H. & Huganir, R. L. (2018). The AMPA Receptor Code of Synaptic Plasticity. *Neuron,* **100**(2), 314-329.

Dingledine, R., Borges, K., Bowie, D. & Traynelis, S. F. (1999). The glutamate receptor ion channels. *Pharmacol Rev,* **51**(1), 7-61.

Dionisio, S., Brown, H., Lander, C., Airey, C., Lehn, A., Nooruddin, H. & Blum, S. (2013). Immunoglobulin-responsive refractory epilepsy--3 cases with a similar EEG pattern. *Seizure,* **22**(5), 403-8.

Dravet, C. & Oguni, H. (2013). Dravet syndrome (severe myoclonic epilepsy in infancy). *Handb Clin Neurol,* **111**, 627-33.

Dravid, S. M. Y., H; Traynelis, S.F (2009). AMPA Receptors: Molecular Biology and Pharmacology. *In:* Squire, L. R. (ed.) *Encyclopedia of Neuroscience.* Elsevier.

Duncan, G. E., Inada, K., Koller, B. H. & Moy, S. S. (2010). Increased sensitivity to kainic acid in a genetic model of reduced NMDA receptor function. *Brain Res,* **1307**, 166-76.

Ekizoglu, E., Tuzun, E., Woodhall, M., Lang, B., Jacobson, L., Icoz, S., Bebek, N., Gurses, C., Gokyigit, A., Waters, P., Vincent, A. & Baykan, B. (2014). Investigation of neuronal autoantibodies in two different focal epilepsy syndromes. *Epilepsia,* **55**(3), 414-22.

Elkon, K. & Casali, P. (2008). Nature and functions of autoantibodies. *Nat Clin Pract Rheumatol,* **4**(9), 491-8.

Engelborghs, S., D'Hooge, R. & De Deyn, P. P. (2000). Pathophysiology of epilepsy. *Acta Neurol Belg,* **100**(4), 201-13.

Fang, Z., Yang, Y., Chen, X., Zhang, W., Xie, Y., Chen, Y., Liu, Z. & Yuan, W. (2017). Advances in Autoimmune Epilepsy Associated with Antibodies, Their Potential Pathogenic Molecular Mechanisms, and Current Recommended Immunotherapies. *Front Immunol,* **8**, 395.

Farmakidis, C., Pasnoor, M., Dimachkie, M. M. & Barohn, R. J. (2018). Treatment of Myasthenia Gravis. *Neurol Clin,* **36**(2), 311-337.

Fisher, R. S., Acevedo, C., Arzimanoglou, A., Bogacz, A., Cross, J. H., Elger, C. E., Engel, J., Forsgren, L., French, J. A., Glynn, M., Hesdorffer, D. C., Lee, B. I., Mathern, G. W., Moshé, S. L., Perucca, E., Scheffer, I. E., Tomson, T., Watanabe, M. & Wiebe, S. (2014). ILAE official report: a practical clinical definition of epilepsy. *Epilepsia,* **55**(4), 475-82.

Fisher, R. S., Cross, J. H., French, J. A., Higurashi, N., Hirsch, E., Jansen, F. E., Lagae, L., Moshe, S. L., Peltola, J., Roulet Perez, E., Scheffer, I. E. & Zuberi, S. M. (2017). Operational classification of seizure types by the International League Against Epilepsy: Position Paper of the ILAE Commission for Classification and Terminology. *Epilepsia,* **58**(4), 522-530.

Fisher, R. S., van Emde Boas, W., Blume, W., Elger, C., Genton, P., Lee, P. & Engel, J. (2005). Epileptic seizures and epilepsy: definitions proposed by the International League Against Epilepsy (ILAE) and the International Bureau for Epilepsy (IBE). *Epilepsia,* **46**(4), 470-2.

Fitzgerald, P. J. (2012). The NMDA receptor may participate in widespread suppression of circuit level neural activity, in addition to a similarly prominent role in circuit level activation. *Behav Brain Res,* **230**(1), 291-8.

Frassoni, C., Spreafico, R., Franceschetti, S., Aurisano, N., Bernasconi, P., Garbelli, R., Antozzi, C., Taverna, S., Granata, T. & Mantegazza, R. (2001). Labeling of rat neurons by anti-GluR3 IgG from patients with Rasmussen encephalitis. *Neurology,* **57**(2), 324-7.

Gable, M. S., Sheriff, H., Dalmau, J., Tilley, D. H. & Glaser, C. A. (2012). The frequency of autoimmune N-methyl-D-aspartate receptor encephalitis surpasses that of individual

viral etiologies in young individuals enrolled in the California Encephalitis Project. *Clin Infect Dis,* **54**(7), 899-904.

Gahring, L., Carlson, N. G., Meyer, E. L. & Rogers, S. W. (2001). Granzyme B proteolysis of a neuronal glutamate receptor generates an autoantigen and is modulated by glycosylation. *J Immunol,* **166**(3), 1433-8.

Gandal, M. J., Sisti, J., Klook, K., Ortinski, P. I., Leitman, V., Liang, Y., Thieu, T., Anderson, R., Pierce, R. C., Jonak, G., Gur, R. E., Carlson, G. & Siegel, S. J. (2012). GABAB-mediated rescue of altered excitatory-inhibitory balance, gamma synchrony and behavioral deficits following constitutive NMDAR-hypofunction. *Transl Psychiatry,* **2**, e142.

Ganor, Y., Besser, M., Ben-Zakay, N., Unger, T. & Levite, M. (2003). Human T cells express a functional ionotropic glutamate receptor GluR3, and glutamate by itself triggers integrin-mediated adhesion to laminin and fibronectin and chemotactic migration. *J Immunol,* **170**(8), 4362-72.

Ganor, Y., Goldberg-Stern, H., Cohen, R., Teichberg, V. & Levite, M. (2014). Glutamate receptor antibodies directed against AMPA receptors subunit 3 peptide B (GluR3B) can be produced in DBA/2J mice, lower seizure threshold and induce abnormal behavior. *Psychoneuroendocrinology,* **42**, 106-17.

Ganor, Y., Gottlieb, M., Eilam, R., Otmy, H., Teichberg, V. I. & Levite, M. (2005). Immunization with the glutamate receptor-derived peptide GluR3B induces neuronal death and reactive gliosis, but confers partial protection from pentylenetetrazole-induced seizures. *Exp Neurol,* **195**(1), 92-102.

Ganor, Y., Teichberg, V. I. & Levite, M. (2007). TCR activation eliminates glutamate receptor GluR3 from the cell surface of normal human T cells, via an autocrine/paracrine granzyme B-mediated proteolytic cleavage. *J Immunol,* **178**(2), 683-92.

Gardoni, F., Stanic, J., Scheggia, D., Benussi, A., Borroni, B. & Di Luca, M. (2021). NMDA and AMPA Receptor Autoantibodies in Brain Disorders: From Molecular Mechanisms to Clinical Features. *Cells,* **10**(1).

Ghosh, S., Sinha, J. K., Khan, T., Devaraju, K. S., Singh, P., Vaibhav, K. & Gaur, P. (2021). Pharmacological and Therapeutic Approaches in the Treatment of Epilepsy. *Biomedicines,* **9**(5).

Gladding, C. M. & Raymond, L. A. (2011). Mechanisms underlying NMDA receptor synaptic/extrasynaptic distribution and function. *Mol Cell Neurosci,* **48**(4), 308-20.

Gleichman, A. J., Spruce, L. A., Dalmau, J., Seeholzer, S. H. & Lynch, D. R. (2012). Anti-NMDA receptor encephalitis antibody binding is dependent on amino acid identity of a small region within the GluN1 amino terminal domain. *J Neurosci,* **32**(32), 11082-94.

Gold, M., Pul, R., Bach, J. P., Stangel, M. & Dodel, R. (2012). Pathogenic and physiological autoantibodies in the central nervous system. *Immunol Rev,* **248**(1), 68-86.

Goldberg-Stern, H., Ganor, Y., Cohen, R., Pollak, L., Teichberg, V. & Levite, M. (2014). Glutamate receptor antibodies directed against AMPA receptors subunit 3 peptide B (GluR3B) associate with some cognitive/psychiatric/behavioral abnormalities in epilepsy patients. *Psychoneuroendocrinology,* **40**, 221-31.

Goldin, A. L. (2006). Expression of Ion Channels in Xenopus Oocytes. *Expression and Analysis of Recombinant Ion Channels.*

Gouaux, E. (2004). Structure and function of AMPA receptors. *J Physiol,* **554**(Pt 2), 249-53.

Granata, T. & Andermann, F. (2013). Rasmussen encephalitis. *Handb Clin Neurol,* **111**, 511-9.

Granata, T., Gobbi, G., Spreafico, R., Vigevano, F., Capovilla, G., Ragona, F., Freri, E., Chiapparini, L., Bernasconi, P., Giordano, L., Bertani, G., Casazza, M., Dalla Bernardina, B. & Fusco, L. (2003). Rasmussen's encephalitis: early characteristics allow diagnosis. *Neurology,* **60**(3), 422-5.

Greco, A., Rizzo, M. I., De Virgilio, A., Conte, M., Gallo, A., Attanasio, G., Ruoppolo, G. & de Vincentiis, M. (2016). Autoimmune epilepsy. *Autoimmun Rev,* **15**(3), 221-5.

Greenwood, J. & Valdes, J. (2016). Perampanel (Fycompa): A Review of Clinical Efficacy and Safety in Epilepsy. *P T,* **41**(11), 683-698.

Greger, I. H., Watson, J. F. & Cull-Candy, S. G. (2017). Structural and Functional Architecture of AMPA-Type Glutamate Receptors and Their Auxiliary Proteins. *Neuron,* **94**, 713-730.

Hamill, O. P., Marty, A., Neher, E., Sakmann, B. & Sigworth, F. J. (1981). Improved patch-clamp techniques for high-resolution current recording from cells and cell-free membrane patches. *Pflugers Arch,* **391**(2), 85-100.

Hammer, C., Stepniak, B., Schneider, A., Papiol, S., Tantra, M., Begemann, M., Sirén, A. L., Pardo, L. A., Sperling, S., Mohd Jofrry, S., Gurvich, A., Jensen, N., Ostmeier, K.,

Lühder, F., Probst, C., Martens, H., Gillis, M., Saher, G., Assogna, F., Spalletta, G., Stöcker, W., Schulz, T. F., Nave, K. A. & Ehrenreich, H. (2014). Neuropsychiatric disease relevance of circulating anti-NMDA receptor autoantibodies depends on blood-brain barrier integrity. *Mol Psychiatry,* **19**(10), 1143-9.

Hansen, K. B., Furukawa, H. & Traynelis, S. F. (2010). Control of assembly and function of glutamate receptors by the amino-terminal domain. *Mol Pharmacol,* **78**(4), 535-49.

Hansen, K. B., Yi, F., Perszyk, R. E., Furukawa, H., Wollmuth, L. P., Gibb, A. J. & Traynelis, S. F. (2018). Structure, function, and allosteric modulation of NMDA receptors. *J Gen Physiol,* **150**(8), 1081-1105.

Hansen, K. B., Yi, F., Perszyk, R. E., Menniti, F. S. & Traynelis, S. F. (2017). NMDA Receptors in the Central Nervous System. *Methods Mol Biol,* **1677**, 1-80.

Haselmann, H., Mannara, F., Werner, C., Planaguma, J., Miguez-Cabello, F., Schmidl, L., Grunewald, B., Petit-Pedrol, M., Kirmse, K., Classen, J., Demir, F., Klocker, N., Soto, D., Doose, S., Dalmau, J., Hallermann, S. & Geis, C. (2018). Human Autoantibodies against the AMPA Receptor Subunit GluA2 Induce Receptor Reorganization and Memory Dysfunction. *Neuron,* **100**(1), 91-105 e9.

He, X. P., Patel, M., Whitney, K. D., Janumpalli, S., Tenner, A. & McNamara, J. O. (1998). Glutamate receptor GluR3 antibodies and death of cortical cells. *Neuron,* **20**(1), 153-63.

Hedegaard, M., Hansen, K. B., Andersen, K. T., Bräuner-Osborne, H. & Traynelis, S. F. (2012). Molecular pharmacology of human NMDA receptors. *Neurochem Int,* **61**(4), 601-9.

Hewitt, S. M., Baskin, D. G., Frevert, C. W., Stahl, W. L. & Rosa-Molinar, E. (2014). Controls for immunohistochemistry: the Histochemical Society's standards of practice for validation of immunohistochemical assays. *J Histochem Cytochem,* **62**(10), 693-7.

Hill, A. J., Jones, N. A., Williams, C. M., Stephens, G. J. & Whalley, B. J. (2010). Development of multi-electrode array screening for anticonvulsants in acute rat brain slices. *J Neurosci Methods,* **185**(2), 246-56.

Hill, C. L. & Stephens, G. J. (2021). An Introduction to Patch Clamp Recording. *Methods Mol Biol,* **2188**, 1-19.

Hnasko, R. M. & McGarvey, J. A. (2015). Affinity Purification of Antibodies. *Methods Mol Biol,* **1318**, 29-41.

Hughes, E. G., Peng, X., Gleichman, A. J., Lai, M., Zhou, L., Tsou, R., Parsons, T. D., Lynch, D. R., Dalmau, J. & Balice-Gordon, R. J. (2010). Cellular and synaptic mechanisms of anti-NMDA receptor encephalitis. *J Neurosci,* **30**(17), 5866-75.

Hunter, D., Jamet, Z. & Groc, L. (2021). Autoimmunity and NMDA receptor in brain disorders: Where do we stand? *Neurobiol Dis,* **147**, 105161.

Husari, K. S. & Dubey, D. (2019). Autoimmune Epilepsy. *Neurotherapeutics,* **16**(3), 685-702.

Iorio, R., Assenza, G., Tombini, M., Colicchio, G., Della Marca, G., Benvenga, A., Damato, V., Rossini, P. M., Vollono, C., Plantone, D., Marti, A., Batocchi, A. P. & Evoli, A. (2015a). The detection of neural autoantibodies in patients with antiepileptic-drug-resistant epilepsy predicts response to immunotherapy. *Eur J Neurol,* **22**(1), 70-8.

Iorio, R., O'Toole, O. & Pittock, S. J. (2015b). Autoimmune and Paraneoplastic Neurological Disorders. *In:* Zigmond, M. J., Rowland, L. P. & Coyle, J. T. (eds.) *Neurobiology of Brain Disorders.* Academic Press.

Irani, S. R., Bera, K., Waters, P., Zuliani, L., Maxwell, S., Zandi, M. S., Friese, M. A., Galea, I., Kullmann, D. M., Beeson, D., Lang, B., Bien, C. G. & Vincent, A. (2010). N-methyl-D-aspartate antibody encephalitis: temporal progression of clinical and paraclinical observations in a predominantly non-paraneoplastic disorder of both sexes. *Brain,* **133**(Pt 6), 1655-67.

Jackman, S. L. & Regehr, W. G. (2017). The Mechanisms and Functions of Synaptic Facilitation. *Neuron,* **94**(3), 447-464.

Jain, A., Lancaster, E., Dalmau, J. & Balice-Gordon, R., J. (2015). Autoantibodies in the CSF of anti-GABA receptor encephalitis patients block activation of GABA receptors in vitro. *Ann Neurol,* **78**.

Janeway, C. A., Travers, P., Walport, M. & Shlomchik, M. J. (2001). Immunobiology: The Immune System in Health and Disease. 5th edition ed. New York: Garland Science.

Jenssen, S., Gracely, E. J. & Sperling, M. R. (2006). How long do most seizures last? A systematic comparison of seizures recorded in the epilepsy monitoring unit. *Epilepsia,* **47**(9), 1499-503.

Jones, B. E., Tovar, K. R., Goehring, A., Jalali-Yazdi, F., Okada, N. J., Gouaux, E. & Westbrook, G. L. (2019). Autoimmune receptor encephalitis in mice induced by active immunization with conformationally stabilized holoreceptors. *Sci Transl Med,* **11**(500).

Karakas, E. & Furukawa, H. (2014). Crystal structure of a heterotetrameric NMDA receptor ion channel. *Science,* **344**(6187), 992-7.

Kazi, R., Dai, J., Sweeney, C., Zhou, H. X. & Wollmuth, L. P. (2014). Mechanical coupling maintains the fidelity of NMDA receptor-mediated currents. *Nat Neurosci,* **17**(7), 914-22.

Kersten, M., Rabbe, T., Blome, R., Porath, K., Sellmann, T., Bien, C. G., Kohling, R. & Kirschstein, T. (2019). Novel Object Recognition in Rats With NMDAR Dysfunction in CA1 After Stereotactic Injection of Anti-NMDAR Encephalitis Cerebrospinal Fluid. *Front Neurol,* **10**, 586.

Kornau, H. C., Kreye, J., Stumpf, A., Fukata, Y., Parthier, D., Sammons, R. P., Imbrosci, B., Kurpjuweit, S., Kowski, A. B., Fukata, M., Pruss, H. & Schmitz, D. (2020). Human Cerebrospinal Fluid Monoclonal LGI1 Autoantibodies Increase Neuronal Excitability. *Ann Neurol,* **87**(3), 405-418.

Kreye, J., Wenke, N. K., Chayka, M., Leubner, J., Murugan, R., Maier, N., Jurek, B., Ly, L.-T., Brandl, D., Rost, B. R., Stumpf, A., Schulz, P., Radbruch, H., Hauser, A. E., Pache, F., Meisel, A., Harms, L., Paul, F., Dirnagl, U., Garner, C., Schmitz, D., Wardemann, H. & Prüss, H. (2016). Human cerebrospinal fluid monoclonal N - methyl-D-aspartate receptor autoantibodies are sufficient for encephalitis pathogenesis. *Brain,* **139**(10), 2641-2652.

Kwan, P. & Brodie, M. J. (2000). Early identification of refractory epilepsy. *N Engl J Med,* **342**(5), 314-9.

Lado, F. A. & Moshé, S. L. (2008). How do seizures stop? *Epilepsia,* **49**(10), 1651-64.

Lavrik, I. N., Golks, A. & Krammer, P. H. (2005). Caspases: pharmacological manipulation of cell death. *J Clin Invest,* **115**(10), 2665-72.

Lee, B. S., Huang, J. S., Jayathilaka, G. D., Lateef, S. S. & Gupta, S. (2010). Production of antipeptide antibodies. *Methods Mol Biol,* **657**, 93-108.

Lee, C. J., Bardoni, R., Tong, C. K., Engelman, H. S., Joseph, D. J., Magherini, P. C. & MacDermott, A. B. (2002). Functional expression of AMPA receptors on central terminals of rat dorsal root ganglion neurons and presynaptic inhibition of glutamate release. *Neuron,* **35**(1), 135-46.

Lee, L. H. & Lu, C. J. (2016). Long-term and Strong Immunotherapy to Treat Anti-N-Methyl- D-Aspartate Receptor Encephalitis with Refractory Status Epilepticus. *Acta Neurol Taiwan,* **25**(3), 99-103.

Lee, S. K. (2014). Old versus New: Why Do We Need New Antiepileptic Drugs? *J Epilepsy Res,* **4**(2), 39-44.

Levite, M. (2014). Glutamate receptor antibodies in neurological diseases: anti-AMPA-GluR3 antibodies, anti-NMDA-NR1 antibodies, anti-NMDA-NR2A/B antibodies, anti-mGluR1 antibodies or anti-mGluR5 antibodies are present in subpopulations of patients with either: epilepsy, encephalitis, cerebellar ataxia, systemic lupus erythematosus (SLE) and neuropsychiatric SLE, Sjogren's syndrome, schizophrenia, mania or stroke. These autoimmune anti-glutamate receptor antibodies can bind neurons in few brain regions, activate glutamate receptors, decrease glutamate receptor's expression, impair glutamate-induced signaling and function, activate blood brain barrier endothelial cells, kill neurons, damage the brain, induce behavioral/psychiatric/cognitive abnormalities and ataxia in animal models, and can be removed or silenced in some patients by immunotherapy. *J Neural Transm (Vienna),* **121**(8), 1029-75.

Levite, M., Chowers, Y., Ganor, Y., Besser, M., Hershkovits, R. & Cahalon, L. (2001). Dopamine interacts directly with its D3 and D2 receptors on normal human T cells, and activates β1 integrin function. *Eur J Immunol,* **31**(3504).

Levite, M., Fleidervish, I. A., Schwarz, A., Pelled, D. & Futerman, A. H. (1999). Autoantibodies to the glutamate receptor kill neurons via activation of the receptor ion channel. *J Autoimmun,* **13**(1), 61-72.

Levite, M. & Hermelin, A. (1999). Autoimmunity to the glutamate receptor in mice--a model for Rasmussen's encephalitis? *J Autoimmun,* **13**(1), 73-82.

Leypoldt, F., Buchert, R., Kleiter, I., Marienhagen, J., Gelderblom, M., Magnus, T., Dalmau, J., Gerloff, C. & Lewerenz, J. (2012). Fluorodeoxyglucose positron emission tomography in anti-N-methyl-D-aspartate receptor encephalitis: distinct pattern of disease. *J Neurol Neurosurg Psychiatry,* **83**(7), 681-6.

Lipman, N. S., Jackson, L. R., Trudel, L. J. & Weis-Garcia, F. (2005). Monoclonal versus polyclonal antibodies: distinguishing characteristics, applications, and information resources. *ILAR J,* **46**(3), 258-68.

Longaretti, F., Dunkley, C., Varadkar, S., Vargha-Khadem, F., Boyd, S. G. & Cross, J. H. (2012). Evolution of the EEG in children with Rasmussen's syndrome. *Epilepsia,* **53**(9), 1539-45.

Loscher, W., Gillard, M., Sands, Z. A., Kaminski, R. M. & Klitgaard, H. (2016). Synaptic Vesicle Glycoprotein 2A Ligands in the Treatment of Epilepsy and Beyond. *CNS Drugs,* **30**(11), 1055-1077.

Lu, W., Shi, Y., Jackson, A. C., Bjorgan, K., During, M. J., Sprengel, R., Seeburg, P. H. & Nicoll, R. A. (2009). Subunit composition of synaptic AMPA receptors revealed by a single-cell genetic approach. *Neuron,* **62**(2), 254-68.

Ludwig, R. J., Vanhoorelbeke, K., Leypoldt, F., Kaya, Z., Bieber, K., McLachlan, S. M., Komorowski, L., Luo, J., Cabral-Marques, O., Hammers, C. M., Lindstrom, J. M., Lamprecht, P., Fischer, A., Riemekasten, G., Tersteeg, C., Sondermann, P., Rapoport, B., Wandinger, K. P., Probst, C., El Beidaq, A., Schmidt, E., Verkman, A., Manz, R. A. & Nimmerjahn, F. (2017). Mechanisms of Autoantibody-Induced Pathology. *Front Immunol,* **8**, 603.

Luscher, C. & Malenka, R. C. (2012). NMDA receptor-dependent long-term potentiation and long-term depression (LTP/LTD). *Cold Spring Harb Perspect Biol,* **4**(6).

Löscher, W., Klitgaard, H., Twyman, R. E. & Schmidt, D. (2013). New avenues for anti-epileptic drug discovery and development. *Nat Rev Drug Discov,* **12**(10), 757-76.

Macdonald, R. L. & Kelly, K. M. (1995). Antiepileptic drug mechanisms of action. *Epilepsia,* **36 Suppl 2**, S2-12.

Malenka, R., C (1994). Synaptic plasticity in the hippocampus: LTP and LTD. *Cell,* **78**(4), 535-538.

Malenka, R. C. (2003). Synaptic plasticity and AMPA receptor trafficking. *Ann N Y Acad Sci,* **1003**, 1-11.

Malina, K., Ganor, Y., Levite, M. & Teichberg, V. I. (2006). Autoantibodies against an extracellular peptide of the GluR3 subtype of AMPA receptors activate both homomeric and heteromeric AMPA receptor channels. *Neurochem Res,* **31**(10), 1181-90.

Malinow, R. (2003). AMPA receptor trafficking and long-term potentiation. *Philos Trans R Soc Lond B Biol Sci,* **358**(1432), 707-14.

Mannoor, K., Xu, Y. & Chen, C. (2013). Natural autoantibodies and associated B cells in immunity and autoimmunity. *Autoimmunity,* **46**(2), 138-47.

Mantegazza, R., Bernasconi, P., Baggi, F., Spreafico, R., Ragona, F., Antozzi, C., Bernardi, G. & Granata, T. (2002). Antibodies against GluR3 peptides are not specific for

Rasmussen's encephalitis but are also present in epilepsy patients with severe, early onset disease and intractable seizures. *J Neuroimmunol,* **131**(1-2), 179-85.

Manto, M., Dalmau, J., Didelot, A., Rogemond, V. & Honnorat, J. (2010). In vivo effects of antibodies from patients with anti-NMDA receptor encephalitis: further evidence of synaptic glutamatergic dysfunction. *Orphanet J Rare Dis,* **5**, 31.

Medina, K. L. (2016). Overview of the immune system. *In:* Pittock, S. J. & Vincent, A. (eds.) *Handb Clin Neurol.* 2016/04/27 ed.

Mellers, J. D. C. (2005). The approach to patients with ‘‘non-epileptic seizures’’. *Postgrad Med J,* **81**, 498-504.

Mikasova, L., De Rossi, P., Bouchet, D., Georges, F., Rogemond, V., Didelot, A., Meissirel, C., Honnorat, J. & Groc, L. (2012). Disrupted surface cross-talk between NMDA and Ephrin-B2 receptors in anti-NMDA encephalitis. *Brain,* **135**(Pt 5), 1606-21.

Miller, S. L. Y., H.H (2017). Neurotransmitters and Neurotransmission in the Developing and Adult Nervous System. *In:* Conn, P. M. (ed.) *Conn's Translational Neuroscience.* Elsevier.

Miya, K., Takahashi, Y. & Mori, H. (2014). Anti-NMDAR autoimmune encephalitis. *Brain Dev,* **36**(8), 645-52.

Moscato, E. H., Peng, X., Jain, A., Parsons, T. D., Dalmau, J. & Balice-Gordon, R. J. (2014). Acute mechanisms underlying antibody effects in anti-N-methyl-D-aspartate receptor encephalitis. *Ann Neurol,* **76**(1), 108-19.

Mullier, B., Wolff, C., Sands, Z. A., Ghisdal, P., Muglia, P., Kaminski, R. M. & André, V. M. (2017). GRIN2B gain of function mutations are sensitive to radiprodil, a negative allosteric modulator of GluN2B-containing NMDA receptors. *Neuropharmacology,* **123**, 322-331.

Needs, H. I., Henley, B. S., Cavallo, D., Gurung, S., Modebadze, T., Woodhall, G. & Henley, J. M. (2019). Changes in excitatory and inhibitory receptor expression and network activity during induction and establishment of epilepsy in the rat Reduced Intensity Status Epilepticus (RISE) model. *Neuropharmacology,* **158**, 107728.

Negrete-Diaz, J. V., Sihra, T. S., Flores, G. & Rodriguez-Moreno, A. (2018). Non-canonical Mechanisms of Presynaptic Kainate Receptors Controlling Glutamate Release. *Front Mol Neurosci,* **11**, 128.

NICE, N. I. f. H. a. C. E. (2021). *Epilepsies: diagnosis and management*.

Niswender, C. M. & Conn, P. J. (2010). Metabotropic glutamate receptors: physiology, pharmacology, and disease. *Annu Rev Pharmacol Toxicol,* **50**, 295-322.

Ong, M. S., Kohane, I. S., Cai, T., Gorman, M. P. & Mandl, K. D. (2014). Population-level evidence for an autoimmune etiology of epilepsy. *JAMA Neurol,* **71**(5), 569-74.

Palese, F., Bonomi, E., Nuzzo, T., Benussi, A., Mellone, M., Zianni, E., Cisani, F., Casamassa, A., Alberici, A., Scheggia, D., Padovani, A., Marcello, E., Di Luca, M., Pittaluga, A., Usiello, A., Borroni, B. & Gardoni, F. (2020). Anti-GluA3 antibodies in frontotemporal dementia: effects on glutamatergic neurotransmission and synaptic failure. *Neurobiol Aging,* **86**, 143-155.

Pan, H., Oliveria, B., Saher, G., Dere, E., Tapken, D., Mitjans, M., Seidel, J., Wesolowski, J., Wakhloo, D., Klein-Schmidt, C., Ronneberg, A., Schwabe, K., Trippe, R., Mätz-Rensing, K., Berghoff, S., Al-Krinawe, Y., Martens, H., Begemann, M., Stöcker, W., Kaup, F., A, Mischke, R., Boretius, S., Nave, K. A., Krauss, J., K, Hollman, M., Lühder, F. & Ehrenreich, H. (2018). Uncoupling the widespread occurrence of anti-NMDAR1 autoantibodies from neuropsychiatric disease in a novel autoimmune model. *Molecular Psychiatry*.

Paoletti, P. (2011). Molecular basis of NMDA receptor functional diversity. *Eur J Neurosci,* **33**(8), 1351-65.

Paoletti, P., Bellone, C. & Zhou, Q. (2013). NMDA receptor subunit diversity: impact on receptor properties, synaptic plasticity and disease. *Nat Rev Neurosci,* **14**(6), 383-400.

Paoletti, P. & Neyton, J. (2007). NMDA receptor subunits: function and pharmacology. *Curr Opin Pharmacol,* **7**(1), 39-47.

Parkin, J. & Cohen, B. (2001). An overview of the immune system. *Lancet,* **357**(9270), 1777-89.

Peng, X., Hughes, E. G., Moscato, E. H., Parsons, T. D., Dalmau, J. & Balice-Gordon, R. J. (2015). Cellular plasticity induced by anti-alpha-amino-3-hydroxy-5-methyl-4-isoxazolepropionic acid (AMPA) receptor encephalitis antibodies. *Ann Neurol,* **77**(3), 381-98.

Perucca, E., French, J. & Bialer, M. (2007). Development of new antiepileptic drugs: challenges, incentives, and recent advances. *Lancet Neurol,* **6**(9), 793-804.

Perucca, P., Carter, J., Vahle, V. & Gilliam, F. G. (2009). Adverse antiepileptic drug effects: toward a clinically and neurobiologically relevant taxonomy. *Neurology,* **72**(14), 1223-9.

Perucca, P. & Gilliam, F. G. (2012). Adverse effects of antiepileptic drugs. *Lancet Neurol,* **11**(9), 792-802.

Planaguma, J., Haselmann, H., Mannara, F., Petit-Pedrol, M., Grunewald, B., Aguilar, E., Ropke, L., Martin-Garcia, E., Titulaer, M. J., Jercog, P., Graus, F., Maldonado, R., Geis, C. & Dalmau, J. (2016). Ephrin-B2 prevents N-methyl-D-aspartate receptor antibody effects on memory and neuroplasticity. *Ann Neurol,* **80**(3), 388-400.

Planagumà, J., Leypoldt, F., Mannara, F., Gutiérrez-Cuesta, J., Martín-García, E., Aguilar, E., Titulaer, M. J., Petit-Pedrol, M., Jain, A., Balice-Gordon, R., Lakadamyali, M., Graus, F., Maldonado, R. & Dalmau, J. (2015). Human N-methyl D-aspartate receptor antibodies alter memory and behaviour in mice. *Brain,* **138**(Pt 1), 94-109.

Platt, S. R. (2007). The role of glutamate in central nervous system health and disease--a review. *Vet J,* **173**(2), 278-86.

Pollak, T. A., Beck, K., Irani, S. R., Howes, O. D., David, A. S. & McGuire, P. K. (2016). Autoantibodies to central nervous system neuronal surface antigens: psychiatric symptoms and psychopharmacological implications. *Psychopharmacology (Berl),* **233**(9), 1605-21.

Purcell, A. W., McCluskey, J. & Rossjohn, J. (2007). More than one reason to rethink the use of peptides in vaccine design. *Nat Rev Drug Discov,* **6**(5), 404-14.

Purves, D., Augustine, G. J., Fitzpatrick, D., Hall, W. C., LaMantia, A.-S., McNamara, J. O. & Williams, S. M. (2004). *Neuroscience*. Sunderland, Massachusetts, USA: Sinauer Associates Inc.

Ramanathan, S., Al-Diwani, A., Waters, P. & Irani, S. R. (2021). The autoantibody-mediated encephalitides: from clinical observations to molecular pathogenesis. *J Neurol,* **268**(5), 1689-1707.

Ramanathan, S., Bleasel, A., Parratt, J., Orr, C., Dale, R. C., Vincent, A. & Fung, V. S. (2014). Characterisation of a syndrome of autoimmune adult onset focal epilepsy and encephalitis. *J Clin Neurosci,* **21**(7), 1169-75.

Ramberger, M., Berretta, A., Tan, J. M. M., Sun, B., Michael, S., Yeo, T., Theorell, J., Bashford-Rogers, R., Paneva, S., O'Dowd, V., Dedi, N., Topia, S., Griffin, R., Ramirez-Franco, J., El Far, O., Baulac, S., Leite, M. I., Sen, A., Jeans, A., McMillan, D., Marshall, D., Anthony, D., Lightwood, D., Waters, P. & Irani, S. R. (2020). Distinctive binding properties of human monoclonal LGI1 autoantibodies determine pathogenic mechanisms. *Brain,* **143**(6), 1731-1745.

Renner, M. C., Albers, E. H., Gutierrez-Castellanos, N., Reinders, N. R., van Huijstee, A. N., Xiong, H., Lodder, T. R. & Kessels, H. W. (2017). Synaptic plasticity through activation of GluA3-containing AMPA-receptors. *Elife,* **6**.

Rho, J. M., Donevan, S. D. & Rogawski, M. A. (1994). Mechanism of action of the anticonvulsant felbamate: opposing effects on N-methyl-D-aspartate and gamma-aminobutyric acidA receptors. *Ann Neurol,* **35**(2), 229-34.

Rogers, S. W., Andrews, P. I., Gahring, L. C., Whisenand, T., Cauley, K., Crain, B., Hughes, T. E., Heinemann, S. F. & McNamara, J. O. (1994). Autoantibodies to glutamate receptor GluR3 in Rasmussen's encephalitis. *Science,* **265**(5172), 648-51.

Saper, C. B. (2009). A guide to the perplexed on the specificity of antibodies. *J Histochem Cytochem,* **57**(1), 1-5.

Scheffer, I. E., Berkovic, S., Capovilla, G., Connolly, M. B., French, J., Guilhoto, L., Hirsch, E., Jain, S., Mathern, G. W., Moshé, S. L., Nordli, D. R., Perucca, E., Tomson, T., Wiebe, S., Zhang, Y. H. & Zuberi, S. M. (2017). ILAE classification of the epilepsies: Position paper of the ILAE Commission for Classification and Terminology. *Epilepsia,* **58**(4), 512-521.

Scheggia, D., Stanic, J., Italia, M., La Greca, F., Zianni, E., Benussi, A., Borroni, B., Di Luca, M. & Gardoni, F. (2021). GluA3 autoantibodies induce alterations in dendritic spine and behavior in mice. *Brain Behav Immun,* **97**, 89-101.

Schmidt, D. & Schachter, S. C. (2014). Drug treatment of epilepsy in adults. *BMJ,* **348**, g254.

Schroeder, H. W., Jr. & Cavacini, L. (2010). Structure and function of immunoglobulins. *J Allergy Clin Immunol,* **125**(2 Suppl 2), S41-52.

Schwenk, J., Baehrens, D., Haupt, A., Bildl, W., Boudkkazi, S., Roeper, J., Fakler, B. & Schulte, U. (2014). Regional diversity and developmental dynamics of the AMPA-receptor proteome in the mammalian brain. *Neuron,* **84**(1), 41-54.

Shi, Q. & Jackowski, G. (1998). One-dimensional polyacrylamide gel electrophoresis. In: B.D. Hames. *Gel Electrophoresis of Proteins: A Practical Approach.* Oxford: Oxford University Press.

Shin, Y. W., Lee, S. T., Park, K. I., Jung, K. H., Jung, K. Y., Lee, S. K. & Chu, K. (2018). Treatment strategies for autoimmune encephalitis. *Ther Adv Neurol Disord,* **11**, 1756285617722347.

Siloşi, I., Siloşi, C. A., Boldeanu, M. V., Cojocaru, M., Biciuşcă, V., Avrămescu, C. S., Cojocaru, I. M., Bogdan, M. & FolcuŢi, R. M. (2016). The role of autoantibodies in health and disease. *Rom J Morphol Embryol,* **57**(2 Suppl), 633-638.

Skwarczynski, M. & Toth, I. (2016). Peptide-based synthetic vaccines. *Chem Sci,* **7**(2), 842-854.

Smith, P. K., Krohn, R. I., Hermanson, G. T., Mallia, A. K., Gartner, F. H., Provenzano, M. D., Fujimoto, E. K., Goeke, N. M., Olson, B. J. & Klenk, D. C. (1985). Measurement of protein using bicinchoninic acid. *Anal Biochem,* **150**(1), 76-85.

Sommer, B., Keinanen, K., Verdoorn, T. A., Wisden, W., Burnashev, N., Herb, A., Kohler, M., Takagi, T., Sakmann, B. & Seeburg, P. H. (1990). Flip and flop: a cell-specific functional switch in glutamate-operated channels of the CNS. *Science,* **249**(4976), 1580-5.

Stafstrom, C. E. & Carmant, L. (2015). Seizures and epilepsy: an overview for neuroscientists. *Cold Spring Harb Perspect Med,* **5**(6).

Steidl, E. M., Neveu, E., Bertrand, D. & Buisson, B. (2006). The adult rat hippocampal slice revisited with multi-electrode arrays. *Brain Res,* **1096**(1), 70-84.

Stern-Bach, Y., Bettler, B., Hartley, M., Sheppard, P. O., O'Hara, P. J. & Heinemann, S. F. (1994). Agonist selectivity of glutamate receptors is specified by two domains structurally related to bacterial amino acid-binding proteins. *Neuron,* **13**(6), 1345-57.

Sukumaran, M., Penn, A. C. & Greger, I. H. (2012). AMPA receptor assembly: atomic determinants and built-in modulators. *Adv Exp Med Biol,* **970**, 241-64.

Suleiman, J., Wright, S., Gill, D., Brilot, F., Waters, P., Peacock, K., Procopis, P., Nibber, A., Vincent, A., Dale, R. C. & Lang, B. (2013). Autoantibodies to neuronal antigens in children with new-onset seizures classified according to the revised ILAE organization of seizures and epilepsies. *Epilepsia,* **54**(12), 2091-100.

Sveinbjornsdottir, S., Sander, J. W., Upton, D., Thompson, P. J., Patsalos, P. N., Hirt, D., Emre, M., Lowe, D. & Duncan, J. S. (1993). The excitatory amino acid antagonist D-CPP-ene (SDZ EAA-494) in patients with epilepsy. *Epilepsy Res,* **16**(2), 165-74.

Szczurowska, E. & Mares, P. (2013). NMDA and AMPA receptors: development and status epilepticus. *Physiol Res,* **62**(Suppl 1), S21-38.

Tammaro, P., Shimomura, K. & Proks, P. (2008). Xenopus oocytes as a heterologous expression system for studying ion channels with the patch-clamp technique. *Methods Mol Biol,* **491**, 127-39.

Taraschenko, O., Fox, H. S., Eldridge, E., Wang, W., Dowd, S. W., Al-Saleem, F., Kattala, C. D., Dessain, S. K. & Dingledine, R. (2021a). Monoclonal Antibodies From Anti-NMDA Receptor Encephalitis Patient as a Tool to Study Autoimmune Seizures. *Front Neurosci,* **15**, 710650.

Taraschenko, O., Fox, H. S., Pittock, S. J., Zekeridou, A., Gafurova, M., Eldridge, E., Liu, J., M, D. S. & Dingledine, R. (2019). A mouse model of seizures in anti-N-methyl-d-aspartate receptor encephalitis. *Epilepsia,* **60**(3), 452-463.

Taraschenko, O., Fox, H. S., Zekeridou, A., Pittock, S. J., Eldridge, E., Farukhuddin, F., Al-Saleem, F., Devi Kattala, C., Dessain, S. K., Casale, G., Willcockson, G. & Dingledine, R. (2021b). Seizures and memory impairment induced by patient-derived anti-N-methyl-D-aspartate receptor antibodies in mice are attenuated by anakinra, an interleukin-1 receptor antagonist. *Epilepsia,* **62**(3), 671-682.

Toledano, M., Britton, J. W., McKeon, A., Shin, C., Lennon, V. A., Quek, A. M., So, E., Worrell, G. A., Cascino, G. D., Klein, C. J., Lagerlund, T. D., Wirrell, E. C., Nickels, K. C. & Pittock, S. J. (2014). Utility of an immunotherapy trial in evaluating patients with presumed autoimmune epilepsy. *Neurology,* **82**(18), 1578-86.

Toledano, M. & Pittock, S. J. (2015). Autoimmune Epilepsy. *Semin Neurol,* **35**(3), 245-58.

Traynelis, S. F., Wollmuth, L. P., McBain, C. J., Menniti, F. S., Vance, K. M., Ogden, K. K., Hansen, K. B., Yuan, H., Myers, S. J. & Dingledine, R. (2010). Glutamate receptor ion channels: structure, regulation, and function. *Pharmacol Rev,* **62**(3), 405-96.

Trier, N., Hansen, P. & Houen, G. (2019). Peptides, Antibodies, Peptide Antibodies and More. *Int J Mol Sci,* **20**(24).

Trier, N. H., Hansen, P. R. & Houen, G. (2012). Production and characterization of peptide antibodies. *Methods,* **56**(2), 136-44.

Trier, N. H. & Houen, G. (2017). Peptide Antibodies in Clinical Laboratory Diagnostics. *Adv Clin Chem,* **81**, 43-96.

Twomey, E. C. & Sobolevsky, A. I. (2018). Structural Mechanisms of Gating in Ionotropic Glutamate Receptors. *Biochemistry,* **57**(3), 267-276.

Twyman, R. E., Gahring, L. C., Spiess, J. & Rogers, S. W. (1995). Glutamate receptor antibodies activate a subset of receptors and reveal an agonist binding site. *Neuron,* **14**(4), 755-62.

Uy, C. E., Binks, S. & Irani, S. R. (2021). Autoimmune encephalitis: clinical spectrum and management. *Pract Neurol,* **21**(5), 412-423.

Varadkar, S., Bien, C. G., Kruse, C. A., Jensen, F. E., Bauer, J., Pardo, C. A., Vincent, A., Mathern, G. W. & Cross, J. H. (2014). Rasmussen's encephalitis: clinical features, pathobiology, and treatment advances. *Lancet Neurol,* **13**(2), 195-205.

Vincent, A. (2005). Mechanisms in myasthenia gravis. *Drug Discovery Today: Disease Mechanisms,* **2**(4), 401-408.

Vincent, A. & Bien, C. G. (2008). Anti-NMDA-receptor encephalitis: a cause of psychiatric, seizure, and movement disorders in young adults. *Lancet Neurol,* **7**(12), 1074-5.

Vincent, A., Lang, B. & Kleopa, K. A. (2006). Autoimmune channelopathies and related neurological disorders. *Neuron,* **52**(1), 123-38.

Vyklicky, V., Korinek, M., Smejkalova, T., Balik, A., Krausova, B., Kaniakova, M., Lichnerova, K., Cerny, J., Krusek, J., Dittert, I., Horak, M. & Vyklicky, L. (2014). Structure, function, and pharmacology of NMDA receptor channels. *Physiol Res,* **63 Suppl 1**, S191-203.

Wagnon, I., Helie, P., Bardou, I., Regnauld, C., Lesec, L., Leprince, J., Naveau, M., Delaunay, B., Toutirais, O., Lemauff, B., Etard, O., Vivien, D., Agin, V., Macrez, R., Maubert, E. & Docagne, F. (2020). Autoimmune encephalitis mediated by B-cell response against N-methyl-d-aspartate receptor. *Brain,* **143**(10), 2957-2972.

Washburn, H. R., Xia, N. L., Zhou, W., Mao, Y. T. & Dalva, M. B. (2020). Positive surface charge of GluN1 N-terminus mediates the direct interaction with EphB2 and NMDAR mobility. *Nat Commun,* **11**(1), 570.

Watson, R., Jiang, Y., Bermudez, I., Houlihan, L., Clover, L., McKnight, K., Cross, J. H., Hart, I. K., Roubertie, A., Valmier, J., Hart, Y., Palace, J., Beeson, D., Vincent, A. & Lang, B. (2004). Absence of antibodies to glutamate receptor type 3 (GluR3) in Rasmussen encephalitis. *Neurology,* **63**(1), 43-50.

WHO. (2019). *WHO Epilepsy Fact Sheet*. URL: http://www.who.int/mediacentre/factsheets/fs999/en/.

Wiendl, H., Bien, C. G., Bernasconi, P., Fleckenstein, B., Elger, C. E., Dichgans, J., Mantegazza, R. & Melms, A. (2001). GluR3 antibodies: prevalence in focal epilepsy but no specificity for Rasmussen's encephalitis. *Neurology,* **57**(8), 1511-4.

Wirenfeldt, M., Clare, R., Tung, S., Bottini, A., Mathern, G. W. & Vinters, H. V. (2009). Increased activation of Iba1+ microglia in pediatric epilepsy patients with Rasmussen's encephalitis compared with cortical dysplasia and tuberous sclerosis complex. *Neurobiol Dis,* **34**(3), 432-40.

Wright, S., Hashemi, K., Stasiak, L., Bartram, J., Lang, B., Vincent, A. & Upton, A. L. (2015). Epileptogenic effects of NMDAR antibodies in a passive transfer mouse model. *Brain,* **138**(Pt 11), 3159-67.

Wright, S. & Vincent, A. (2016). Progress in autoimmune epileptic encephalitis. *Curr Opin Neurol,* **29**(2), 151-7.

Wright, S. K., Rosch, R. E., Wilson, M. A., Upadhya, M. A., Dhangar, D. R., Clarke-Bland, C., Wahid, T. T., Barman, S., Goebels, N., Kreye, J., Pruss, H., Jacobson, L., Bassett, D. S., Vincent, A., Greenhill, S. D. & Woodhall, G. L. (2021). Multimodal electrophysiological analyses reveal that reduced synaptic excitatory neurotransmission underlies seizures in a model of NMDAR antibody-mediated encephalitis. *Commun Biol,* **4**(1), 1106.

Würdemann, T., Kersten, M., Tokay, T., Guli, X., Kober, M., Rohde, M., Porath, K., Sellmann, T., Bien, C. G., Köhling, R. & Kirschstein, T. (2016). Stereotactic injection of cerebrospinal fluid from anti-NMDA receptor encephalitis into rat dentate gyrus impairs NMDA receptor function. *Brain Res,* **1633**, 10-18.

Yeshokumar, A. K. & Pardo, C. A. (2017). Autoimmune Epilepsies. *Semin Pediatr Neurol,* **24**(3), 161-167.

Zanetti, L., Regoni, M., Ratti, E., Valtorta, F. & Sassone, J. (2021). Presynaptic AMPA Receptors in Health and Disease. *Cells,* **10**(9).

Zeiler, F. A., Teitelbaum, J., Gillman, L. M. & West, M. (2014). NMDA antagonists for refractory seizures. *Neurocrit Care,* **20**(3), 502-13.

Zhang, Q., Tanaka, K., Sun, P., Nakata, M., Yamamoto, R., Sakimura, K., Matsui, M. & Kato, N. (2012). Suppression of synaptic plasticity by cerebrospinal fluid from anti-NMDA receptor encephalitis patients. *Neurobiol Dis,* **45**(1), 610-5.

Zhou, Y. & Danbolt, N. C. (2014). Glutamate as a neurotransmitter in the healthy brain. *J Neural Transm (Vienna),* **121**(8), 799-817.

Zhu, S. & Paoletti, P. (2015). Allosteric modulators of NMDA receptors: multiple sites and mechanisms. *Curr Opin Pharmacol,* **20**, 14-23.

Zucker, R. S. & Regehr, W. G. (2002). Short-term synaptic plasticity. *Annu Rev Physiol,* **64**, 355-405.

9. Appendices

9.1. Vector maps of recombinant plasmid pcDNA3.1(-) NR1-4a Hs and pcDNA3.1(+) NR2B Hs

The plasmids used for HEK cell transfections described in section 2.2.1 were obtained from UCB (Braine, Belgium), shown in Figure 9.1 and 9.2.

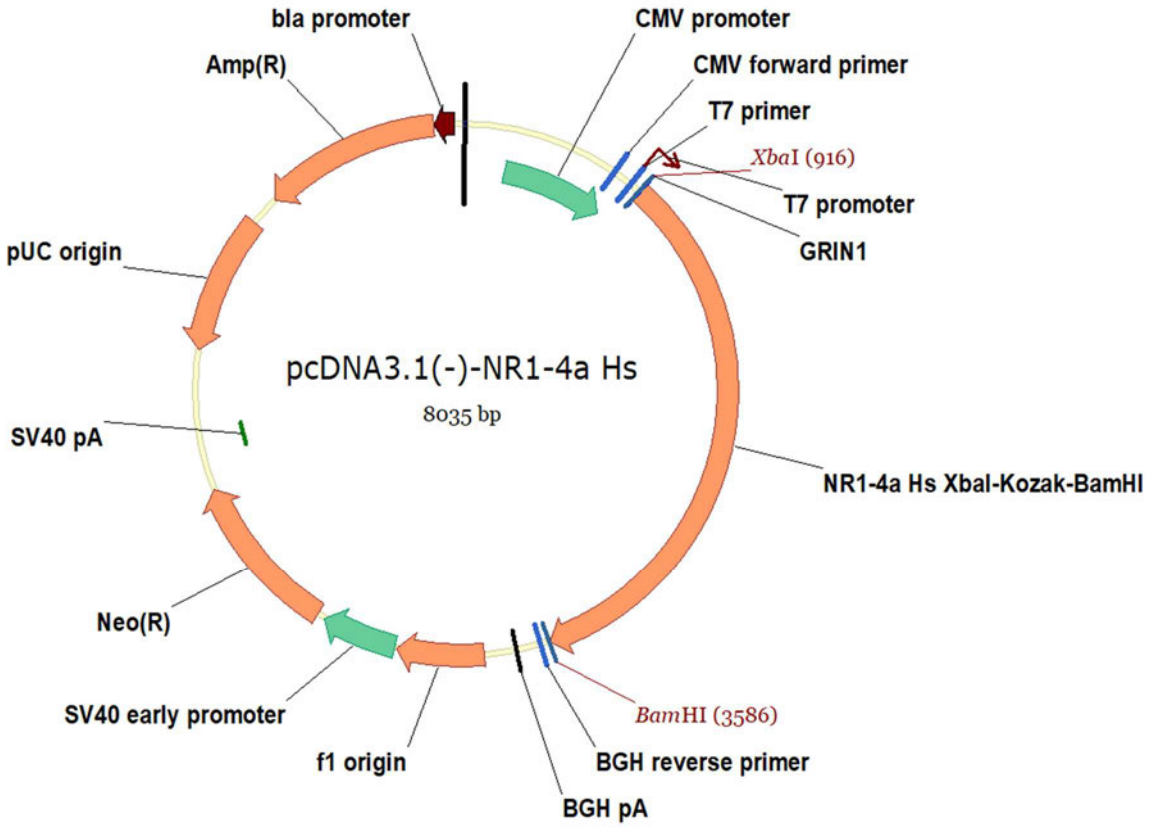

Figure 9.1: Vector map for pcDNA3.1(-)-NR1-4a Hs, used for HEK cell transfections described in section 2.2.1.

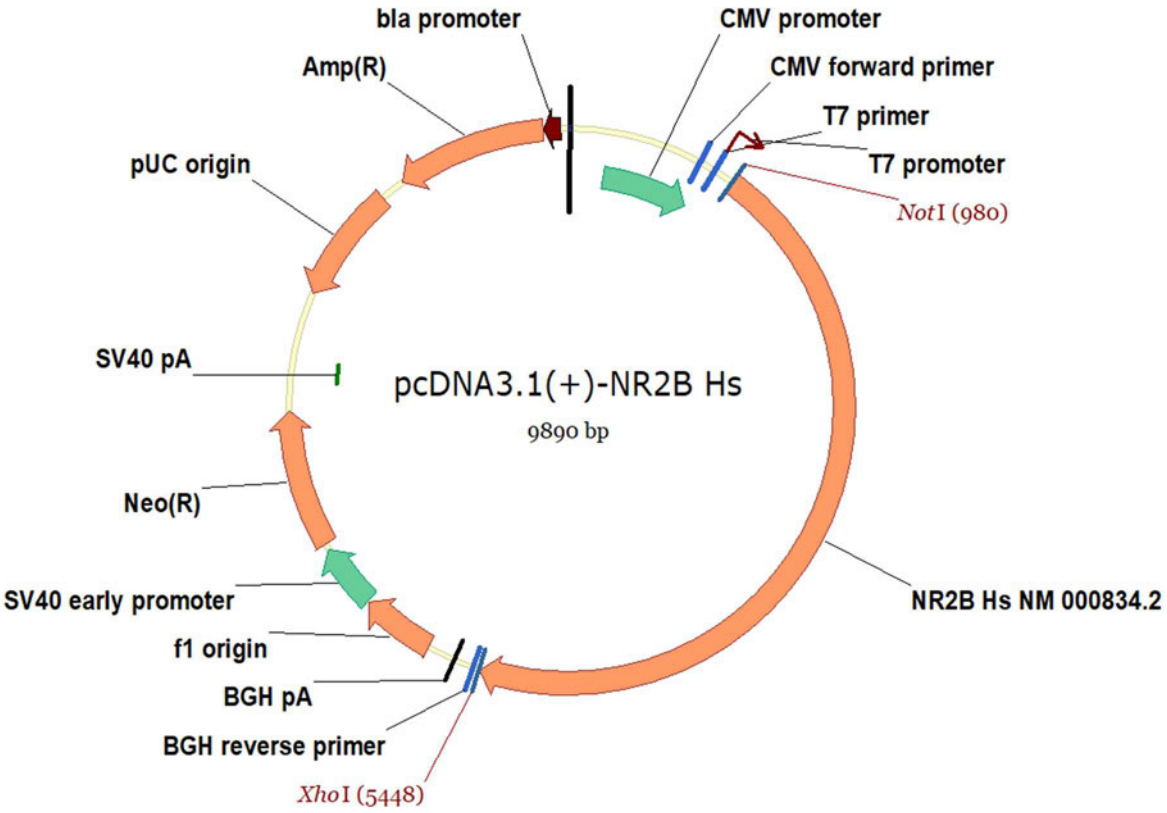

Figure 9.2: Vector map for pcDNA3.1(-)-NR1-4a Hs, used for HEK cell transfections described in section 2.2.1.

9.2 Optimisation of organotypic hippocampal brain slice cultures

This appendix presents a summary of optimisation experiments performed throughout this thesis, but not formally used and no Aabs were applied.

9.2.1 Organotypic hippocampal brain slice cultures (OHSCs)

Postnatal day 7 C57BL6/J mice (male and female) were sacrificed, and brains removed. 400µm slices were performed as described in Chapter 2 on a Leica vibratome using ice cold, carboxygenated dissection media (GBSS supplemented with 1% D-glucose and 300µm kynurenic acid). Slices were left to recover for 30 min - 1 h then placed in pre-warmed culture plates containing inserts (Millipore, UK). Slices were cultured for up to 15 days. At DIV 3, 6, 9, 12 and 15 the slices were removed, and activity was measured by placing over the electrodes on multi-electrode arrays (MEAs). Slices were cultured in a defined medium (Table 15), where medium was changed the day after plating, and every 2 days thereafter.

Table 15: Summary of reagents used in organotypic culture medium

Reagent	Final Concentration	Component	Function	Supplier
BME	25%	Vitamins, amino acids and inorganic salts	Basal medium for supporting growth	Gibco
Heat inactivated Horse serum	12.5%	N/A	Growth factors promote cell proliferation	Gibco
HBSS	12.5%	Nutrients	Maintain pH	Gibco
GlutaMax	2mM	L-alanyl-L-glutamine dipeptide	Essential amino acids (stabilised form of L-Glutamine)	Gibco
D+Glucose	2mg/ml	Glucose	Source of energy	Sigma
Amphotericin B	0.25µg/ml	Antifungal	Prevents contamination of yeast and fungi	Gibco
Penicillin/Streptomycin	50U/ml/50µg/ml	Antibiotic	Prevents growth of gram-positive and -negative bacteria	Gibco

9.2.2 Spontaneous epileptic bursting in OHSCs

Spontaneous epileptiform activity was measured and recorded across OHSCs using MEAs. As detailed previously, prior to recording, MEAs were thoroughly cleaned using Terg-A-Zyme, tap water, distilled water and 100% methanol before being subjected to plasma cleaning. OHSCs on well inserts were removed from culture and inverted onto the recording area of the MEAs, and carefully positioned over the electrodes using a microscope. Slices were weighted down with a harp to ensure constant contact with the electrodes. OHSCs were maintained in culture medium and baseline spontaneous activity was recorded for 10 min. Signals were amplified by a 60-channel head-stage amplifier (MEA60 System, MCS) and simultaneously

sampled at 10 kHz per channel on all 60 channels. Data acquisition to a computer was carried out using the software MC_Rack which monitored and recorded data for offline analysis at a later date.

9.3 Additional AMPAR Aabs Western blots

This appendix presents addition blots probed with AMPAR Aabs, as well as a commercial AMPAR antibody, negative control IgG and secondary-only control.

9.3.1 AMPAR Aabs detect GluR3, but also other non-specific bands

Western blots were performed as described in Section 2.2.1.2, with primary cortical cell lysate and whole brain lysates being run on SDS-PAGE and subsequently probed with AMPAR Aabs, (c)AMPAR, rIgG (negative) control as well as a secondary antibody only (negative) control. AMPAR Aabs detected a band at just above 100 kDa (as expected, GluR3 molecular weight 101 kDa; Figure 9.3A) in whole brain lysate, as well as a band at ~60 kDa. Fainter bands can also be seen at 80 kDa (Figure 9.3A), which may be represent different glycosylated states of the protein, or alternatively may be caused by non-AMPAR specific IgG binding, as seen with our generated NMDAR Aabs (see section 3.3.2). AMPAR Aabs detected a band at ~60 kDa in primary cortical cell lysate, with additional fainter bands being detected at 80 kDa and 50 kDa but failed to detect a band at the expected size of 101 kDa. The commercial anti-AMPAR antibody, detected two prominent bands at 100 kDa and 70 kDa in both samples, with an additional band just above 100 kDa being detected in whole brain lysate (Figure 9.3A).

No-primary antibody negative controls resulted in no bands being detected (Figure 9.3A), and the loading control antibody (GAPDH) was able to produce clean blots with a single band at the expected molecular weight of 37 kDa (Figure 9.3B), the class-specific negative control rIgG consistently produced detected multiple bands at different molecular weights (Figure 9.3A). This may be due to the nature of control used; as it is from a naïve non-immunised rabbit, it likely will contain other antibodies, some of which may be binding to targets within our lysates.

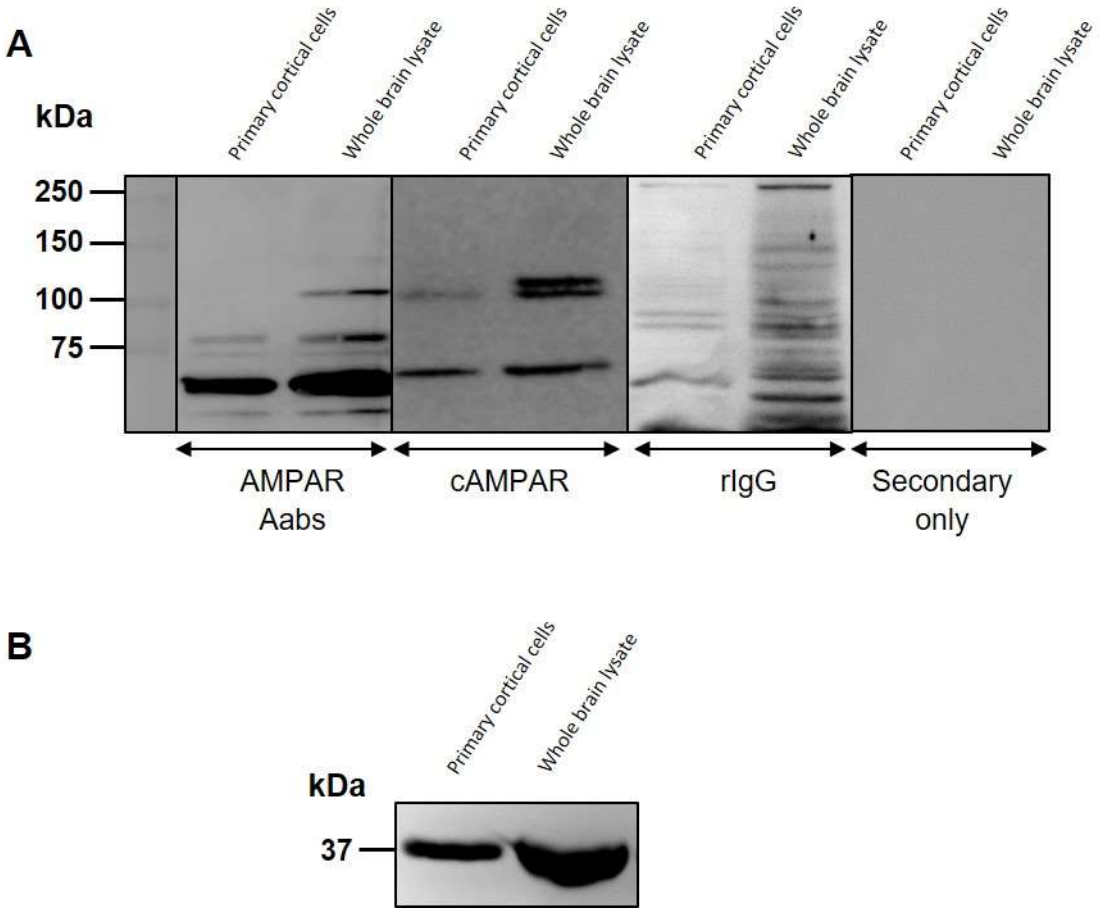

Figure 9.3: Western blot assessing binding specificity of protein A purified AMPAR Aabs to mouse whole brain lysate and cortical cell lysate. (A) AMPAR Aabs elicited a band at the correct size (101 kDa), similar to that of cAMPAR; a commercial anti-AMPAR antibody. The class-specific negative control rIgG elicited a multitude of bands in both primary cortical lysate and whole brain lysate, whereas the no secondary only control did not elicit any bands. **(B)** Representative blot of the loading control GAPDH, showing that clean, single band blots were able to be obtained using the protocol employed (note the different size bands are due to different amounts of protein loaded per sample (10µg primary cortical cell lysate compared to 50µg whole brain lysate). Representative blots selected from n=3 technical replicates.

9.4 Acute and chronic incubation of primary neurons with AMPAR Aabs resulted in significant differences in cumulative inter-event intervals

Significant differences in sEPSC cumulative inter-event interval distributions were observed following AMPAR Aabs 30min incubation when compared to IgG incubated cells, and when compared to pre-treatment baselines. These differences were also observed when broken down into 10 min bins ($p<0.0001$; Kolmogorov-Smirnov test; Figure 9.4A-I).

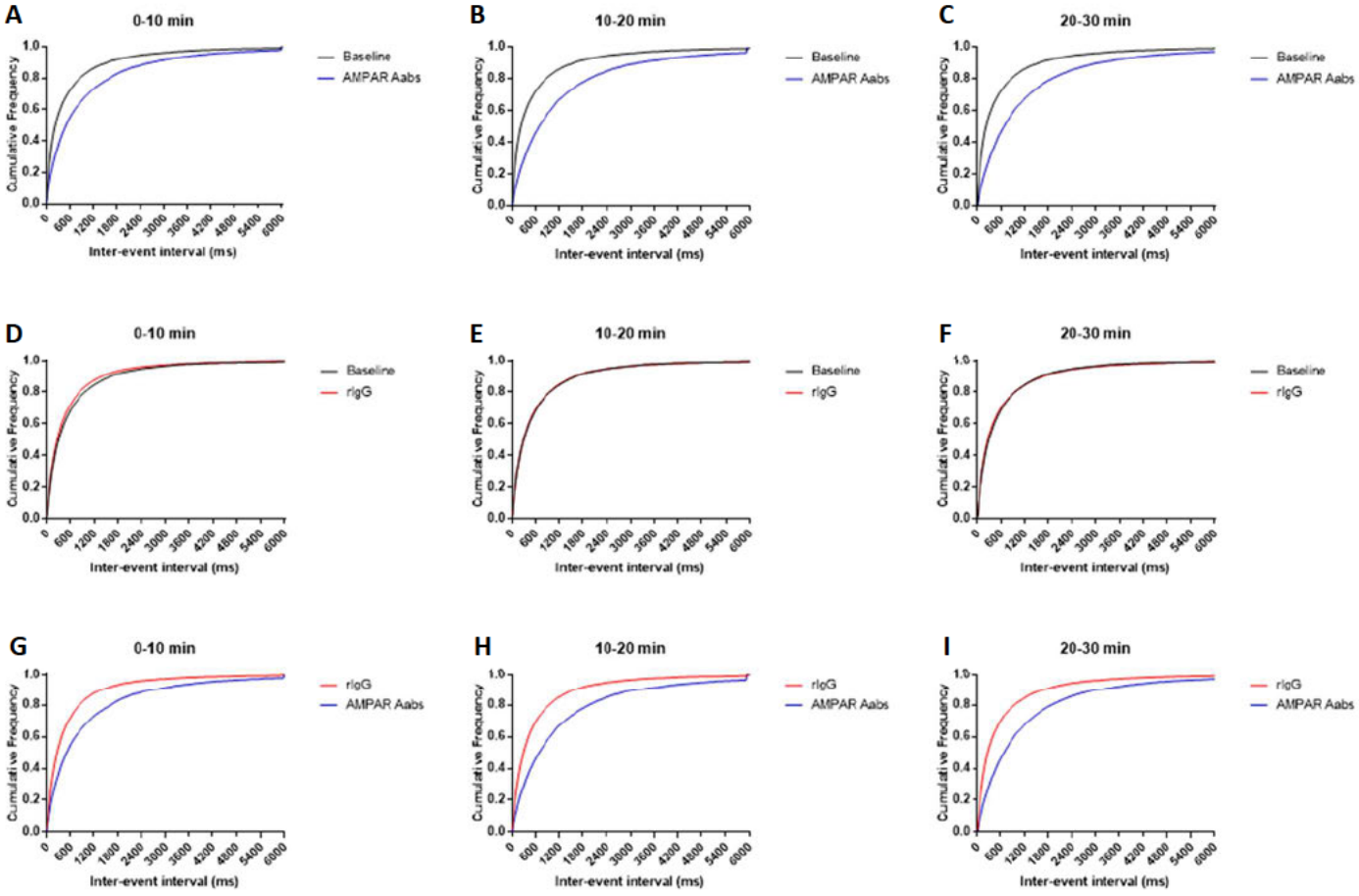

Figure 9.4: Effects of acute (30 min) AMPAR Aabs and rIgG application on sEPSC cumulative inter-event interval. Cumulative inter-event intervals were analysed in 10 min bins and compared to pre-treatment baselines. **A**-**C**: 0-10 min, 10-20 min and 20-30 min bins resulted in significant differences in cumulative inter-event intervals were observed following AMPAR Aab 30 min incubation when compared to its pre-treatment baseline ($p < 0.0001$ A-C). **D**-**F:** 0-10 min, 10-20 min and 20-30 min bins resulted in significant differences in cumulative inter-event intervals were observed following rIgG 30 min incubation when compared to its pre-treatment baseline ($p < 0.0001$, $p = 0.33$ and $p = 0.0003$ respectively). **G**-**I:** 0-10 min, 10-20 min and 20-30 min bins resulted in significant differences in cumulative inter-event intervals were observed following AMPAR Aab 30 min incubation when compared to its pre-treatment baseline ($p < 0.0001$ G-I). Data were collected from 14-22 cells over three separate neuronal culture and analysed via Kolmogorov-Smirnov test.

Significant differences in mEPSC cumulative inter-event interval distributions were also observed following AMPAR Aabs 30min incubation when compared to IgG incubated cells, and when compared to pre-treatment baselines. These differences were also observed when broken down into 10 min bins ($p<0.0001$; Kolmogorov-Smirnov test; Figure 9.5A-I).

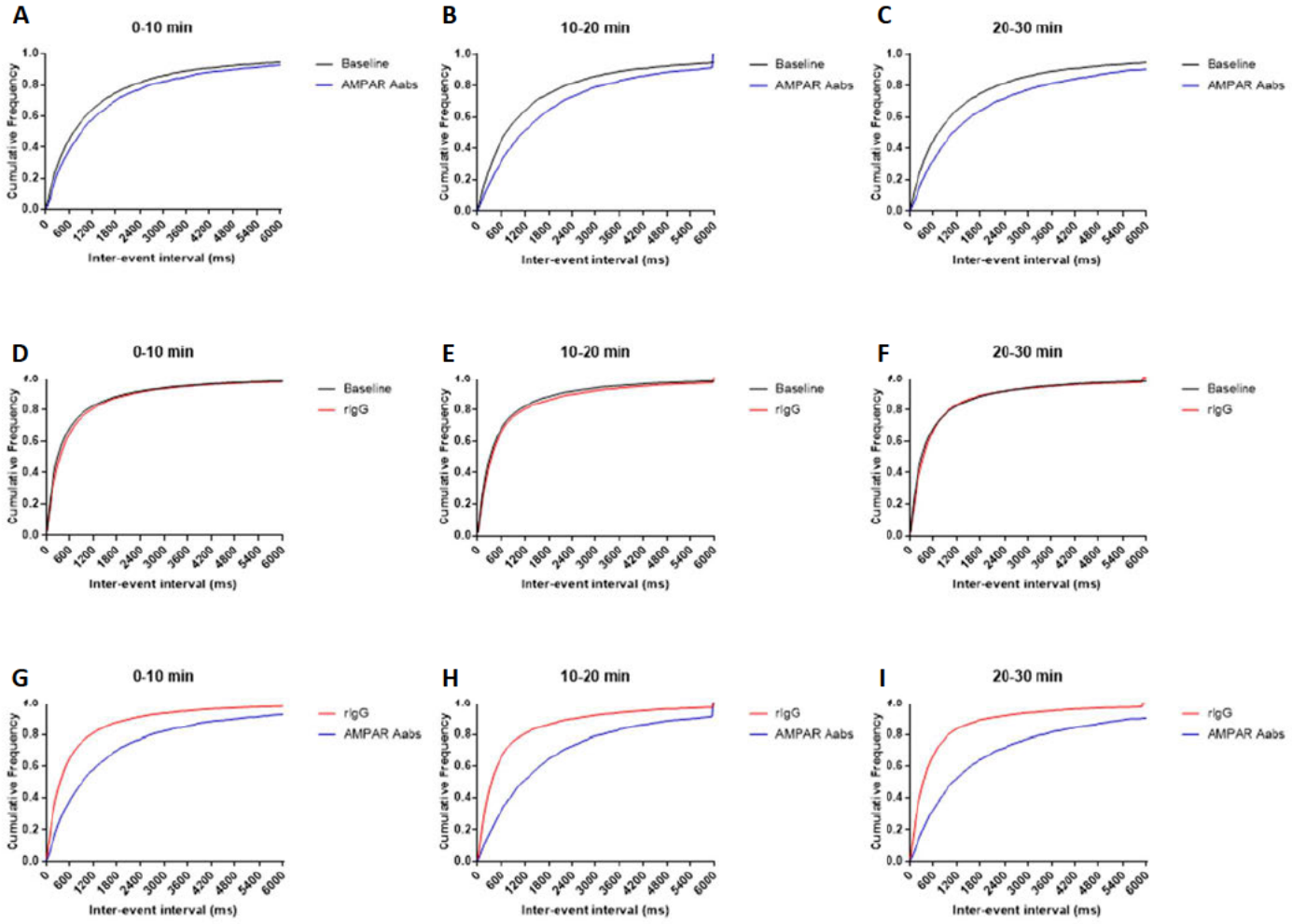

Figure 9.5: Effects of acute (30 min) AMPAR Aabs and rIgG application on mEPSC cumulative inter-event interval. Cumulative inter-event intervals were analysed in 10 min bins and compared to pre-treatment baselines. **A-C:** 0-10 min, 10-20 min and 20-30 min bins resulted in significant differences in cumulative inter-event intervals were observed following AMPAR Aab 30 min incubation when compared to its pre-treatment baseline ($p < 0.0001$ A-C). **D-F:** 0-10 min, 10-20 min and 20-30 min bins resulted in significant differences in cumulative inter-event intervals were observed following rIgG 30 min incubation when compared to its pre-treatment baseline ($p < 0.0001$ D-F). **G-I:** 0-10 min, 10-20 min and 20-30 min bins resulted in significant differences in cumulative inter-event intervals were observed following AMPAR Aab 30 min incubation when compared to its pre-treatment baseline ($p < 0.0001$ G-I). Data were collected from 14-22 cells over three separate neuronal culture and analysed via Kolmogorov-Smirnov test.

9.5 Preliminary cell death experiments following AMPAR Aab incubation

This appendix presents a summary of a preliminary experiment performed, but not formally analysed and therefore not included in the main body of the thesis.

9.5.1 No obvious changes in neuronal cell death were observed following acute or chronic AMPAR Aab incubation

Following on from the functional experiments in Chapter 6, where AMPAR Aabs were found to significantly reduce sEPSC and mEPSC frequency, a pilot study was performed investigating levels of neuronal cell death. Primary neurons were incubated with AMPAR Aabs or negative control IgG for 30 min and 24 h and labelled to detect Cleaved caspase 3 to try and identify any changes in levels of neuronal cell death, similar to that seen previously (Levite *et al.*, 1999; Ganor *et al.*, 2005).

No obvious changes in neuronal cell death were observed between those neurons incubated with AMPAR Aabs, those with negative control IgG, or those only in culture medium, following either acute (30 min) or chronic (24 h) incubation (as shown in Figures 9.6 and 9.7 respectively). However, as this was a preliminary experiment, not enough replicates were conducted for any statistical analysis to be performed, therefore no conclusions can be made regarding this.

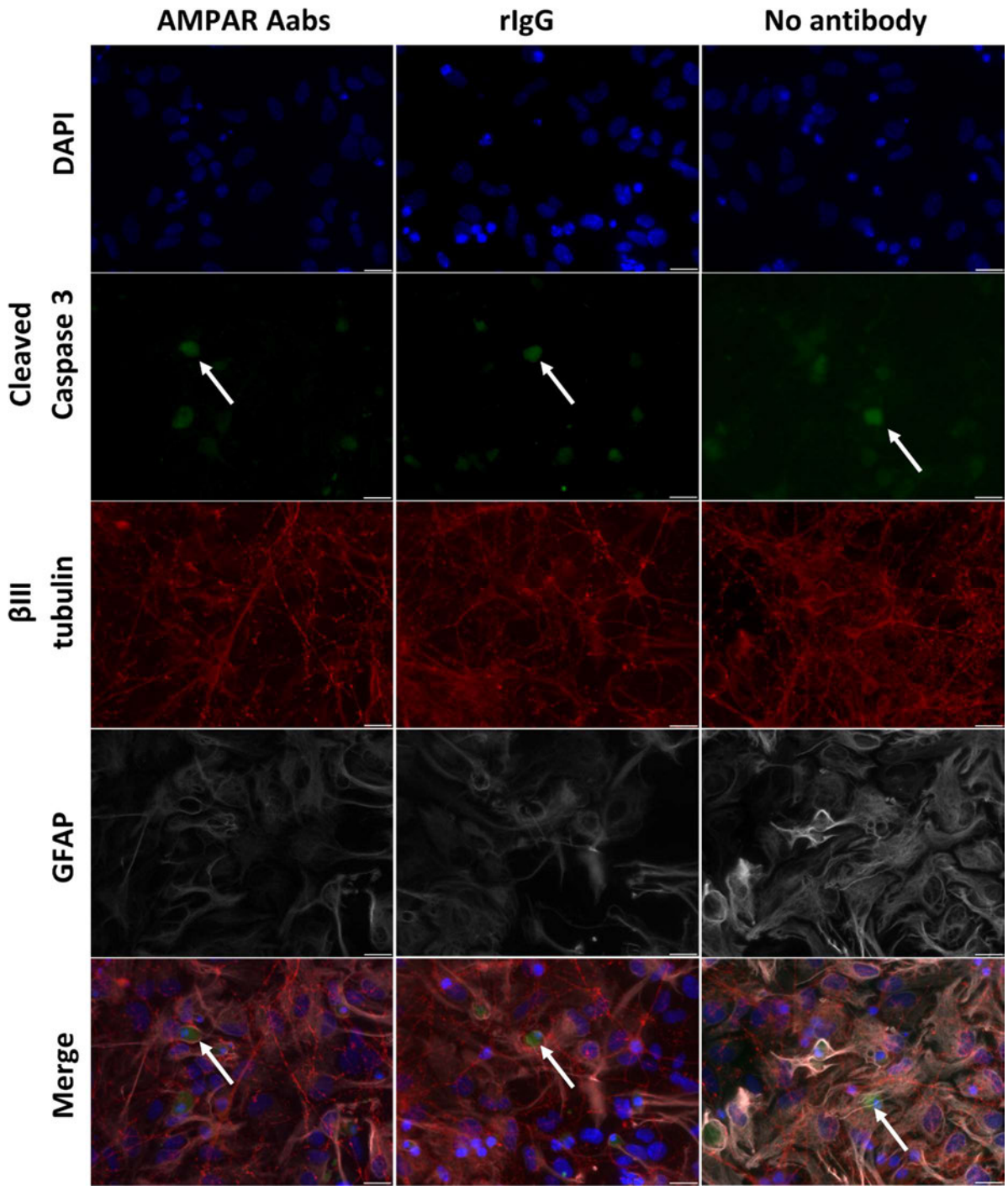

Figure 9.6: Immunocytochemical staining of fixed primary hippocampal neurons. Cells incubated either AMPAR Aabs or rIgG for 30 min prior to fixing and staining with cleaved caspase 3 (green, 1:50, as shown by white arrows), βIII tubulin (red, 1:500) and GFAP (white, 1:400) did not exhibit any obvious differences in levels of neuronal cell death. Scale = 20µm. Representative image selected from n=3 technical replicates (from one biological replicate).

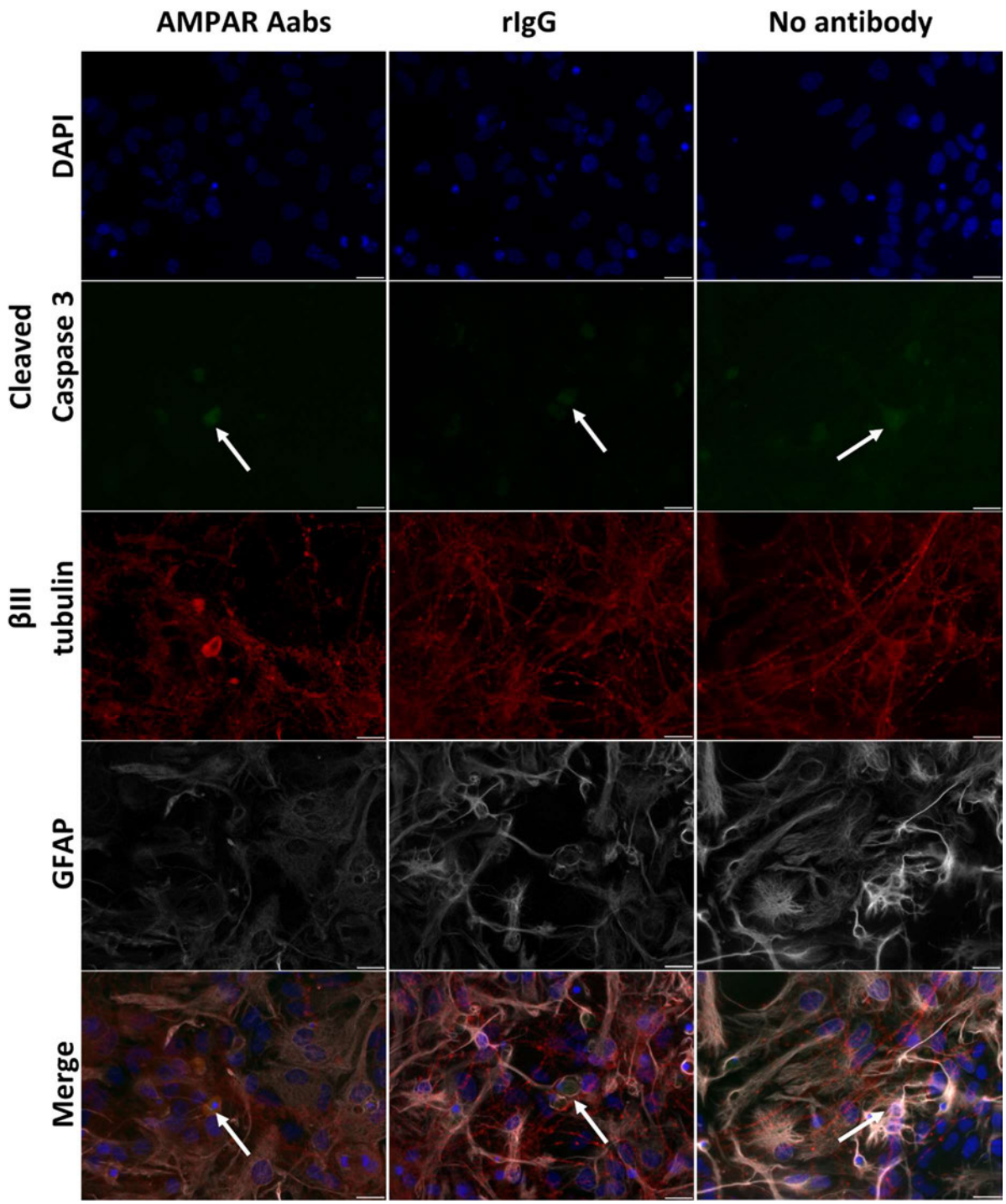

Figure 9.7: Immunocytochemical staining of fixed primary hippocampal neurons. Cells incubated either AMPAR Aabs or rIgG for 24 h prior to fixing and staining with cleaved caspase 3 (green, 1:50, as shown by white arrows), βIII tubulin (red, 1:500) and GFAP (white, 1:400) did not exhibit any obvious differences in levels of neuronal cell death. Scale = 20µm. Representative image selected from n=3 technical replicates (from one biological replicate).